OUKA
The University of Osaka
Institutional Knowledge Archive

Title	Synthesis and Evaluation of Catalytic Activity of Triarylboranes for Reductive Alkylation of Amino Acids Using Molecular Hydrogen
Author(s)	久田, 悠靖
Citation	大阪大学, 2026, 博士論文
Version Type	VoR
URL	https://doi.org/10.18910/105415
rights	
Note	

The University of Osaka Institutional Knowledge Archive : OUKA

https://ir.library.osaka-u.ac.jp/

The University of Osaka

Doctoral Dissertation

Synthesis and Evaluation of Catalytic Activity of Triarylboranes for Reductive Alkylation of Amino Acids Using Molecular Hydrogen

Yusei Hisata

January, 2026

Graduate School of Engineering

The University of Osaka

Preface and Acknowledgements

This study in this thesis has been carried out under the direction of Emeritus Professor Dr. Sensuke Ogoshi and Associate Professor Dr. Yoichi Hoshimoto at the Department of Applied Chemistry, Graduate School of Engineering, The University of Osaka from April 2021 to March 2026. This thesis describes the synthesis and evaluation of catalytic activity of triarylboranes for reductive alkylation of amino acids using molecular hydrogen.

First of all, I would like to express my heartfelt gratitude to Associate Professor Dr. Yoichi Hoshimoto for a large number of invaluable suggestions, discussions, heartful encouragement, and inspiring leadership, which have profoundly enriched all of my entire Ph.D. study, related research, and my life. I would like to thank the rest of my thesis committee: Professor Dr. Koji Hirano and Professor Dr. Mamoru Tobisu for their insightful comments and encouragement, but also for the hard question which invented me to widen my research from various perspectives.

I would like to express my gratitude to Emeritus Professor Dr. Sensuke Ogoshi for his invaluable guidance, for watching over us with care, and for engaging in thoughtful discussions that have inspired and enriched my study. I would like to give my special thanks to Associate Professor Dr. Ryohei Doi (Tokyo Metropolitan University), postdoctoral fellows Dr. Amit Kumar Jaiswal, Dr. Anil Chauhan and Dr. Oluwaseyi Aderemi Ajala for their continuous guidance, advice and assistance. I am also deeply grateful to Ms. Yukiko Mori, Ms. Chika Sugiki, and Ms. Yuri Kishimoto for their kind help and heart-warming encouragement.

I thank my fellow labmates: Mr. Daiki Kitazoe, Mr. Koki Kajiwara, Mr. Lueangratana Pacharapaul and Ms. Reina Okamoto, for the heartful encouragements to each other, improving together, and for all the fun we have had in our laboratory life and private time. I am deeply indebted to my respectful seniors in the Ogoshi Group: Dr. Yasuhiro Yamauchi, Dr. Mahiro Sakuraba, Dr. Shun Nagai, Dr. Taiki Hashimoto, Mr. Kenta Goto, Mr. Masashi Yasuda and Mr. Takuya Tsuruta for their helpful advice and kind encouragements. I thank all of my juniors in the Ogoshi Group: Mr. Keisuke Nozaki, Mr. Naoki Kajita, Mr. Taiki Negoro, Mr. Yutaka Mondori, Mr. Yuyang Zhou, Ms. Setsuka Homma, Mr. Kenta Koh, Mr. Nobutaka Mito, Mr. Taichi Morishita, Mr. Chihiro Yamaguchi, Mr. Genki Yamaguchi, Mr. Yusuke Goto, Mr. Ryosuke Harada, Mr. Naoya Iwamoto, Mr. Kimitaka Kambe, Mr. Yusuke Tokura, Mr. Koki Baba, Mr. Daina Morishita, Mr. Hayato Nishiguchi, Mr. Masakazu Tanigawa, Mr. Toshiki Taguchi and Mr. Riku Ikeda for their helpful assistance and heartful communications. I also thank the visiting research students: Mr. Coco, Ms. Shishkova and Mr. Kaufmann sharing good times.

I have also received a lot of advice from other groups for my Ph.D. study. I explain my gratitude to Professor Dr. Takashi Washio (Kansai University) and Professor Dr. Shinobu Takizawa (The University of Osaka) for meaningful suggestions to theoretical studies in Capter 1. I would like to express my special thanks to the Analytical Instrumentation Facility, Graduate School of Engineering, The University of Osaka, for the measurement of spectral and analytical data. Especially, I am grateful to Associate Professor Dr. Yoshiya Fukumoto and Assistant Professor Dr. Kyoko Inoue for thier advice for the nuclear magnetic resonance analyses, and technical specialist Mr. Hiroaki Tanaka for his advice for the mass spectrometry.

My sincere thanks also go to Professor Dr. Lukas J. Goossen (Ruhr University Bochum), who provided me an opportunity to join his group as a visiting research student (from September 2023 to November 2023 in Bochum, Germany). I am also grateful to his labmates: Dr. Daniel Sowa Prendes, Dr. Mykhailo Kondratiuk, Dr. Bingxiang Xie, Dr. Fluorian Papp, Dr. Gregor Heinrich, Ms. Elmira Nadirova, Dr. Jogendra Kumar, Ms. Johanna Stemmer, Mr. Nagesh Sankaran, Mr. Sourav Manna, Mr. Pierpaolo Satta, Mr. Mattia Saviozzi, Mr. Jie Shen, Ms. Kate Gerhard and Ms. Martyna Rybka for sharing wonderful time and their grateful help.

I acknowledge a grant from the Japan Society for the Promotion of Science (JSPS) Research Fellowship for Young Scientists (DC2), covering the period from April 2024 to March 2026.

Finally, I would like to express my utmost gratitude to my parents, brother, and sister: Mr. Seiji Hisata, Ms. Chiaki Hisata, Mr. Kosei Hisata, and Ms. Mari Hisata for their attentive support and warm encouragement.

January 6, 2026.

Yusei Hisata

Yusei Hisata

Contents

General Introduction 1

Chapter 1 6

In-Silico-Assisted Derivatization of Triarylboranes for the Catalytic Reductive Functionalization of Aniline-Derived Amino Acids and Peptides with H_2

Chapter 2 59

An Isolated Lithium ortho-Carboranyl Cuprate Complex for the Synthesis of Multiple-Carborane-Substituted Arenes from (Hetero)Aryl Bromides and Chlorides

Chapter 3 117

Triarylboranes Bearing (*ortho*-Carboran-1-yl)aryl Groups for Catalytic Hydrogenation with Pure or Crude H_2

Conclusion 136

List of Publications 137

Abbreviations

The following abbreviations are used in this thesis.

2-MeTHF	2-methyltetrahydrofuran
Å	angstrom
Ac	acetate
AIM	Atoms in molecules analysis
AN	accepter number
aq.	aqueous
Ar	aryl
atm	atmospheric pressure
BAr_3	triarylborane
$BF_3 \cdot Et_2O$	boron trifluoride diethyl etherate
br	broad
Bu	butyl
C_6D_6	deuterated benzene
ca.	circa
cal	calorie
calcd	calculated
cat.	catalyst
CBT	carboranyl-group transfer ratio
CCDC	Cambridge Crystallographic Data Centre
CD_2Cl_2	deuterated dichloromethane
cf.	confer
CH_4	methane
CI	chemical ionization
CO	carbon monoxide
CO_2	carbon dioxide
conv.	conversion
COSY	correlation spectroscopy
CPME	cyclopentyl methyl ether
°	degree(s)
°C	degrees Celsius
d	doublet
δ	chemical shift of NMR signal in ppm
DART	direct analysis in real time
DBU	1,8-diazabicyclo[5.4.0]undec-7-ene
DFT	density functional theory
DIPEA	N,N-diisopropylethylamine
DME	dimethoxyethane
DMF	dimethylformamide

E_{DEF}	deformation energy
e.g.	exempli gratia
EI	electron ionization
EQ	equilibrium structure
Eq.	equation
equiv.	equivalent
Et	ethyl
Et_2O	diethyl ether
EtOAc	ethyl acetate
FLP	frustrated Lewis pair
FMO	frontier molecular orbitals
GB	grove box
GB-AN	Gutmann-Beckett accepter number
GC	gas chromatography
GPR	Gaussian process regression
GPy	Gaussian Process library in Python
h	hour(s)
H_2	molecular hydrogen
HOBt	1-hydroxybenzotriazole
HOMO	highest occupied molecular orbital
HPLC	high performance liquid chromatography
HRMS	high-resolution mass spectra
Hz	hertz
i	iso
i.e.	id est
IRC	intrinsic reaction coordinate
J	coupling constant in NMR
k	kilo
LA	Lewis acid
LB	Lewis base
LDA	lithium diisopropylamide
Li-1	lithiated *o*-carborane
Li/Cu-1	lithium bis(o-carboranyl)cuprate complex
Li/Cu-2	isophthalonitrile-coordinated cuprate
Li/Cu-3	tricyclohexylphosphine-coordinated cuprate
LUMO	lowest unoccupied molecular orbital
M	mole per liter
m	multiplet
m	meta
MALDI-TOF	matrix-assisted laser desorption/ionization time-of-flight
Me	methyl
Me_4Si	tetramethylsilane
Mes	mesityl

MHz	mega hertz
min	minute(s)
ML	machine learning
mL	milliliter
µL	microliter
mol	mole
MS	mass spectrometry
MSiv	molecular sieve
MTHP	4-methyltetrahydropyran
n	normal
NCS	N-chlorosuccinimide
n.d.	not detected
NMR	nuclear magnetic resonance
o	ortho
p	para
PCy_3	tricyclohexylphosphine
Ph	phenyl
$PhCF_3$	benzotrifluoride
PhCN	benzonitrile
Pin	pinacolato
Pr	propyl
q	quartet
q(B)	Mulliken charge on boron
q(C)	Mulliken charge on ipso-carbon
ref.	reference
rt	room temperature
s	singlet
SC	single crystal
sec	second
sept	septet
t	triplet
t	tertiary
TCI	Tokyo Chemical Industry
TFA	trifluoroacetic acid
THC	tetrahedral character
THF	tetrahydrofuran
TMD	2,2,4-trimethyl-1,3-dioxolane
TOF	turnover frequency
TON	turnover number
TS	transition state
V	volume
vs	versus
w/o	without

wt%	weight percent
XRD	X-ray diffraction

General Introduction

Reductive alkylation of amines using carbonyl compounds is a well-known process for synthesizing functionalized amines, which involves the *in-situ* formation of imines and subsequent reaction with reductants (Figure 1).

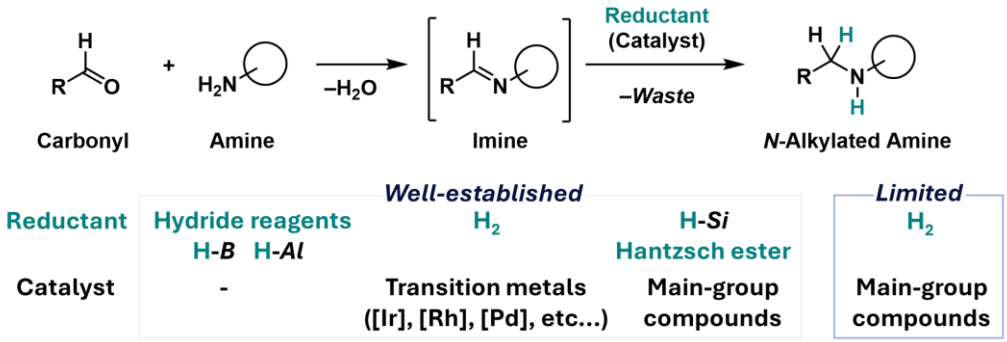


Figure 1. Reductive alkylation of amines with aldehydes.

Improving atom efficiency and reducing environmental impact in reductive alkylation processes are regarded as "a key green chemistry research area" in pharmaceuticals processes.[1] In this context, using molecular hydrogen (H_2) as a reductant can reduce waste generation to only H_2O. Indeed, the combination of transition metal catalysts and H_2 has been used for the reductive alkylation of amines; however, the residual toxicity of the metals has remained a concern.[2,3] Reaction systems using hydrosilanes or the Hantzsch ester as reductants have also been developed in the presence of less toxic main group catalysts, while these reactions produce more than stoichiometric amounts of waste.[4,5] Therefore, the catalytic reductive alkylation of amines using H_2 with less toxic triarylboranes (BAr_3) has been thought of as an ideal method for functionalizing amines.

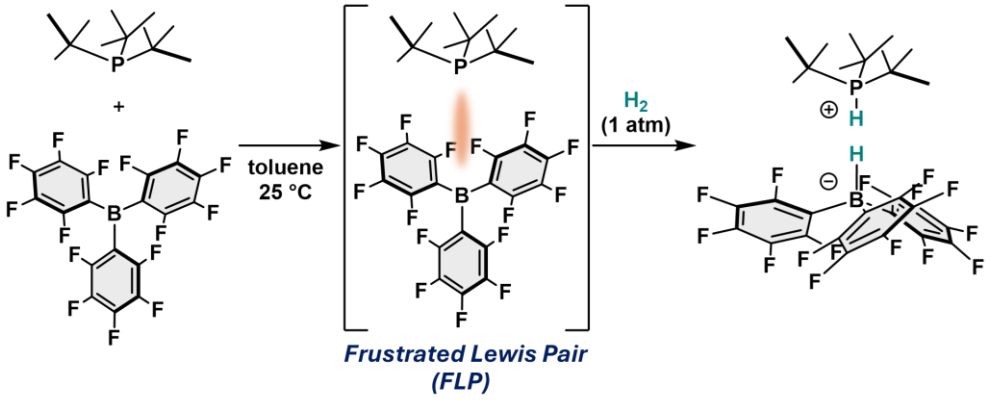


Figure 2. Heterolytic cleavage of H_2 through FLP

The BAr_3-reported catalytic hydrogenation proceeds via the generation of frustrated Lewis pairs (FLPs) that are comprised of Lewis bases and BAr_3 and cooperatively activate small molecules such as H_2,[6–13] CO[14–16] and CO_2[17–23]. For example, as shown in Figure 2, the heterolysis of H_2 proceeds via the generation of an FLP species comprising ^{t}Bu$_3$P and B(C_6F_5)$_3$, quantitatively yielding [^{t}Bu$_3$PH][HB(C_6F_5)$_3$].[24] In addition, BAr_3-

catalyzed hydrogenation of unsaturated molecules such as imines and *N*-heteroaromatics using H_2 has been reported to proceed through the key FLP-mediated H_2 cleavage step.

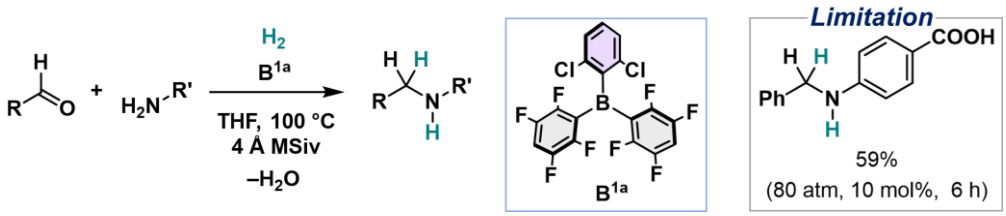


Figure 3. $\mathbf{B^{1a}}$-catalyzed reductive alkylation of amines with aldehydes, reported by our group (ref. 25).

Previously, our group reported the reductive alkylation of amines using $\mathbf{B^{1a}}$ as a catalyst and H_2 as a reductant, with only H_2O as a byproduct (Figure 3).[25] In this system, tetrahydrofuran (THF), used as a solvent, also acts as a Lewis basic component that comprises an FLP with $\mathbf{B^{1a}}$, and such FLP species would mediate the heterolytic cleavage of H_2. While this system is compatible with a wide range of amines, the use of amino acids produced the corresponding alkylated products in only moderate yields, even under harsh reaction conditions. Furthermore, the number of BAr_3 compounds applicable to catalytic hydrogenation reactions has remained limited, making their thorough screening/optimization still challenging.[26–30] Against this background, the author carried out a diversification of BAr_3 catalysts using *in-silico* approaches and applied them to the catalytic reductive alkylation of amino acids and peptides with H_2 and aldehydes.

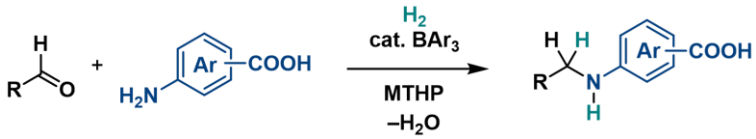


Figure 4. Developed BAr_3-catalyzed reductive alkylation for aniline-derived amino acids.

In Chapter 1, the density functional theory (DFT) calculations were employed to construct an *in-silico* library of BAr_3 and to obtain various theoretical parameters related to the structure and reactivity of BAr_3. A machine learning regression model was developed using the library calculation results as explanatory variables and the catalytic turnover efficiency (TOF) in the reductive alkylation of aniline-derived amino acids as the objective variable. Optimization of the BAr_3 structure through the regression model enabled the development of a reductive alkylation for aniline-derived amino acids.

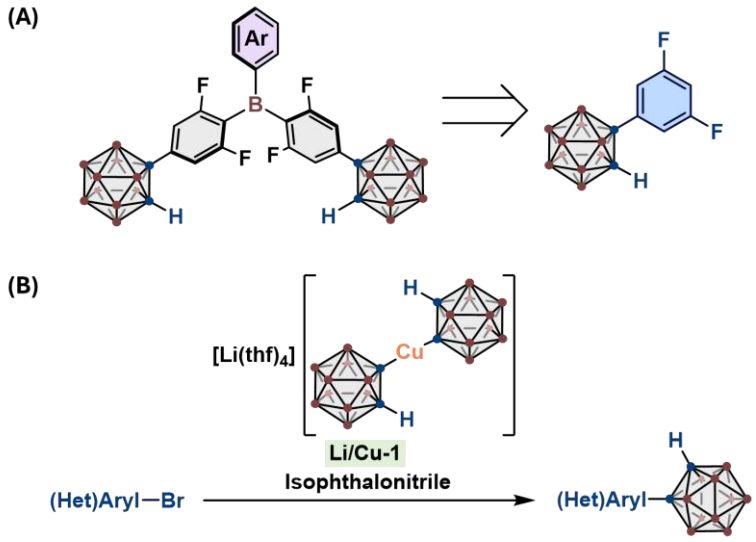


Figure 5. (A) The targeted triarylboranes and a starting material required for their synthesis. (B) Synthesis of carboranyl arenes using **Li/Cu-1**.

In Chapter 2, the author explored suitable boranes that can efficiently catalyze the reductive alkylation of natural amino acid derivatives and identified that some heteroleptic BAr_3 compounds bearing (*o*-carboran-1-yl)aryl groups may function (Figure 5a).[31–37] To this end, the author optimized the synthetic method for synthesizing (*o*-carboran-1-yl)arenes based on the isolation of lithium bis(*o*-carboran-1-yl)cuprate (**Li/Cu-1**) reagent (Figure 5b), as the reported procedures for synthesizing (*o*-carboran-1-yl)arenes were not suitable for transforming aryl bromide substrates.[38–43]

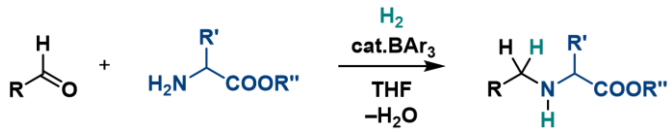


Figure 6. BAr_3-catalyzed reductive alkylation for natural amino acid derivatives.

In Chapter 3, the author developed heteroleptic BAr_3 compounds bearing (*o*-carboran-1-yl)aryl groups and applied them to the reductive alkylation of natural amino acid derivatives.

Finally, this thesis is summarized in the Conclusion.

References and Notes

1. Bryan, M. C.; Dunn, P. J.; Entwistle, D.; Gallou, F.; Koenig, S. G.; Hayler, J. D.; Hickey, M. R.; Hughes, S.; Kopach, M. E.; Moine, G.; Richardson, P.; Roschangar, F.; Steven, A.; Weiberth, F. J. *Green Chem.* **2018**, *20*, 5082–5103.
2. Reshi, N. U. D.; Saptal, V. B.; Beller, M.; Bera, J. K. *ACS Catal.* **2021**, *11*, 13809–13837.
3. Nugent, T. C.; El-Shazly, M. C *Adv. Synth. Catal.* **2010**, *352*, 753–819.
4. Fasano, V.; Radcliffe, J. E.; Ingleson, M. J. *ACS Catal.* **2016**, *6*, 1793–1798.
5. Wang, Q.; Chen, J.; Feng, X.; Du, H. *Org. Biomol. Chem.* **2018**, *16*, 1448–1451.
6. van der Zee, L. J. C.; Hofman, J.; van Gaalen, J. M.; Slootweg, J. C. *Chem. Soc. Rev.* **2024**, *53*, 4862–4876.

7. Khan, M. N.; van Ingen, Y.; Boruah, T.; McLauchlan, A.; Wirth, T.; Melen, R. L. *Chem. Sci.* **2023**, *14*, 13661–13695.
8. Stephan, D. W. *J. Am. Chem. Soc.* **2021**, *143*, 20002–20014.
9. Li, N.; Zhang, W. X. *Chinese J. Chem.* **2020**, *38*, 1360–1370.
10. Carden, J. L.; Dasgupta, A.; Melen, R. L. *Chem. Soc. Rev.* **2020**, *49*, 1706–1725.
11. Lam, J.; Szkop, K. M.; Mosaferi, E.; Stephan, D. W. *Chem. Soc. Rev.* **2019**, *48*, 3592–3612.
12. Hoshimoto, Y.; Ogoshi, S. *ACS Catal.* **2019**, *9*, 5439–5444.
13. Paradies, J. *Eur. J. Org. Chem.* **2019**, 283–294.
14. Stephan, D. W. *Chem. Soc. Rev.* **2023**, *52*, 4632–4643.
15. Stephan, D. W.; Erker, G. *Chem. Sci*. **2014**, *5*, 2625–2641.
16. Stephan, D. W.; Erker, G. *Angew. Chem., Int. Ed.* **2010**, *49*, 46–76.
17. Ashley, A. E.; Thompson, A. L.; O'Hare, D. *Angew. Chem., Int. Ed.* **2009**, *48*, 9839–9843.
18. Mömming, C. M.; Otten, E.; Kehr, G.; Fröhlich, R.; Grimme, S.; Stephan, D. W.; Erker, G. *Angew. Chem., Int. Ed.* **2009**, *48*, 6643–6646.
19. Tran, S. D.; Tronic, T. A.; Kaminsky, W.; Heinekey, D. M.; Mayer, J. M. *Inorg. Chim. Acta* **2011**, *369*, 126–132.
20. Voss, T.; Mahdi, T.; Otten, E.; Fröhlich, R.; Kehr, G.; Stephan, D. W.; Erker, G. *Organometallics* **2012**, *31*, 2367–2378.
21. Liu, Y.-L.; Kehr, G.; Daniliuc, C. G.; Erker, G. *Chem. Sci.* **2017**, *8*, 1097–1104.
22. Jian, Z.; Kehr, G.; Daniliuc, C. G.; Wibbeling, B.; Erker, G. *Dalton Trans.* **2017**, *46*, 11715–11721.
23. Jie, X.; Sun, Q.; Daniliuc, C. G.; Knitsch, R.; Hansen, M. R.; Eckert, H.; Kehr, G.; Erker, G. *Chem. Eur. J.* **2020**, *26*, 1269.
24. Welch, G. C.; Stephan, D. W. *J. Am. Chem. Soc.* **2007**, *129*, 1880–1881.
25. Hoshimoto, Y.; Kinoshita, T.; Hazra, S.; Ohashi, M.; Ogoshi, S. *J. Am. Chem. Soc.* **2018**, *140*, 7292–7300.
26. Gyömöre, Á.; Bakos, M.; Földes, T.; Pápai, I.; Domján, A.; Soós, T. *ACS Catal.* **2015**, *5*, 5366–5372.
27. Dorkó, É.; Kótai, B.; Földes, T.; Gyömöre, Á.; Pápai, I.; Soós, T. *J. Organomet. Chem.* **2017**, *847*, 258–262.
28. Berger, S. M.; Ferger, M.; Marder, T. B. *Chem. Eur. J.* **2021**, *27*, 7043–7058.
29. He, J.; Rauch, F.; Finze, M.; Marder, T. B. *Chem. Sci.* **2021**, *12*, 128–147.
30. Sakuraba, M.; Hoshimoto, Y. *Synthesis* **2024**, *56*, 3421–3430.
31. Lee, Y. H.; Lee, H. D.; Ryu, J. Y.; Lee, J.; Lee, M. H. *J. Organomet. Chem.* **2017**, *846*, 81–87.
32. Kim, S. Y.; Lee, A. R.; Cho, Y. J.; Son, H. J.; Han, W. S.; Kang, S. O. *J. Organomet. Chem.* **2015**, *798*, 245–251.
33. Nghia, N. Van; Jana, S.; Sujith, S.; Ryu, J. Y.; Lee, J.; Lee, S. U.; Lee, M. H. *Angew. Chem., Int. Ed.* **2018**, *57*, 12483–12488.
34. Choi, B. H.; Lee, J. H.; Hwang, H.; Lee, K. M.; Park, M. H. *Organometallics* **2016**, *35*, 1771–1777.
35. Song, K. C.; Kim, H.; Lee, K. M.; Lee, Y. S.; Do, Y.; Lee, M. H. *Dalton Trans.* **2013**, *42*, 2351–2354.
36. Lee, K. M.; Huh, J. O.; Kim, T.; Do, Y.; Lee, M. H. *Dalton Trans.* **2011**, *40*, 11758–11764.
37. Huh, J. O.; Kim, H.; Lee, K. M.; Lee, Y. S.; Do, Y.; Lee, M. H. *Chem. Commun.* **2010**, *46*, 1138–1140.

38. Coult, R.; Fox, M. A.; Gill, W. R.; Herbertson, P. L.; MacBride, J. A. H.; Wade, K. *J. Organomet. Chem.* **1993**, *462*, 19–29.
39. Anderson, K. P.; Mills, H. A.; Mao, C.; Kirlikovali, K. O.; Axtell, J. C.; Rheingold, A. L.; Spokoyny, A. M. *Tetrahedron* **2019**, *75*, 187–191.
40. Sun, M.; Feng, L.; Lu, J. Y. *Org. Lett.* **2024**, *26*, 3697–3702.
41. Lu, J. Y.; Zhao, B.; Du, Y.; Yang, J.; Lu, J. *Org. Biomol. Chem.* **2019**, *17*, 7438–7441.
42. Tang, C.; Xie, Z. *Angew. Chem., Int. Ed.* **2015**, *54*, 7662–7665.
43. Frixa, C.; Scobie, M.; Black, S. J.; Thompson, A. S.; Threadgill, M. D. *Chem. Commun.* **2002**, 2876–2877.

Chapter 1

In-Silico-Assisted Derivatization of Triarylboranes for the Catalytic Reductive Functionalization of Amino Acids with H_2

Abstract: Cheminformatics-based machine learning (ML) has assisted in determining optimal reaction conditions, including catalyst structures, in the field of synthetic chemistry. However, such ML-focused strategies have remained largely unexplored in the context of catalytic molecular transformations using Lewis-acidic main-group elements, probably due to the absence of a candidate library and effective guidelines (parameters) for the prediction of the activity of main-group elements. Here, the construction of a triarylborane library and its application to an ML-assisted approach for the catalytic reductive alkylation of amino acids with aldehydes and H_2 is reported. The obtained results suggest that the deformation energy serves as a useful parameter for Gaussian process regression to construct adequate models for predicting the turnover frequencies of triarylboranes under the applied model reaction conditions, while Gaussian process regression based on the energy levels of the lowest unoccupied molecular orbitals (LUMOs), including the empty p-orbitals of boron tend to underestimate the turnover frequency. The optimal borane, i.e., B(2,3,5,6-Cl_4-C_6H)(2,6-F_2-3,5-$(CF_3)_2$-$C_6H)_2$, effectively catalyzes the reductive functionalization of aniline-derived amino acids and C-terminal-protected peptides in the presence of 4-methyltetrahydropyrane and H_2, generating H_2O as the sole byproduct.

1.1 Introduction

Catalysis is a fact of our daily lives. A wide variety of important commercial chemical substances are currently produced on both the fine and bulk scales in the presence of molecular catalysts that have been optimized based on specific factors such as efficiency, toxicity, cost, or a combination thereof. Recent advancements in cheminformatics-based machine learning (ML) offer chemists a way to bypass traditional Edisonian empiricism and develop more efficient approaches to optimizing catalysts.[1–4] Several groups have reported successful demonstrations of ML-driven optimizations of homogeneous catalysts such as phosphoric acids and Lewis-basic ligands for metal-based catalysts involving phosphines, *N*-heterocyclic carbenes, and nitrogen-based ligands.[5–18]

Recent progress in frustrated Lewis pairs (FLPs)[19,20] has expanded the practical and sustainable application of main-group catalysis, e.g., enabling the hydrogenation of unsaturated molecules without toxic/precious metals.[21–26] In this context, the main-group-catalyzed reductive alkylation of amines with carbonyl compounds and H_2 via the generation of FLP species has been widely accepted as a waste-minimizing process that generates valuable *N*-alkylated amines, whereby H_2O is the only by-product.[23,27–31] Our research group[30] and that of Soós[28] have independently shown that triarylboranes effectively catalyze the reductive alkylation of a variety of amines with aldehydes in the presence of H_2. Moreover, our group has demonstrated that an FLP that consists of Soós' borane, i.e., B(2,6-Cl_2-C_6H_3)(2,3,5,6-F_4-$C_6H)_2$ (**B**$^{\mathbf{1a}}$),[27] and tetrahydrofuran (THF) exhibits good functional-group tolerance for aniline derivatives including halogens, hydroxyl, and amide groups (Figure 1.1A).[30] Based on mechanistic studies, the author proposed dual catalysis of **B**$^{\mathbf{1a}}$ in the formation

of imine intermediates and the hydrogenation of the imines via the generation of the FLP species (Figure 1.1B). However, the direct reductive alkylation of amino acids with H_2 has remained challenging, and such reactions have proceeded in only low-to-moderate yields even under forcing conditions. In terms of toxicity, the solvent THF, which also acts here as a Lewis base to generate FLPs with boranes (Figure 1.1B), should be replaced with a less hazardous chemical.[32,33] Given the central role of the reductive alkylation of amines using carbonyl compounds in the synthesis of, e.g., pharmaceuticals, bio-active molecules, and agrochemicals,[34–36] the development of a straightforward and greener protocol for derivatizing amino acids and peptides would be worthwhile.

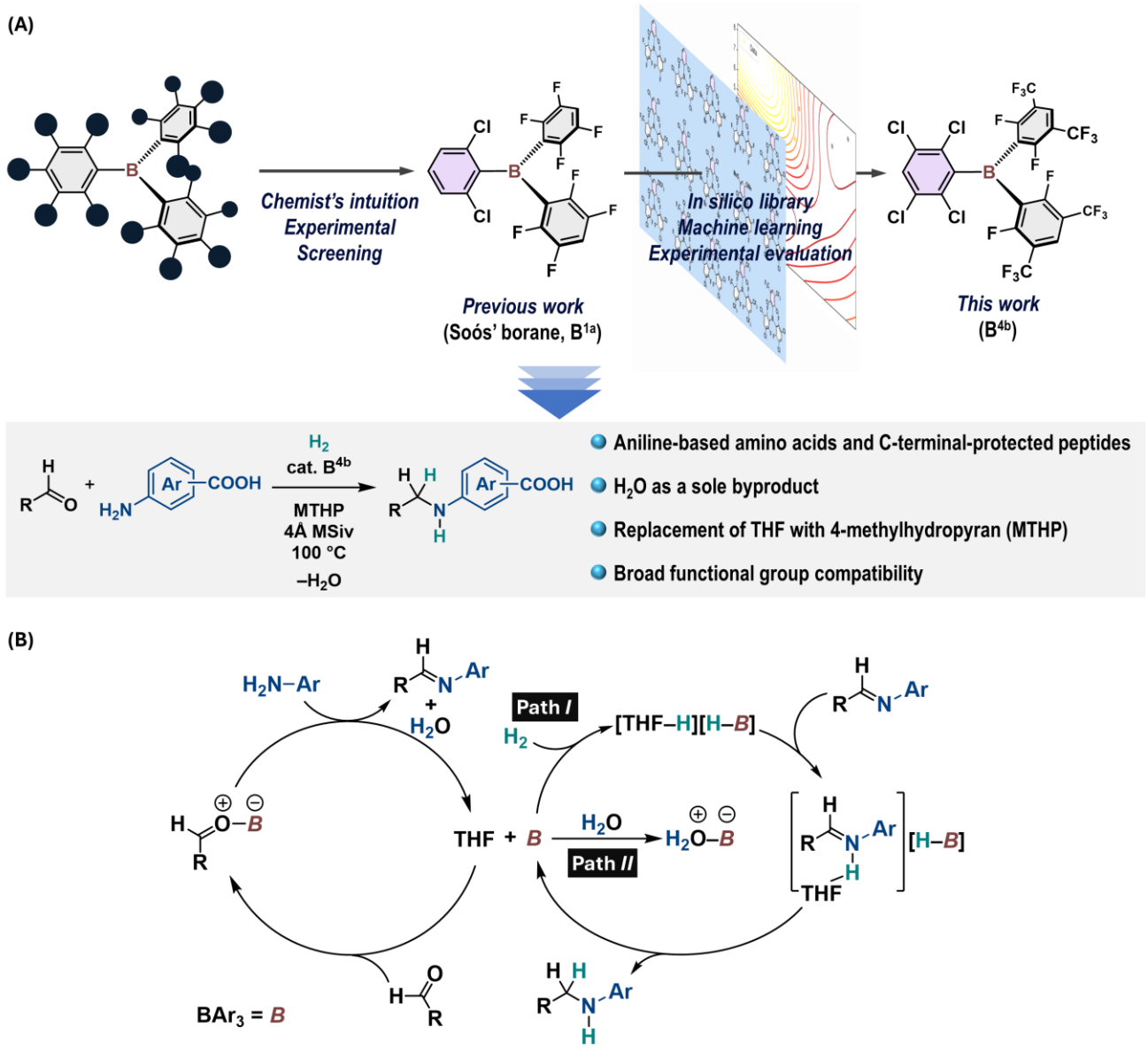


Figure 1.1. Context of this work. (A) Schematic representation of the concept of this study. (B) Proposed dual catalysis of triarylborane in the catalytic reductive alkylation of amines with aldehydes; ***B*** = triarylborane; **LB** = THF or MTHP.

To this end, the author envisioned an ML-assisted approach to identify a suitable triarylborane that is able to efficiently catalyze the reductive alkylation of amino acids and peptides with H_2 through the construction of an *in-silico* library that includes a variety of unprecedented triarylboranes. The synthesis of triarylboranes with unprecedented substitution patterns is typically a laborious and time-consuming process that often requires several weeks or even months for optimization. However, once the optimal procedures have been obtained, the optimized conditions can often be extrapolated, which is much faster. Therefore, using an ML-assisted approach to streamlining the selection of triarylborane candidates has the potential to significantly accelerate the optimization process and therefore the entire research process. Moreover, through the construction of this *in-silico* library, the author aimed to contribute to the structural diversification of triarylboranes beyond the archetypical $B(C_6F_5)_3$,[37–40] which should expand the utility of this compound class in catalysis, materials science, and other areas. It should be noted that Dyson, Corminboeuf and co-workers have demonstrated the hydrogenation of CO_2 to yield a formate salt [DBU–H][H–COO], which was catalyzed by an FLP consisting of tris(*p*-bromo)tridurylborane and 1,8-diazabicyclo[5.4.0]undec-7-ene (DBU).[41] They identified this combination of borane and DBU using a cheminformatics-assisted approach that profiled the theoretically predicted catalyst activity based on the intrinsic acidity and basicity of the Lewis components.

Herein, the author reports the construction of an *in-silico* library with 54 triarylboranes, including 46 unprecedented structures, which was used for the ML-assisted identification of the optimal borane for the catalytic reductive alkylation of aniline-derived amino acids and peptides with aldehydes and H_2 (Figure 1.1A). The author also explored the functional-group compatibility of the present system using the functional group evaluation (FGE) kit recently proposed by Morimoto, Oshima and co-workers,[42] which is based on the concept of robustness screening that has been proposed by Glorius and co-workers.[43,44]

1.2 Results and Discussion

1.2.1 Theoretical and experimental variables collection

The author started an investigation with the construction of an *in-silico* library of triarylboranes using the strategy described below. Generally, the author explored triarylboranes that seemed to be synthetically accessible using common procedures.[37,40] Optimization of the gas-phase structures of the 54 boranes shown in Figure 1.2A was accomplished using DFT calculations at the *ω*B97X-D/6-311+G(d,p)//*ω*B97X-D/6-31G(d,p) level. The 53 explored heteroleptic boranes $\mathbf{B}^{xy}$ (*x* = **1**–**6**, *y* = **a**–**w**) include two 2,6-F_2-3,5-R_2-C_6H groups, and their core structures are classified as $\mathbf{B}^{1}$–$\mathbf{B}^{6}$ depending on the R groups, i.e., $\mathbf{B}^{x}$(R) = $\mathbf{B}^{1}$(F), $\mathbf{B}^{2}$(Cl), $\mathbf{B}^{3}$(Br), $\mathbf{B}^{4}$(CF_3), and $\mathbf{B}^{5}$(H), whereas $\mathbf{B}^{6}$ includes 2,6-F_2-3-Cl-C_6H_2 groups. With these core structures, the author combined 23 aryl groups (**a**–**w**), and completed the construction of the borane library with the addition of $B(C_6F_5)_3$. It should be noted that boranes $\mathbf{B}^{xa}$ (*x* = 1–3, 5, 6), $\mathbf{B}^{1v}$, and $\mathbf{B}^{1w}$ were known before the construction of this library,[27,30,45–47] and their reactivity in the hydrogenation of unsaturated molecules inspired us when designing the library molecules. In fact, $\mathbf{B}^{1a}$ has previously been employed for the catalytic reductive alkylation of aniline derivatives to generate active FLP species with THF,[30] and thus, *in-silico* derivatization of $\mathbf{B}^{1a}$ was carried out via substitution of the *meta* and/or *para* H atoms in the 2,6-Cl_2-C_6H_3 group with Cl, Br, CF_3, OMe, OCF_3 or C_6F_5 groups. The author further conducted extensive *in-silico* derivatization of $\mathbf{B}^{2a}$ and $\mathbf{B}^{3a}$, given that

these boranes exhibit far superior catalytic activity than $\mathbf{B^{1a}}$, $\mathbf{B^{6a}}$, and $B(C_6F_5)_3$ in the hydrogenation of *N*-heteroaromatics using a gaseous mixture of $H_2/CO/CO_2/CH_4$.[45] In these cases, the author envisioned that the modulation of the intrinsic Lewis acidity of the triarylboranes, i.e., the energy levels of the LUMO, which includes the p orbital on the boron center,[48] as well as the remote back-strain[49] that would influence the stability of the four-coordinated tetrahedral Lewis base–borane adducts. The introduction of 2,6-Br_2-C_6H_3 (**j**) and its derivatives (**k**–**r**) into the $\mathbf{B^2}$ core was also explored, as the author expected an increase in the front strain that influences the accessibility of the Lewis bases to the boron centers.[37]

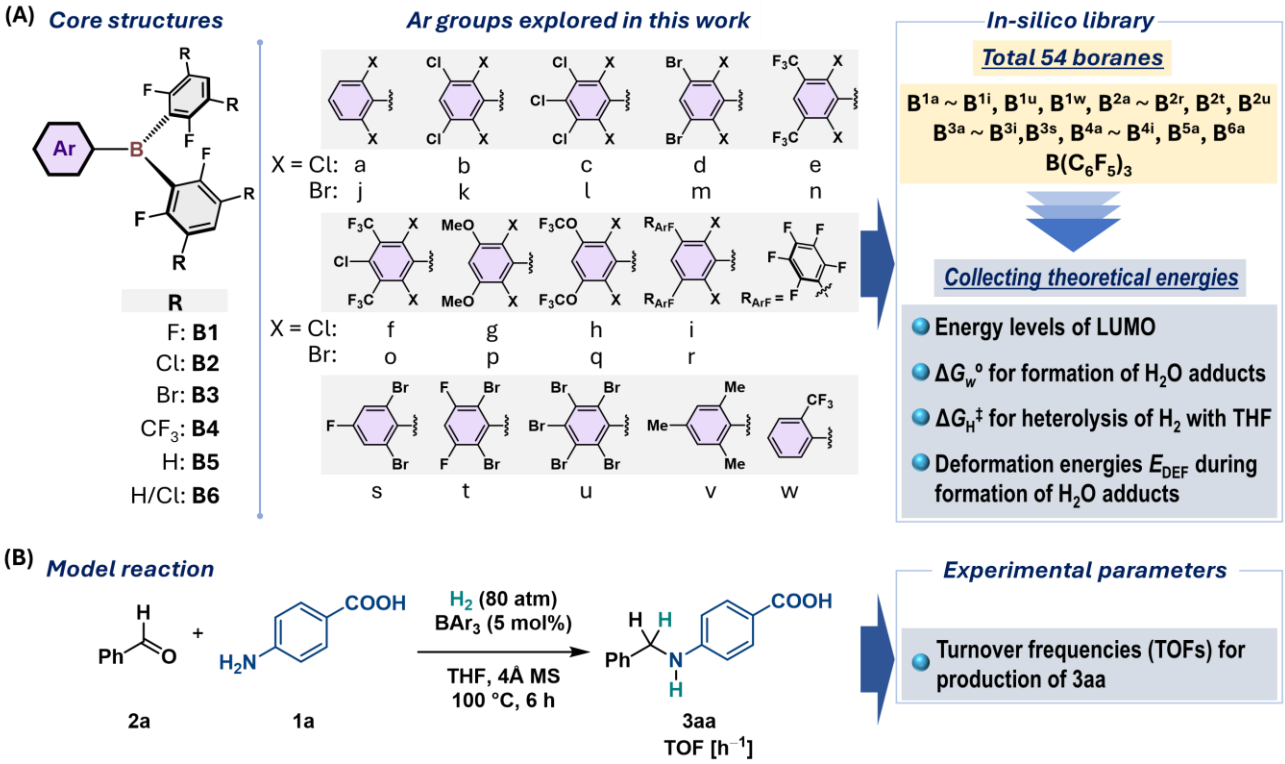


Figure 1.2. Experiment designs. (A) The *in-silico* library of triarylboranes explored in this work. The structure of $\mathbf{B^6}$ includes 2,6-F_2-3-Cl-C_6H_2 groups. (B) The model reaction for obtaining the experimental parameters (turnover frequencies per hour) used in this work.

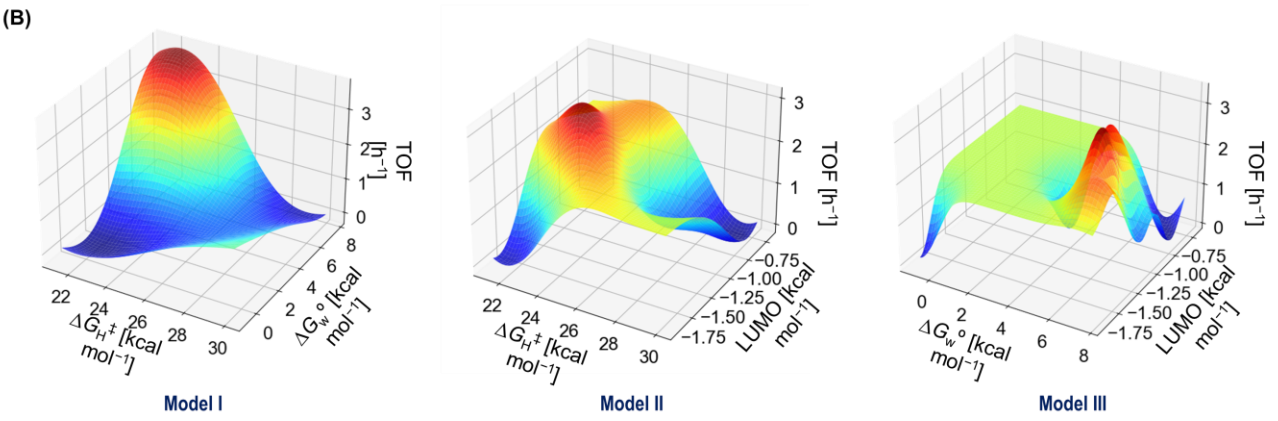
The author subsequently obtained the theoretical parameters. The author thought that the use of structural parameters obtained from the gas-phase optimization of $\mathbf{B^{xy}}$ would not play a critical role in predicting the reactivity of the triarylboranes under the chosen conditions, given that no substantial differences were observed among them (Table 1.S4). Thus, the author obtained the following energetic parameters, calculated at the ωB97X-D/6-311+G(d,p)//ωB97X-D/6-31G(d,p) level: (i) the energy levels of the LUMOs [eV], which include the p orbitals on the boron atoms, (ii) the energy barriers ($\Delta G_H^{\ddagger}$) [kcal mol^{-1}] for the heterolytic cleavage of H_2 with the combination of $\mathbf{B^{xy}}$ and THF, and (iii) the relative Gibbs energy values ($\Delta G_w°$) [kcal mol^{-1}] for the formation of the H_2O–$\mathbf{B^{xy}}$ adducts with respect to [H_2O + $\mathbf{B^{xy}}$]. These theoretical values are shown in Figure 1.3A for selected boranes. For parameter (ii), the author has previously proposed that the heterolytic cleavage

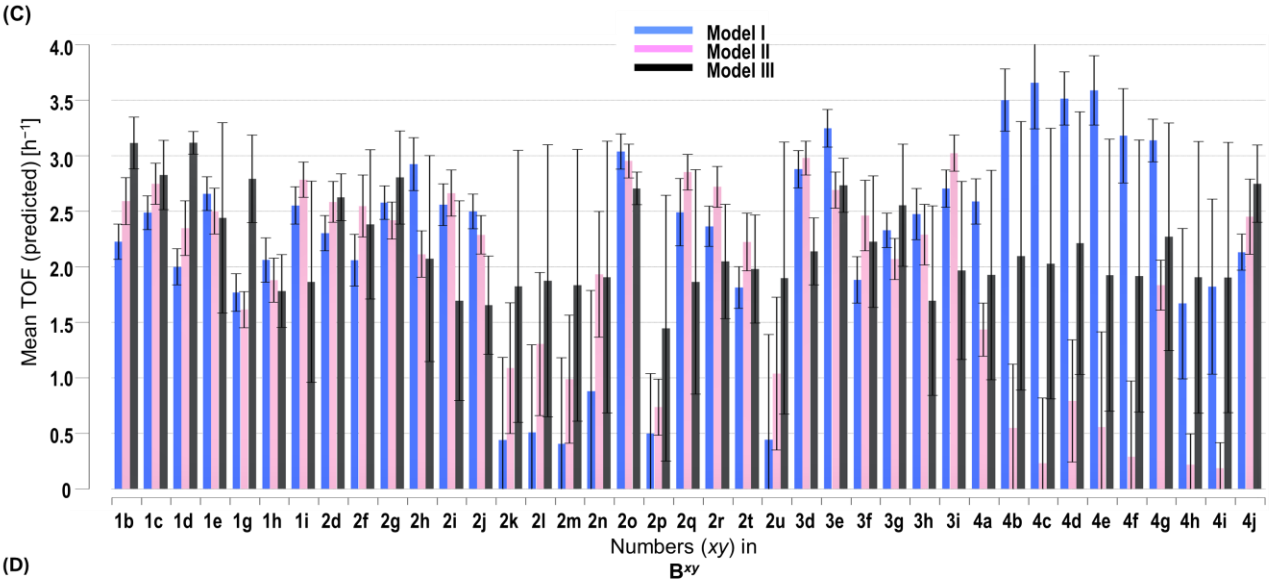
of H_2 by FLPs should be involved in the rate-determining event of the **B^{1a}**-catalyzed reductive alkylation of amines (Path I in Figure 1.1B).[30] For parameter (iii), H_2O could be a potential quencher of the triarylborane catalysts via the formation of adducts (Path II in Figure 1.1B) followed by proto-deboronation.[50] In this context, the author envisioned that boranes **B^{xy}** that exhibit larger $\Delta G_w°$ and smaller $\Delta G_H^‡$ values should show superior performance as Lewis acids for the generation of more active FLPs with ethereal components. It should also be mentioned here that the author theoretically optimized a structure that included a sole imaginary frequency related to the H−H bond cleavage; however, to reduce the calculation costs, the author performed an IRC calculation only for selected cases and confirmed their validity as a possible transition state structure.

Next, the author turned attention to collecting experimental data for the reported triarylboranes (**B^{xa}**, x = 1–3, 5, 6; **B^{1v}**; **B^{1w}**; $B(C_6F_5)_3$) and newly synthesized boranes (**B^{1f}**; **B^{2y}**, y = b, c, e; **B^{3y}**, y = b, c, s); the latter compounds were used to analyze the influence of the derivatization of the 2,6-Cl_2-C_6H_3 structure. The author obtained the turnover frequency (TOF in h^{-1}; Figure 1.3A) as an experimental parameter calculated based on the yield of **3aa** from the reductive alkylation of amino acid **1a** with benzaldehyde (**2a**) and H_2 in the presence of 5 mol% **B^{xy}** under the shown conditions as a model reaction (Figure 1.2B). The design of this model reaction is based on the potential of **B^{1a}** to produce **3aa** in approximately 50% yield after 6 h (i.e., TOF = 1.67 h^{-1}), as this consideration allows for a clearer evaluation of the positive and negative effects of structural derivatization during the optimization of **B^{xy}**.

(A)

	B^{1a}	B^{1f}	B^{1v}	B^{1w}	B^{2a}	B^{2b}	B^{2c}	B^{2e}	B^{3a}	B^{3b}	B^{3c}	B^{3s}	B^{5a}	B^{6a}	$B(C_6F_5)_3$
LUMO	−1.33	−1.64	−0.92	−1.25	−1.31	−1.48	−1.53	−1.62	−1.28	−1.45	−1.50	−1.35	−1.03	−0.71	−1.93
$\Delta G_w°$	+5.2	+4.1	+7.7	+4.4	+5.6	+6.3	+6.5	+7.0	+5.5	+6.5	+6.6	+6.9	+6.1	+6.6	−0.9
$\Delta G_H^‡$	+25.5	+23.3	+30.1	+28.7	+24.4	+24.1	+24.5	+24.7	+24.5	+24.5	+24.5	+25.9	+25.4	+28.7	+21.3
TOF	1.87	1.80	0	0.90	2.70	3.20	2.87	2.67	2.70	2.93	2.87	1.63	1.97	0.10	1.33





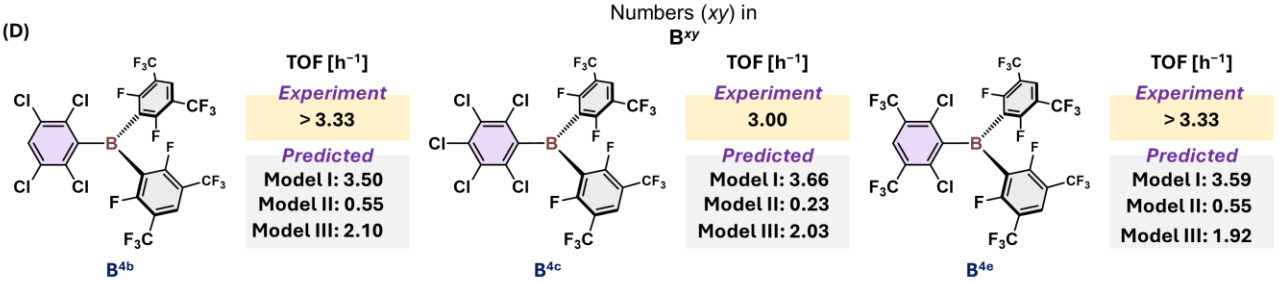


Figure 1.3. Optimization of B^{xy}. (A) LUMO energy level [eV], $\Delta G_w°$ [kcal mol^{-1}], and $\Delta G_H^‡$ [kcal mol^{-1}] for selected boranes B^{xy}. TOFs [h^{-1}] calculated based on the yield of **3aa** under the model conditions are also shown. (B) Gaussian process regression using the programming library GPy for the prediction of the TOF values. The theoretical values of the parameters $\Delta G_w°$ and $\Delta G_H^‡$ (**Model I**), the LUMO level and $\Delta G_H^‡$ (**Model II**), or the LUMO level and $\Delta G_w°$ (**Model III**) were used. (C) Comparison of the TOF values predicted using **Models I**,

II, or **III**. Error bars represent 1σ standard deviation. (D) Comparison of the experimental and predicted TOF values for $\mathbf{B^{4b}}$, $\mathbf{B^{4c}}$, and $\mathbf{B^{4e}}$.

1.2.2 Reaction conditions optimization

With the theoretical and experimental parameters in hand, Gaussian process regression (GPR), which is a radial basis function kernel-based statistical-learning algorithm, using GPy (a programming library for GPR),[51] was applied to construct a model to predict the TOF values for the production of **3aa** (it should be noted here that unless stated otherwise, mean values are presented for the theoretically predicted TOF values). GPR using GPy constructs a regression model using a limited number of observed data through ML and searches for a subsequent adequate parameter value of $\mathbf{B^{xy}}$ using the surrogate model. Note that GPR analysis has been widely explored in depth in information science and is characterized by the availability of a wide range of acquisition functions. Hence, its performance and flexibility to address various types of problems can be expected to efficiently promote the exploration of wide-ranging experimental conditions.[52] The author evaluated the accuracy of each GPR model based on the coefficient of determination (Q^2) of the leave-one-out (LOO) cross-validation using either training or validation data. It is noteworthy that higher Q^2 values approaching 1 indicate a more robust explanation for the data. The author carried out the initial GPR analysis using the experimental TOF values and pairs of two of the three theoretical parameters (LUMO energy level, $\Delta G_w°$, and $\Delta G_H^{‡}$) obtained for the 15 boranes shown in Figure 1.3A as training data. This GPR analysis resulted in three distinct models, labelled **Model I** ($\Delta G_w°$ vs $\Delta G_H^{‡}$; $Q^2 = 0.75$), **II** (LUMO level vs $\Delta G_H^{‡}$; $Q^2 = 0.76$), and **III** (LUMO level vs $\Delta G_w°$; $Q^2 = 0.21$) (Figure 1.3B). A significantly lower Q^2 of **Model III** would indicate its insufficient reliability. Subsequently, the author used the theoretical parameters of the other 39 triarylboranes to predict their TOF values using these three models. The author found intriguing inconsistencies among the TOF values for the $\mathbf{B^4}$ derivatives that contain *meta*-CF_3 groups predicted using **Model I** and those predicted using **Model II** (Figure 1.3C), albeit that the Q^2 values of **Model I** and **II** were identical at this stage. For example, when **Model I** was applied, the TOF values of $\mathbf{B^{4b}}$, $\mathbf{B^{4c}}$, and $\mathbf{B^{4e}}$ were predicted to be 3.50, 3.66, and 3.59, respectively; however, using **Model II**, the corresponding TOF values were predicted to be 0.55, 0.23, and 0.55, respectively (Figures 1.3C and 1.3D). A critical difference between **Model I** and **Model II** is the use of the LUMO energy levels in the GPR analysis. Thus, to evaluate whether the LUMO levels can serve here as a critical parameter for the prediction of the TOF for the production of **3aa**, the author additionally synthesized $\mathbf{B^{4b}}$, $\mathbf{B^{4c}}$, and $\mathbf{B^{4e}}$, and confirmed that these boranes demonstrate excellent activity for the reductive alkylation of **1a** with **2a** under the model reaction conditions as predicted by **Model I** (Figure 1.3D). The author updated each model additionally using the experimental TOF values of $\mathbf{B^{4b}}$, $\mathbf{B^{4c}}$, and $\mathbf{B^{4e}}$ to construct **Model I′** ($Q^2 = 0.73$), **II′** ($Q^2 = 0.28$), and **III′** ($Q^2 = 0.28$) (Table 1.S3). These results convinced us of the superiority of **Model I′** for the prediction of the catalytic activity of $\mathbf{B^{xy}}$ under the applied conditions. Based on synthetic accessibility considerations, the author decided to employ $\mathbf{B^{4b}}$ as the optimal catalyst in the following experiments. These results also suggest that the employment of a combination of theoretical parameters related to the rate-determining step (e.g., $\Delta G_H^{‡}$ in this work) and the (potential) catalyst deactivation step (e.g., ΔG_w in this work)

is decisive, whereas a parameter related to intrinsic Lewis acidity of triarylboranes, such as the LUMO energy level, is inappropriate for the prediction of the catalytic activity of triarylboranes under the applied conditions.

The author also aimed to investigate relatively unexplored theoretical parameters for the construction of a regression-based model for the prediction of the catalytic activity of triarylboranes. In this context, the author explored the deformation energy (E_{DEF}) [kcal mol^{-1}] that can be used to evaluate the degree of remote back-strain,[49] where E_{DEF} represents the energetic penalty associated with the change in the conformation at the boron center from trigonal planar to tetrahedral upon the formation of adducts between Lewis bases (LBs) and triarylboranes.[48,53,54] The author calculated the E_{DEF}(LB) values for 18 boranes shown in Figure 1.4A via the gas-phase optimization of their H_2O or THF adducts (i.e., $E_{DEF}(H_2O)$ and E_{DEF}(THF)) followed by energy-decomposition analysis at the RI-DSD-PBEP86-D3BJ/ma-Def2-QZVPP//PBEh-3c/Def2-SVP level. The GPR analysis with E_{DEF}(LB) and $\Delta G_H^{\ddagger}$ using the experimental TOF values resulted in the construction of **Model IV** (LB = H_2O; $Q^2 = 0.59$) and **V** (LB = THF; $Q^2 = 0.51$) with an acceptable reliability (Figure 1.4B). Interestingly, these Q^2 values were found to be insensitive to the differences in H_2O and THF. For further comparison, the author also prepared **Model VI** (q(B) vs $\Delta G_H^{\ddagger}$; $Q^2 = 0.09$) and **VII** (q(C) vs $\Delta G_H^{\ddagger}$; $Q^2 = -0.31$), wherein Mulliken charges [e] on the boron atoms and their average values on three *ipso*-carbon atoms in $\mathbf{B}^{xy}$ are given as q(B) and q(C), respectively; however, the reliability of these models was found to be insufficient. These results thus suggest that E_{DEF} should be a valuable parameter to explore during the ML-based optimization of triarylboranes, as the estimation of E_{DEF} through the optimization of structurally simple molecules (i.e., boranes, Lewis bases such as H_2O, and their adducts) is technically easier than the calculation of the activation energies, which is only feasible after the optimization of transition states.

(A)

	B^{1a}	B^{1f}	B^{1v}	B^{1w}	B^{2a}	B^{2b}	B^{2c}	B^{2e}	B^{3a}	B^{3b}	B^{3c}	B^{3s}	B^{4b}	B^{4c}	B^{4e}	B^{5a}	B^{6a}	$B(C_6F_5)_3$
$E_{DEF}(H_2O)$	+21.6	+25.4	+17.6	+16.2	+20.6	+22.1	+22.0	+23.6	+20.0	+21.7	+21.7	+21.4	+21.9	+23.3	+22.4	+21.0	+20.3	+18.4
E_{DEF}(THF)	+27.7	+31.4	+27.8	+23.0	+28.6	+29.9	+30.1	+29.8	+28.5	+29.9	+30.1	+31.2	+29.7	+29.9	+29.9	+30.9	+31.2	+25.8
q(B)	+0.31	+0.31	+0.15	+0.25	+0.27	+0.30	+0.33	+0.27	+0.32	+0.28	+0.28	+0.26	+0.27	+0.26	+0.37	+0.24	+0.26	+0.37
q(C)	−0.17	−0.17	−0.14	−0.16	−0.14	−0.19	−0.20	−0.17	−0.16	−0.17	−0.16	−0.16	−0.16	−0.15	−0.17	−0.13	−0.15	−0.21

(B)

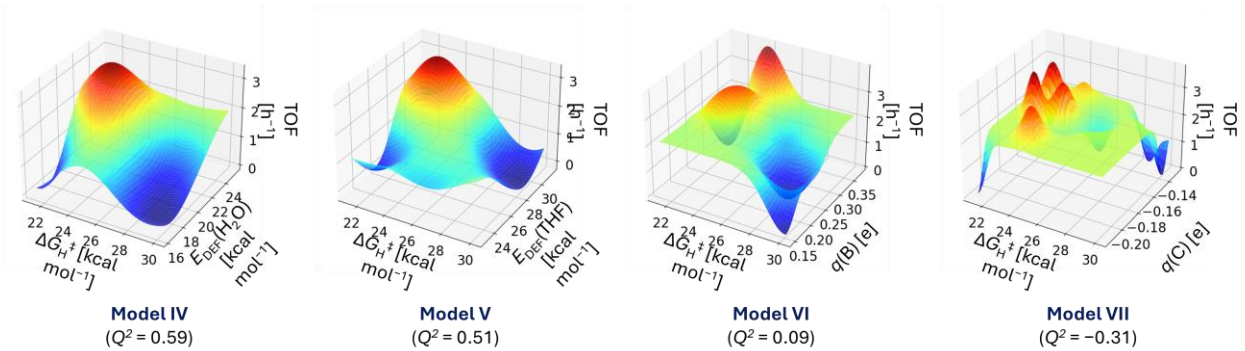


Figure 1.4. Exploring theoretical parameters. (A) Theoretical parameters calculated for the selected $\mathbf{B}^{xy}$. Deformation energies [kcal mol^{-1}], including $E_{DEF}(H_2O)$ and E_{DEF}(THF), were calculated at the RI-DSD-PBEP86-D3BJ/ma-Def2-QZVPP//PBEh-3c/Def2-SVP level. Mulliken charges [e], q(B) (values on the boron

atoms) and q(C) (averaged values of three *ipso*-carbons), were calculated at the PBEh-3c/Def2-SVP level. (B) Gaussian process regression with GPy for the prediction of TOF values [h^{-1}], using $E_{DEF}(H_2O)$ and $\Delta G_H^{\ddagger}$ (**Model IV**), E_{DEF}(THF) and $\Delta G_H^{\ddagger}$ (**Model V**), q(B) and $\Delta G_H^{\ddagger}$ (**Model VI**), and q(C) and $\Delta G_H^{\ddagger}$ (**Model VII**).

With the optimal triarylborane $\mathbf{B^{4b}}$ in hand, the author modified the reaction conditions to reduce its environmental impact and thus establish a greener and more sustainable system. In this context, the use of an alternative reaction solvent that could also act as a Lewis base to generate an FLP with $\mathbf{B^{4b}}$ was initially explored, given the recent demand for the replacement of hazardous THF with alternative ethereal compounds that exhibit lower toxicity combined with high chemical and thermal stability.[32] In the presence of 40 atm H_2, the reductive alkylation of **1a** with **2a** was carried out using THF, 2-methyltetrahydrofuran (2-MeTHF), cyclopentyl methyl ether (CPME), 4-methyltetrahydropyran (MTHP), or 2,2,4-trimethyl-1,3-dioxolane (TMD) (Figure 1.5A). While THF provided a superior result (50%) compared to 2-MeTHF (38%) and CPME (18%), **3aa** was generated in 59% yield when MTHP was used. Prolongation of the reaction time to 24 h resulted in the formation of **3aa** in 72% yield; however, the removal of the 4Å MSiv caused a decrease in the yield of **3aa** to 42%. Finally, increasing the H_2 pressure to 60 atm resulted in the formation of **3aa** in 95% yield after a period of 24 h. The use of TMD did not furnish any **3aa**. It should be noted that MTHP can be easily separated from water (its solubility in H_2O is ~1.5 wt%) and removed under reduced pressure due to its strong hydrophobicity and low heat of vaporization, although its employment as a greener solvent has been limited in organic synthesis compared with the use of 2-MeTHF and CPME.[32,33] Moreover, to clarify the benefit of using MTHP over THF, the author compared the activation energies for the heterolytic cleavage of H_2 by the combination of $\mathbf{B^{4b}}$ and THF or MTHP at the ωB97X-D/6-311+G(d,p)//ωB97X-D/6-31G(d,p) level (Figure 1.5B). A possible transition state was found in both cases, and that in the case of MTHP was found to be more stabilized (TS_{MTHP} = +21.8 kcal mol^{-1}) than that in the case involving THF (TS_{THF} = +23.2 kcal mol^{-1}). The author attributes this stabilization to the increased structural flexibility of the tetrahydropyrane motif relative to THF, which allows the formation of efficient non-covalent interactions (NCIs) between the F/Cl atoms in $\mathbf{B^{4b}}$ and the H atoms in MTHP. The participation of such NCIs was confirmed using the quantum theory of atoms in molecules (AIM) method (for details, see Figure 1.S13).[55,56]

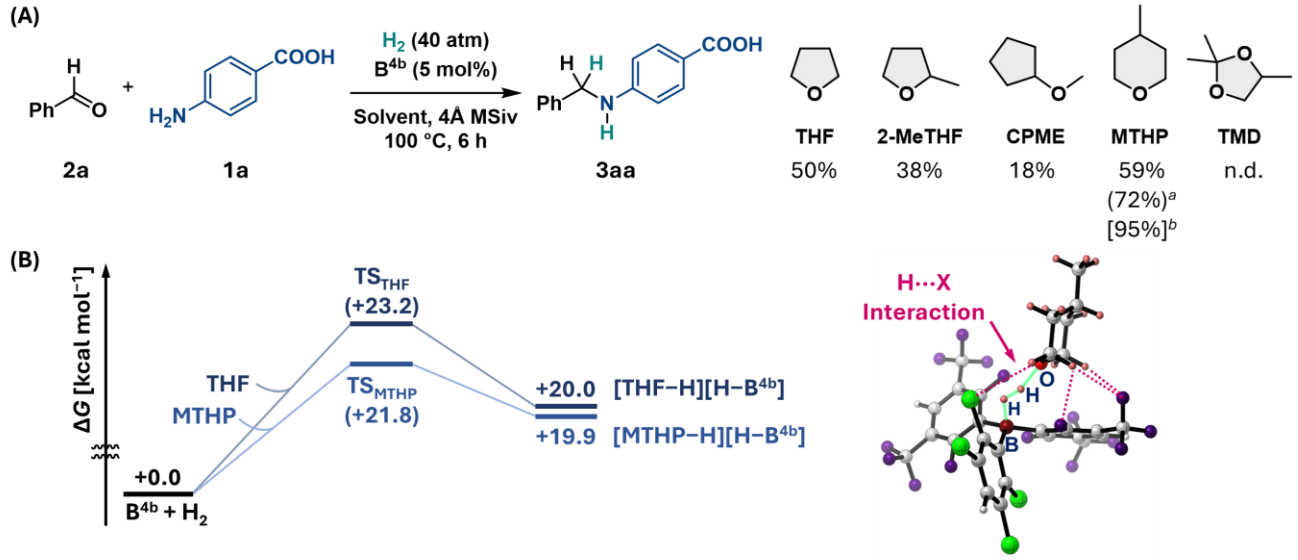


Figure 1.5. Optimization of reaction conditions. (A) Exploration of greener Lewis-basic solvents. Reaction conditions: **1a** (0.4 mmol, 0.05 M), **2a** (1.0 equiv.), **B^{4b}** (5 mol%), and 4Å MSiv (100 mg) were mixed in the solvent, followed by pressurization with H_2 (40 atm). The yield of **3aa** was determined via ^{1}H NMR analysis. [a]24 h. [b]60 atm H_2 for 24 h. (B) Relative Gibbs free energies [kcal mol^{-1}] with respect to [**B^{4b}** + H_2 + LB], where LB is either MTHP or THF, calculated at the *ω*B97X-D/6-311+G(d,p)//*ω*B97X-D/6-31G(d,p) level. The structure of TS_{MTHP} is also shown. Pairs of atoms involved in H···X (F/Cl) interactions that were found using AIM analysis are indicated by dashed lines (H: pink; B: brown; C: gray; O: red; F: purple; Cl: light green).

1.2.3 Functional-group compatibility

The **B^{4b}**-catalyzed reductive alkylation of **1a** with **2a** in MTHP using H_2 (40 atm) demonstrated remarkable compatibility toward a variety of additives (**Add.0**–**Add.21**) (Figure 1.6). All these experiments were carried out twice, and mean values [%] are given for the yield of **3aa**, the recovered additive, and the imine intermediate 4-(benzylideneamino)benzoic acid formed *in situ* through the **B^{4b}**-catalyzed condensation of **1a** and **2a** (left cycle in Figure 1.1B). Initially, the author carried out a control experiment using **Add.0**, which confirmed that the yields of **3aa** and the remaining imine were consistent (72% and 28%, respectively) with those of the reaction conducted without **Add.0** (Figures 1.5A and 1.6). Relative to the control experiment, the reductive alkylation among **1a**, **2a**, and H_2 proceeded without a significant change in the yield of **3aa**, the recovered additives, or imine intermediates for additives with ketone (**Add.3**/**Add.13**), primary amide (**Add.4**), aryl bromide/iodide including alkyl ether (**Add.6**/**Add.7**), allylic ether (**Add.8**), terminal alkyne (**Add.9**), enone (**Add.12**), nitrile (**Add.15**), and ester (**Add.20**) moieties. It is also noteworthy that additives including sulfhydryl (**Add.16**) and sulfide (**Add.17**) moieties did not affect the present reaction, whereas such sulfur-containing compounds can be critical inhibitors in transition-metal-based catalysis and organocatalysis.[42] On the other hand, the hydrogenation of the imine intermediates was suppressed in the presence of aliphatic/aromatic carboxy (**Add.1**/**Add.14**), aliphatic hydroxyl (**Add.2**), bulky silyl ether (**Add.10**), pinacolatoboryl (**Add.18**), and *N*-*tert*-butoxycarbonyl (Boc) (**Add.21**) moieties, as these functional groups include either a Lewis-basic or -acidic site that can kinetically inhibit the formation of the FLP consisting of **B^{4b}** and MTHP. In fact, the quantitative

recovery of the additives after a period of 24 h was confirmed, without the generation of any other significant byproduct, i.e., the sum of the yields of **3aa** and the imine was always ~95%. In contrast, the formation of **3aa** was largely suppressed under reaction conditions including *N*-heteroaromatic moieties such as an imidazole (**Add.5**) and an indole (**Add.19**), as these heteroaromatic units can react with $\mathbf{B^{4b}}$ to form Lewis adducts and/or with aldehydes to complicate the system. In the case of **Add.11,** which includes an epoxide moiety, **3aa** was only produced in 13% yield, and a significant loss of **Add.11** was confirmed after the reaction. Given that Lewis-acidic triarylboranes mediate the ring-opening transformation of epoxides,[57,58] the $\mathbf{B^{4b}}$-catalyzed ring-opening reaction of **Add.11** to give the corresponding aldehyde can be expected to compete with the targeted reaction (see 1.4 Supporting information for details).

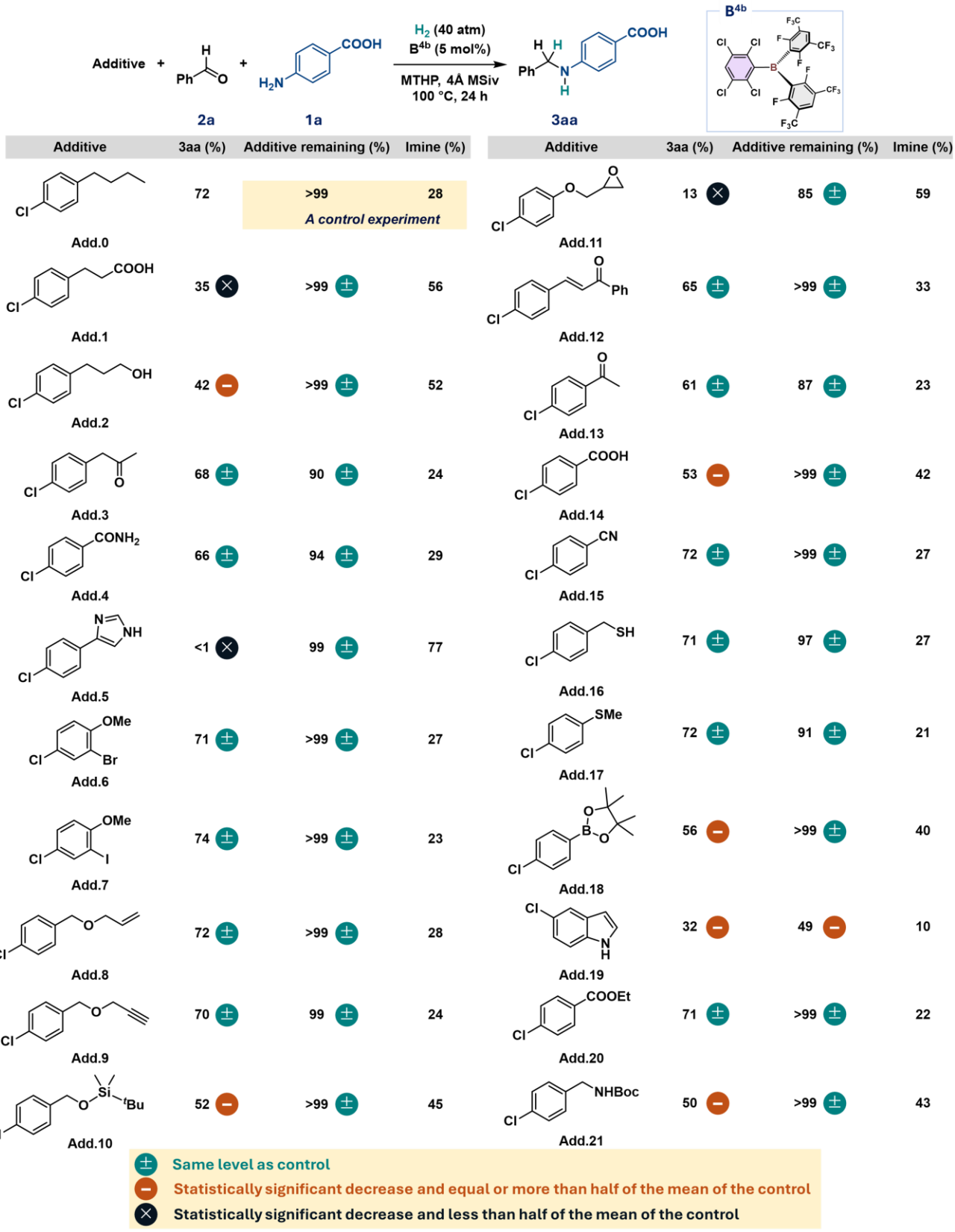


Figure 1.6. Exploring functional-group compatibility. Reaction conditions: **1a** (0.4 mmol, 0.05 M), **2a** (1.0 equiv.), additive (1.0 equiv.), **B**^{4b} (5 mol%) and 4Å MSiv (100 mg) were mixed in MTHP, followed by pressurization with H_2 (40 atm). The mean values of two experiments are given, which were determined via ^{1}H

NMR analysis.

1.2.4 Scope study

Finally, the author applied the combination of **B**^{4b} and MTHP for the reductive alkylation of aniline-derived amino acids and peptide derivatives in the presence of H_2 (Figure 1.7). Aminosalicylic acids **1b** and **1c** were effectively alkylated under the optimized conditions, and **3ba** and **3ca** were obtained in 90% and 93% yield, respectively; 60 atm of H_2 was used in the latter case. For comparison, under a pressure of 80 atm of H_2 in THF, **3ba** and **3ca** were furnished in 47% and 70% yield in the presence of 10 mol% and 15 mol% **B**^{1a}, respectively, which again demonstrates the advantages of the present system using **B**^{4b} and MTHP in terms of synthetic efficiency and sustainability. The reductive alkylation of anthranilic acid (**1d**), which is also known as vitamin L1, 5-aminoisophthalic acid (**1e**), and 4-aminophenylacetic acid (**1f**) afforded **3da**, **3ea**, and **3fa** in excellent yield using 40–60 atm of H_2. In contrast, the author recognized that aliphatic amino acids (or their imine derivatives) and substrates insoluble in MTHP were not suitable. For example, aspartic acid (**1g**) is insoluble in MTHP, and no reaction took place when **1g** was employed under otherwise identical conditions. Esterification of the carboxy group in 3-amino-4,4-dimethylpentanoic acid effectively improved its solubility in MTHP; however, the hydrogenation of the imine derived from **1h** and **2a** did not occur. Based on these results, the author prepared alanine- and *S*-methylcysteine-based peptides **1i** and **1j**, and subjected them to the optimal reaction conditions; alkylated peptides **3ia** and **3ja** were obtained in 95% and 55% yield, respectively. In terms of the scope of aldehydes, 3,5-bis(trifluoromethyl)benzaldehyde (**2b**) furnished **3ab** in 93% yield, but 3,5-di-*tert*-butylbenzaldehyde (**2c**) gave **3ac** in merely 38%. In the latter case, a significant amount of **2c** remained unreacted, indicating difficulties associated with the formation of the imine intermediate due to the decreased electrophilicity of the aldehyde moiety. A comparable result was obtained when *p*-tolualdehyde (**2d**) was used with respect to the case using **2a**, and **3ad** was afforded in 80% yield. As confirmed by the aforementioned robustness screening, the **B**^{4b}/MTHP system exhibited remarkable functional-group compatibility in the reductive alkylation of aniline derivatives to afford **3ka**−**3sa** in excellent yield. Given that harsh conditions, including 80 atm of H_2, 10 mol% borane, and/or a longer reaction time were required for the reactions with **1l**, **1m**, and **1q** in the reported **B**^{1a}/THF system, the present **B**^{4b}/MTHP system clearly demonstrates its advantages.

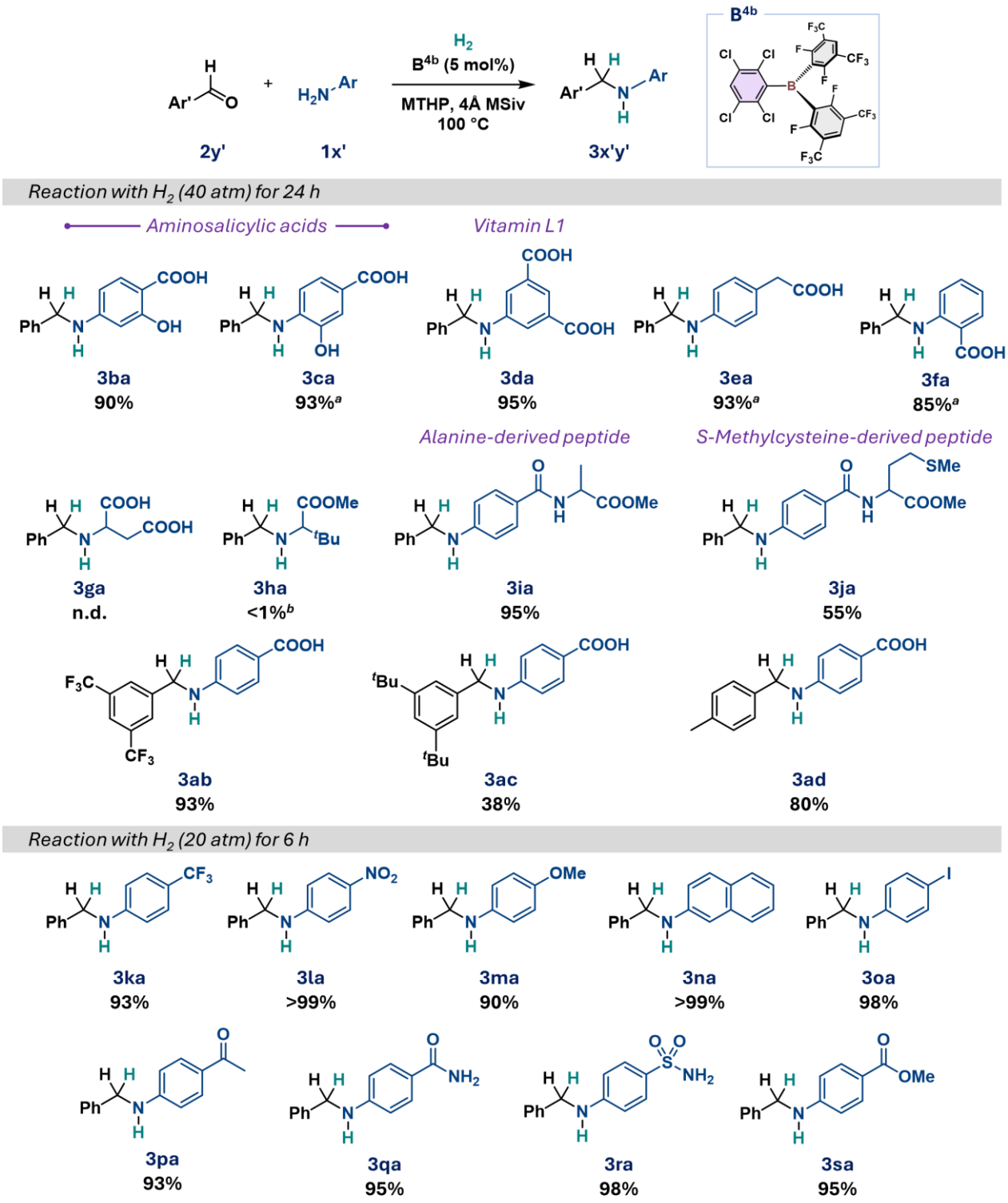


Figure 1.7. The B^{4b}-catalyzed reductive alkylation of aniline derivatives (1b−1s) with aldehydes (2a−d) using H_2 in MTHP. General conditions: **1** (0.4 mmol, 0.05 M), **2** (1.0 equiv), B^{4b} (5 mol%), and 4Å MSiv (100 mg) were mixed in MTHP, followed by pressurization with H_2. Yields of isolated products are given. [a]60 atm H_2. [b]The formation of the imine in >99% was confirmed.

1.3 Conclusion

The present study demonstrates an *in-silico*-assisted approach to designing triarylboranes that exhibit promising reactivity as main-group catalysts for the reductive alkylation of aniline-derived amino acids with H_2. The author has constructed an *in-silico* library of triarylboranes, including 46 unprecedented boranes, and obtained their theoretical parameters using DFT calculations. Guided by Gaussian process regression (GPR) using theoretical and experimental parameters, the author identified the optimal triarylborane, i.e., B(2,3,5,6-Cl_4-C_6H)(2,6-F_2-3,5-$(CF_3)_2$-$C_6H)_2$ (**B^{4b}**). Through the evaluation of the regression-based models, the author confirmed that the use of a parameter related to an intrinsic Lewis acidity of the triarylboranes (e.g., LUMO energy level and Mulliken charge on the boron atom) as one of the variables for the GPR analysis may lead to an underestimation when predicting the catalyst activity (TOF in h^{-1}) under the optimized reaction conditions. Moreover, the author proposes that the deformation energy (E_{DEF}) may serve as a potentially useful parameter to construct an adequate model. The author also identified that 4-methyltetrahydropyran (MTHP) is a superior Lewis-basic solvent for not only the generation of FLP species with **B^{4b}**, but also for the realization of a more practical and less-hazardous reaction system compared to a system using THF. In fact, the **B^{4b}**-catalyzed reductive alkylation using aldehydes as an alkylating reagent and H_2 in MTHP proceeded efficiently even in the presence of a variety of additives, showcasing its broad functional-group compatibility. Aniline-derived amino acids and C-terminal-protected peptides were alkylated in good-to-excellent yields under the optimized conditions with the concomitant generation of H_2O as the byproduct.

1.4 Supporting information

1.4.1 General considerations

Unless otherwise noted, all manipulations were conducted under a N_2 atmosphere using standard Schlenk line or grove box (GB) techniques. ^{1}H, ^{11}B, ^{13}C, ^{19}F, and ^{31}P NMR spectra were recorded on a Bruker AVANCE III 400 or at 25 °C. The chemical shifts in the ^{1}H NMR spectra were recorded relative to Me_4Si or residual protonated solvent ($CHCl_3$ (δ 7.26), $CDCl_2H$ (δ 5.32), C_6D_5H (δ 7.16)). The chemical shifts in the ^{11}B NMR spectra were recorded relative to $BF_3{\cdot}Et_2O$. The chemical shifts in the ^{13}C spectra were recorded relative to Me_4Si or deuterated solvent ($CDCl_3$ (δ 77.16), CD_2Cl_2 (δ 53.84), C_6D_6 (δ 128.06)). The chemical shifts in the ^{19}F NMR spectra were recorded relative to α,α,α-trifluorotoluene (δ −65.64). The chemical shifts in the ^{31}P NMR spectra were recorded relative to 85% H_3PO_4 as an external standard. Assignment of the resonances in ^{1}H and ^{13}C NMR spectra was based on ^{1}H–^{1}H COSY, HMQC, and HMBC experiments. High resolution mass spectrometry (HRMS) and elementary analyses were performed at the Instrumental Analysis Center, Faculty of Engineering, The University of Osaka. Exact mass spectra were recorded on a double-focusing mass spectrometer (JMS-700; JEOL). X-ray crystal data were collected with Rigaku XtaLAB Synergy equipping with the HyPix-6000HE detector.

1.4.2 Materials

All commercially available reagents including super-dehydrated solvents (*n*-hexane, toluene, tetrahydrofuran, and Et_2O), were purchased from Sigma Aldrich, TCI, and Wako Pure Chemical Industries, and used as received. Benzene-d_6 was distilled from sodium benzophenone ketyl prior to use. CD_2Cl_2 was once

degassed by several freeze-pump-thaw cycles and stored inside GB over molecular sieves (4 Å). 4-Methyltetrahydropyran (MTHP) was provided from Kuraray Co., Ltd., and used after distillation using sodium benzophenone ketyl. Compounds **Add.0**−**Add.21** (functional group evaluation kit) shown in Figure 1.6 was provided by Morimoto, Oshima and co-workers (Graduate School of Pharmaceutical Sciences, Kyushu University), and used after dried in vacuo overnight.[42] Metrical data for the solid-state structures are available from Cambridge Crystallographic Data Centre: CCDC 2295627 (**B**^{1f}), 2295628 (**B**^{2b}), 2295633 (**B**^{2c}), 2295634 (**B**^{2e}), 2295629 (**B**^{3b}), 2295635 (**B**^{3c}), 2295631 (**B**^{3s}), 2295632 (**B**^{4b}), 2295630 (**B**^{4e}).

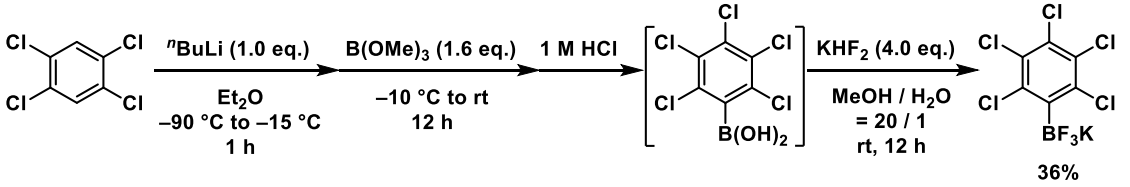
1.4.3 Preparation of reagents

1.4.3.1 Preparation of trifluoro(2,3,5,6-tetrachlorophenyl)-λ^4-borane, potassium salt



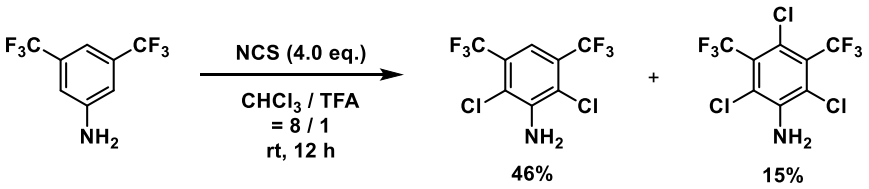
At −90 °C, ^{n}BuLi (17.9 mL in *n*-hexane, 1.58 M, 27.8 mmol) was added to 1,2,4,5-tetrachlorobenzene (6.00 g, 27.8 mmol) in Et_2O (50 mL). The mixture was slowly allowed to warm to −10 °C for 1 h. When the solution became clear, $B(OMe)_3$ (4.96 mL, 44.5 mol) was added to this reaction mixture. The mixture was allowed to warm to rt, and stirred for 12 h. Then, HCl (1M 50 mL) was added to the resultant mixture at rt, stirred for 15 min, and the resultant organic layer was extracted with Et_2O. The combined organic layer was washed with brine, dried over anhydrous Na_2SO_4, and all volatiles were removed in vacuo after filtration. The resultant solid was then washed with *n*-hexane and dried in vacuo, giving a pale yellow solid. A methanol solution of the pale-yellow solid (100 mL) was mixed with H_2O (5 mL) and KHF_2 (6.67 g, 111.0 mmol) and stirred at rt in a PE-bottle. After 12 h of stirring, extraction with acetone through a glass filter and the following removal of all volatiles furnished a white solid. After extraction with acetone, filtration, and evaporation yielded a solid that was purified via the chromatography on a silica gel (*n*-hexane/EtOAc = 1/2) and removal of all volatiles in vacuo afforded trifluoro(2,3,5,6-tetrachlorophenyl)-λ^4-borane, potassium salt as a white solid (3.21 g, 9.99 mmol, 36%) **^{1}H NMR** (400 MHz, DMSO-d_6, rt, δ/ppm): 7.68 (s, 1H, Ar-*H*). **^{11}B NMR** (128 MHz, DMSO-d_6, rt, δ/ppm): 1.68 (q, $^1J_{B,F}$ = 29.4 Hz). **^{13}C{^{1}H} NMR** (100 MHz, DMSO-d_6, rt, δ/ppm): 135.1, 130.8, 128.3. A signal of the ipso-carbon with respect to the boron atoms was not identified. **^{19}F NMR** (376 MHz, DMSO-d_6, rt, δ/ppm): −135.7 (q, $^2J_{F,F}$ = 41.0 Hz, 3F). **HRMS** (FAB$^-$): m/z Calculated for $C_6HBCl_4F_3$ ([M]$^-$) 280.8883, found 280.8860.

1.4.3.2 Preparation of trifluoro(perchlorophenyl)-λ^4-borane, potassium salt



At −90 °C, ^{n}BuLi (17.9 mL in *n*-hexane, 1.58 M, 21.1 mmol) was added to perchlorobenzene (6.00 g, 21.1 mmol) in Et_2O (50 mL). The mixture was slowly allowed to warm to −15 °C for 1 h. When the solution became clear, the reaction mixture was treated with $B(OMe)_3$ (3.76 mL, 33.8 mmol). The mixture was allowed to warm to rt, and stirred for 12 h. Then, HCl (1M 50 mL) was added to the resultant mixture at rt, stirred for 15 min, and the resultant organic layer was extracted with Et_2O.The combined organic layer was washed with brine, dried over anhydrous Na_2SO_4, and all volatiles were then washed with hexane and dried in vacuo, giving a pale yellow solid. A methanol solution of the pale-yellow solid (100 mL) was mixed with H_2O (5 mL) and KHF_2 (5.07 g, 84.3 mmol) in a PE-bottle, and stirred at rt. After 12 h of stirring, extraction with acetone through a glass filter and the following removal of all volatiles furnished a white solid. After extraction with acetone, filtration, and evaporation yielded a solid that was purified via the chromatography on a silica gel (*n*-hexane/EtOAc = 1/1) and removal of all volatiles in vacuo afforded trifluoro(perchlorophenyl)-λ^4-borane, potassium salt as a pale yellow solid (2.71 g, 7.61 mmol, 36%). **^{11}B NMR** (128 MHz, C_6D_6, rt, δ/ppm): 1.62 (q, $^{1}J_{B,F}$ = 29.1 Hz). **^{13}C{^{1}H} NMR** (100 MHz, DMSO-d_6, rt, δ/ppm): 136.2, 131.9 (d, J = 23.0 Hz), 130.4, 129.7 (d, J = 21.0 Hz). **^{19}F NMR** (376 MHz, DMSO-d_6, rt, δ/ppm): −132.5 (q, $^{2}J_{F,F}$ = 42.6 Hz, 3F). **HRMS** (FAB^-): m/z Calculated for $C_6BCl_5F_3$ ($[M]^-$) 314.8493, found 314.8488.

1.4.3.3 Preparation of 2,6-dichloro-3,5-bis(trifluoromethyl)aniline and 2,4,6-trichloro-3,5-bis(trifluoromethyl)aniline[59]



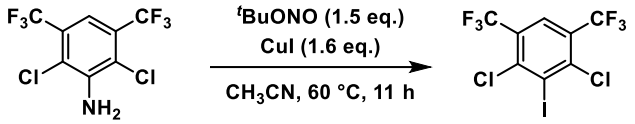
This reaction was carried out under air. To a solution of trifluoroacetic acid (45.7 mL) and N-chlorosuccinimide (77.98 g, 584.8 mmol, 4.0 equiv) in $CHCl_3$ (365 mL) was added 3,5-bis(trifluoromethyl)aniline (33.5 g, 146.2 mmol) at rt. After stirring 12 h, sat. $NaHCO_3$ aq. was added followed by addition of sat. $Na_2S_2O_3$ aq. Then the organic layer was extracted with $CHCl_3$ and washed with brine, dried over anhydrous Na_2SO_4, and all volatiles were removed in vacuo after filtration. Then, distillation (0.2 mmHg, 90 °C) of the resultant mixture was carried out to afford 2,6-dichloro-3,5-bis(trifluoromethyl)aniline as a fraction that eventually became a white solid (19.9 g, 66.8 mmol, 46%). The residue was purified by the chromatography on a silica gel (100% hexane) followed by removal of all volatiles in vacuo, resulting in isolation of 2,4,6-trichloro-3,5-bis(trifluoromethyl)aniline as a pale-yellow solid (7.31 g, 22.0 mmol, 15%).

Identification of 2,6-dichloro-3,5-bis(trifluoromethyl)aniline:
^{1}H NMR (400 MHz, $CDCl_3$, rt, δ/ppm): 7.39 (s, 1H, Ar-*H*), 5.02 (brs, 2H, N*H*). **^{13}C{^{1}H} NMR** (100 MHz, $CDCl_3$, rt, δ/ppm): 143.4, 127.5 (q, $^{2}J_{C,F}$ = 32.3 Hz), 122.3 (q, $^{1}J_{C,F}$ = 274 Hz), 120.3, 113.5 (t, $^{3}J_{C,F}$ = 5.6 Hz). **^{19}F NMR** (376 MHz, $CDCl_3$, rt, δ/ppm): −66.2 (s, 6F). **HRMS** (EI^+): m/z Calculated for $C_8H_3Cl_2F_6N$ ($[M]^+$) 296.9547, found 296.9551.

Identification of 2,4,6-trichloro-3,5-bis(trifluoromethyl)aniline:

^{1}H NMR (400 MHz, $CDCl_3$, rt, δ/ppm): 5.15 (s, 2H, N*H*). **^{13}C{^{1}H} NMR** (100 MHz, $CDCl_3$, rt, δ/ppm): 142.2, 127.0 (q, $^2J_{C,F}$ = 30.1 Hz), 122.4 (q, $^1J_{C,F}$ = 276 Hz), 121.3, 118.3. **^{19}F NMR** (376 MHz, $CDCl_3$, rt, δ/ppm): −57.8 (s, 6F). **HRMS** (EI^+): m/z Calculated for $C_8H_2Cl_3F_6N$ ($[M]^+$) 330.9157, found 330.9164.

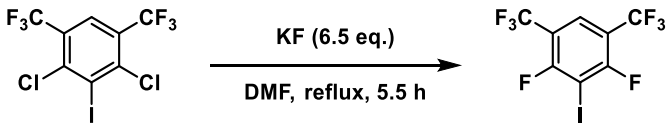
1.4.3.4 Preparation of 2,4-Cl_2-3-I-1,5-$(CF_3)_2$-C_6H[60]



66%

In CH_3CN (65 mL), a mixture of CuI (14.1 g, 78.9 mmol, 1.6 equiv) and 2,6-dichloro-3,5-bis(trifluoromethyl)aniline (14.7 g, 49.3 mmol) was stirred at 60 °C. To this solution, ^{t}BuONO (8.80 mL, 74.2 mmol, 1.5 equiv) was added slowly and the resultant mixture was stirred for 11 h at 60 °C. The reaction was then cooled to rt, diluted with *n*-hexane/EtOAc (v/v = 5/1), and filtered through a celite pad. To the resultant solution, sat. $Na_2S_2O_3$ aq. was added, and washed with brine, dried over anhydrous Na_2SO_4, and all volatiles were removed in vacuo after filtration. The resultant mixture was purified by the chromatography on a silica gel (hexane/EtOAc = 99/1). Removal of all volatiles in vacuo afforded 2,4-Cl_2-3-I-1,5-$(CF_3)_2$-C_6H as a colorless crystal (13.3 g, 32.5 mmol, 66%). **^{1}H NMR** (400 MHz, $CDCl_3$, rt, δ/ppm): 8.05 (s, 1H, Ar-*H*). **^{13}C{^{1}H} NMR** (100 MHz, $CDCl_3$, rt, δ/ppm): 142.8, 127.7 (q, $^2J_{C,F}$ = 32.6 Hz), 126.2−126.0 (m, *C*-H), 121.6 (q, $^1J_{C,F}$ = 274 Hz), 113.0. **^{19}F NMR** (376 MHz, $CDCl_3$, rt, δ/ppm): −66.8 (s, 6F). **HRMS** (EI^+): m/z Calculated for $C_8HCl_2F_6I$ ($[M]^+$) 407.8404, found 407.8403.

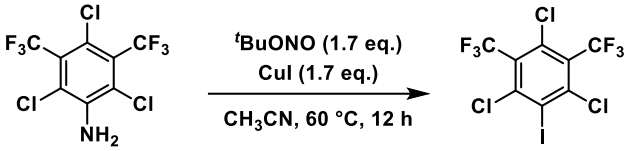
1.4.3.5 Preparation of 2,4-F_2-3-I-1,5-$(CF_3)_2$-C_6H[61]



85%

In DMF (6.0 mL), 2,4-Cl_2-3-I-1,5-$(CF_3)_2$-C_6H (14.1 g, 34.5 mmol) and KF (13.0 g, 224.1 mmol, 6.5 equiv) were mixed, and the resultant suspension was stirred at 160 °C for 5.5 h. Then the mixture was allowed to cool to rt. Followed by addition of H_2O (50 mL), and the organic layer was extracted with *n*-hexane/EtOAc (v/v = 5/1) and washed with brine, dried over anhydrous Na_2SO_4, and all volatiles were removed in vacuo after filtration. The resultant mixture was purified by the chromatography on a silica gel (100% hexane). Removal of all volatiles in vacuo afforded 2,4-F_2-3-I-1,5-$(CF_3)_2$-C_6H as a colorless solid (11.0 g, 29.2 mmol, 85%). **^{1}H NMR** (400 MHz, $CDCl_3$, rt, δ/ppm): 7.92 (t, $^4J_{H,F}$ = 7.2 Hz, Ar-*H*). **^{13}C{^{1}H} NMR** (100 MHz, $CDCl_3$, rt, δ/ppm): 162.5 (dd, $^1J_{F,F}$ = 261 Hz, $^4J_{C,F}$ = 5.9 Hz), 126.5 (m, 2H), 121.1 (q, $^2J_{C,F}$ = 273 Hz), 116.2−114.8 (m), 75.3 (t, $^2J_{F,F}$ = 29.6 Hz). **^{19}F NMR** (376 MHz, $CDCl_3$, rt, δ/ppm): −64.7 (d, $^4J_{F,F}$ = 14.4 Hz, 6F), −86.3 (m, 4F). **HRMS** (EI^+): m/z Calculated for $C_8Cl_3F_6I$ ($[M]^+$) 407.8404, found 407.8403.

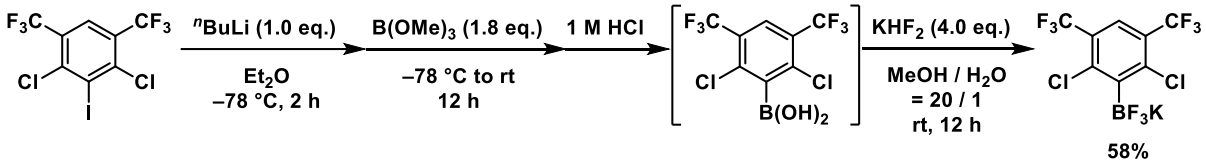
1.4.3.6 Preparation of 1,3,5-Cl_3-2-I-4,6-$(CF_3)_2$-C_6[60]



61%

Under N_2 atmosphere, CuI (5.94 g, 31.2 mmol, 1.7 equiv) and 2,4,6-trichloro-3,5-bis(trifluoromethyl)aniline (6.10 g, 18.3 mmol) were dissolved in CH_3CN (40 mL) and stirred at 60 °C. Then, ^{t}BuONO (3.69 mL, 31.2 mmol, 1.7 equiv) was added slowly and the mixture was stirred for 12 h while maintained at 60 °C. The reaction mixture was then cooled to rt, diluted with *n*-hexane/EtOAc (v/v = 5/1), and filtered through a celite pad. To the resultant solution, sat. $Na_2S_2O_3$ aq. was added, and the organic layer was washed with brine, dried over anhydrous Na_2SO_4, and all volatiles were removed in vacuo after filtration. The resultant mixture was purified by the chromatography on a silica gel (hexane/EtOAc = 99/1). Removal of all volatiles in vacuo afforded 1,3,5-Cl_3-2-I-4,6-$(CF_3)_2$-C_6 as a colorless solid (4.91 g, 11.1 mmol, 61%). **$^{13}C\{^1H\}$ NMR** (100 MHz, $CDCl_3$, rt, δ/ppm): 143.5, 136.1, 127.6 (q, $^2J_{C,F}$ = 30.5 Hz), 121.7 (q, $^1J_{C,F}$ = 276 Hz), 113.4. **^{19}F NMR** (376 MHz, $CDCl_3$, rt, δ/ppm): −58.3 (s, 6F). **HRMS** (EI^+): m/z Calculated for $C_8Cl_3F_6I$ ($[M]^+$) 441.8014, found 441.8024.

1.4.3.7 Preparation of (2,6-dichloro-3,5-bis(trifluoromethyl)phenyl)trifluoro-λ^4-borane

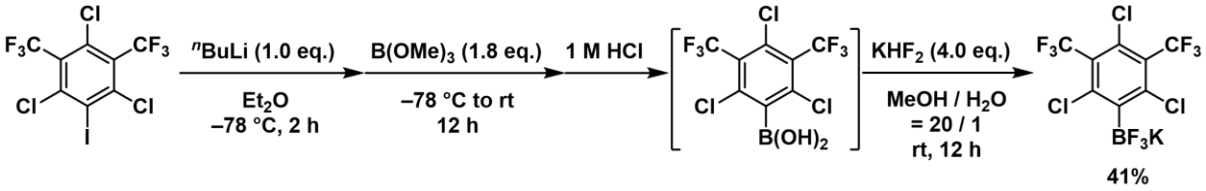


58%

At −78°C, ^{n}BuLi (6.06 mL in *n*-hexane, 1.58 M) (9.6 mmol) was added to 2,4-Cl_2-3-I-1,5-$(CF_3)_2$-C_6H (3.92 g, 9.59 mmol) in Et_2O (40 mL) over 15 min. The reaction solution was stirred at −78 °C for 2 h, then $B(Ome)_3$ (1.92 mL, 17.2 mmol, 1.8 equiv) was added to the reaction mixture. The mixture was allowed to warm to rt, and stirred for 12 h. Then, HCl (1M 50 mL) was added to the resultant mixture at rt, stirred for 15 min, and the resultant organic layer was extracted with Et_2O. The combined organic layer was washed with brine, dried over anhydrous Na_2SO_4, and all volatiles were removed in vacuo after filtration. The resultant solid was then washed with hexane and dried in vacuo, giving a pale yellow solid. A methanol solution of the pale yellow solid (100 mL) was mixed with H_2O (5 mL) and KHF_2 (2.30 g, 38.3 mmol, 4.0 equiv) in a PE-bottle, and stirred at rt. After 12 h of stirring, extraction with acetone through a glass filter and the following removal of all volatiles furnished a white solid. After extraction with acetone, filtration, and evaporation yielded a solid that was washed with *n*-hexane followed by dried in vacuo, which afforded (2,6-dichloro-3,5-bis(trifluoromethyl)phenyl)trifluoro-λ^4-borane, potassium salt as a white solid (2.15 g, 5.53 mmol, 58%) **^1H NMR** (400 MHz, DMSO-d_6, rt, δ/ppm): 7.83 (s, 1H, Ar-*H*). **^{11}B NMR** (128 MHz, DMSO-d_6, rt, δ/ppm): 1.70 (q, $^1J_{B,F}$ = 44.2 Hz). **$^{13}C\{^1H\}$ NMR** (100 MHz, DMSO-d_6, rt, δ/ppm): 141.3, 125.6 (q, $^2J_{C,F}$ = 30.3 Hz), 124.1−123.9 (m), 122.8 (q, $^1J_{C,F}$ = 271 Hz). A signal of the ipso-carbon with respect to the boron atoms was not identified. **^{19}F NMR** (376 MHz, DMSO-d_6, rt, δ/ppm): −64.3 (s, 6F), −134.8 (q, $^2J_{F,F}$ = 41.2 Hz, 3F). **HRMS**

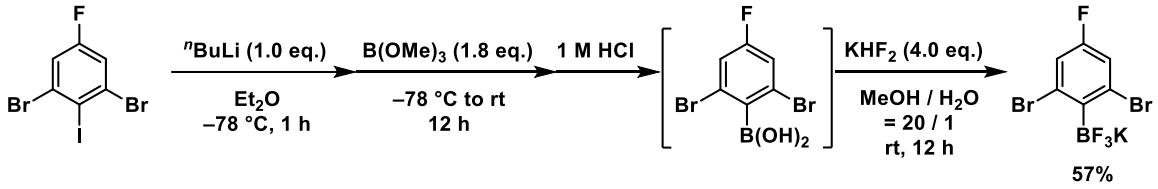
(FAB⁻): m/z Calculated for $C_8HBF_9Cl_2$ ([M]⁻) 348.9410, found 348.9398.

1.4.3.8 Preparation of trifluoro(2,4,6-trichloro-3,5-bis(trifluoromethyl)phenyl)-λ^4-borane, potassium salt



At −78°C, ^{n}BuLi (4.64 mL in *n*-hexane, 1.58 M, 7.20 mmol) was added to 1,3,5-Cl_3-2-I-4,6-$(CF_3)_2$-C_6 (3.19 g, 7.20 mmol) in Et_2O (35 mL) over 15 min. The reaction solution was stirred at −78 °C for 2 h, then $B(OMe)_3$ (1.44 mL, 13.0 mmol, 1.8 equiv) was added to the reaction mixture over 5 min. The mixture was allowed to warm to rt, and stirred for 12 h. Then, HCl (1M 50 mL) was added to the resultant mixture at rt, stirred for 15 min, and the resultant organic layer was extracted with Et_2O. The combined organic layer was washed with brine, dried over anhydrous Na_2SO_4, and all volatiles were removed in vacuo after filtration. The resultant solid was washed with *n*-hexane and dried in vacuo, giving a brownish solid. A methanol solution of the solid (100 mL) was mixed with H_2O (5 mL) and KHF_2 (1.73 g, 28.8 mmol, 4.0 equiv) in a PE-bottle, and stirred at rt. After 12 h of stirring, extraction with acetone, filtration, and evaporation yielded a solid that was washed with *n*-hexane followed by dried in vacuo, giving trifluoro(2,4,6-trichloro-3,5-bis(trifluoromethyl)phenyl)-λ^4-borane, potassium salt as a pale yellow solid (1.26 g, 29.8 mmol, 41%). **^{11}B NMR** (128 MHz, DMSO-d_6, rt, δ/ppm): 1.60 (q, $^1J_{B,F}$ = 42.5 Hz). **^{13}C{^{1}H} NMR** (100 MHz, DMSO-d_6, rt, δ/ppm): 142.9, 131.1, 125.0, 122.7 (q, $^1J_{C,F}$ = 277 Hz). A signal of the ipso-carbon with respect to the boron atoms was not identified. **^{19}F NMR** (376 MHz, DMSO-d_6, rt, δ/ppm): −56.0 (s, 6F), −134.2 (q, $^2J_{F,F}$ = 41.8 Hz, 3F). **HRMS** (FAB⁻): m/z Calculated for $C_8BF_9Cl_3$ ([M]⁻) 382.9020, found 382.9037.

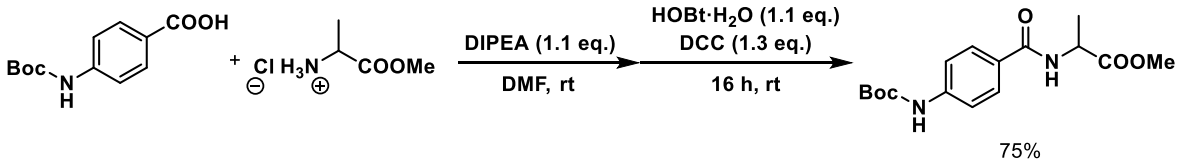
1.4.3.9 Preparation of (2,6-dibromo-4-fluorophenyl)trifluoro-λ^4-borane, potassium salt



At −78 °C, ^{n}BuLi (8.67 mL in *n*-hexane, 1.52 M) (13.2 mmol) was added to 1,3-Br_2-5-F-2-I-C_6H_2 (5.00 g, 13.2 mmol) in Et_2O (40 mL) over 15 min. The reaction solution is stirred at −78 °C for 1 h, then $B(OMe)_3$ (2.64 mL, 23.7 mmol, 1.8 equiv) was added to the reaction mixture. The mixture was allowed to warm to rt and stirred for 12 h. Then, HCl (1M 50 mL) was added to the resultant mixture at rt, stirred for 15 min, and the resultant organic layer was extracted with Et_2O. The combined organic layer was washed with brine, dried over anhydrous Na_2SO_4, and all volatiles were removed in vacuo after filtration. The resultant solid was then washed with hexane and dried in vacuo, giving a pale yellow solid. A methanol solution of the solid (100 mL) was mixed with H_2O (5 mL) and KHF_2 (3.16 g, 52.6 mmol, 4.0 equiv) in a PE-bottle, and stirred at rt. After 12

h of stirring, extraction with acetone, filtration, and evaporation yielded a solid that was washed with *n*-hexane followed by dried in vacuo, giving (2,6-dibromo-4-fluorophenyl)trifluoro-λ^4-borane, potassium salt as a white solid (2.70 g, 7.51 mmol, 57%) **^{1}H NMR** (400 MHz, DMSO-d_6, rt, δ/ppm): 7.30 (d, $^3J_{H,F}$ = 8.8 Hz, 2H, Ar-*H*). **^{11}B NMR** (128 MHz, DMSO-d_6, rt, δ/ppm): 1.71 (q, $^1J_{B,F}$ = 44.7 Hz). **^{13}C{^{1}H} NMR** (100 MHz, DMSO-d_6, rt, δ/ppm): 159.4 (d, $^1J_{C,F}$ = 247 Hz), 127.7 (d, $^3J_{C,F}$ = 9.0 Hz), 119.1 (d, $^2J_{C,F}$ = 22.0 Hz). A signal of the ipso-carbon with respect to the boron atoms was not identified. **^{19}F NMR** (376 MHz, DMSO-d_6, rt, δ/ppm): −119.9 (t, $^2J_{F,H}$ = 8.6 Hz, 1F), −135.7 (q, $^2J_{F,F}$ = 43.4 Hz, 3F). **HRMS** (FAB$^-$): m/z Calculated for $C_6H_2BF_4Br_2$ ([M]$^-$) 318.8558, found 318.8566.

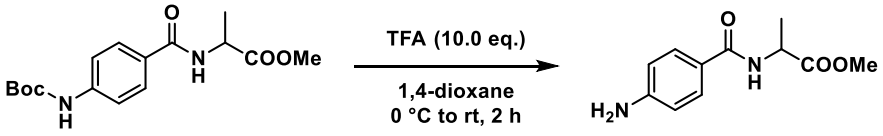
1.4.3.10 Preparation of methyl (4-((tert-butoxycarbonyl)amino)benzoyl)alaninate[62]



75%

Methyl DL-alaninate hydrochloride (848 mg, 6.32 mmol, 2.0 equiv) was suspended in dry DMF (32 mL) and solubilized by addition of dry DIPEA (1.10 mL, 6.3 mmol, 2.0 equiv). To this solution,. 4-((tert-butoxycarbonyl)amino)benzoic acid (750 mg, 3.16 mmol), HOBt·H_2O (533 mg, 348 mmol, 1.1 equiv), and DCC (848 mg, 4.11 mmol, 1.3 equiv) were added. The solution was stirred 16 h at rt, and then all volatiles were removed in vacuo. The residue was dissolved in EtOAc and washed with brine. The organic layer was dried over anhydrous Na_2SO_4, and the crude product was purified by a flash column chromatography on a silica gel (*n*-hexane/EtOAc = 1/1). Removal of all volatiles in vacuo afforded methyl (4-((tert-butoxycarbonyl)amino)benzoyl)-D-alaninate as a colorless solid (759.1 mg, 2.36 mmol, 75%). **^{1}H NMR** (400 MHz, $CDCl_3$, rt, δ/ppm): δ 7.74 (d, J = 8.6 Hz, 2H, Ar-*H*), 7.43 (d, J = 8.5 Hz, 2H, Ar-*H*), 6.58−6.80 (m, 2H, Ar-*H*), 4.79 (q, J = 7.2 Hz, 1H, C*H*CH_3), 3.79 (s, 3H, COOCH_3), 1.52 (s, 9H, C(CH_3)$_3$).

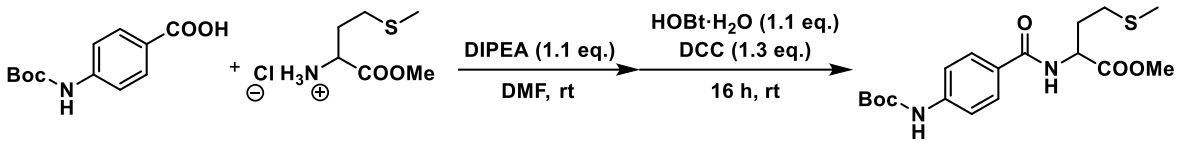
1.4.3.11 Preparation of methyl (4-((tert-butoxycarbonyl)amino)benzoyl)alaninate[62]



68%

Trifluoroacetic acid (475 µL, 6.2 mmol, 10.0 equiv) was slowly added to a solution of methyl (4-((tert-butoxycarbonyl)amino)benzoyl)alaninate (200 mg, 0.62 mmol) in 1,4-dioxane (10 mL) at 0 °C. The reaction mixture was allowed to warm to rt and stirred for 2 h. After addition of H_2O (2 mL), the solution was evaporated in vacuo to give the crude mixture. The crude products were purified by a flash column chromatography on a silica gel (*n*-hexane/EtOAc = 7/3) afforded methyl (4-aminobenzoyl)alaninate as a white solid (94.2 mg, 0.42 mmol, 68%). **^{1}H NMR** (400 MHz, $CDCl_3$, rt, δ/ppm): 7.64 (dd, J = 7.1, J = 1.9 Hz, 2H, Ar-*H*), 6.67 (d, J = 8.6 Hz, 2H, Ar-*H*), 6.53 (m, 1H, Ar-*H*), 4.79 (p, J = 7.2 Hz, 1H, C*H*CH_3), 3.78 (s, 3H, COOCH_3), 1.50 (d, J = 7.2 Hz, 2H, CHCH_3). A resonance of NH_2 was not identified.

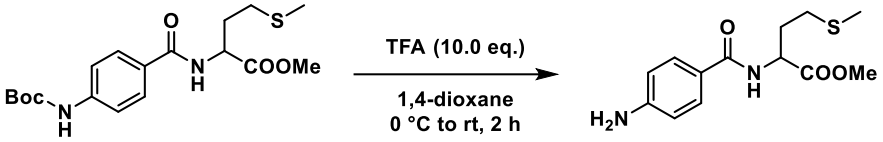
1.4.3.12 Preparation of methyl (4-((tert-butoxycarbonyl)amino)benzoyl)methioninate[63]



63%

Methyl methioninate hydrochloride (1.80 g, 8.44 mmol, 2.0 equiv) was suspended in dry DMF (30 mL) and solubilized by addition of dry DIPEA (1.47 mL, 8.44 mmol, 2.0 equiv). To this solution, 4-((tert-butoxycarbonyl)amino)benzoic acid (1.0 g, 4.22 mmol), HOBt·H_2O (710 mg, 4.6 mmol, 1.1 equiv) and DCC (1.13 g, 5.48 mmol, 1.3 equiv) were added. The solution was stirred 16 h at rt, and then all volatiles were removed in vacuo. The residue was dissolved in EtOAc and washed with brine. The organic layer was dried over anhydrous Na_2SO_4, and the crude products were purified by a flash column chromatography on a silica gel (*n*-hexane/EtOAc = 1/1). Removal of all volatiles in vacuo afforded methyl (4-((tert-butoxycarbonyl)amino)benzoyl)methioninate as a white solid (1.01 g, 2.64 mmol, 63%). **^{1}H NMR** (400 MHz, $CDCl_3$, rt, δ/ppm): δ 7.76 (d, J = 8.7 Hz, 2H, Ar-*H*), 7.44 (d, J = 8.6 Hz, 2H, Ar-*H*), 6.88 (d, J = 7.5 Hz, 1H, Ar-*H*), 6.70 (s, 1H, CON*H*), 4.91 (m, 1H, CON*H*), 3.79 (s, 3H, COOCH_3), 2.52−2.65 (m, 2H, CH_2-S), 2.11 (s, 3H, S-CH_3), 2.05−2.34 (m, 2H, CH-CH_2-CH_2).

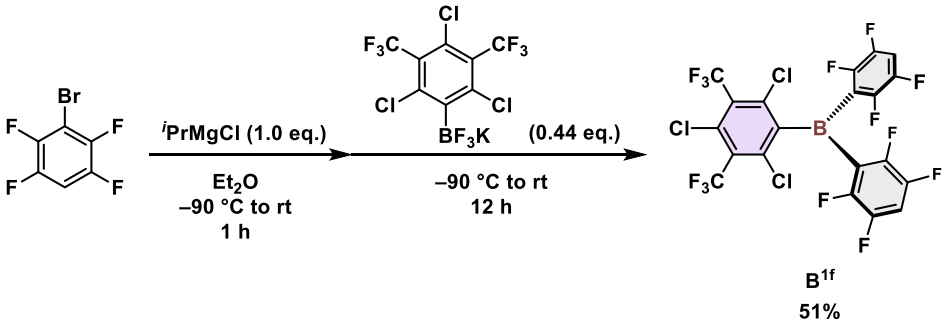
1.4.3.13 Preparation of methyl (4-aminobenzoyl)methioninate[64]



32%

Trifluoroacetic acid (2.0 mL, 26.1 mmol, 10.0 equiv) was slowly added to a solution of methyl (4-((tert-butoxycarbonyl)amino)benzoyl)methioninate (1.0 g, 2.62 mmol) in 1,4-dioxane (40 mL) at 0 °C. The reaction mixture was allowed to warm to rt and stirred for 2 h. After addition of H_2O (2 mL), the solution was evaporated in vacuo to give the crude mixture. The crude product was purified by a flash column chromatography on a silica gel (*n*-hexane/EtOAc = 1/1), affording methyl (4-aminobenzoyl)alaninate as a white solid (238 mg, 0.84 mmol, 32%). **^{1}H NMR** (400 MHz, $CDCl_3$, rt, δ/ppm): 7.65 (d, J = 8.6 Hz, 2H, Ar-*H*), 6.73 (d, J = 7.7 Hz, 1H, N*H*), 6.67 (d, J = 8.6 Hz, 2H, Ar-*H*), 4.86−4.95 (m, 1H, C*H*CH_2), 3.79 (s, 3H, COOCH_3), 2.52−2.61 (m, 2H, CH_2S), 2.11 (s, 3H, SCH_3), 2.03−2.33 (m, 2H, CHC$H_2$$CH_2$). A resonance of NH_2 was not identified.

1.4.3.14 Preparation of **B^{1f}**



A solution of *p*-C_6F_4HBr (314 µL, 2.56 mmol, 1.0 equiv, 0.17 M in Et_2O) was slowly treated with ^{i}PrMgCl (2.56 mL, 2.56 mmol, 1.0 equiv, 1.0 M in Et_2O) at −90 °C, and stirred for 1 h (−90 °C to rt).The resultant solution was transferred into a suspension of trifluoro(2,4,6-trichloro-3,5-bis(trifluoromethyl)phenyl)-λ^4-borane, potassium salt (475 mg, 1.12 mmol, 0.44 equiv, 0.22 M in Et_2O) at −90 °C. The reaction mixture was then allowed to warm to rt, and stirred for another 12 h. After the removal of all volatiles in vacuo, the residue was dissolved in *n*-hexane and then passed through a celite pad, concentrated in vacuo and washed with *n*-hexane (cooled to −20 °C prior to use) to afford **B^{1f}** as a white solid (396 mg, 0.57 mmol, 51%) after removal of all volatiles in vacuo. A single crystal of **B^{1f}** was obtained from a saturated solution of **B^{1f}** in toluene layered by *n*-hexane at −20 °C. **^{1}H NMR** (400 MHz, C_6D_6) , rt, δ/ppm): 6.23−6.14 (m, 2H, Ar-*H*). **^{11}B NMR** (128 MHz, C_6D_6, rt, δ/ppm): 63.4 (brs). **^{13}C{^{1}H} NMR** (100 MHz, C_6D_6, rt, δ/ppm): 150.1−149.0 (m), 147.6−147.0 (m), 145.3−144.7 (m), 137.4, 137.0, 127.2, 126.6, 122.5 (q, $^{1}J_{C,F}$ = 276 Hz), 119.7, 112.6. A signal of the ipso-carbon with respect to the boron atoms was not identified. **^{19}F NMR** (376 MHz, C_6D_6, rt, δ/ppm): −58.0 (s, 6F), −131.7–−131.8 (m, 4F), −140.3–−140.4 (m, 4F). **X-ray** data for (**B^{1f}**)$_{1/2}$: M = 312.69, colorless, monoclinic, *C*2/c (#15), a = 14.0805(6) Å, b = 11.5258(4) Å, c = 13.9271(6) Å, α = 90°, β = 110.209(5)°, γ = 90°, V = 2121.07(16) Å^3, Z = 8, *Dcalcd* = 1.958 g/cm^3 , T = 173 K, R_1 (wR_2) = 0.0409 (0.1136).

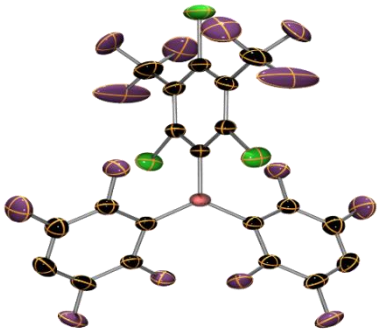
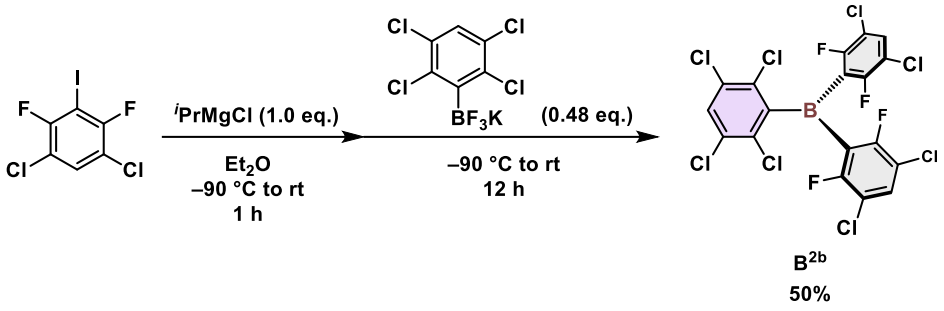


Figure 1.S1. Molecular structure of **B^{1f}** with ellipsoids set at 50% probability. H atoms are omitted for clarity.

1.4.3.15 Preparation of **B^{2b}**



A solution of 1,5-Cl_2-2,4-F_2-3-I-C_6H (1.51 g, 4.9 mmol, 1.0 equiv, 0.16 M in Et_2O) was slowly treated with ^{i}PrMgCl (4.90 mL, 1.0 equiv, 1.0 M in Et_2O) at −90 °C. After stirred for 1 h (−90 °C to rt), the resultant solution was transferred into a suspension of trifluoro(2,3,5,6-tetrachlorophenyl)-λ^4-borane, potassium salt (750 mg, 2.33 mmol, 0.48 equiv, 0.46 M in Et_2O) at −90 °C. The reaction mixture was then allowed to warm to rt, and stirred for another 12 h. After the removal of all volatiles in vacuo, the residue was dissolved in a small amount of toluene and then passed through a celite pad, then concentrated in vacuo and washed with *n*-hexane (cooled to −20 °C prior to use) to afford **B^{2b}** as a white solid (683 mg, 1.16 mmol, 50%) after removal of all volatiles in vacuo. A single crystal of **B^{2b}** was obtained from a saturated solution of **B^{2b}** in toluene layered by *n*-hexane at rt. **^{1}H NMR** (400 MHz, C_6D_6, rt, δ/ppm): 6.91 (s, 1H, Ar-*H*), 6.82 (t, $^{4}J_{H,F}$ = 7.6 Hz, 2H, Ar-*H*). **^{11}B NMR** (128 MHz, C_6D_6, rt, δ/ppm): 65.9 (brs). **^{13}C{^{1}H} NMR** (100 MHz, C_6D_6, rt, δ/ppm): 159.3 (dd, $^{1}J_{C,F}$ = 256 Hz, $^{4}J_{C,F}$ = 9.8 Hz), 143.9, 136.9 (d, J = 4.8 Hz), 132.3 , 131.9 (d, J = 4.2 Hz), 130.5 , 118.3−117.6 (m), 117.7−117.4 (m). **^{19}F NMR** (376 MHz, C_6D_6, rt, δ/ppm): −103.5 (d, $^{4}J_{F,F}$ = 6.8 Hz, 4F). **X-ray** data for **B^{2b}**: M = 589.61, colorless, monoclinic, $P2_1/c$ (#14), a = 12.7067(3) Å, b = 10.6167(2) Å, c = 16.0053(4), α = 90°, β = 100.320(2)°, γ = 90°, V = 2124.24(8) Å^3, Z = 4, $Dcalcd$ = 1.844 g/cm^3 , T = 123 K, R_1 (wR_2) = 0.0388 (0.1002).

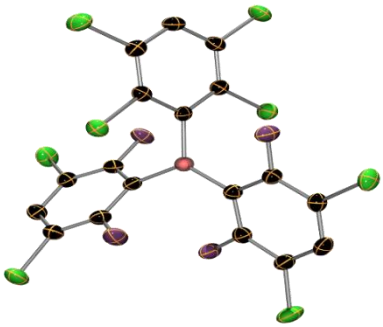
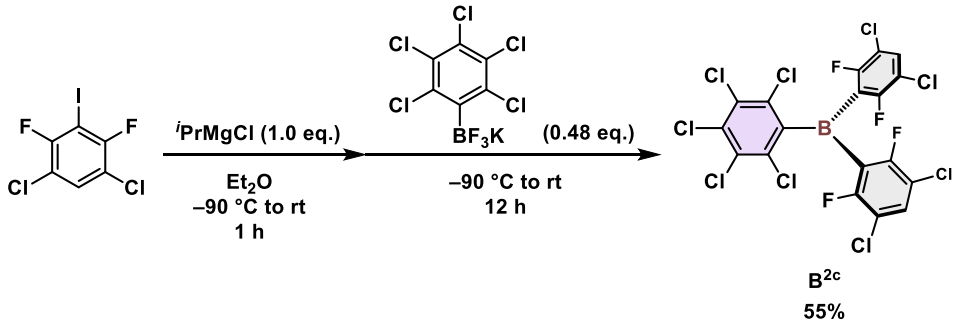


Figure 1.S2. Molecular structure of **B^{2b}** with ellipsoids set at 50% probability. H atoms are omitted for clarity.

1.4.3.16 Preparation of **B^{2c}**



A solution of 1,5-Cl_2-2,4-F_2-3-I-C_6H (1.37 mg, 4.42 mmol, 1.0 equiv, 0.15 M in Et_2O) was slowly treated with ^{i}PrMgCl (4.50 mL, 1.0 equiv, 1.0 M in Et_2O) at −90 °C, and stirred for 1 h (−90 °C to rt). The resultant solution was transferred into a suspension of trifluoro(perchlorophenyl)-λ^4-borane, potassium salt (750 mg, 2.11 mmol, 0.48 equiv, 0.42 M in Et_2O) at −90 °C. The reaction mixture was then allowed to warm to rt, and stirred for another 12 h. After the removal of all volatiles in vacuo, the residue was dissolved in toluene (10 mL × 4) and then passed through a celite pad, then concentrated in vacuo and washed with *n*-hexane to afford **B^{2c}** as a white solid (716 mg, 1.15 mmol, 55%) after removal of all volatiles in vacuo. A single crystal of **B^{2c}** was obtained from a saturated solution of **B^{2c}** in toluene layered by *n*-hexane at −20 °C. **^{1}H NMR** (400 MHz, C_6D_6, rt, δ/ppm): 6.80 (t, $^{4}J_{H,F}$ = 7.6 Hz, 1H, Ar-*H*). **^{11}B NMR** (128 MHz, C_6D_6, rt, δ/ppm): 61.3 (brs). **^{13}C{^{1}H} NMR** (100 MHz, C_6D_6, rt, δ/ppm): 159.2 (dd, $^{1}J_{C,F}$ = 256 Hz, $^{4}J_{C,F}$ = 9.8 Hz), 141.4 (brs), 137.0 (d, J = 5.3 Hz), 135.2, 132.4, 131.2, 118.3−117.9 (m), 117.6−117.4 (m). **^{19}F NMR** (376 MHz, C_6D_6, rt, δ/ppm): −103.5 (d, $^{4}J_{F,F}$ = 7.5 Hz, 4F). **X-ray** data for **B^{2c}**: M = 624.06, colorless, monoclinic, $P2_1/c$ (#14), a = 8.5443(2) Å, b = 19.4719(5) Å, c = 13.7797(3) Å, α = 90°, β = 104.919(2)°, γ = 90°, V = 2215.30(9) Å^3, Z = 4, $Dcalcd$ = 1.871 g/cm^3 , T = 123 K, R_1 (wR_2) = 0.0583 (0.1666).

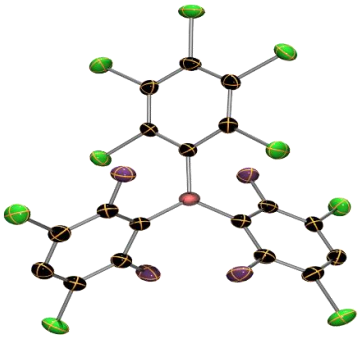
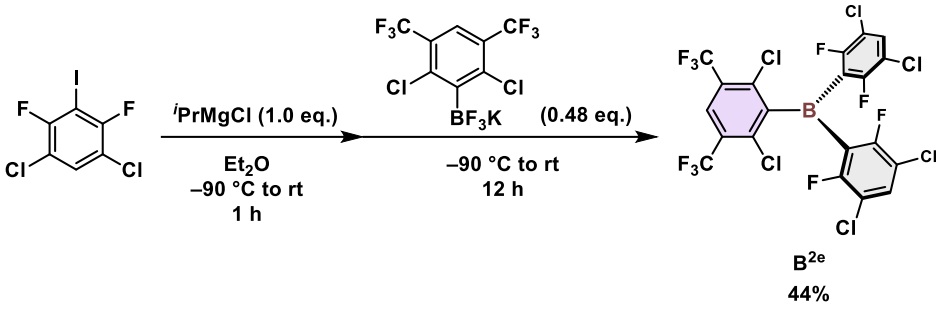


Figure 1.S3. Molecular structure of **B^{2c}** with ellipsoids set at 50% probability. H atoms are omitted for clarity.

1.4.3.17 Preparation of **B^{2e}**



A solution of 1,5-Cl_2-2,4-F_2-3-I-C_6H (833 mg, 2.70 mmol, 1.0 equiv, 0.18 M in Et_2O) was slowly treated with ^{i}PrMgCl (2.70 mL, 1.0 equiv, 1.0 M in Et_2O) at −90 °C, and stirred for 1 h (−90 °C to rt). The resultant solution was transferred into a suspension of (2,6-dichloro-3,5-bis(trifluoromethyl)phenyl)trifluoro-λ^4-borane, potassium salt (500 mg, 1.29 mmol, 0.48 equiv, 0.16 M in Et_2O) at −90 °C. The reaction mixture was then allowed to warm to rt, and stirred for another 12 h. After the removal of all volatiles in vacuo, the residue was dissolved in toluene (5 mL × 4) and then passed through a celite pad, then concentrated in vacuo and washed with *n*-pentane to afford **B^{2e}** as a white solid (411 mg, 0.57 mmol, 44%) after removal of all volatiles in vacuo. A single crystal of **B^{2e}** was obtained from a saturated solution of **B^{2e}** in toluene layered by *n*-hexane at −20 °C. **^{1}H NMR** (400 MHz, C_6D_6) , rt, δ/ppm): 7.47 (s, 1H, Ar-*H*), 6.82−6.78 (m, 2H, Ar-*H*). **^{11}B NMR** (128 MHz, C_6D_6, rt, δ/ppm): 63.2 (brs). **^{13}C{^{1}H} NMR** (100 MHz, C_6D_6, rt, δ/ppm): 159.2 (dd, $^{1}J_{C,F}$ = 255 Hz, $^{4}J_{C,F}$ = 9.7 Hz), 146.5, 137.3, 136.2, 127.4−127.3 (m), 126.3, 122.3 (q, $^{1}J_{C,F}$ = 272 Hz), 118.4−118.0 (m), 117.5−117.1 (m). **^{19}F NMR** (376 MHz, C_6D_6, rt, δ/ppm): −65.3 (s, 6F), −103.7 (s, 4F). **X-ray** data for **B^{2e}**: M = 656.73, colorless, orthorhombic, *P*bca (#61), a = 15.5239(4) Å, b = 11.5011(3) Å, c = 26.6249(6) Å, α = 90°, β = 90°, γ = 90°, V = 4753.7(2) Å^3, Z = 8, *Dcalcd* = 1.835 g/cm^3, T = 123 K, R_1 (wR_2) = 0.0478 (0.1363).

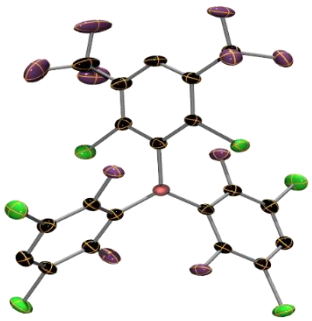
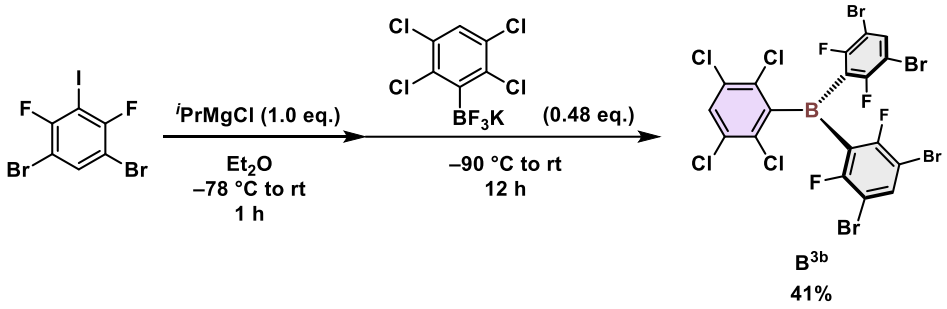


Figure 1.S4. Molecular structure of **B^{2e}** with ellipsoids set at 50% probability. H atoms are omitted for clarity.

1.4.3.18 Preparation of **B^{3b}**



A solution of 1,5-Br_2-2,4-F_2-3-I-C_6H (1.30 g, 3.26 mmol, 1.0 equiv, 0.10 M in Et_2O) was slowly treated with ^{i}PrMgCl (3.32 mL, 1.0 equiv, 1.0 M in Et_2O) at −78 °C, and stirred for 1 h (−78 °C to rt). The resultant solution was transferred into a suspension of trifluoro(2,3,5,6-tetrachlorophenyl)-λ^4-borane, potassium salt (500 mg, 1.55 mmol, 0.48 equiv, 0.31 M in Et_2O) at −90 °C. The reaction mixture was then allowed to warm to rt, and stirred for another 12 h. After the removal of all volatiles in vacuo, the residue was dissolved in $PhCF_3$ and then passed through a celite pad, then concentrated in vacuo and washed with *n*-pentane to afford **B^{3b}** as a white solid (491 mg, 0.64 mmol, 41%) after removal of all volatiles in vacuo. A single crystal of **B^{3b}** was obtained from a saturated solution of **B^{3b}** in toluene layered by *n*-hexane at −20 °C. **^{1}H NMR** (400 MHz, C_6D_6) , rt, δ/ppm): 7.21 (t, J = 7.2 Hz, 2H, Ar-*H*), 6.87 (s, 1H, Ar-*H*). **^{11}B NMR** (128 MHz, C_6D_6, rt, δ/ppm): 58.1 (brs). **^{13}C{^{1}H} NMR** (100 MHz, C_6D_6, rt, δ/ppm): 160.5 (dd, $^{1}J_{C,F}$ = 253 Hz, $^{4}J_{C,F}$ = 9.9 Hz), 143.5, 141.8, 131.9, 131.4 (d, J = 4.3 Hz), 130.1, 117.3, 105.4 (d, J = 26.4 Hz). **^{19}F NMR** (376 MHz, C_6D_6, rt, δ/ppm): −94.6 (d, $^{4}J_{F,F}$ = 7.0 Hz, 4F) **X-ray** data for **[(B^{3b})$_2$·C_6H_{14}]**: M = 1621.0, colorless, monoclinic, $P2_1/c$ (#14), a = 26.6350(3) Å, b = 10.24640(1) Å, c = 19.2265(2) Å, α = 90°, β = 101.1980(10)°, γ = 90°, V = 5147.26(1) Å^3, Z = 4, *Dcalcd* = 2.092 g/cm^3 , T = 123 K, R_1 (wR_2) = 0.0368 (0.0969).

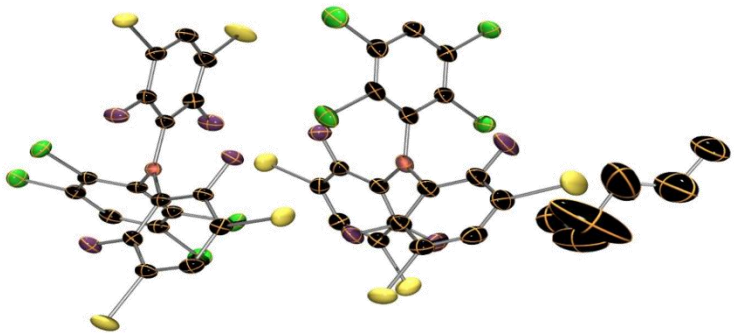
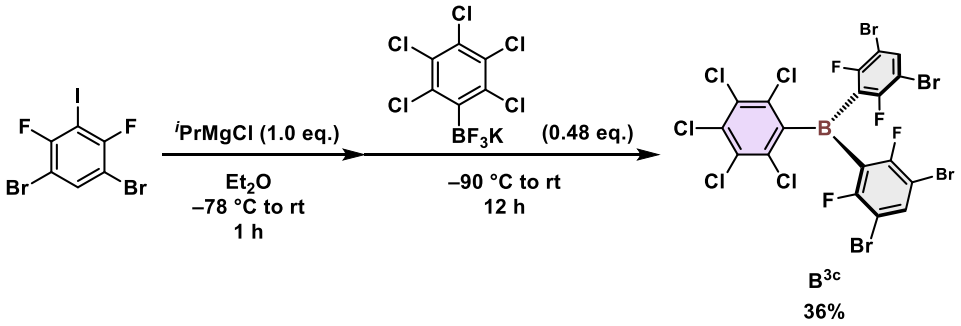


Figure 1.S5. Molecular structure of **[(B^{3b})$_2$·C_6H_{14}]** with ellipsoids set at 50% probability. H atoms are omitted for clarity.

1.4.3.19 Preparation of **B^{3c}**



A solution of 1,5-Br_2-2,4-F_2-3-I-C_6H (1.17 g, 2.95 mmol, 1.0 equiv, 0.20 M in Et_2O) was slowly treated with ^{i}PrMgCl (3.32 mL, 1.0 equiv, 1.0 M in Et_2O) at −78 °C, and stirred for 1 h (−78 °C to rt). The resultant solution was transferred into a suspension of trifluoro(perchlorophenyl)-λ^4-borane, potassium salt (500 mg, 1.40 mmol, 0.48 equiv, 0.28 M in Et_2O) at −90 °C. The reaction mixture was then allowed to warm to rt, and stirred for another 12 h. After the removal of all volatiles in vacuo, the residue was dissolved in $PhCF_3$ (10 mL × 5) and then passed through a celite pad, then concentrated in vacuo and washed with *n*-hexane to afford **B^{3c}** as a white solid (411 mg, 0.51 mmol, 36%) after removal of all volatiles in vacuo. A single crystal of **B^{3c}** was obtained from a saturated solution of **B^{3c}** in toluene layered by *n*-hexane at −20 °C. **^{1}H NMR** (400 MHz, C_6D_6, rt, δ/ppm): 7.19 (t, J = 7.3 Hz, 2H, Ar-*H*). **^{11}B NMR** (128 MHz, C_6D_6, rt, δ/ppm): 63.9 (brs). **^{13}C{^{1}H} NMR** (100 MHz, C_6D_6, rt, δ/ppm): 160.5 (dd, $^{1}J_{C,F}$ = 254 Hz, $^{4}J_{C,F}$ = 9.9 Hz), 141.8, 134.7, 132.0, 130.9, 117.4−117.3 (m), 105.6−105.2 (m). A signal of the ipso-carbon with respect to the boron atoms was not identified. **^{19}F NMR** (376 MHz, C_6D_6, rt, δ/ppm): −94.7 (d, $^{4}J_{F,F}$ = 7.1 Hz, 4F). **X-ray** data for **B^{3c}**: M = 801.86, colorless, monoclinic, $P2_1/c$ (#14), a = 8.61989(3) Å, b = 19.8121(6) Å, c = 14.3343(6) Å, α = 90°, β = 106.628(4)°, γ = 90°, V = 2345.59(15) Å^3, Z = 4, $Dcalcd$ = 2.271 g/cm^3 , T = 123 K, R_1 (wR_2) = 0.0504 (0.1406).

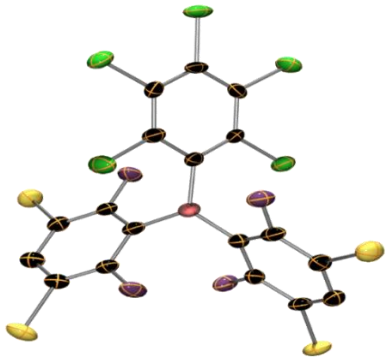
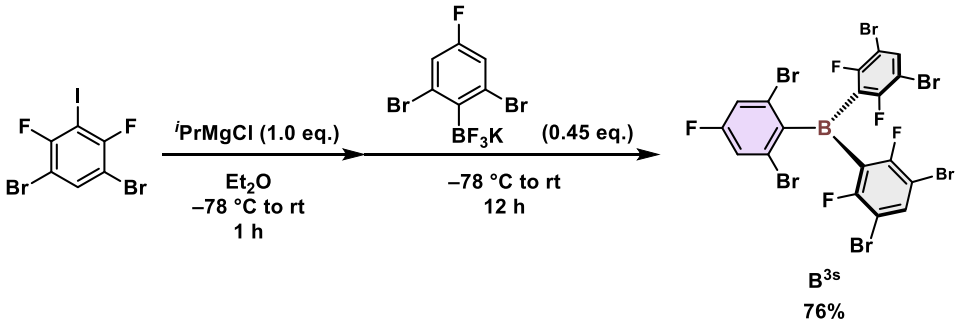


Figure 1.S6. Molecular structure of **B^{3c}** with ellipsoids set at 50% probability. H atoms are omitted for clarity.

1.4.3.20 Preparation of **B^{3s}**



A solution of 1,5-Br_2-2,4-F_2-3-I-C_6H (2.38 g, 5.98 mmol, 1.0 equiv, 0.24 M in Et_2O) was slowly treated with ^{i}PrMgCl (5.98 mL, 1.0 equiv, 1.0 M in Et_2O) at −78 °C, and stirred for 1 h (−78 °C to rt). The resultant solution was transferred into a suspension of (2,6-dibromo-4-fluorophenyl)trifluoro-λ^4-borane, potassium salt (1.0 g, 2.78 mmol, 0.45 equiv, 0.56 M in Et_2O) at −78 °C. The reaction mixture was then allowed to warm to rt, and stirred for another 12 h. After the removal of all volatiles in vacuo, the residue was dissolved in toluene (10 mL × 4) and then passed through a celite pad, then concentrated in vacuo and washed with *n*-hexane to afford **B^{3s}** as a white solid (1.71 g, 2.12 mmol, 76%) after removal of all volatiles in vacuo. A single crystal of **B^{3s}** was obtained from a saturated solution of **B^{3s}** in toluene layered by *n*-hexane at −20 °C. **^{1}H NMR** (400 MHz, C_6D_6, rt, δ/ppm): 7.27 (t, J = 7.2 Hz, 2H, Ar-*H*), 6.66 (d, J = 7.6 Hz, 2H, Ar-*H*). **^{11}B NMR** (128 MHz, C_6D_6, rt, δ/ppm): 67.0 (brs). **^{13}C{^{1}H} NMR** (100 MHz, C_6D_6, rt, δ/ppm): 163.0 (d, $^1J_{C,F}$ = 255 Hz), 160.6 (dd, $^1J_{C,F}$ = 253 Hz, $^4J_{C,F}$ = 9.9 Hz), 141.6, 141,2, 128.6, 123.3 (d, J = 9.8), 119.0−118.4 (m), 105.8−105.4 (m). **^{19}F NMR** (376 MHz, C_6D_6, rt, δ/ppm): −94.4 (d, $^4J_{F,F}$ = 7.2 Hz, 4F), −110.7 (t, $^3J_{F,H}$ = 8.1 Hz, 1F). **X-ray** data for (**B^{3s}**)$_2$ M = 1610.96, colorless, triclinic, *P*-1 (#2), a = 8.4152(2) Å, b = 15.7132(4) Å, c = 16.5779(4) Å, α = 80.300(2)°, β = 84.953(2)°, γ = 81.608(2)°, V = 2133.10(9) Å^3, Z = 2, *Dcalcd* = 2.508 g/cm^3 , T = 123 K, R_1 (wR_2) = 0.0391 (0.0805).

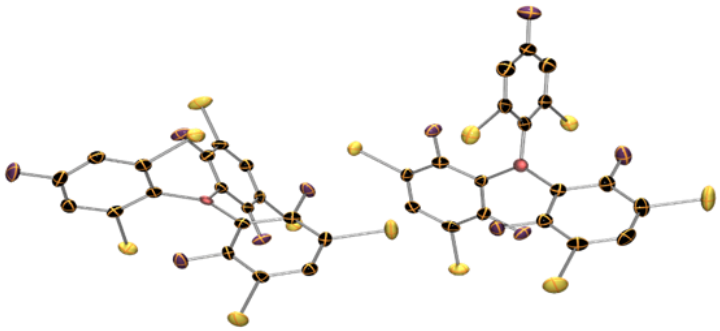
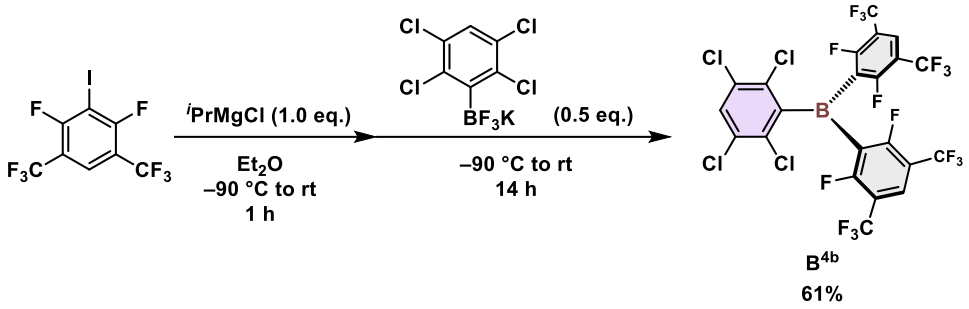


Figure 1.S7. Molecular structure of (**B^{3s}**)$_2$ with ellipsoids set at 50% probability. H atoms are omitted for clarity.

1.4.3.21 Preparation of **B^{4b}**



A solution of 2,4-F_2-3-I-1,5-$(CF_3)_2$-C_6H (4.58 g, 12.2 mmol, 1.0 equiv, 0.24 M in Et_2O) was slowly treated with ^{i}PrMgCl (12.2 mL, 1.0 equiv, 1.0 M in THF) at −90 °C, and stirred for 1 h (−90 °C to rt). The resultant solution was transferred into a suspension of trifluoro(2,3,5,6-tetrachlorophenyl)-λ^4-borane, potassium salt (1.92 mg, 5.97 mmol, 0.5 equiv, 1.20 M in Et_2O) at −90 °C. The reaction mixture was then allowed to warm to rt, and stirred for another 14 h. After the removal of all volatiles in vacuo, the residue was dissolved in toluene and then passed through a celite pad, then concentrated in vacuo. Recrystallization from *n*-hexane at −20 °C afforded **B^{4b}** as a colorless crystal (2.62 g, 3.62 mmol, 61%) after removal of all volatiles in vacuo. **^{1}H NMR** (400 MHz, C_6D_6, rt, δ/ppm): 7.45 (t, $^{4}J_{H,F}$ = 7.4 Hz, 2H, Ar-*H*), 6.79 (s, 1H, Ar-*H*). **^{11}B NMR** (128 MHz, C_6D_6, rt, δ/ppm): 60.1 (brs). **^{13}C{^{1}H} NMR** (100 MHz, C_6D_6, rt, δ/ppm): 165.1 (dd, $^{1}J_{C,F}$ = 326 Hz, $^{3}J_{C,F}$ = 10.7 Hz), 142.3, 132.6 (d, J = 5.8 Hz) , 132.2, 130.1, 124.5, 121.3 (q, $^{1}J_{C,F}$ = 271 Hz), 117.3−117.1 (m) 116.2−115.2 (m). **^{19}F NMR** (376 MHz, C_6D_6, rt, δ/ppm): −64.5 (d, J = 12.9 Hz, 6F), −95.3 (d, $^{4}J_{F,F}$ = 5.6 Hz, 4F). **X-ray** data for **B^{4b}**: M = 723.85, colorless, monoclinic, $P2_1/c$ (#14), a = 8.64150(1) Å, b = 10.1745(2) Å, c = 29.3722(4) Å, α = 90°, β = 94.7370(1)°, γ = 90°, V = 2573.67(7) Å^3, Z = 4, $Dcalcd$ = 1.868 g/cm^3 , T = 173 K, R_1 (wR_2) = 0.0490 (0.1391).

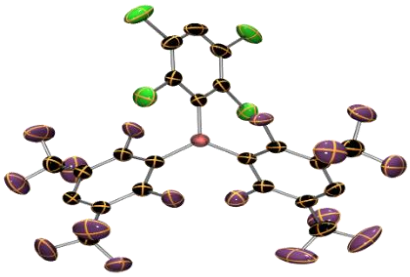
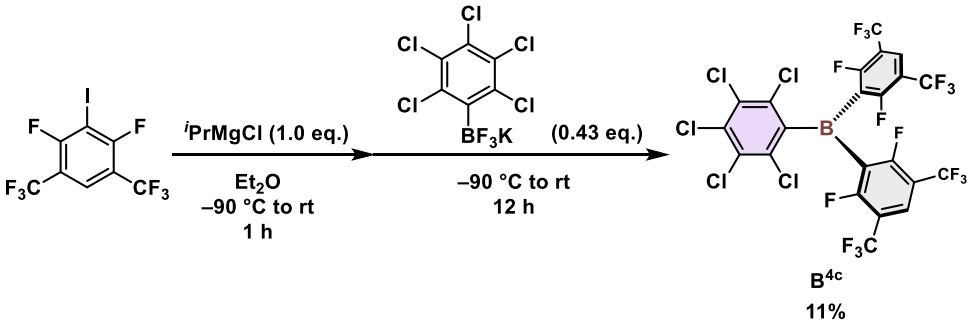


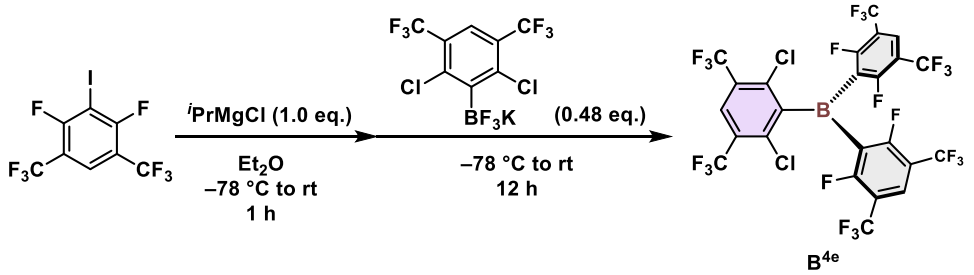
Figure 1.S8. Molecular structure of **B^{4b}** with ellipsoids set at 50% probability. H atoms are omitted for clarity.

1.4.3.22 Preparation of **B^{4c}**



A solution of 2,4-F_2-3-I-1,5-$(CF_3)_2$-C_6H (2.38 g, 6.32 mmol, 1.0 equiv, 0.42 M in Et_2O) was slowly treated with ^{i}PrMgCl (6.32 mL, 1.0 equiv, 1.0 M in Et_2O) at −90 °C, and stirred for 1 h (−90 °C to rt). The resultant solution was transferred into a suspension of trifluoro(perchlorophenyl)-λ^4-borane, potassium salt (1.00 g, 2.81 mmol, 0.43 equiv, 0.56 M in Et_2O) at −90 °C. The reaction mixture was then allowed to warm to rt, and stirred for another 12 h. After the removal of all volatiles in vacuo, the residue was dissolved in $PhCF_3$ (5 mL × 4) and then passed through a celite pad, then concentrated in vacuo. Recrystallization from *n*-hexane at −20 °C afforded **B^{4c}** as a colorless crystal (240 mg, 0.30 mmol, 11%) after removal of all volatiles in vacuo. **^{1}H NMR** (400 MHz, C_6D_6, rt, δ/ppm): 7.46 (t, $^{4}J_{H,F}$ = 7.4 Hz, 2H, Ar-*H*). **^{11}B NMR** (128 MHz, C_6D_6, rt, δ/ppm): 64.5 (brs). **^{13}C{^{1}H} NMR** (100 MHz, C_6D_6, rt, δ/ppm): 165.1 (d, $^{1}J_{C,F}$ = 278 Hz), 136.2, 132.8, 132.3, 130.8, 121.5 (q, $^{1}J_{C,F}$ = 272 Hz), 116.3−115.4 (m). Signals of the ipso-carbon with respect to the boron atoms were not identified. **^{19}F NMR** (376 MHz, C_6D_6, rt, δ/ppm): −64.5 (d, J = 12.8 Hz, 6F), −95.3 (d, $^{4}J_{F,F}$ = 5.6 Hz, 4F).

1.4.3.23 Preparation of **B^{4e}**



A solution of 2,4-F_2-3-I-1,5-$(CF_3)_2$-C_6H (3.40 g, 9.04 mmol, 1.0 equiv, 0.18 M in Et_2O) was slowly treated with ^{i}PrMgCl (9.05 mL, 1.0 equiv, 1.0 M in Et_2O) at −78 °C, and stirred for 1 h (−78 °C to rt). The resultant solution was transferred into a suspension of (2,6-dichloro-3,5-bis(trifluoromethyl)phenyl)trifluoro-λ^4-borane, potassium salt (1.42 mg, 4.41 mmol, 0.48 equiv, 0.88 M in Et_2O) at −78 °C. The reaction mixture was then allowed to warm to rt, and stirred for another 12 h. After the removal of all volatiles in vacuo, the residue was dissolved in toluene (5 mL × 4) and then passed through a celite pad, and then concentrated in vacuo. Recrystallization of the resultant solids with *n*-pentane at −20 °C afforded **B^{4e}** as a colorless crystal (suitable for XRD analysis), which included trace unidentified impurities. While tried to remove them by continuous extraction and recrystallization from *n*-pentane, we failed to obtain **B^{4e}** as an analytically pure sample. Therefore, we used **B^{4e}** including trace impurities for the following experiments. **^{1}H NMR** (400 MHz, C_6D_6, rt, δ/ppm): 7.53 (t, $^{4}J_{H,F}$ = 7.8 Hz, 2H, Ar-*H*), 7.44 (s, 1H, Ar-*H*). **^{19}F NMR** (376 MHz, C_6D_6, rt, δ/ppm): −64.6–

−64.8 (m, 12F), −65.5–−65.7 (s, 6F), −95.5 (s, 4F). Due to a limited amount of a solid, we failed to collect sufficient quality of ^{13}C NMR spectrum. **X-ray** data for $\mathbf{B^{4e}}$: M = 790.97, colorless, orthorhombic, *P*bcn (#60), a = 16.8886(5) Å, b = 12.9910(4) Å, c = 12.8554(4)Å, α = 90°, β = 90°, γ = 90°, V = 2820.47(15) Å^3, Z = 4, $Dcalcd$ = 1.863 g/cm^3, T = 193 K, R_1 (wR_2) = 0.0578 (0.1670).

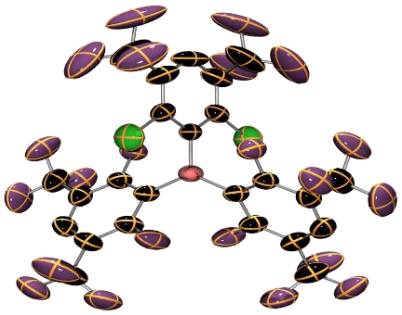


Figure 1.S9. Molecular structure of $\mathbf{B^{4e}}$ with ellipsoids set at 50% probability. H atoms are omitted for clarity.

1.4.4 Collection of experimental data

A 30 mL autoclave was charged with **1a** (0.40 mmol), **2a** (0.40 mmol), triarylborane (0.02 mmol, 5 mol%), 4Å MSiv (100 mg) and THF (8 mL). Once sealed, the vessel was pressurized with H_2 (80 atm) and heated at 100 °C for 6 h. The reaction mixture was then cooled to rt, degassed, extracted with acetone, and passed through a glass filter. Subsequently, the filtrate was concentrated in vacuo to give crude mixture. The yield of **3aa** was determined by NMR analysis using 1,3,5-trimethoxybenzen as an internal standard.

1.4.5 Comparison of Lewis acidity among $\mathbf{B^{xy}}$ by Gutmann-Beckett method

A J. Young tube was charged with $\mathbf{B^{xy}}$ (0.03 mmol), $Et_3P{=}O$ (1.3 mg, 0.01 mmol, 0.33 equiv), and CD_2Cl_2 (0.5 mL). Then, the ^{31}P NMR analyses were conducted. The acceptor number (AN) was calculated according to the literature and summarized in Table 1.S1.

Table 1.S1. Comparison of Lewis acidity based on the Gutmann-Beckett method.

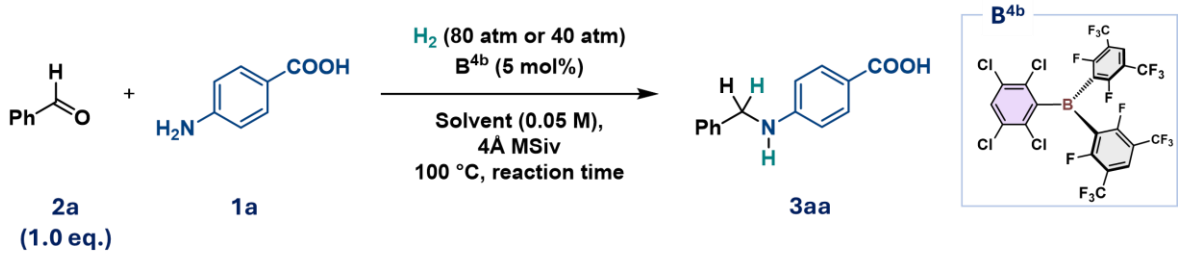
$\mathbf{B^{xy}}$	$\mathbf{B^{1a}}$	$\mathbf{B^{1f}}$	$\mathbf{B^{1v}}$	$\mathbf{B^{1w}}$	$\mathbf{B^{2a}}$	$\mathbf{B^{2b}}$	$\mathbf{B^{2c}}$	$\mathbf{B^{2e}}$	$\mathbf{B^{3a}}$
δ_p	75.0	76.5	71.6	76.1	74.8	75.7	76.0	76.2	74.7
AN	75	79	68	78	75	77	77	78	75

$\mathbf{B^{xy}}$	$\mathbf{B^{3b}}$	$\mathbf{B^{3c}}$	$\mathbf{B^{3s}}$	$\mathbf{B^{4b}}$	$\mathbf{B^{4c}}$	$\mathbf{B^{4e}}$	$\mathbf{B^{5a}}$	$\mathbf{B^{6a}}$	$\mathbf{B(C_6F_5)_3}$
δ_p	75.6	75.9	75.3	76.7	76.9	77.2	72.0	73.4	77.7
AN	77	77	76	79	80	80	69	72	81

1.4.6 Effect of solvents

A 30 mL autoclave was charged with **1a** (0.40 mmol), **2a** (0.40 mmol), $\mathbf{B^{4b}}$ (0.02 mmol), 4Å MSiv (100 mg) and MTHP (8 mL). Once sealed, the vessel was pressurized with H_2 (40 or 80 atm) and heated at 100 °C for 6–24 h. The reaction mixture was then cooled to rt, degassed, extracted with acetone, and passed

through a glass filter. Subsequently, the filtrate was concentrated in vacuo to give crude mixture. The yield of **3aa** was determined by NMR analysis using 1,3,5-trimethoxybenzen as an internal standard. Results are summarized in Figure 1.S10.



2a (1.0 eq.) 1a 3aa

Entry	H_2 (atm)	Solvent	Reaction time (h)	MSiv (mg)	3aa (%)
1	80	THF	6	100	>99
2	40	THF	6	100	50
3	40	MTP	6	100	59
4	40	1,4-dioxane	6	100	24
5	40	CPME	6	100	18
6	40	2-MeTHF	6	100	38
7	40	2,2,4-Triethyl-1,3-dioxane	6	100	-
8	40	MTHP	24	100	72
9	40	MTHP	24	none	42

Figure 1.S10. Effect of solvents

1.4.7 Robustness screening with FGE kit

1.4.7.1 Exploring functional-group compatibility

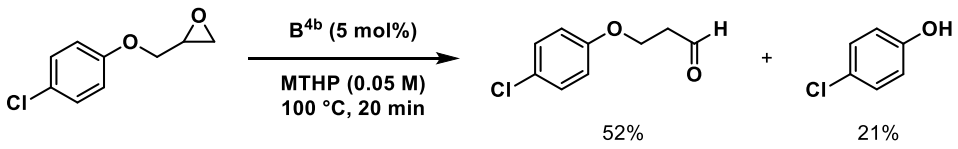
A 30 mL autoclave was charged with **1a** (0.40 mmol), **2a** (0.40 mmol), **B^{4b}** (0.02 mmol, 5 mol%), 4Å MSiv (100 mg), and MTHP (8 mL). Once sealed, the vessel was pressurized with H_2 (40 or 60 atm) and the reaction mixture was stirred at 100 °C for 24 h. Then degassed at rt followed by addition of acetone, the resultant mixture was filtered to remove MS and other solids when generated. The yield of **3aa** was determined by NMR analysis using 1,3,5-trimethoxybenzen as an internal standard. Results are summarized in Table 1.S2.

Table 1.S2. Results on robustness screen

Entry	3aa (%)	Additive remaining (%)	Imine (%)	Note
A0-1	72	>99	29	
A0-2	71	>99	27	
A1-1	40	>99	57	
A1-2	31	>99	54	
A2-1	42	>99	52	
A2-2	42	99	51	
A3-1	66	95	27	
A3-2	71	85	20	
A4-1	69	>99	27	
A4-2	63	88	30	
A5-1	0	>99	72	
A5-2	0	>99	81	
A6-1	72	>99	28	
A6-2	70	99	27	
A7-1	75	>99	21	
A7-2	73	98	25	
A8-1	72	>99	30	
A8-2	72	>99	25	
A9-1	69	99	22	
A9-2	71	99	26	
A10-1	53	>99	45	
A10-2	52	>99	44	

Entry	3aa (%)	Additive remaining (%)	Imine (%)	Note
A11-1	16	86	62	3-(4-chlorophenoxy)propanal was observed.
A11-2	11	85	55	3-(4-chlorophenoxy)propanal was observed.
A12-1	66	>99	33	
A12-2	65	>99	34	
A13-1	60	87	25	
A13-2	63	87	20	
A14-1	57	99	41	
A14-2	49	>99	43	
A15-1	73	99	26	
A15-2	72	>99	29	
A16-1	70	>99	26	
A16-2	72	95	28	
A17-1	71	89	20	
A17-2	72	94	23	
A18-1	59	>99	38	
A18-2	54	>99	41	
A19-1	33	45	9	
A19-2	32	53	12	
A20-1	67	>99	23	
A20-2	75	99	21	
A21-1	48	>99	44	
A21-2	51	>99	41	

1.4.7.2 **B^{4b}**-catalyzed ring opening of **Add.11**



In MTHP (21.6 mL), **Add.11** (200 mg, 1.08 mmol) and **B^{4b}** (39.2 mg, 54.1 μmol, 5 mol%) was mixed and the solution was stirred at 100 °C for 20 min. Then, H_2O was added, and the organic layer was extracted with EtOAc, washed with brine, dried over anhydrous Na_2SO_4, and filtered. Removal of all volatiles gave a crude mixture which was further purified by a flash column chromatography on a silica gel (hexane/EtOAc = 9/1), giving 3-(4-chlorophenoxy)propanal as colorless liquid (103.5 mg, 0.56 mmol, 52%) and 4-chlorophenol

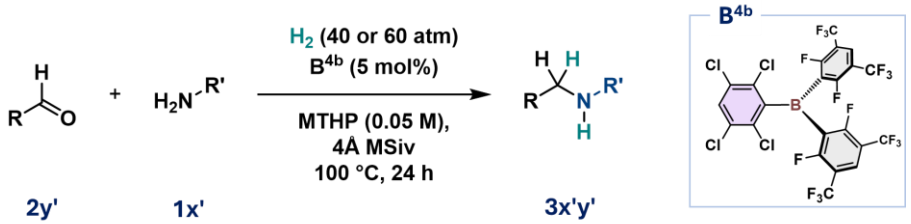
as a colorless solid (29.2 mg, 0.23 mmol, 21%).

Identification of 3-(4-chlorophenoxy)propanal:
^{1}H NMR (400 MHz, $CDCl_3$, rt, δ/ppm): 9.86 (t, J = 1.4 Hz, 1H, C*H*O), 7.23−7.21 (m, 2H, Ar-*H*), 6.85−6.80 (m, 2H, Ar-*H*), 4.27 (t, J = 6.0 Hz, 2H, CH_2), 2.90 (dt, J = 6.0 Hz, J = 1.4 Hz, 2H, CH_2). **^{13}C{^{1}H} NMR** (100 MHz, $CDCl_3$, rt, δ/ppm): 200.0 (d, J = 6.0 Hz), 157.2, 129.5, 126.2, 115.9, 62.0, 43.3. **HRMS** (EI$^+$): m/z Calculated for $C_9H_9ClO_2$ ([M]$^+$) 184.0291, found 184.0290.

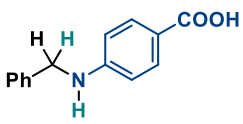
Identification of 4-chlorophenol[65]
^{1}H NMR (400 MHz, $CDCl_3$, rt, δ/ppm): 7.18 (d, J = 8.8 Hz, 2H, Ar-*H*), 6.77 (d, J = 8.8 Hz, 2H, Ar-*H*), 5.48 (brs, 1H, O*H*).

1.4.8 Reductive alkylation of 1 with 2 for preparation of 3

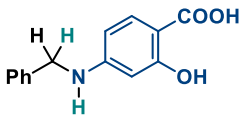
1.4.8.1 Reactions with aniline derived amino acids



General: A 30 mL autoclave was charged with **1x′** (0.40 mmol), **2y′** (0.40 mmol), **B^{4b}** (0.02 mmol), 4Å MSiv (100 mg), and MTHP (8 mL). Once sealed, the vessel was pressurized with H_2 (40 or 60 atm) and the reaction mixture was stirred at 100 °C for 24 h. Then degassed at rt followed by addition of acetone, the resultant mixture was filtered to remove MSiv and other solids when generated. Subsequently, all volatiles were removed in vacuo to give **3x′y′** that was purified by a flash column chromatography on silica gel.

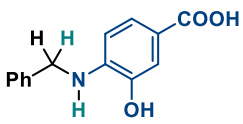


4-(Benzylamino)benzoic acid (3aa)[30]: The general procedure was followed with **2a** (42.4 mg, 0.40 mmol), **1a** (54.9 mg, 0.40 mmol), **B^{4b}** (14.5 mg, 0.02 mmol), and H_2 (60 atm). Purification by a flash column chromatography on silica gel (*n*-hexane/EtOAc = 2/1) afforded **3aa** as a colorless solid (85.4 mg, 0.38 mmol, 95%). **^{1}H NMR** (400 MHz, $CDCl_3$, rt, δ/ppm): 7.92 (d, J = 8.8 Hz, 2H, Ar-*H*), 7.39−7.28 (m, 5H, $C_6H_5CH_2$), 6.61 (d, J = 8.8 Hz, 2H, Ar-*H*), 4.41 (s, 2H, CH_2). Resonances of COOH and NH were not identified.

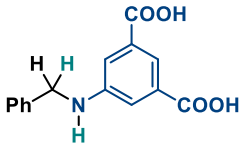


4-(Benzylamino)-2-hydroxybenzoic acid (3ba)[30]: The general procedure was followed with **2a** (42.4 mg, 0.40 mmol), **1b** (61.3 mg, 0.40 mmol), **B^{4b}** (14.5 mg, 0.02 mmol), and H_2 (40 atm). Purification by a flash column chromatography on silica gel (*n*-hexane/EtOAc = 1/1) afforded **3ba** as a brown solid (87.1 mg, 0.36 mmol, 90%). **^{1}H NMR** (400 MHz, DMSO-d_6, rt, δ/ppm): δ 12.6 (brs, 1H, COO*H*), 7.43 (d, J = 8.8 Hz, 1H, Ar-*H*). 7.34–7.32 (m, 4H, Ar-*H*), 7.27–7.22 (m,

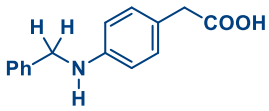
1H, Ar-*H*), 7.08 (brs, *J* = 5.6 Hz, 1H, N-*H*), 6.19 (d, *J* = 8.8, *J* = 2.4 Hz, 1H, Ar-*H*), 5.93 (d, *J* = 2.0 Hz, 1H, Ar-*H*), 4.31 (d, *J* = 6.0 Hz, 2H, CH_2). Resonances of OH were not identified.



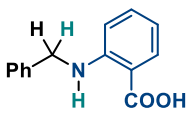
4-(Benzylamino)-3-hydroxybenzoic acid (3ca)[30]: The general procedure was followed with **2a** (42.4 mg, 0.40 mmol), **1c** (61.3 mg, 0.40 mmol), **B^{4b}** (14.5 mg, 0.02 mmol), and H_2 (40 atm). Purification by a flash column chromatography on silica gel (*n*-hexane/EtOAc = 1/1) afforded **3ca** as a pink solid (88.9 mg, 0.37 mmol, 93%). **^{1}H NMR** (400 MHz, DMSO-d_6, rt, δ/ppm): δ 12.0 (brs, 1H, COO*H*), 7.63 (d, *J* = 8.7 Hz, 2H, Ar-*H*), 7.36−7.28 (m, 4H, Ar-*H*), 7.26−7.20 (m, 1H, Ar-*H*), 7.02 (t, *J* = 6.0 Hz, 1H, N*H*), 6.59 (d, *J* = 8.8 Hz, 2H, Ar-*H*), 4.33 (d, *J* = 6.0 Hz, 2H, CH_2). A resonance of OH was not identified.



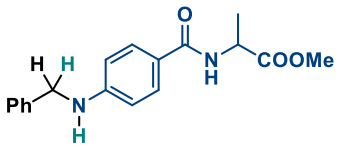
5-(Benzylamino)isophthalic acid (3da): The general procedure was followed with **2a** (42.4 mg, 0.40 mmol), **1d** (72.5 mg, 0.40 mmol), **B^{4b}** (14.5 mg, 0.02 mmol), and H_2 (40 atm). Purification by a flash column chromatography on silica gel (*n*-hexane/EtOAc = 1/3) afforded **3da** as a colorless solid (104.1 mg, 0.38 mmol, 95%). **^{1}H NMR** (400 MHz, DMSO-d_6, rt, δ/ppm): 12.9 (brs, 2H, COO*H*), 7.69−7.66 (m, 1H, Ar-*H*), 7.28−7.38 (m, 6H, Ar-*H*), 7.19−7.26 (m, 1H, Ar-*H*), 6.85 (t, *J* = 5.4 Hz, 1H, N*H*), 4.34 (d, *J* = 5.2 Hz, 2H, CH_2). **^{13}C{^{1}H} NMR** (100 MHz, DMSO-d_6, rt, δ/ppm): 167.1, 149.0, 139.4, 131.7, 128.4, 127.1, 126.8, 117.5, 116.6, 46.3. **HRMS** (EI$^+$): m/z Calculated for $C_{15}H_{13}NO_4$ ([M]$^+$) 271.0845, found 271.0850.



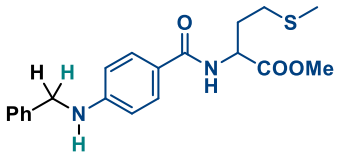
2-(4-(Benzylamino)phenyl)acetic acid (3ea): The general procedure was followed with **2a** (42.4 mg, 0.40 mmol), **1e** (60.5 mg, 0.40 mmol), **B^{4b}** (14.5 mg, 0.02 mmol), and H_2 (40 atm). Purification by a flash column chromatography on silica gel (*n*-hexane/EtOAc = 1/3) afforded **3ea** as a pink solid (88.8 mg, 0.37 mmol, 93%).**^{1}H NMR** (400 MHz, DMSO-d_6, rt, δ/ppm): 12.1 (brs, 1H, COO*H*), 7.37−7.15 (m, 5H, C_6H_5-CH_2), 6.91 (d, *J* = 8.4 Hz, 2H, Ar-*H*), 6.50 (d, *J* = 8.4 Hz, 2H, Ar-*H*), 6.15 (brs, 1H, N*H*), 4.24 (s, 2H, NHCH_2), 3.32 (s, 2H, CH_2COOH, (overlap with a H_2O peak)). **^{13}C{^{1}H} NMR** (100 MHz, DMSO-d_6, rt, δ/ppm): 173.3, 147.4, 140.3, 129.7, 128.2, 127.1, 126.6, 121.9, 112.2, 46.5. **HRMS** (EI$^+$): m/z Calculated for $C_{15}H_{15}NO_2$ ([M]$^+$) 241.1103, found 241.1093.



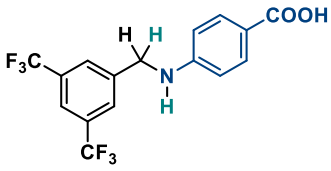
2-(Benzylamino)benzoic acid (3fa)[31]: The general procedure was followed with **2a** (42.4 mg, 0.40 mmol), **1f** (54.9 mg, 0.40 mmol), **B^{4b}** (14.5 mg, 0.02 mmol), and H_2 (40 atm). Purification by a flash column chromatography on silica gel (*n*-hexane/EtOAc = 1/1) afforded **3fa** as a colorless solid (77.01 mg, 0.34 mmol, 85%). **^{1}H NMR** (400 MHz, DMSO-d_6, rt, δ/ppm): 8.30 (brs, 1H, COO*H*), 7.80 (d, *J* = 7.8 Hz, 2H, Ar-*H*), 7.19−7.38 (m, 6H), 6.66 (d, *J* = 8.5 Hz, 1H, Ar-*H*), 6.55 (t, *J* = 7.5 Hz, 1H, N*H*), 4.45 (s, 2H).



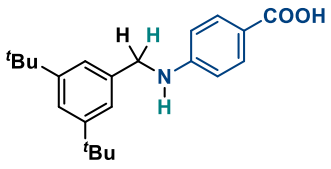
Methyl(4-(benzylamino)benzoyl)-D-alaninate (3ia): The general procedure was followed with **2a** (42.4 mg, 0.40 mmol), **2i** (88.9 mg, 0.40 mmol), **B**^{4b} (14.5 mg, 0.02 mmol), and H_2 (40 atm). Purification by a flash column chromatography on silica gel (*n*-hexane/EtOAc = 99/1) afforded **3ia** as a white solid (117.2 mg, 0.38 mmol, 95%). **^{1}H NMR** (400 MHz, $CDCl_3$, rt, δ/ppm): 7.65 (dd, J = 6.9, J = 1.9 Hz, 1H, Ar-*H*), 7.39−7.26 (m, 5H), 6.61 (dd, J = 6.9, J = 1.9 Hz, 1H, Ar-*H*), 6.52 (d, J = 7.0 Hz, 1H, CON*H*), 4.78 (q, J = 7.2 Hz, 1H, C*H*CH$_3$), 4.42 (brs, 1H, N*H*), 4.38 (s, 2H, CH_2), 3.78 (s, 3H, COOCH_3), 1.49 (d, J = 7.2 Hz, 3H, CHCH_3). A resonance of NH was not identified. **^{13}C{^{1}H} NMR** (100 MHz, DMSO-d_6, rt, δ/ppm): 174.0, 166.6, 150.9, 138.6, 128.8, 128.7, 128.4 (d, J = 7.5 Hz), 122.2, 111.9, 52.5 (d, J = 8.2 Hz), 48.3 (d, J = 2.2 Hz), 47.7, 18.8 (d, J = 4.9 Hz). **HRMS** (EI$^+$): m/z Calculated for $C_{18}H_{20}N_2O_3$ ([M]$^+$) 312.1474, found 312.1468.



Methyl (4-(benzylamino)benzoyl)methioninate (3ja): The general procedure was followed with **2a** (42.4 mg, 0.40 mmol), **1j** (112.9 mg, 0.40 mmol), **B**^{4b} (14.5 mg, 0.02 mmol), and H_2 (40 atm). Purification by a flash column chromatography on silica gel (*n*-hexane/EtOAc = 7/3) afforded **3ja** as a white solid (81.2 mg, 0.22 mmol, 55%). **^{1}H NMR** (400 MHz, $CDCl_3$, rt, δ/ppm): 7.56 (d, J = 8.7 Hz, 2H, Ar-*H*), 7.31−7.18 (m, 5H, Ar-*H*), 6.67 (d, J = 7.6 Hz, 1H, CON*H*), 6.52 (d, J = 8.8 Hz, 2H, Ar-*H*), 4.75−4.84 (m, 1H, C*H*CH$_2$), 4.30 (s, 2H, C$_6$H$_5$CH_2), 3.68 (s, 3H, COOCH_3), 2.55−2.40 (m, 2H, CH_2S), 2.23−1.93 (m, 2H, CHCH_2), 2.01 (s, 3H, SCH_3). A resonance of NH was not identified. **^{13}C{^{1}H} NMR** (100 MHz, $CDCl_3$, rt, δ/ppm): 173.0, 167.1, 151.1, 138.6, 129.0, 128.9, 127.6, 127.5, 122.0, 112.0 (d, J = 4.8 Hz), 52.7 (d, J = 9.3 Hz), 52.0 (d, J = 4.7 Hz), 47.8 (t, J = 5.8 Hz), 31.9, 30.2, 15.6. **HRMS** (EI$^+$): m/z Calculated for $C_{20}H_{24}N_2O_3NaS$ ([M]$^+$) 395.1400, found 395.1381.

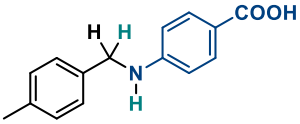


4-((3,5-Bis(trifluoromethyl)benzyl)amino)benzoic acid (3ab): The general procedure was followed with **1a** (54.9 mg, 0.40 mmol), 3,5-bis(trifluoromethyl)benzaldehyde **2b** (96.8 mg, 0.40 mmol), **B**^{4b} (14.5 mg, 0.02 mmol), and H_2 (40 atm). Purification by a flash column chromatography on silica gel (*n*-hexane/EtOAc = 9/1) afforded **3ab** as a white solid (135.3 mg, 0.37 mmol, 93%). **^{1}H NMR** (400 MHz, $CDCl_3$, rt, δ/ppm): 7.94 (d, 2H, Ar-*H*), 7.81 (m, 3H, Ar-*H*), 6.60 (d, J = 8.6 Hz, 2H, Ar-*H*), 4.71 (brs, 1H, N*H*), 4.56 (s, 2H, CH_2). Resonances of COOH were not identified. **^{13}C{^{1}H} NMR** (100 MHz, $CDCl_3$, rt, δ/ppm): 171.8, 151.7, 141.4, 132.6, 132.3 (d, $^2J_{C,F}$ = 33.1 Hz), 127.3, 123.3 (q, 2C, $^1J_{C,F}$ = 272 Hz), 121.8, 119.0, 112.1, 47.1. **^{19}F NMR** (376 MHz, $CDCl_3$, rt, δ/ppm): −66.1 (s, 6F). **HRMS** (EI$^+$): m/z Calculated for $C_{16}H_{10}F_6NO_2$ ([M]$^+$) 362.0610, found 362.0621.



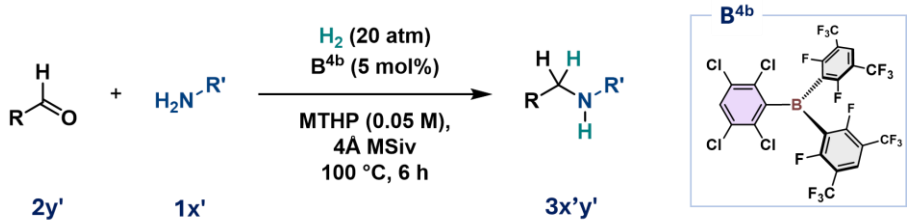
4-((3,5-Bis(trifluoromethyl)benzyl)amino)benzoic acid (3ac): The general procedure was followed with **1a** (54.9 mg, 0.40 mmol), **2c** (87.3 mg, 0.40 mmol), **B**^{4b} (14.5 mg, 0.02 mmol), and H_2 (40 atm). Purification by a flash column chromatography on silica gel (*n*-hexane only) afforded **3ac** as a white solid (50.8

mg, 0.15 mmol, 38%). **^{1}H NMR** (400 MHz, $CDCl_3$, rt, δ/ppm): 7.98 (d, J = 8.4 Hz, 2H, Ar-*H*), 7.41 (s, 1H, N*H*), 7.22 (d, J = 1.6 Hz, 2H, Ar-*H*), 6.66 (d, J = 8.8 Hz, 2H, Ar-*H*), 4.38 (s, 2H, CH_2), 1.35 (s, 18H, C(CH_3)$_3$). Resonances of COOH were not identified. **^{13}C{^{1}H} NMR** (100 MHz, $CDCl_3$, rt, δ/ppm): 172.6, 152.7, 151.6, 137.3, 132.5, 122.2, 121.9, 117.7, 111.7, 48.6, 35.0, 31.6 (d, J = 4.9 Hz). **HRMS** (EI$^+$): m/z Calculated for $C_{22}H_{28}NO_2$ ([M]$^+$) 338.2115, found 338.2123.

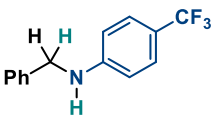


4-((4-Methylbenzyl)amino)benzoic acid (3ad): The general procedure was followed with **1a** (54.9 mg, 0.40 mmol), **2d** (48.1 mg, 0.40 mmol), **B^{4b}** (14.5 mg, 0.02 mmol), and H_2 (40 atm). Purification by a flash column chromatography on silica gel (*n*-hexane/EtOAc = 9/1) afforded **3ad** as a pink solid (74.1 mg, 0.32 mmol, 80%). **^{1}H NMR** (400 MHz, $CDCl_3$, rt, δ/ppm): 7.92 (d, J = 8.8 Hz, 2H, Ar-*H*), 7.26−7.15 (m, 4H, Ar-*H*), 6.60 (d, J = 8.8 Hz, 2H, Ar-*H*), 4.36 (s, 2H, CH_2), 2.35 (s, 3H, CH_3). Resonances of COOH were not identified. **^{13}C{^{1}H} NMR** (100 MHz, $CDCl_3$, rt, δ/ppm): 172.0, 152.6, 137.5, 135.3, 132.5, 129.6, 127.6, 117.7, 111.8, 47.6, 21.2. **HRMS** (EI$^+$): m/z Calculated for $C_{15}H_{14}NO_2$ ([M]$^+$) 240.1019, found 240.1030.

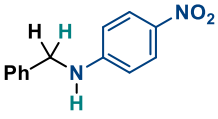
1.4.8.2 Reactions with substituted anilines



General: A 30 mL autoclave was charged with **1x′** (0.40 mmol), **2y′** (0.40 mmol), **B^{4b}** (0.02 mmol), 4Å MSiv (100 mg), and MTHP (8 mL). Once sealed, the vessel was pressurized with H_2 (20 atm) and the reaction mixture was stirred at 100 °C for 6 h. Then degassed at rt followed by addition of acetone, the resultant mixture was filtered to remove MS and other solids when generated. Subsequently, all volatiles were removed in vacuo to give **3x′y′** that was purified by a flash column chromatography on silica gel.

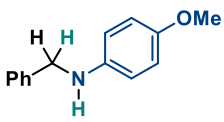


***N*-benzyl-4-(trifluoromethyl)aniline (3ka)[30]:** The general procedure was followed with **2a** (42.4 mg, 0.40 mmol), **1k** (64.4 mg, 0.40 mmol), **B^{4b}** (14.5 mg, 0.02 mmol), and H_2 (20 atm). Purification by a flash column chromatography on silica gel (*n*-hexane only) afforded **3ka** as a white solid (93.1 mg, 0.37 mmol, 93%). **^{1}H NMR** (400 MHz, $CDCl_3$, rt, δ/ppm): 7.41–7.28 (m, 7H, Ar-*H*), 6.63 (d, J = 8.8 Hz, 2H, Ar-*H*), 4.38 (brs, 3H, CH_2 and N*H*).

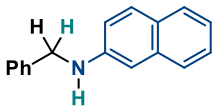


***N*-benzyl-4-nitroaniline (3la)[30]:** The general procedure was followed with **2a** (42.4 mg, 0.40 mmol), **1l** (55.2 mg, 0.40 mmol), **B^{4b}** (14.5 mg, 0.02 mmol), and H_2 (20 atm). Purification by a flash column chromatography on silica gel (*n*-hexane/EtOAc = 1/1) afforded **3la** as a yellow solid (90.3 mg, 0.40 mmol, >99%). **^{1}H NMR** (400 MHz, $CDCl_3$, rt, δ/ppm): 8.11–8.07

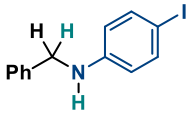
(m, 2H, Ar-*H*), 7.40–7.30 (m, 5H, Ar-*H*), 6.60–6.56 (m, 2H, Ar-*H*), 4.84 (brs, 1H, N*H*), 4.43 (d, *J* = 5.6 Hz, 2H, CH_2).



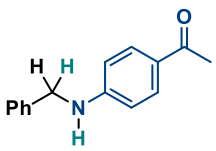
***N*-benzyl-4-methoxyaniline (3ma)[30]:** The general procedure was followed with **2a** (42.4 mg, 0.40 mmol), **1m** (49.3 mg, 0.40 mmol), **B^{4b}** (14.5 mg, 0.02 mmol), and H_2 (20 atm). Purification by a flash column chromatography on silica gel (*n*-hexane only) afforded **3ma** as a white solid (76.0 mg, 0.36 mmol, 90%). **^{1}H NMR** (400 MHz, $CDCl_3$, rt, *δ*/ppm): 7.47–7.42 (m, 4H, Ar-*H*), 7.38–7.35 (m, 1H, Ar-*H*), 6.88 (d, *J* = 8.8 Hz, 2H, Ar-*H*), 6.68 (d, *J* = 8.8 Hz, 2H, Ar-*H*), 4.35 (s, 2H, CH_2), 3.81 (brs, 4H, OCH_3 and N*H*).



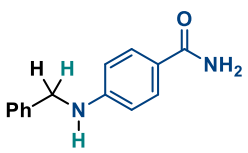
***N*-benzylnaphthalen-2-amine (3na)[30]:** The general procedure was followed with **2a** (42.4 mg, 0.40 mmol), **1n** (87.3 mg, 0.40 mmol), **B^{4b}** (14.5 mg, 0.02 mmol), and H_2 (20 atm). Purification by a flash column chromatography on silica gel (*n*-hexane only) afforded **3na** as a brownish solid (92.6 mg, 0.40 mmol, >99%). **^{1}H NMR** (400 MHz, $CDCl_3$, rt, *δ*/ppm): 7.69–7.58 (m, 3H, Ar-*H*), 7.44–7.28 (m, 6H, Ar-*H*), 7.22–7.18 (m, 1H, Ar-*H*), 6.94–6.91 (m, 1H, Ar-*H*), 6.85 (d, *J* = 2.0 Hz, 1H, Ar-*H*), 4.45 (s, 2H, CH_2), 4.21 (brs, 1H, N*H*).



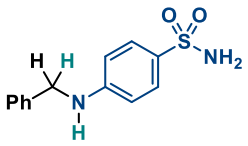
***N*-benzyl-4-iodoaniline (3oa)[30]:** The general procedure was followed with **2a** (42.4 mg, 0.40 mmol), **1o** (87.3 mg, 0.40 mmol), **B^{4b}** (14.5 mg, 0.02 mmol), and H_2 (20 atm). Purification by a flash column chromatography on silica gel (*n*-hexane only) afforded **3oa** as a pale yellow solid (120.3 mg, 0.39 mmol, 98%). **^{1}H NMR** (400 MHz, $CDCl_3$, rt, *δ*/ppm): 7.43–7.39 (m, 2H, Ar-*H*), 7.37–7.27 (m, 5H, Ar-*H*), 6.43–6.40 (m, 2H, Ar-*H*), 4.30 (d, *J* = 5.2 Hz, 2H, CH_2), 4.10 (brs, 1H, N*H*).



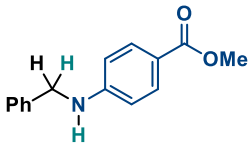
1-(4-(benzylamino)phenyl)ethan-1-one (3pa)[30]: The general procedure was followed with **2a** (42.4 mg, 0.40 mmol), **1p** (54.1 mg, 0.40 mmol), **B^{4b}** (14.5 mg, 0.02 mmol), and H_2 (20 atm). Purification by a flash column chromatography on silica gel (hexane/EtOAc = 1/1) afforded **3pa** as a pale yellow solid (83.1 mg, 0.37 mmol, 93%). **^{1}H NMR** (400 MHz, $CDCl_3$, rt, *δ*/ppm): 7.84–7.81 (m, 2H, Ar-*H*), 7.39–7.28 (m, 5H, Ar-*H*), 6.62–6.58 (m, 2H, Ar-*H*), 4.58 (brs, 1H, N*H*), 4.41 (d, *J* = 5.6 Hz, 2H, CH_2), 2.49 (s, 3H, CH_3).



4-(benzylamino)benzamide (3qa)[30]: The general procedure was followed with **2a** (42.4 mg, 0.40 mmol), **1q** (54.5 mg, 0.40 mmol), **B^{4b}** (14.5 mg, 0.02 mmol), and H_2 (20 atm). Purification by a flash column chromatography on silica gel (EtOAc) afforded **3qa** as a white solid (86.7 mg, 0.38 mmol, 95%). **^{1}H NMR** (400 MHz, DMSO-d_6, rt, *δ*/ppm): 7.59 (d, *J* = 8.8 Hz, 2H, Ar-*H*), 7.51 (brs, 1H, one of NH_2), 7.35–7.30 (m, 4H, Ar-*H*), 7.25–7.21 (m, 1H, Ar-*H*), 6.83 (brs, 1H, other peak of NH_2), 6.78 (t, *J* = 6.0 Hz, 1H, N*H*), 6.55 (d, *J* = 8.8 Hz, 2H, Ar-*H*), 4.31 (d, *J* = 6.0 Hz, 2H, CH_2). Resonances of N*H* were not identified.



4-(benzylamino)benzenesulfonamide (3ra)[30]**:** The general procedure was followed with **2a** (42.4 mg, 0.40 mmol), **1r** (68.9 mg, 0.40 mmol), **B**[4b] (14.5 mg, 0.02 mmol), and H_2 (20 atm). Purification by a flash column chromatography on silica gel (*n*-hexane only) afforded **3ra** as a pale yellow solid (103.1 mg, 0.39 mmol, 98%). **^{1}H NMR** (400 MHz, DMSO-d_6, rt, δ/ppm): 7.47 (d, J = 8.8 Hz, 2H, Ar-*H*), 7.33–7.32 (m, 4H, Ar-*H*), 7.26–7.21 (m, 1H, N*H*), 6.99 (t, J = 6.0 Hz, 1H, Ar-*H*), 6.88 (brs, 2H, NH_2), 6.62 (d, J = 8.8 Hz, 2H, Ar-*H*). 4.33 (d, J = 6.0 Hz, 2H, CH_2).



Methyl 4-(benzylamino)benzoate (3sa)[30]**:** The general procedure was followed with **2a** (42.4 mg, 0.40 mmol), **1s** (60.5 mg, 0.40 mmol), **B**[4b] (14.5 mg, 0.02 mmol), and H_2 (20 atm). Purification by a flash column chromatography on silica gel (*n*-hexane only) afforded **3sa** as a white solid (92.2 mg, 0.38 mmol, 95%). **^{1}H NMR** (400 MHz, $CDCl_3$, rt, δ/ppm): 7.87–7.84 (m, 2H, Ar-*H*), 7.38–7.27 (m, 5H, Ar-*H*), 6.61–6.57 (m, 2H, Ar-*H*), 4.49 (brs, 1H, N*H*), 4.39 (d, *J* = 5.2 Hz, 2H, CH_2), 3.85 (s, 3H, COOCH_3).

1.4.9 Monitoring the formation of 3aa

A MTHP solution of **1a** (137.1 mg, 1.0 mmol, [**1a**] = 0.050 M), **2a** (106.1 mg, 1.0 mmol, [**2a**] = 0.050 M), **B**^{4b} (36.2 mg, 0.050 mmol), was prepared. Then, this reaction mixture was equally divided into 10 autoclave reactors (V = 10 mL), and 4 Å molecular sieves (25 mg) were added to each solution, affording a 2.0 mL of MTHP solution ([**1a**] = [**2a**] = 0.050 M). Once sealed, each vessel was pressurized with H_2 (40 atm) and the reaction mixture was stirred at 100 °C. After heating for the certain reaction period, a resultant crude mixture was filtered to remove MS, dried in vacuo. The yield of **3aa** was calculated by ^{1}H NMR analyses using 1,3,5-trimethoxybenzene as an internal standard. The obtained time-concentration profile was shown in Figure 1.S11, showing obvious similarity with the **B**^{1a}-catalyzed reductive alkylation of amines with aldehydes.[30] We thus calculated TOFs used in GPR analysis based on the following equation:

TOF (h^{-1}) = yield of **3aa** (%)/ reaction time (h)

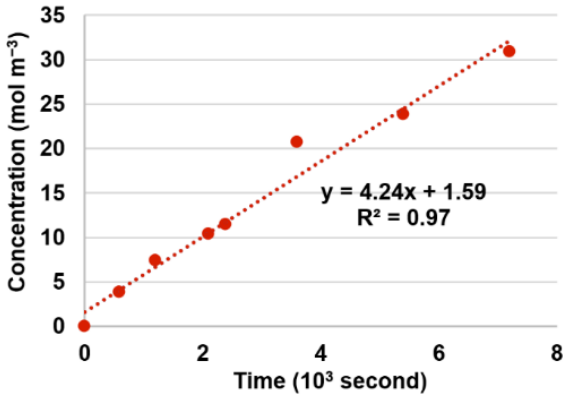
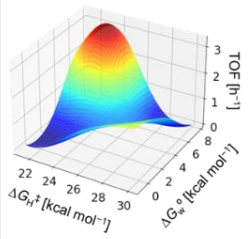
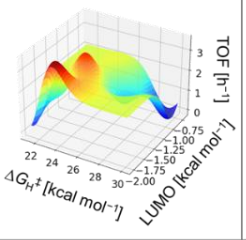
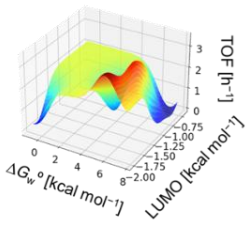
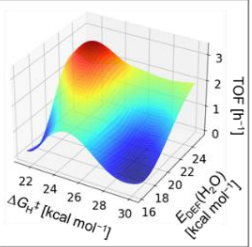
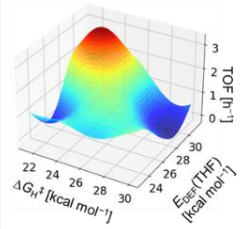
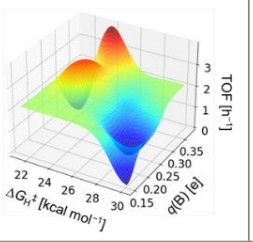
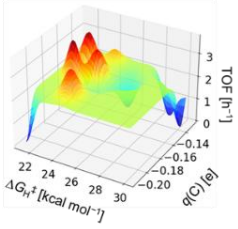
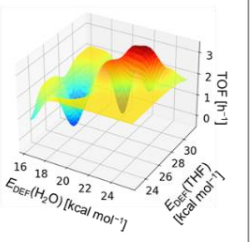


Figure 1.S11. Concentration vs. time profiles of the production of **3aa**

1.4.10 Gaussian process regression for Model I to V

The code and .csv folder for all theoretical values used in this work can be found in the Zenode repository, see DOI: 10.5281/zenodo.8420295.

Table 1.S3. Q^2 values of Model I – VIII

Model No.	I	II	III	IV
3D surface				
Theoretical value combinations	$\Delta G_H^{\ddagger}$ vs ΔG_w°	$\Delta G_H^{\ddagger}$ vs LUMO	$\Delta G w^{\circ}$ vs LUMO	$\Delta G_H^{\ddagger}$ vs $E_{DEF}(H_2O)$
Q^2 (Leave one out)	0.78	0.23	0.23	0.59
Model No.	**V**	**VI**	**VII**	**VIII**
3D surface				
Theoretical value combinations	$\Delta G_H^{\ddagger}$ vs E_{DEF}(THF)	$\Delta G_H^{\ddagger}$ vs q(B)	$\Delta G_H^{\ddagger}$ vs q(C)	$E_{DEF}(H_2O)$ vs E_{DEF}(THF)
Q^2 (Leave one out)	0.51	0.09	-0.31	0.16

1.4.11 Theoretical studies

1.4.11.1 Computational details

The density functional theory (DFT) calculations were performed with Gaussian 16 (Revision C.01) software.[67] All the structures were optimized at the ωB97X-D[68] level of theory with the 6-31G(d,p) basis sets. Frequency calculations were performed to verify that intermediates have no imaginary frequency, whereas the transition state structures have only one imaginary frequency. For selectd transition state structures, the appropriateness of the connections between each reactant and product via the transition state was confirmed using intrinsic reaction coordinate (IRC).[69] Single-point energy calculations were carried out at ωB97X-D/6-311+G(d,p)/gas-phase level of theory otherwise noted. The reported Gibbs free energies were calculated at 298.15 K. These calculations involve a certain margin of error.

For the calculation of deformation energies (E_{DEF}), the ORCA 5.0.3 program package was applied.[70–73] Gas phase equilibrium structures for $\mathbf{H_2O{-}B^{xy}}$ and $\mathbf{THF{-}B^{xy}}$ adducts have been obtained on the PBEh-3c/Def2-SVPS6 level of theory, which was also applied for the frequency analysis to verify that these structures have no imaginary frequency.

E_{DEF} values were obtained by computing the single point energies (RI-DSDPBEP86-D3BJ/ma-Def2-QZVPP) of B^{xy} units in the structures of each $\mathbf{H_2O{-}B^{xy}}$ and $\mathbf{THF{-}B^{xy}}$ adducts, and subtraction from the energies in the relaxed states.[48]

1.4.11.2 Comparison of geometrical parameters in $\mathbf{B}^{xy}$ and $\mathbf{H_2O{-}B}^{xy}$ adducts

From the optimized geometrical parameters of B^{xy} at the PBEh-3c/Def2-SVPS6 level, we obtained the following four indices: (i) q(B) (the Mulliken charge on boron atom in B^{xy}); (ii) q(C) (the averaged value of the Mulliken charge on *ipso*-carbon atoms; (iii) Mayer's bonded valence on B; and (iv) the averaged value of the Mayer's bonded valence of *ipso*-carbon atoms. These results are summarized in Table 1.S3.

Table 1.S3. Comparison of theoretical parameters in $\mathbf{B}^{xy}$

B^{xy}	B^{1a}	B^{1b}	B^{1c}	B^{1d}	B^{1e}	B^{1f}	B^{1g}	B^{1h}	B^{1i}	B^{1v}
q(B)	0.3118	0.2793	0.2539	0.2739	0.2765	0.3077	0.2685	0.2751	0.2724	0.15
q(C)	-0.166	-0.147	-0.125	-0.143	-0.147	-0.166	-0.149	-0.162	-0.139	-0.137
Mayer bond order on B	3.218	3.305	3.328	3.307	3.296	3.232	3.313	3.307	3.298	3.42
Mayer bond order on ipso-C	3.767	3.774	3.753	3.768	3.767	3.771	3.775	3.786	3.758	3.742

B^{xy}	B^{1w}	B^{2a}	B^{2b}	B^{2c}	B^{2d}	B^{2e}	B^{2f}	B^{2g}	B^{2h}	B^{2i}
q(B)	0.252	0.265	0.2975	0.3326	0.2163	0.2691	0.2843	0.2607	0.2875	0.2645
q(C)	-0.157	-0.14	-0.194	-0.202	-0.139	-0.172	-0.184	-0.175	-0.203	-0.172
Mayer bond order on B	3.368	3.279	3.237	3.159	3.398	3.301	3.277	3.318	3.268	3.302
Mayer bond order on ipso-C	3.754	3.736	3.765	3.758	3.757	3.76	3.749	3.769	3.779	3.755

B^{xy}	B^{2j}	B^{2k}	B^{2l}	B^{2m}	B^{2n}	B^{2o}	B^{2p}	B^{2q}	B^{2r}	B^{2t}
q(B)	0.2252	0.2825	0.2312	0.2163	0.2484	0.2607	0.2448	0.2842	0.2488	0.2465
q(C)	-0.141	-0.191	-0.161	-0.146	-0.185	-0.183	-0.173	-0.208	-0.172	-0.141
Mayer bond order on B	3.352	3.257	3.348	3.399	3.359	3.313	3.341	3.26	3.33	3.346
Mayer bond order on ipso-C	3.741	3.772	3.756	3.787	3.759	3.758	3.771	3.777	3.764	3.793

B^{xy}	B^{2u}	B^{3a}	B^{3b}	B^{3c}	B^{3d}	B^{3e}	B^{3f}	B^{3g}	B^{3h}	B^{3i}
q(B)	0.2465	0.3179	0.2843	0.2829	0.2469	0.2542	0.3673	0.2596	0.2662	0.2681
q(C)	-0.157	-0.157	-0.17	-0.159	-0.137	-0.156	-0.189	-0.158	-0.171	-0.17
Mayer bond order on B	3.345	3.169	3.331	3.248	3.327	3.34	3.23	3.319	3.313	3.289
Mayer bond order on ipso-C	3.883	3.747	3.757	3.743	3.762	3.768	3.715	3.774	3.786	3.763

B^{xy}	B^{3s}	B^{4a}	B^{4b}	B^{4c}	B^{4d}	B^{4e}	B^{4f}	B^{4g}	B^{4h}	B^{4i}
q(B)	0.2569	0.2859	0.2659	0.2618	0.2648	0.3718	0.2772	0.2564	0.2873	0.2537
q(C)	-0.146	-0.167	-0.157	-0.149	-0.147	-0.17	-0.159	-0.168	-0.165	-0.145
Mayer bond order on B	3.31	3.241	3.304	3.307	3.305	3.245	3.28	3.306	3.244	3.322
Mayer bond order on ipso-C	3.766	3.768	3.772	3.755	3.766	3.715	3.761	3.776	3.779	3.765

B^{xy}	B^{4j}	B^{5a}	B^{6a}	BCF
q(B)	0.2208	0.2443	0.258	0.3749
q(C)	-0.119	-0.13	-0.147	-0.213
Mayer bond order on B	3.351	3.317	3.306	3.184
Mayer bond order on ipso-C	3.751	3.757	3.756	3.655

From the optimized geometrical parameters of $H_2O{-}B^{xy}$ adducts, we obtained the following two indices for the evaluation of the degree of geometrical deviation from the ideal tetrahedral geometry around the boron center: (i) τ_δ(B) = $\{360 - (\alpha + \beta)/141 \times \beta/\alpha\}$, where α and β are the largest and second largest C−B−C angles;[74] (ii) a tetrahedral character (THC),[75] calculated by the following equation (θ = X−B−C, X = O or C; n

= 1 − 6):

$$\mathrm{THC} = [1 - \frac{\sum_{n=1-6}|109.5-\theta_n|}{27}] \times 100$$

When the boron center adopts ideal tetrahedral geometry, both τ_5(B) and THC provide each 1.0 and 100 as their maximum, and smaller values thus suggest that the boron atom adopts more distorted tetrahedral geometry. Results are summarized in Table 1.S4.

Table 1.S4. Comparison of geometrical parameters in **H_2O−B^{xy}** adducts

B^{xy}	B^{1a}	B^{1b}	B^{1c}	B^{1d}	B^{1e}	B^{1f}	B^{1g}	B^{1h}	B^{1i}	B^{1v}
τ_5(B)	0.88	0.87	0.87	0.86	0.87	0.86	0.9	0.86	0.88	0.9
O–B	1.63	1.65	1.65	1.64	1.63	1.64	1.65	1.64	1.64	1.67
av. B–C_{Ar}	1.63	1.63	1.63	1.63	1.63	1.63	1.63	1.63	1.63	1.63
THC (%)	91.6	88.7	88.6	90.1	91.5	90.2	90.8	90.1	90.2	87.6

B^{xy}	B^{1w}	B^{2a}	B^{2b}	B^{2c}	B^{2d}	B^{2e}	B^{2f}	B^{2g}	B^{2h}	B^{2i}
τ_5(B)	0.87	0.88	0.87	0.87	0.87	0.87	0.88	0.89	0.87	0.87
O–B	1.69	1.64	1.65	1.65	1.65	1.64	1.64	1.65	1.64	1.63
av. B–C_{Ar}	1.63	1.63	1.63	1.63	1.63	1.63	1.63	1.63	1.63	1.63
THC (%)	83.5	90.1	90.1	90	90	90.7	89.8	89.8	90.7	89.7

B^{xy}	B^{2j}	B^{2k}	B^{2l}	B^{2m}	B^{2n}	B^{2o}	B^{2p}	B^{2q}	B^{2r}	B^{2t}
τ_5(B)	0.88	0.88	0.89	0.88	0.9	0.89	0.89	0.87	0.87	0.89
O–B	1.65	1.65	1.65	1.65	1.66	1.66	1.65	1.64	1.65	1.64
av. B–C_{Ar}	1.63	1.64	1.63	1.63	1.63	1.63	1.63	1.63	1.63	1.63
THC (%)	89.2	89	88.6	89.3	87.8	87.4	89.1	89.5	89.8	89.9

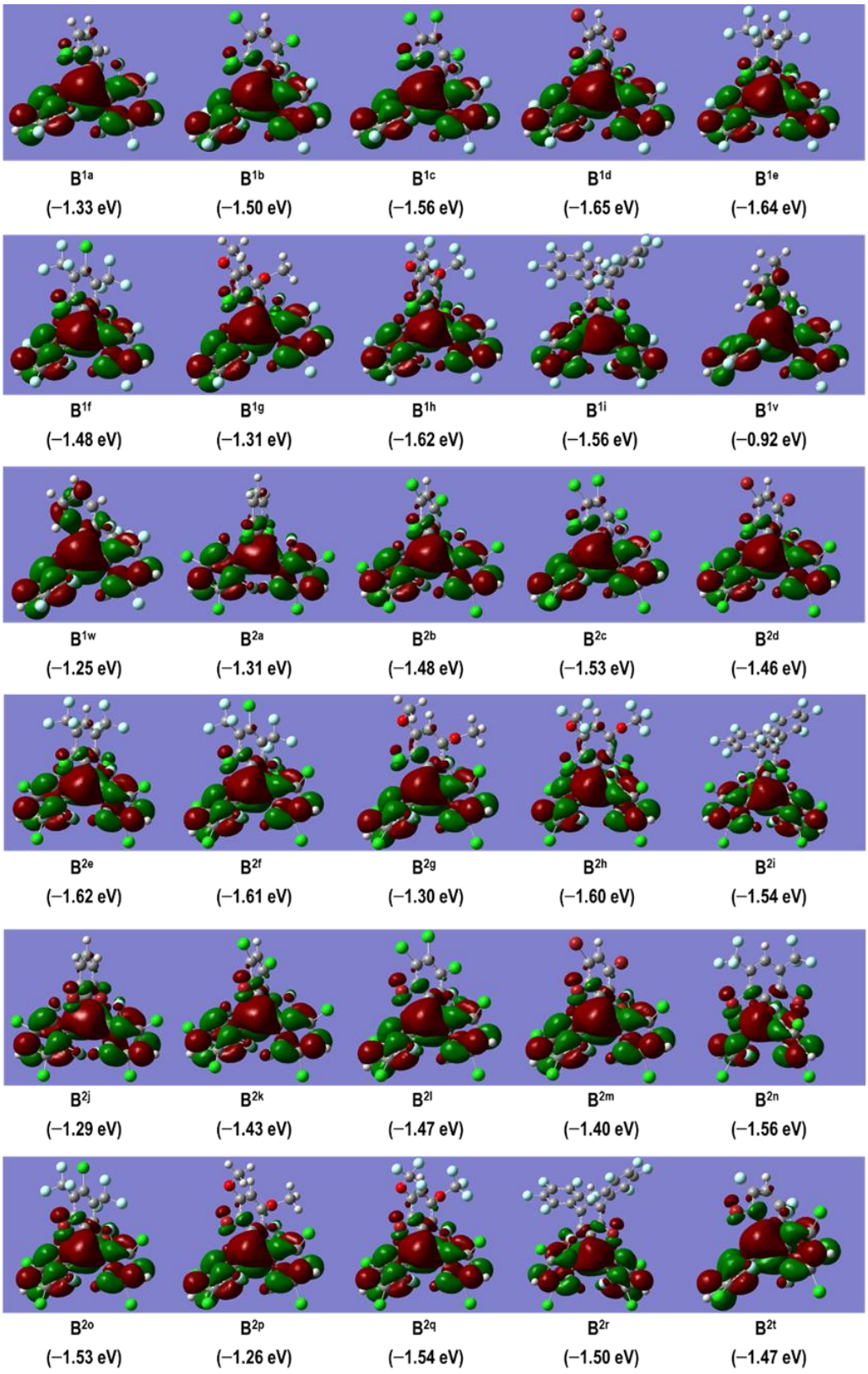
B^{xy}	B^{2u}	B^{3a}	B^{3b}	B^{3c}	B^{3d}	B^{3e}	B^{3f}	B^{3g}	B^{3h}	B^{3i}
τ_5(B)	0.89	0.89	0.88	0.88	0.88	0.88	0.87	0.88	0.89	0.87
O–B	1.65	1.65	1.65	1.65	1.65	1.65	1.65	1.65	1.64	1.64
av. B–C_{Ar}	1.63	1.63	1.63	1.63	1.63	1.63	1.63	1.63	1.63	1.63
THC (%)	89.1	89.8	89.7	89.7	89.6	89.3	89.5	88.6	89.7	90.6

B^{xy}	B^{3s}	B^{4a}	B^{4b}	B^{4c}	B^{4d}	B^{4e}	B^{4f}	B^{4g}	B^{4h}	B^{4i}
τ_5(B)	0.87	0.88	0.87	0.86	0.88	0.88	0.91	0.91	0.87	0.88
O–B	1.65	1.66	1.64	1.64	1.65	1.65	1.65	1.65	1.64	1.64
av. B–C_{Ar}	1.63	1.63	1.63	1.63	1.63	1.63	1.63	1.63	1.63	1.63
THC (%)	89.7	88.8	89.2	91.1	89.8	88.7	88.4	89.3	91.5	90.5

B^{xy}	B^{4j}	B^{5a}	B^{6a}	BCF
τ_5(B)	0.88	0.88	0.88	0.92
O–B	1.66	1.66	1.65	1.64
av. B–C_{Ar}	1.63	1.62	1.63	1.62
THC (%)	87.3	89.3	90.1	92.5

1.4.11.3 Selected frontier molecular orbitals (FMOs) for $\mathbf{B}^{xy}$

FMOs including the p orbitals of the boron, calculated at the *ω*B97X-D/6-311+G(d,p)//*ω*B97X-D/6-31G(d,p) level, are shown in Figure 1.S12.



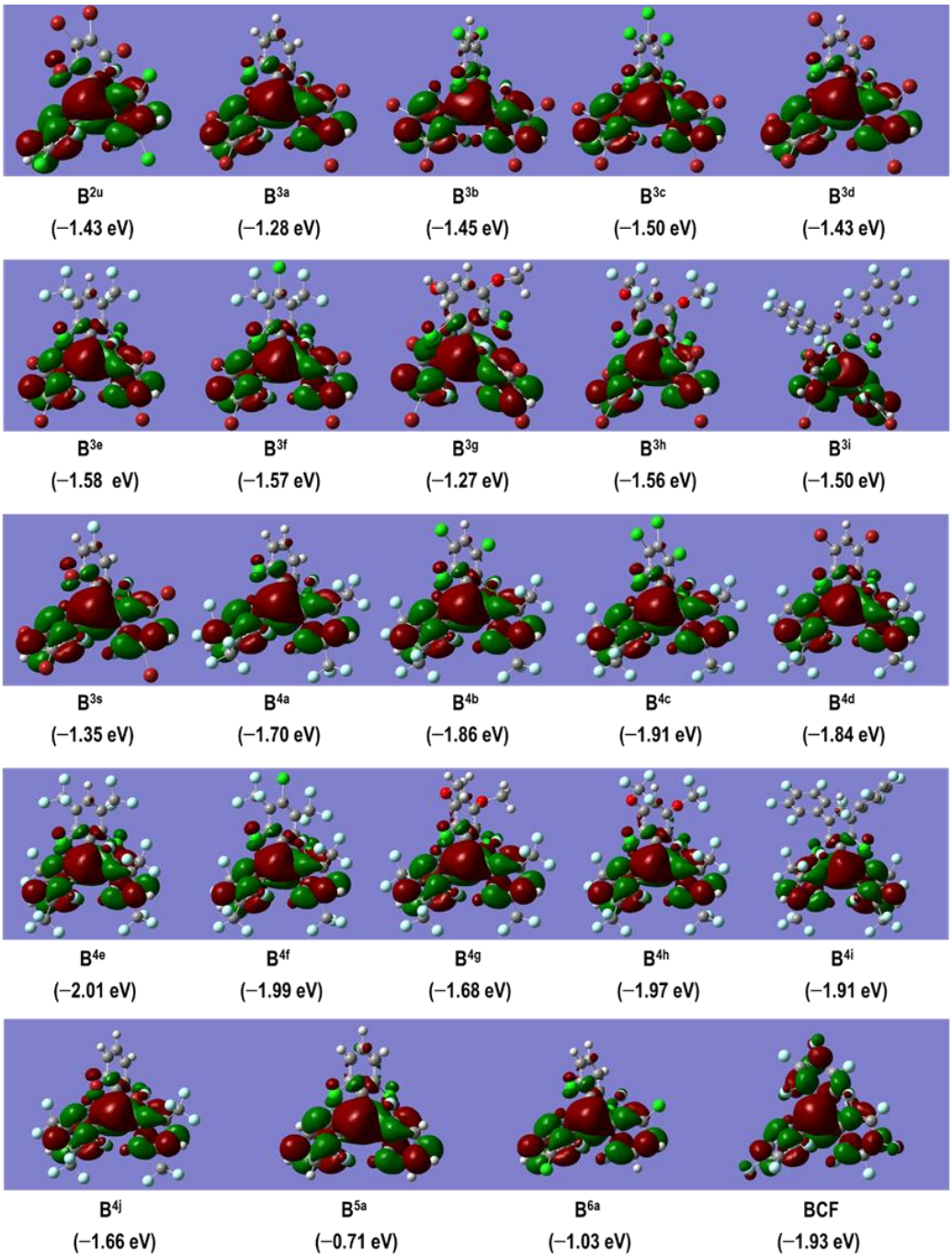


Figure 1.S12. Selected FMOs (LUMO in most cases) for $\mathbf{B}^{xy}$

1.4.11.4 Results of AIM analysis

The AIM calculation for TS_{MTHP} was carried out using AIMAll program (Version 19.10.12),[76] in which wave functional files were prepared based on the SCF density at the aforementioned level of theory (Figure 1.S13 and Table 1.S5).

The AIM bond paths (white lines), bond critical points (BCP; $e\ r_{Bohr}^{-3}$; green dots; their numbers are also shown)

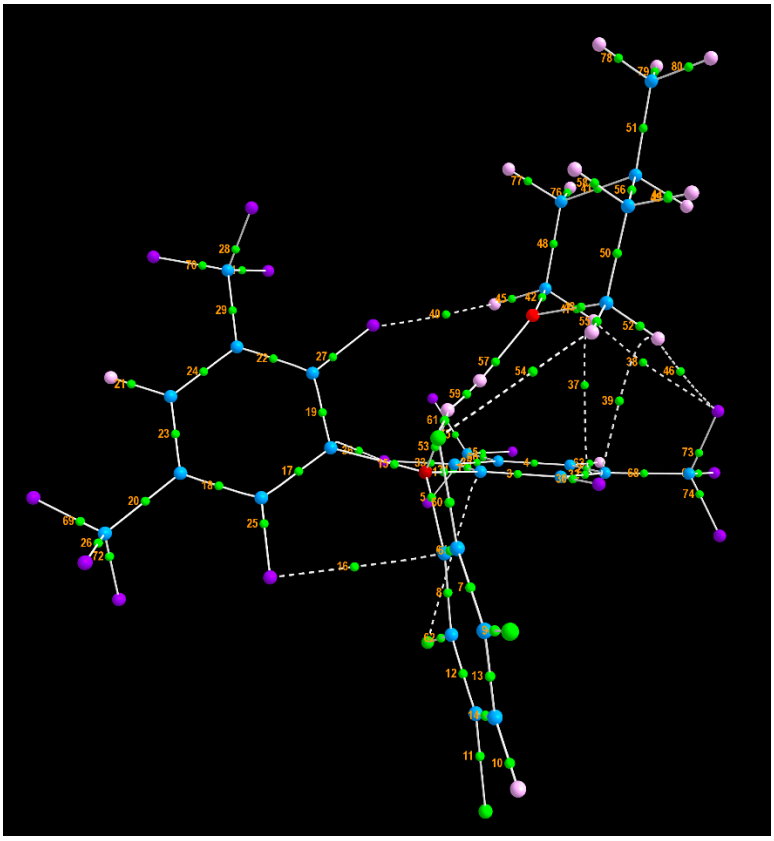


Figure 1.S13. Selected AIM results for TS_{MTHP}. NCIs are shown in dashed white lines.

Table 1.S5. Selected AIM parameters for TS_{MTHP}

BCP #	*Atoms*	*Rho*	*DelSqRho*	*DI(A|B)*	*G*	*V*
1	C39 - C40	0.31064	-0.872215	1.313351	0.108375	-0.434803
2	C1 - C3	0.308379	-0.851426	1.352646	0.104611	-0.422078
3	C38 - C40	0.311195	-0.873115	1.314894	0.11105	-0.440378
4	C2 - C3	0.309371	-0.8565	1.36354	0.105145	-0.424415
5	C4 - B32	0.158987	-0.131622	0.468655	0.120762	-0.274429
6	C4 - C5	0.299061	-0.791262	1.348826	0.103678	-0.405171
7	C5 - C7	0.306155	-0.834229	1.314593	0.10023	-0.409016
8	C4 - C6	0.29849	-0.790667	1.328525	0.101827	-0.401322
9	C7 - Cl66	0.201781	-0.306528	1.116421	0.067615	-0.211863
10	C9 - H35	0.283391	-0.989694	0.926677	0.034697	-0.316818
11	C8 - Cl67	0.20246	-0.308815	1.118565	0.067846	-0.212896

12	C6 - C8	0.307415	-0.840735	1.319861	0.101085	-0.412354
13	C7 - C9	0.312872	-0.88084	1.354102	0.107073	-0.434356
14	C8 - C9	0.311935	-0.876592	1.345696	0.10574	-0.430628
15	C10 - B32	0.159275	-0.096169	0.466036	0.129069	-0.28218
16	C4 - F16	0.012244	0.048313	0.041486	0.010718	-0.009358
17	C10 - C11	0.310338	-0.868787	1.331531	0.108517	-0.434231
18	C11 - C13	0.311035	-0.875057	1.282576	0.102104	-0.422972
19	C10 - C12	0.311909	-0.87901	1.321812	0.111147	-0.442047
20	C13 - C43	0.267043	-0.69597	0.890759	0.059355	-0.292702
21	C15 - H37	0.286189	-1.01143	0.910493	0.033453	-0.319764
22	C12 - C14	0.314646	-0.893078	1.301642	0.106271	-0.435812
23	C13 - C15	0.310053	-0.859738	1.369829	0.105765	-0.426464
24	C14 - C15	0.308246	-0.851838	1.351468	0.104228	-0.421416
25	C11 - F16	0.26331	0.212207	0.822398	0.406292	-0.759532
26	C43 - F49	0.278238	-0.242389	0.697554	0.329099	-0.718796
27	C12 - F17	0.252922	0.229359	0.801062	0.390441	-0.723543
28	C44 - F45	0.276378	-0.244356	0.694471	0.324696	-0.710481
29	C14 - C44	0.267762	-0.700142	0.892702	0.060055	-0.295145
30	F18 - C38	0.256581	0.208177	0.809046	0.392679	-0.733313
31	B32 - C40	0.156459	-0.078992	0.455046	0.129087	-0.277921
32	C1 - C38	0.312969	-0.884089	1.286575	0.104446	-0.429914
33	F19 - C39	0.263238	0.217947	0.819929	0.4074	-0.760313
34	C41 - F55	0.279748	-0.239787	0.699097	0.332896	-0.725738
35	C2 - C39	0.31178	-0.878491	1.284524	0.102773	-0.425169
36	C10 - F19	0.011967	0.047838	0.040173	0.010441	-0.008923
37	C1 - H23	0.007599	0.023011	0.017925	0.004739	-0.003725
38	H23 - F51	0.00524	0.019774	0.015257	0.004205	-0.003467
39	F18 - H26	0.008384	0.03625	0.018069	0.007745	-0.006428
40	F17 - H24	0.010454	0.044296	0.029192	0.00947	-0.007866
41	C57 - C59	0.241527	-0.545887	0.961434	0.056133	-0.248737
42	O20 - C21	0.235168	-0.238496	0.807561	0.246988	-0.5536
43	O20 - C22	0.2361	-0.246077	0.81482	0.24665	-0.554819
44	C57 - H58	0.273178	-0.904965	0.921413	0.042758	-0.311757
45	C21 - H24	0.287117	-1.010442	0.895638	0.034324	-0.321259
46	H26 - F51	0.00564	0.021329	0.018171	0.004538	-0.003743
47	C21 - H23	0.280653	-0.958771	0.892506	0.03672	-0.313132
48	C21 - C59	0.251465	-0.601381	0.966286	0.05836	-0.267065
49	C25 - H28	0.273152	-0.907715	0.938973	0.042059	-0.311046

50	C22 - C25	0.251396	-0.601236	0.967259	0.058082	-0.266472
51	C57 - C62	0.243315	-0.557879	0.984019	0.056237	-0.251943
52	C22 - H26	0.282229	-0.969869	0.893733	0.035863	-0.314193
53	H30 - B32	0.103927	0.16877	0.257519	0.12025	-0.198308
54	H27 - Cl33	0.005414	0.016203	0.03026	0.003268	-0.002485
55	C22 - H27	0.284563	-0.993078	0.905021	0.034726	-0.317723
56	C25 - C57	0.241359	-0.544957	0.961003	0.056128	-0.248496
57	O20 - H31	0.101652	0.101265	0.23731	0.068999	-0.112682
58	C25 - H29	0.273255	-0.906542	0.932077	0.04207	-0.310775
59	H30 - H31	0.182147	-0.548597	0.425402	0.024519	-0.186187
60	C5 - Cl33	0.194556	-0.281643	1.083614	0.065706	-0.201822
61	H30 - Cl33	0.019899	0.066945	0.091872	0.014681	-0.012627
62	C6 - Cl34	0.199058	-0.295167	1.095549	0.067247	-0.208286
63	C3 - H36	0.286053	-1.01027	0.910389	0.033474	-0.319516
64	Cl34 - C40	0.013628	0.046576	0.071868	0.009987	-0.008329
65	C41 - F54	0.275133	-0.222841	0.690078	0.328037	-0.711784
66	C2 - C41	0.267081	-0.695885	0.889959	0.059224	-0.292419
67	C42 - F52	0.277385	-0.21626	0.693527	0.33436	-0.722786
68	C1 - C42	0.268142	-0.701741	0.895113	0.060773	-0.296982
69	C43 - F50	0.274885	-0.222863	0.689287	0.327546	-0.710809
70	C44 - F47	0.276263	-0.219748	0.691933	0.33118	-0.717297
71	C44 - F46	0.27795	-0.244301	0.696846	0.328001	-0.717077
72	C43 - F48	0.278913	-0.242029	0.698318	0.330603	-0.721713
73	C42 - F51	0.269689	-0.261432	0.685694	0.306104	-0.677566
74	C42 - F53	0.281379	-0.23396	0.70221	0.337794	-0.734078
75	C41 - F56	0.277855	-0.244844	0.696376	0.327676	-0.716564
76	C59 - H61	0.273087	-0.90734	0.938758	0.042068	-0.310971
77	C59 - H60	0.273554	-0.90861	0.93041	0.041646	-0.310445
78	C62 - H64	0.271525	-0.896548	0.953923	0.04304	-0.310216
79	C62 - H65	0.272522	-0.90359	0.95837	0.042882	-0.311662
80	C62 - H63	0.272474	-0.903232	0.95853	0.042915	-0.311637

1.5 References and notes

1. Vogiatzis, K. D.; Polynski, M. V.; Kirkland, J. K.; Townsend, J.; Hashemi, A.; Liu, C.; Pidko, E. A. *Chem. Rev.* **2019**, *119*, 2453–2523.
2. Toyao, T.; Maeno, Z.; Takakusagi, S.; Kamachi, T.; Takigawa, I.; Shimizu, K. *ACS Catal.* **2020**, *10*, 2260–2297.
3. Foscato, M.; Jensen, V. R. *ACS Catal.* **2020**, *10*, 2354–2377.

4. Matsubara, S. *Chem. Lett.* **2021**, *50*, 475–481.
5. Zahrt, A. F.; Athavale, S. V.; Denmark, S. E. *Chem. Rev.* **2020**, *120*, 1620–1689.
6. Rinehart, N. I.; Zahrt, A. F.; Henle, J. J.; Denmark, S. E. *Acc. Chem. Res.* **2021**, *54*, 2041–2054.
7. Crawford, J. M.; Kingston, C.; Toste, F. D.; Sigman, M. S. *Acc. Chem. Res.* **2021**, *54*, 3136–3148.
8. Liles, J. P.; Rouget-Virbel, C.; Wahlman, J. L. H.; Rahimoff, R.; Crawford, J. M.; Medlin, A.; O'Connor, V. S.; Li, J.; Roytman, V. A.; Toste, F. D.; Sigman, M. S. *Chem* **2023**, *9*, 1518–1537.
9. Chen, H.; Yamaguchi, S.; Morita, Y.; Nakao, H.; Zhai, X.; Shimizu, Y.; Mitsunuma, H.; Kanai, M. *Cell Reports Phys. Sci.* **2021**, *2*, 100679.
10. Gensch, T.; Dos Passos Gomes, G.; Friederich, P.; Peters, E.; Gaudin, T.; Pollice, R.; Jorner, K.; Nigam, A.; Lindner-D'Addario, M.; Sigman, M. S.; Aspuru-Guzik, A. *J. Am. Chem. Soc.* **2022**, *144*, 1205–1217.
11. Xu, J.; Grosslight, S.; Mack, K. A.; Nguyen, S. C.; Clagg, K.; Lim, N.-K.; Timmerman, J. C.; Shen, J.; White, N. A.; Sirois, L. E.; Han, C.; Zhang, H.; Sigman, M. S.; Gosselin, F. *J. Am. Chem. Soc.* **2022**, *144*, 20955–20963.
12. Karl, T. M.; Bouayad-Gervais, S.; Hueffel, J. A.; Sperger, T.; Wellig, S.; Kaldas, S. J.; Dabranskaya, U.; Ward, J. S.; Rissanen, K.; Tizzard, G. J.; Schoenebeck, F. *J. Am. Chem. Soc.* **2023**, *145*, 15414–15424.
13. Goebel, J. F.; Löffler, J.; Zeng, Z.; Handelmann, J.; Hermann, A.; Rodstein, I.; Gensch, T.; Gessner, V. H.; Gooßen, L. J. *Angew. Chem., Int. Ed.* **2023**, *62*, e202216160.
14. Huang, H.; Zong, H.; Bian, G.; Yue, H.; Song, L. *J. Org. Chem.* **2014**, *79*, 9455–9464.
15. See, X. Y.; Wen, X.; Wheeler, T. A.; Klein, C. K.; Goodpaster, J. D.; Reiner, B. R.; Tonks, I. A. *ACS Catal.* **2020**, *10*, 13504–13517.
16. Mukai, M.; Nagao, K.; Yamaguchi, S.; Ohmiya, H. *Bull. Chem. Soc. Jpn.* **2022**, *95*, 271–277.
17. Wang, J.-W.; Li, Z.; Liu, D.; Zhang, J.-Y.; Lu, X.; Fu, Y. *J. Am. Chem. Soc.* **2023**, *145*, 10411–10421.
18. Cordova, M.; Wodrich, M. D.; Meyer, B.; Sawatlon, B.; Corminboeuf, C. *ACS Catal.* **2020**, *10*, 7021–7031.
19. Stephan, D. W.; Erker, G. *Angew. Chem., Int. Ed.* **2015**, *54*, 6400–6441.
20. Jupp, A. R.; Stephan, D. W. *Trends Chem.* **2019**, *1*, 35–48.
21. Weicker, S. A.; Stephan, D. W. *Bull. Chem. Soc. Jpn.* **2015**, *88*, 1003–1016.
22. Scott, D. J.; Fuchter, M. J.; Ashley, A. E. *Chem. Soc. Rev.* **2017**, *46*, 5689–5700.
23. Hoshimoto, Y.; Ogoshi, S. *ACS Catal.* **2019**, *9*, 5439–5444.
24. Fasano, V.; Ingleson, M. J. *Synthesis* **2018**, *50*, 1783–1795.
25. Paradies, J. *Acc. Chem. Res.* **2022**, *56*, 821–834.
26. Feng, X.; Du, H. *Tetrahedron Lett.* **2014**, *55*, 6959–6964.
27. Gyömöre, Á.; Bakos, M.; Földes, T.; Pápai, I.; Domján, A.; Soós, T. *ACS Catal.* **2015**, *5*, 5366–5372.
28. Dorkó, É.; Szabó, M.; Kótai, B.; Pápai, I.; Domján, A.; Soós, T. *Angew. Chem., Int. Ed.* **2017**, *56*, 9512–9516.
29. Sapsford, J. S.; Scott, D. J.; Allcock, N. J.; Fuchter, M. J.; Tighe, C. J.; Ashley, A. E. *Adv. Synth. Catal.* **2018**, *360*, 1066–1071.
30. Hoshimoto, Y.; Kinoshita, T.; Hazra, S.; Ohashi, M.; Ogoshi, S. *J. Am. Chem. Soc.* **2018**, *140*, 7292–7300.
31. Zhao, J.; Liu, S.; Liu, S.; Ding, W.; Liu, S.; Chen, Y.; Du, P. *J. Org. Chem.* **2022**, *87*, 1194–1207.

32. Bijoy, R.; Agarwala, P.; Roy, L.; Thorat, B. N. *Org. Process Res. Dev.* **2022**, *26*, 480–492.
33. Samoilov, V.; Ni, D.; Goncharova, A.; Zarezin, D.; Kniazeva, M.; Ladesov, A.; Kosyakov, D.; Bermeshev, M.; Maximov, A. *Molecules* **2020**, *25*, 1723.
34. Bryan, M. C.; Dunn, P. J.; Entwistle, D.; Gallou, F.; Koenig, S. G.; Hayler, J. D.; Hickey, M. R.; Hughes, S.; Kopach, M. E.; Moine, G.; Richardson, P.; Roschangar, F.; Steven, A.; Weiberth, F. J. *Green Chem.* **2018**, *20*, 5082–5103.
35. Murugesan, K.; Senthamarai, T.; Chandrashekhar, V. G.; Natte, K.; Kamer, P. C. J.; Beller, M.; Jagadeesh, R. V. *Chem. Soc. Rev.* **2020**, *49*, 6273–6328.
36. Roughley, S. D.; Jordan, A. M. *J. Med. Chem.* **2011**, *54*, 3451–3479.
37. Carden, J. L.; Dasgupta, A.; Melen, R. L. *Chem. Soc. Rev.* **2020**, *49*, 1706–1725.
38. He, J.; Rauch, F.; Finze, M.; Marder, T. B. *Chem. Sci.* **2021**, *12*, 128–147.
39. Kumar, G.; Roy, S.; Chatterjee, I. *Org. Biomol. Chem.* **2021**, *19*, 1230–1267.
40. Berger, S. M.; Ferger, M.; Marder, T. B. *Chem. Eur. J.* **2021**, *27*, 7043–7058.
41. Das, S.; Turnell-Ritson, R. C.; Dyson, P. J.; Corminboeuf, C. *Angew. Chem., Int. Ed.* **2022**, *61*, e202208987.
42. Saito, N.; Nawachi, A.; Kondo, Y.; Choi, J.; Morimoto, H.; Ohshima, T. *Bull. Chem. Soc. Jpn.* **2023**, *96*, 465–474.
43. Collins, K. D.; Glorius, F. *Nat. Chem.* **2013**, *5*, 597–601.
44. Collins, K. D.; Glorius, F. *Acc. Chem. Res.* **2015**, *48*, 619–627.
45. Hashimoto, T.; Asada, T.; Ogoshi, S.; Hoshimoto, Y. *Sci. Adv.* **2022**, *8*, eade0189.
46. Erős, G.; Nagy, K.; Mehdi, H.; Pápai, I.; Nagy, P.; Király, P.; Tárkányi, G.; Soós, T. *Chem. Eur. J.* **2012**, *18*, 574–585.
47. Dorkó, É.; Kótai, B.; Földes, T.; Gyömöre, Á.; Pápai, I.; Soós, T. *J. Organomet. Chem.* **2017**, *847*, 258–262.
48. Erdmann, P.; Greb, L. *Angew. Chem., Int. Ed.* **2022**, *61*, e202114550.
49. Sakuraba, M.; Morishita, T.; Hashimoto, T.; Ogoshi, S.; Hoshimoto, Y. *Synlett* **2023**, *34*, 2187–2192.
50. Fasano, V.; Radcliffe, J. E.; Ingleson, M. J. *ACS Catal.* **2016**, *6*, 1793–1798.
51. The GPy authors. GPy: A Gaussian process framework in python. http://github.com/SheffieldML/Gpy.
52. Kondo, M.; Wathsala, H. D. P.; Sako, M.; Hanatani, Y.; Ishikawa, K.; Hara, S.; Takaai, T.; Washio, T.; Takizawa, S.; Sasai, H. *Chem. Commun.* **2020**, *56*, 1259–1262.
53. Rodrigues Silva, D.; de Azevedo Santos, L.; Freitas, M. P.; Fonseca Guerra, C.; Hamlin, T. A. *Chem. Asian J.* **2020**, *15*, 4043–4054.
54. Timoshkin, A. Y.; Davydova, E. I.; Sevastianova, T. N.; Suvorov, A. V.; Schaefer, H. F. *Int. J. Quantum Chem.* **2002**, *88*, 436–440.
55. Kumar, P. S. V.; Raghavendra, V.; Subramanian, V. *J. Chem. Sci.* **2016**, *128*, 1527–1536.
56. Macchi, P.; Sironi, A. *Coord. Chem. Rev.* **2003**, *238–239*, 383–412.
57. Bhagat, M. N.; Bennett, C. K.; Chang, G.-F.; Zhu, Y.; Raghuraman, A.; Belowich, M. E.; Nguyen, S. T.; Broadbelt, L. J.; Notestein, J. M. *ACS Catal.* **2019**, *9*, 9663–9670.
58. Andrea, K. A.; Kerton, F. M. *ACS Catal.* **2019**, *9*, 1799–1809.
59. Prakash, M.; Itoh, Y.; Fujiwara, Y.; Takahashi, Y.; Takada, Y.; Mellini, P.; Elboray, E. E.; Terao, M.;

Yamashita, Y.; Yamamoto, C.; Yamaguchi, T.; Kotoku, M.; Kitao, Y.; Singh, R.; Roy, R.; Obika, S.; Oba, M.; Wang, D. O.; Suzuki, T. *J. Med. Chem.* **2021**, *64*, 15810–15824.

60. Godfrey, N. A.; Schatz, D. J.; Pronin, S. V. *J. Am. Chem. Soc.* **2018**, *140*, 12770–12774.
61. Pallesen, J.; Møllerud, S.; Frydenvang, K.; Pickering, D. S.; Bornholdt, J.; Nielsen, B.; Pasini, D.; Han, L.; Marconi, L.; Kastrup, J. S.; Johansen, T. N. *ACS Chem. Neurosci.* **2019**, *10*, 1841–1853.
62. Benke, B. P.; Madhavan, N. *Bioorganic Med. Chem.* **2015**, *23*, 1413–1420.
63. Zhao, M.; Robert, D.; Jung, L. *Eur. J. Med. Chem.* **1993**, *28*, 949–954.
64. Beckett, M. A.; Strickland, G. C.; Holland, J. R.; Varma, K. S. *Polymer* **1996**, *37*, 4629–4631.
65. Pal, M.; Parasuraman, K.; Yeleswarapu, K. R. *Org. Lett.* **2003**, *5*, 349–352.
66. Kwong, F. Y.; Klapars, A.; Buchwald, S. L. *Org. Lett.* **2002**, *4*, 581–584.
67. Frisch, M. J.; Trucks, G. W.; Schlegel, H. B.; Scuseria, G. E.; Robb, M. A.; Cheeseman, J. R.; Scalmani, G.; Barone, V.; Petersson, G. A.; Nakatsuji, H.; Li, X.; Caricato, M.; Marenich, A. V.; Bloino, J.; Janesko, B. G.; Gomperts, R.; Mennucci, B.; Hratchian, H. P.; Ortiz, J. V.; Izmaylov, A. F.; Sonnenberg, J. L.; Williams-Young, D.; Ding, F.; Lipparini, F.; Egidi, F.; Goings, J.; Peng, B.; Petrone, A.; Henderson, T.; Ranasinghe, D.; Zakrzewski, V. G.; Gao, J.; Rega, N.; Zheng, G.; Liang, W.; Hada, M.; Ehara, M.; Toyota, K.; Fukuda, R.; Hasegawa, J.; Ishida, M.; Nakajima, T.; Honda, Y.; Kitao, O.; Nakai, H.; Vreven, T.; Throssell, K.; Montgomery, J. A., Jr.; Peralta, J. E.; Ogliaro, F.; Bearpark, M. J.; Heyd, J. J.; Brothers, E. N.; Kudin, K. N.; Staroverov, V. N.; Keith, T. A.; Kobayashi, R.; Normand, J.; Raghavachari, K.; Rendell, A. P.; Burant, J. C.; Iyengar, S. S.; Tomasi, J.; Cossi, M.; Millam, J. M.; Klene, M.; Adamo, C.; Cammi, R.; Ochterski, J. W.; Martin, R. L.; Morokuma, K.; Farkas, O.; Foresman, J. B.; Fox, D. J. Gaussian, Inc., Wallingford CT, 2016.
68. Chai, J. D.; Head-Gordon, M. *Phys. Chem. Chem. Phys.* **2008**, *10*, 6615–6620.
69. Fukui, K. *Acc. Chem. Res.* **1981**, *14*, 363–368.
70. Becke, A. D.; Johnson, E. R. *J. Chem. Phys.* **2005**, *122*, 154104.
71. Grimme, S.; Antony, J.; Ehrlich, S.; Krieg, H. *J. Chem. Phys.* **2010**, *132*, 154104.
72. Johnson, E. R.; Becke, A. D. *J. Chem. Phys.* **2005**, *123*, 024101.
73. Grimme, S.; Ehrlich, S.; Goerigk, L. *J. Comput. Chem.* **2011**, *32*, 1456–1465.
74. Erdmann, P.; Greb, L. *Angew. Chem., Int. Ed.* **2022**, *61*, e202114550.
75. Reineke, M. H.; Sampson, M. D.; Rheingold, A. L.; Kubiak, C. P. *Inorg. Chem.* **2015**, *54*, 3211–3217.
76. Höpfl, H. *J. Organomet. Chem.* **1999**, *581*, 129−149.
77. Keith, T. A. AIMAll (Version 19.10.12, Professional): Computational Chemistry Using the Quantum Theory of Atoms in Molecules (QTAIM). TK Gristmill Software, Overland Park, KS, 2017. Available at: http://aim.tkgristmill.com/.

Chapter 2

An Isolated Lithium *ortho*-Carboranyl Cuprate Complex for the Synthesis of Multiple-Carborane-Substituted Arenes from (Hetero)Aryl Bromides and Chlorides

Abstract: Carborane-substituted arenes have emerged as versatile building blocks in medicinal chemistry, materials science, and coordination chemistry owing to the unique three-dimensional aromaticity, exceptional stability, and bioisosteric properties of carboranes. However, the existing synthetic routes to carborane-substituted arenes via C–C bond formation often rely on complex, laborious, and poorly reproducible *in-situ* procedures using aryl iodides, thus severely limiting the scope of their practical applications. As the synthesis of *o*-carboranyl groups substituted arenes is essential for introducing these moieties as substituents on BAr_3 the primary focus of this study. Here, the author reports the isolation and characterization of a lithium bis(*o*-carboran-1-yl)cuprate complex (**Li/Cu-1**) that enables the efficient "dump-and-stir" synthesis of carborane-substituted arenes from readily available aryl bromides and chlorides. Remarkably, isophthalonitrile functions as a ligand for the Li center in **Li/Cu-1**, leaving the carboranyl-cuprate unit available for the oxidative addition to aryl halides. This represents a paradigm shift from traditional approaches using pyridines as ligands for Cu centers. Our method provides access to a diverse array of unprecedented molecules, including multiple-carborane-substituted or carborane-fused arenes, thereby converting a hitherto difficult transformation in synthetic chemistry into a practical and scalable process.

2.1 Introduction

The reaction system optimized in Chapter 1 could not be applied to natural amino acid derivatives, prompting further catalyst screening to develop a reductive alkylation system. DL-valine methyl ester, easily purified from its hydrochloride salt, was employed as a model substrate (Figure 2.1A); however, the reported BAr_3 provided only low to moderate yields, making multidimensional regression modeling unreasonable. To rationalize catalyst performance, the relative Gibbs energy values ($\Delta G_{PO}°$) [kcal mol^{-1}] for the formation of $Et_3PO{-}BAr_3$ adducts with respect to [Et_3PO + BAr_3] were calculated as a descriptor for the relative comparison of the Lewis acidity.[1] These theoretical values, summarized in Figure 2.1A, revealed that lower yields are obtained when the $\Delta G_{PO}°$ values are significantly negative or nearly zero, albeit it suggests that a better yield would be obtained with a borane having $\Delta G_{PO}°$ values around –15 to –10. Conventional substituents introduced on the Ar groups of BAr_3 have been predominantly limited to alkyl, fluoro, chloro, and trifluoromethyl groups; therefore, the author systematically computed $\Delta G_{PO}°$ values for BAr_3 bearing hitherto unexplored substituents. Notably, a BAr_3 featuring *o*-(carboran-1-yl)aryl groups (**B^7**) exhibited $\Delta G_{PO}° = -10.6$ kcal mol^{-1} (Figure 2.1B), indicating its unique reactivity. To access this promising **B^7**, a large-scale synthesis of *o*-carboranyl arenes was required; however, the reported methods for synthesizing *o*-carboranyl arenes suffer from a narrow substrate scope and limited scalability. Consequently, Chapter 2 focuses on developing a practical and scalable route to *o*-carboranyl arenes as precursors for advanced BAr_3 catalysts.

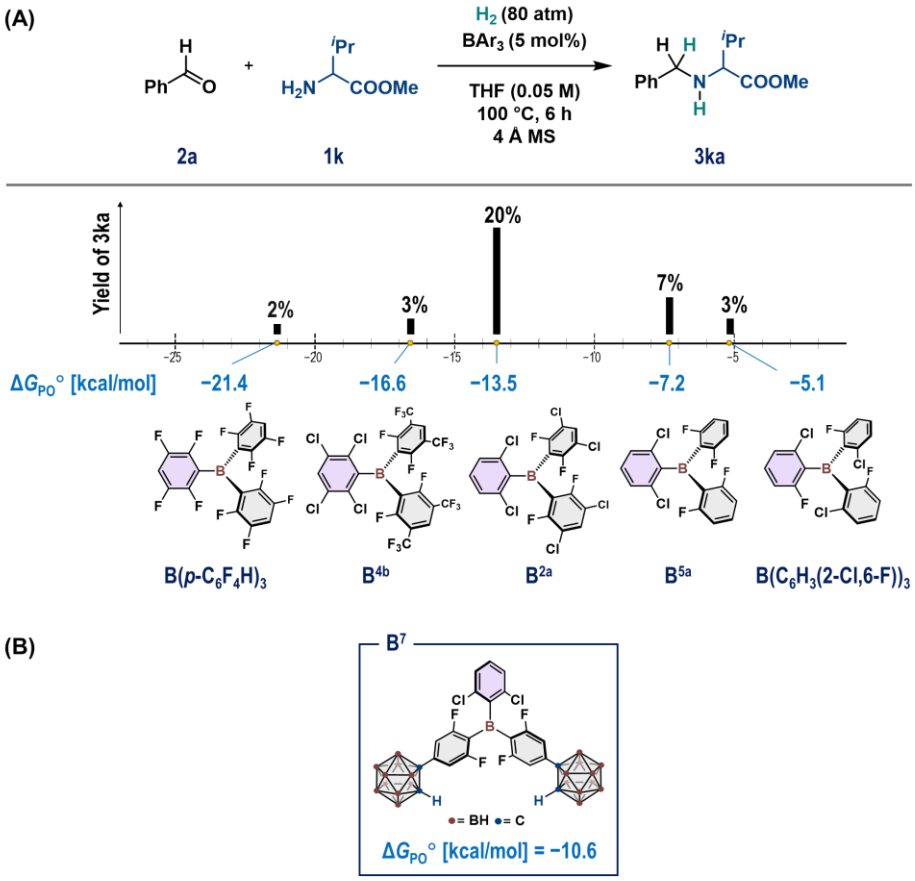


Figure 2.1. Screening for optimal catalysts for reductive alkylation of natural amino acid derivatives. (A) Relationship between $\Delta G_{PO}°$ and reaction yield for selected BAr_3 catalysts. (B) Computed $\Delta G_{PO}°$ values for **B**^{7}

Achieving operational simplicity in molecular synthesis is a key goal in modern synthetic chemistry. Simple and operationally facile methods using well-characterized isolated reagents can considerably expand the scope and applicability of reported synthetic methods by reducing the complex experimental manipulations required for the *in-situ* preparation of reactive species. Such "dump-and-stir" methods are highly desirable, especially for introducing expensive but multifunctional substituents into versatile molecular frameworks. For example, the synthesis of (hetero)arenes bearing *closo*-1,2-carborane (*o*-carborane, *o*-1,2-$C_2B_{10}H_{12}$; Figure 2.2A) via C–C bond formation using isolable and readily available carboranyl-metal nucleophiles and (hetero)aryl electrophiles is highly practical. In fact, such *C*-arylated *o*-carborane derivatives have been extensively applied in diverse fields, including medicinal,[2,3] materials, and coordination chemistry,[4-13] owing to the distinctive properties of carboranes, such as neutron absorption, high thermal stability, high chemical stability toward oxidants and strong acids, three-dimensional electron delocalization (3D aromaticity),[14] remarkable hydrophobicity, and comparable pseudospherical size to both adamantane and the effective spherical volume occupied by a rotating phenyl ring (i.e., bioisosterism).[2,15] Given that a variety of biphenyl-based bioactive compounds have found applications in our daily lives,[16] strategic bioisosteric replacement of one of their phenyl groups with carboranes is worth exploring in the interest of pursuing underexplored molecular applications.[17-19] Unfortunately, hitherto reported synthetic procedures are characterized by a severely limited

range of accessible (*o*-carboran-1-yl)arenes.

Several pioneering methods have been developed for the synthesis of (*o*-carboran-1-yl)arenes via C–C bond formation between *in-situ*-generated *o*-carboranyl-metal (i.e., Cu, Ni, Pd) species and aryl iodides from commercially available *o*-carborane (Figure 2.2A).[20-26] These methods constitute alternative approaches to access this class of compounds without using toxic and explosive decaborane ($B_{10}H_{14}$) under harsh conditions.[2,27] However, these transition-metal-mediated processes usually involve laborious multistep manipulations, including the *in-situ* generation of active *o*-carboranyl-lithium or -magnesium species at low temperatures in ethereal solvents (e.g., THF or 1,2-dimethoxyethane (DME)) and the transmetalation with transition metals followed by coupling with aryl iodides, often requiring solvent exchange to appropriate hydrocarbon solvents (e.g., toluene or xylene),[28,29] which has prevented extending these approaches to more synthetically accessible aryl bromides and chlorides and often result in poor reproducibility. For example, to achieve an efficient C–C bond formation between carboranyl-copper species **CB-Cu$_1$**, which remains elusive,[30] and aryl halides via the so-called Ullman-type mechanism,[31] the equilibrium involving **CB-Cu$_1$**, carboranyl-lithium species (**CB-Li$_1$** and **CB-Li$_2$**),[33] and other copper species (**CB-Li$_1$Cu$_1$** and **CB-Cu$_2$**) should be precisely regulated to avoid undesired side reactions such as the formation of bis-*o*-carborane triggered by **CB-Cu$_2$** (Figure 2.2B).[20,21] Nevertheless, the presence of salts (LiX and CuX) in the equilibrium renders controlling these reactions difficult, and their complete removal during the aforementioned multistep procedures is challenging. In addition, **CB-Cu$_1$** cannot be expected to be sufficiently stable under the hitherto reported reaction conditions, as evident from the low to moderate efficiency described in previous reports.

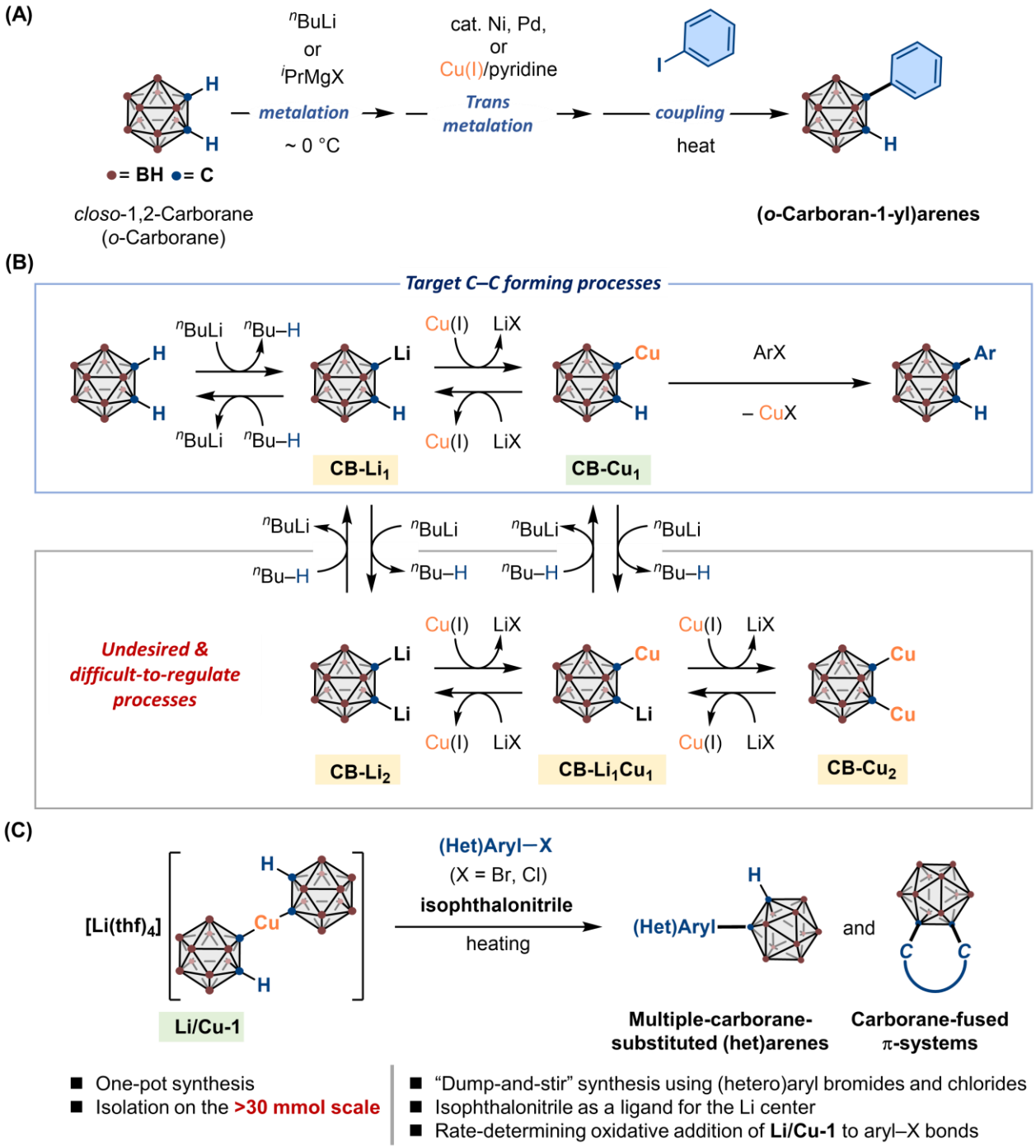


Figure 2.2. Synthesis of (*o*-carboran-1-yl)arenes via C−C bond formation. (A) Schematic representation of reported *in-situ* procedures using *o*-carborane and aryl iodides. (B) Selected species proposed to be generated *in situ* under Ullmann-type conditions using ^{n}BuLi and Cu(I) salts. (C) This work: a 'dump-and-stir' synthesis of multiple-carborane-substituted or carborane-fused (hetero)arenes.

During our investigations to expand the library of triarylboranes,[34,35] the author examined the incorporation of multiple *o*-carboranyl groups in single arenes using readily available CuCl and 1,4-dibromobenzene (**A1**) as a model substrate in the presence of pyridine, which has been proposed as a suitable

ligand for **CB-Cu$_1$** species by Wade and co-workers.[21] However, these reactions are complicated, and 1-bromo-4-(*o*-carboran-1-yl)benzene (**C1**) was predominantly obtained in < 30% yield, even after an extensive screening of conditions (Figure 2.S31), while the yield of the targeted 1,4-bis(*o*-carboran-1-yl)benzene (**B1**) remained < 5% (for the structures of **B1** and **C1**, see Figure 2.3B). A nickel-catalyzed procedure reported by Xie and co-workers[36] was also unsuccessful under the applied conditions using **A1** (Figure 2.S32). Therefore, the author envisioned that a dump-and-stir method using an isolated *o*-carboranyl-copper reagent could potentially afford efficiently multiple-carborane-substituted arenes from readily available aryl halides (Figure 2.2C). Herein, the author reports the development of a decagram-scale (> 30 mmol) synthesis of lithium bis(*o*-carboran-1-yl)cuprate **Li/Cu-1**, which proved to be sufficiently reactive in C–C bond-forming reactions with a variety of (hetero)aryl bromides and chlorides. Moreover, the author demonstrates the key role of isophthalonitrile as a ligand for the Li center in **Li/Cu-1** to effectively stabilize a transition state for the rate-determining oxidative addition step; whereas pyridine- or phosphine-derived ligands, which tend to coordinate to the Cu center, are unsuitable for this reaction. The author also performed preliminary mechanistic studies on the Ullmann-type coupling involving **Li/Cu-1**.

2.2 Results and Discussion

To establish a dump-and-stir method for the efficient synthesis of multiple-carborane-substituted arenes, a readily isolable and well-characterized reagent containing the *o*-carboranyl group is essential. To this end, the author initially isolated (*o*-carboran-1-yl)Li(thf)$_3$ (**Li-1**) (Figure 2.3A), given that the *in-situ* generation of carboranyl-lithium species and subsequent carborane transfer is a common procedure for constructing chemical bonds between *o*-carborane and electrophiles (Figure 2.3A). The molecular structure of **Li-1** was unambiguously confirmed by a single-crystal X-ray diffraction (SC-XRD) analysis (Figure 2.S4). It should be also noted that an identical structure has previously been proposed for **Li-1** by Willans and co-workers based on calculated NMR data.[33] **Li-1** was isolated as a white powder that can be easily handled, whereas isolation of the corresponding **CB-Li** species bearing DME was unsuccessful. Subsequently, the author mixed **Li-1** with CuCl (1.1 equiv) in THF at room temperature, assuming that these compounds would react in a 1:1 stoichiometry to furnish the **CB-Cu$_1$** species shown in Figure 2.2B. However, the author eventually confirmed the formation of unprecedented lithium bis(*o*-carboran-1-yl)cuprate complex **Li/Cu-1**, which was isolated in 94% yield as a brownish solid after optimizing the stoichiometry of CuCl to 0.55 equivalents with respect to **Li-1**.[32] Finally, the author established a straightforward one-pot procedure to synthesize **Li/Cu-1** on a decagram scale (19.9 g, 30.9 mmol, 89% isolated yield) using *o*-carborane (69.3 mmol), ^{n}BuLi (1.0 equiv), and CuCl (0.55 equiv). The molecular structure of **Li/Cu-1** was determined unambiguously via multinuclear NMR and SC-XRD analyses (Figure 2.3A, right). The Cu center in **Li/Cu-1** exhibits a linear geometry with a C1-Cu-C2 angle of 176.73(9)° and is located almost equidistant between the C1 and C2 atoms, whereby the Cu–C1 and Cu–C2 bonds are approximately 1.91 Å. **Li/Cu-1** is stable under an inert-gas atmosphere, showing no observable decomposition after one month, although it decomposes rapidly in the presence of air/moisture. It dissolves in CH_2Cl_2 and ethereal solvents such as THF, DME, and 1,4-dioxane, whereas it exhibits limited solubility in aromatic hydrocarbon solvents such as toluene and $PhCF_3$. On the basis of these properties, the author concluded

that **Li/Cu-1** could potentially serve as a useful reagent for introducing *o*-carboranyl groups into arenes using a dump-and-stir method.

Employing the isolated **Li/Cu-1** reagent facilitated the rapid and thorough optimization of the reaction conditions using **A1** as a model substrate (Figure 2.3B). In the hitherto reported Cu-mediated Ullmann-type coupling reactions for the synthesis of (*o*-carboran-1-yl)arenes, pyridines have been predominantly used as ligands for the Cu center.[21] In fact, the author confirmed that the carboranyl-group transfer ratio (CBT; Figure 2.3B), for which a value of 100% means that two carboranyl groups in a single **Li/Cu-1** molecule are transferred to give **B1**, increased to 37% in the presence of pyridine (yield of **B1** = 10%, yield of **C1** = 54%; run 2) compared to the results without additives (CBT = 26%; run 1). Nevertheless, electron-rich pyridine derivatives such as 4-dimethylaminopyridine (CBT = 13%; run 3) and 4,4'-di-*tert*-butyl-2,2'-bipyridine (CBT = 23%; run 4) did not lead to improved results. Remarkably, the CBT value was significantly enhanced to 60% when 4-cyanopyridine was employed, affording **B1** and **C1** in 25% and 69% yield, respectively (run 5), demonstrating that both carboranyl groups in **Li/Cu-1** can be transferred to electrophiles. The author therefore explored the effectiveness of 3- and 2-cyano-substituted pyridines (runs 6 and 7); however, the CBT values decreased in both cases, although 3-cyanopyridine still afforded better results (CBT = 44%, yield of **B1** = 13%, yield of **C1** = 61%) than pyridine (run 2). Subsequently, the author performed a control experiment using benzonitrile (run 8), confirming that the carboranyl-group transfer from **Li/Cu-1** to **A1** still occurred to produce **B1** (15%) and **C1** (56%). Benzonitrile derivatives have been rarely employed as additives in Cu-mediated C–C bond formation reactions.[31] The addition of isophthalonitrile (run 10) or terephthalonitrile (run 11) resulted in further improved CBT values (64% and 62%, respectively); however, phthalonitrile (CBT = 12%; run 9) and 1,3,5-tricyanobenzene (CBT = 28%; run 12) were ineffective. To confirm the key role of two cyano groups as coordinating units, the author examined electron-deficient and electron-rich benzonitriles (runs 13 and 14), finding that the CBT values considerably decreased compared to those obtained with benzonitrile, isophthalonitrile, and terephthalonitrile (runs 8, 10, and 11). These results demonstrate that the additional cyano groups in isophthalonitrile and terephthalonitrile act not only as electron-withdrawing substituents, but also as secondary coordination sites (*vide infra*). Further modification of isophthalonitrile by substituting H atoms with F atoms also failed to improve the results (CBT = 40%, yield of **B1** = 13%, yield of **C1** = 54%; run 15). The formation of **B1** and **C1** was not observed when using PCy_3 or benzyl cyanide, and only a trace amount of **C1** (7%) was obtained in the presence of Cl_3CCN.

Given these results, the author subsequently employed isophthalonitrile to perform the solvent screening (Figure 2.3C). Interestingly, ethereal solvents (i.e., THF, DME, or 1,4-dioxane) that fully dissolve **Li/Cu-1** furnished rather low CBT values (< 45%). A higher CBT value of 66%, similar to that obtained in toluene (64%), was obtained when the reaction was conducted in *n*-hexane, even though the system appeared heterogeneous. Cyclohexane also afforded **B1** (25%) and **C1** (75%), resulting in a CBT of 63%. The corresponding carboranyl transfer did not proceed satisfactorily in $PhCF_3$, DMF, CH_3CN, or $CHCl_3$. Considering the limited solubility of most (hetero)aryl bromides in hexanes, the author used toluene when exploring the substrate scope. It should also be noted that a significant decrease in CBT values was observed in the co-presence of CuCl and/or LiCl additives, both of which coexist in the equilibrium under the reported *in-*

situ experimental conditions (Figure 2.2B), demonstrating the importance of using the isolated **Li/Cu-1** (Figure 2.S3, runs 10-13). After optimization of other reaction parameters (Figure 2.S3), the dump-and-stir protocol for synthesizing **B1** as the main product was set as follows: **A1** (0.25 mmol, [**A1**] = 0.5 M) was treated with two equivalents of **Li/Cu-1** (i.e., 1.00 mmol of *o*-carboranyl groups) and isophthalonitrile in toluene, and the resultant heterogeneous mixture was stirred for 16 h at 100 °C (Figure 2.3D). Under these conditions, **B1** was isolated in 98% yield (i.e., 0.49 mmol of *o*-carboranyl units were incorporated) by column chromatography, while 0.46 mmol of *o*-carborane was recovered, demonstrating that the present procedure allows minimizing the loss of valuable carboranyl groups. Isophthalonitrile was also recovered in 94% yield (0.47 mmol). Therefore, our method is characterized by operational simplicity and high efficiency in introducing multiple *o*-carboranyl groups into aryl cores and in recovering the valuable *o*-carborane reagent.

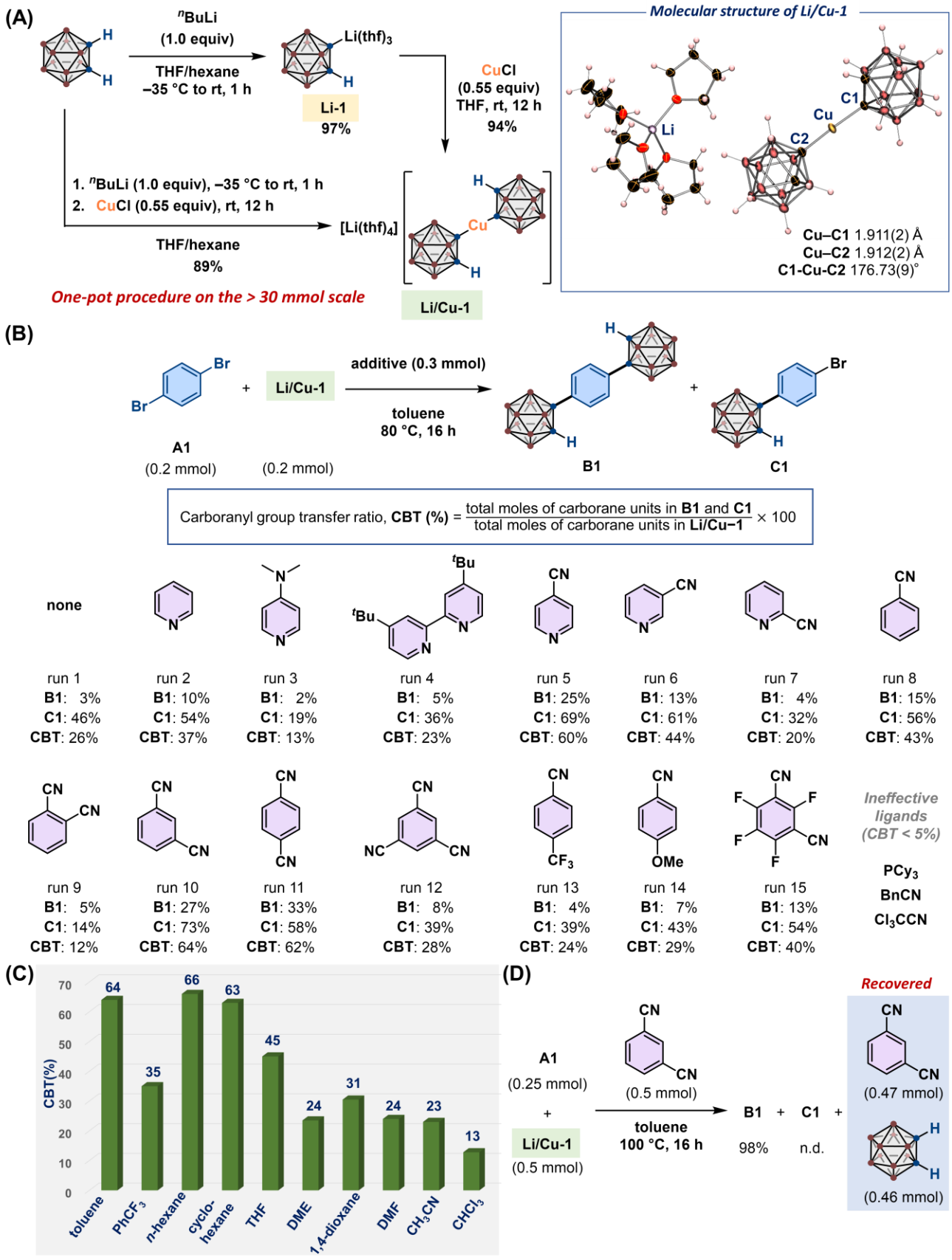


Figure 2.3. Isolation and application of lithium bis(*o*-carboranyl)cuprate Li/Cu-1. (A) Synthesis of **Li/Cu-1**. The molecular structure of **Li/Cu-1** in the crystalline state was determined by an SC-XRD analysis (thermal

ellipsoids are shown at 30% probability). (B) Ligand screening for the coupling reaction between **A1** and **Li/Cu-1**. (C) Solvent effects. (D) Optimized reaction conditions for the synthesis of **B1**. Isolated yields are shown. For carborane or carboranyl groups, brown spheres represent B–H units and blue spheres represent C atoms, as shown in Figure 2.2A.

Next, the author applied the optimized conditions for the synthesis of a variety of multiple-carboranyl-substituted arenes (**B2**–**B12**) from the corresponding aryl bromides (**A2**–**A12**) (Figure 2.4) using equimolar amounts of **Li/Cu-1** and isophthalonitrile with respect to the number of Br atoms in **each substrate**. For example, the reaction between 1,3,5-$Br_3C_6H_3$ (**A2,** 0.25 mmol) and **Li/Cu-1** (0.75 mmol, i.e., 1.50 mmol of *o*-carboranyl units) proceeded in the presence of isophthalonitrile (0.75 mmol) to afford tris(*o*-carboran-1-yl)benzene (**B2**), which was isolated in 90% yield and unambiguously characterized by an SC-XRD analysis. Importantly, **B2** was also synthesized from 1,3,5-$Cl_3C_6H_3$ (**A2′**) under the optimized reaction conditions in 71% yield, demonstrating the wide applicability of the present method for incorporating multiple *o*-carboranyl groups in aryl cores. In fact, *o*-carboranyl groups were multiply introduced into naphthalene and pyrene cores in **A3** and **A4**, respectively, to afford **B3** (86%) and **B4** (63%). The solid-state structures of these compounds revealed distorted arene frameworks resulting from the steric repulsion between the bulky *o*-carboranyl groups and the adjacent C–H bonds. These results were also reproduced in the DFT-optimized gas-phase structures of **B3** and **B4** (Figure 2.S42). In particular, the repulsion between the C–H bonds in the pyrene K-region (i.e., C7–H, C8–H, C13–H, and C14–H) and the adjacent *o*-carboranyl C/B–H bonds induced helicity in **B4** with C1–C5–C6–C7, C2-C11-C9-C8, C3-C10-C12-C13, and C4-C16-C15-C14 torsion angles of −21.4(5)°, 19.6(5)°, 18.9(5)°, and −17.7(5)°, respectively. 1,3-Dibromoazulene (**A5**) was successfully converted into 1,3-bis(*o*-carboran-1-yl)azulene (**B5**), which was isolated as a purple solid in 95% yield and unambiguously characterized by an SC-XRD analysis. 1,4-Dibromobenzenes **A6** and **A8**, which bear fluorine or methoxy groups at the 2,5-positions, afforded the corresponding bis-carboranyl benzenes (**B6** and **B8**) in excellent yields. Additionally, a gram-scale experiment using **A7** (4.84 g, 17.8 mmol) also proceeded efficiently to afford 2,4-difluoro derivative **B7** in a 49% isolated yield (3.49 g). The author also synthesized *N*-(*o*-carboran-1-yl)aryl carbazole **B9** in 86% yield, demonstrating the practicality of our dump-and-stir method given that *N*-aryl carbazoles have attracted much attention for their applications in organic light-emitting diodes (OLEDs), particularly as hole-transporting materials, bipolar hosts, and thermally activated delayed fluorescence (TADF) emitters.[38] Two *o*-carboranyl groups were introduced in dibromo-substituted pyrazine and pyridazine cores (**A10**-**A12**) to afford **B10** (52%), **B11** (97%), and **B12** (93%), respectively.

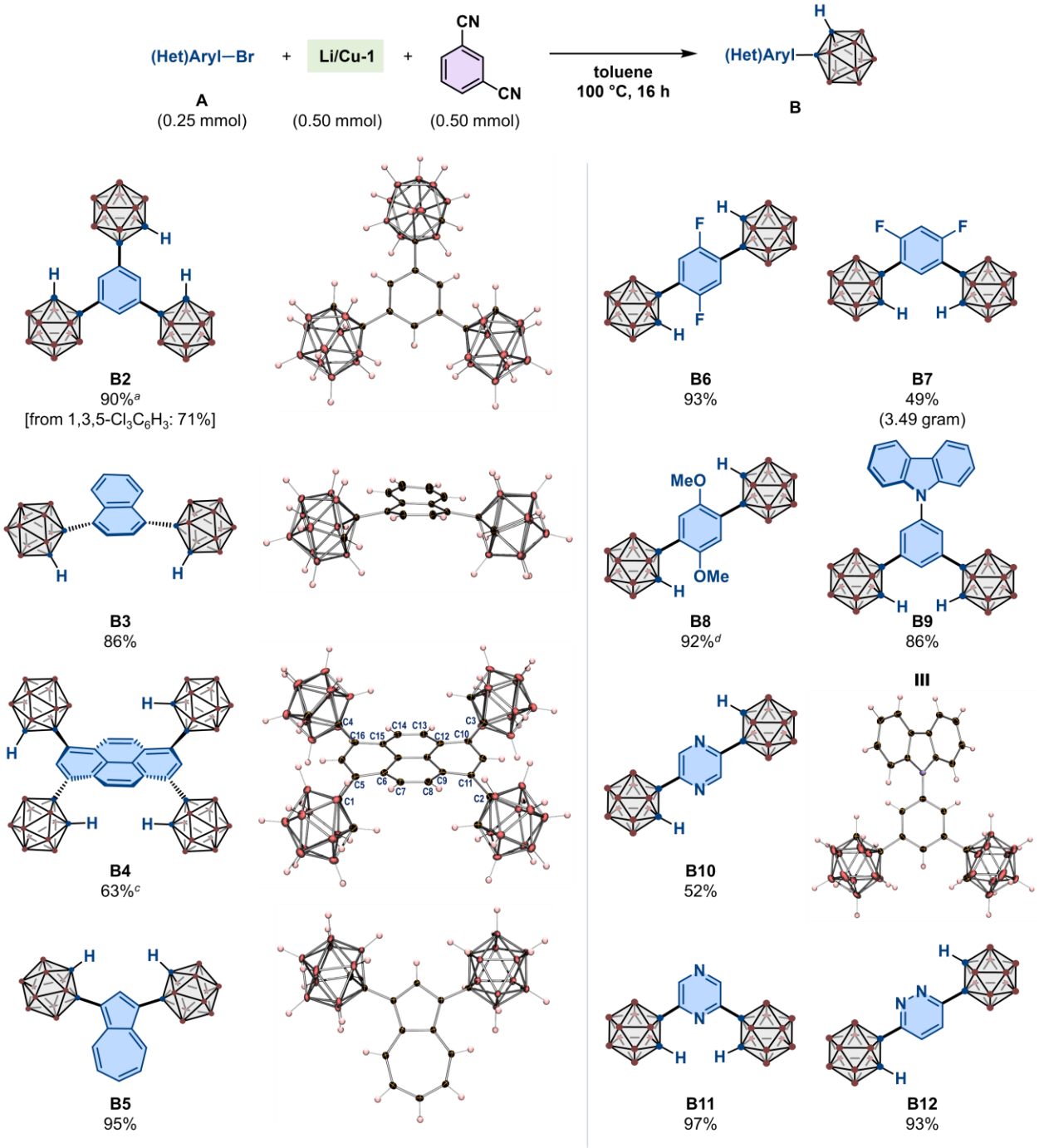


Figure 2.4. Synthesis of B2–B12. Unless otherwise noted, the reactions were performed using the optimized conditions shown in Figure 2.3D; isolated yields are given. Molecular structures of **B2–B5**, and **B9,** determined by SC-XRD analyses, are shown with thermal ellipsoids at 30% probability (solvate molecules are omitted for clarity). [a]0.75 mmol of **Li/Cu-1** and isophthalonitrile were used. [c]1.00 mmol of **Li/Cu-1** and isophthalonitrile were used. [d]Reaction time: 32 h. For carborane or carboranyl groups, brown spheres represent B–H units and blue spheres represent C atoms, as shown in Figure 2.2A.

Subsequently, the author synthesized monocarboranyl arenes **C13–C30** by simply mixing equimolar amounts of aryl bromides, **Li/Cu-1**, and isophthalonitrile in toluene, followed by stirring at 100 °C (Figure

2.5A). These results highlight several characteristics of **Li/Cu-1** in terms of reactivity. First, the present system tolerates Lewis-acidic (e.g., the pinacolato boron group in **A14**) and -basic (e.g., N, S, or O-heterocycles in **A23**–**A30**) functional groups, affording a variety of (*o*-carboran-1-yl)arenes in high to excellent isolated yield.[41] In particular, **C20** and **C21** feature a fusion of strongly electron-withdrawing and 3D-aromatic carboranes with stimuli-responsive spirobenzopyran and 1,8-naphthalimide cores, which have been widely applied in materials and biological sciences.[39,40] However, the presence of acidic protons in **A16** (–OH) and **A17** (–NH) affected the reaction progress owing to protonation of the Cu–carboranyl bonds. In these cases, the author added 1.5 equivalents of **Li/Cu-1** (i.e., 3.0 equiv of *o*-carboranyl units) and isophthalonitrile with respect to each substrate, and eventually isolated **C16** and **C17** in 80% and 88% yield, respectively. Again, in the latter case, *o*-carborane and isophthalonitrile were easily recovered in excellent yield from the crude mixture. Moreover, **C22**, a bioisostere analogue of flurbiprofen, which exhibits versatile pharmaceutical properties (e.g., anti-inflammatory, antifungal, and analgesic),[16] was prepared in 61% yield from **A22** without protection of the carboxylic group. Second, **Li/Cu-1** can distinguish aryl bromides from the corresponding chlorides and fluorides when different halogen substituents coexist in a single molecule, thus enabling the selective synthesis of **C18** (98%), **C19** (93%), and **C23** (80%). Our approach is also valuable as a method complementary to the nucleophilic aromatic substitution using 2-halopyridines and *in-situ*-generated carboranyl-lithium species (e.g., **Li-1** in Figure 2.3A). For example, Lu and co-workers have reported the selective substitution of the 2-Cl atom in 5-bromo-2-chloropyridine (**A23**) while the 5-Br atom remained intact,[29] whereas the 5-Br atom selectively reacted in our system to afford **C23** with a 2-Cl atom. To further confirm the applicability of the present *C*-carboranylation method to aryl chlorides, 4-chlorotoluene (**A13′**), 4-chlorophenol (**A16′**), and 4-chloro-2-cyanopyridine (**A24′**) were subjected to the optimal reaction conditions, affording **C13**, **C16** and **C24** in 71%, 54% and 26% yield, respectively. The corresponding carboranylation of 4-iodotoluene (**A13′′**) proceeded effectively even at 60 °C to afford **C13** in 95% yield after 48 h. Importantly, through the formation of these compounds, the author did not observe the chemical shift (δ_H 3.81) that suggests the formation of bis-*o*-carborane, which tends to be formed easily through the generation of CB-Cu_2 species in aromatic hydrocarbon solvents (Figure 2.2B),[42] manifesting the benefit to use well-identified isolated **Li/Cu-1** reagent.

The author then attempted the construction of 2,2′-bis(*o*-carboran-1-yl)biphenyl using 2,2′-dibromobiphenyl (**A31**) under the optimized conditions; however, carborane-fused biphenyl **D31** was obtained in nearly quantitative yield (Figure 2.5B). Similarly, bithiophene-fused **D32 (96%)** and **D33** (86%) as well as naphthalene-fused **D34** (40%) were obtained. These results demonstrate another practical application of **Li/Cu-1** for the construction of carborane-fused π-conjugated (hetero)arenes, as some of these intriguing compounds were previously obtained in low to moderate yield from reactions between decaborane (or its thiol adducts) and alkynes that were also prepared through multistep Pd-catalyzed coupling processes.[43-45]

Through the synthesis of novel carborane-substituted products (e.g., **B2**–**B12**, **C14**, **C17**, **C20**–**C24**, **C26**–**C28**, and **D33**) and their SC-XRD analysis, the author found that the carboranyl C–C bond lengths are ca. 1.65 Å, with rather larger values (~1.68 Å) observed when the carboranes are introduced in sterically crowded environments such as **B3**, **B4**, and **C27**. It should also be noted that the unreacted C–H bonds in the carborane units remain in **B1**–**B12** and **C13**–**C30**, which could afford further molecular derivatization. The ^{1}H NMR

chemical shifts of these C–H bonds vary depending on the surrounding environments and tend to shift downfield when adjacent heteroatoms that can form hydrogen bonding interactions are present.

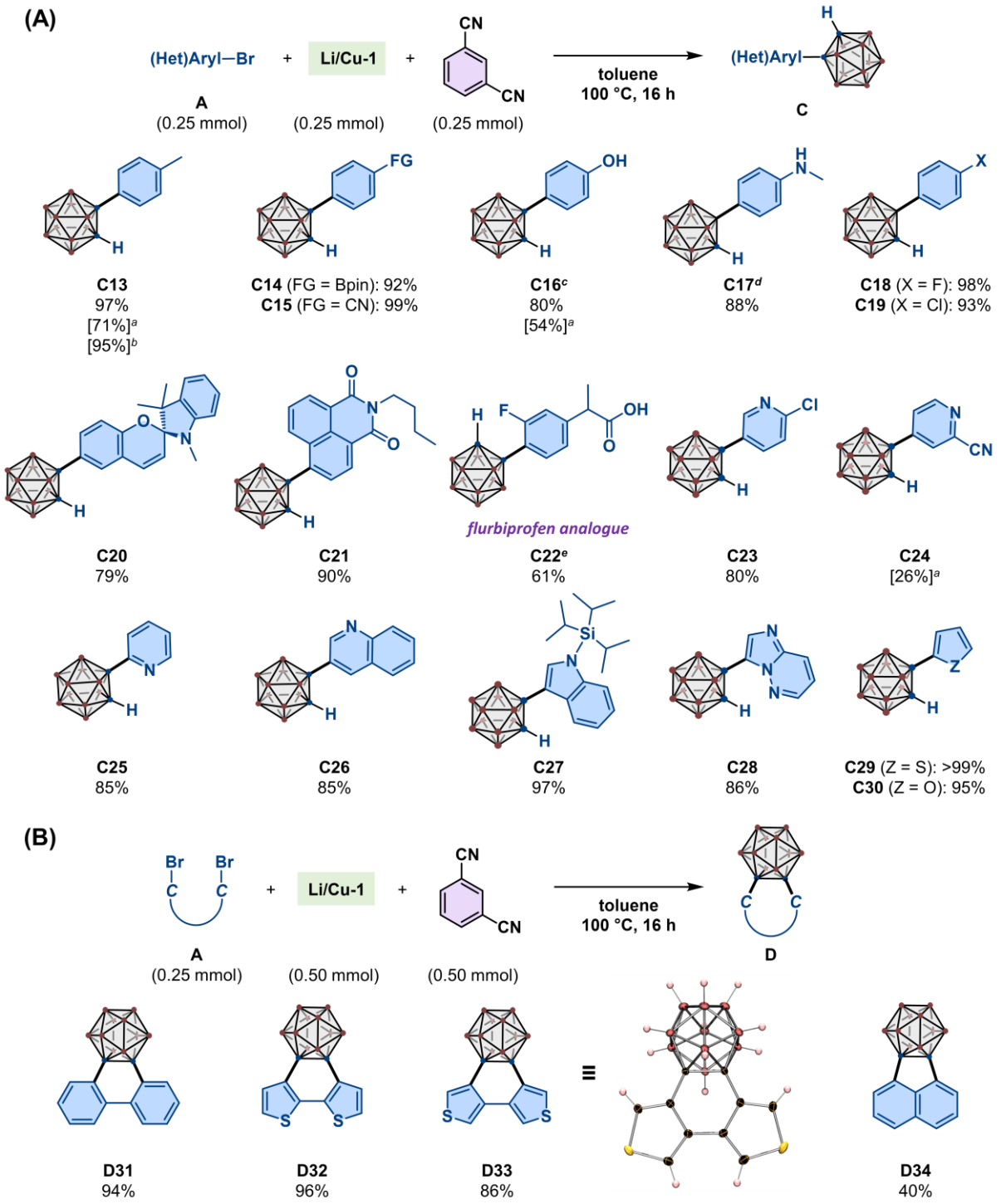


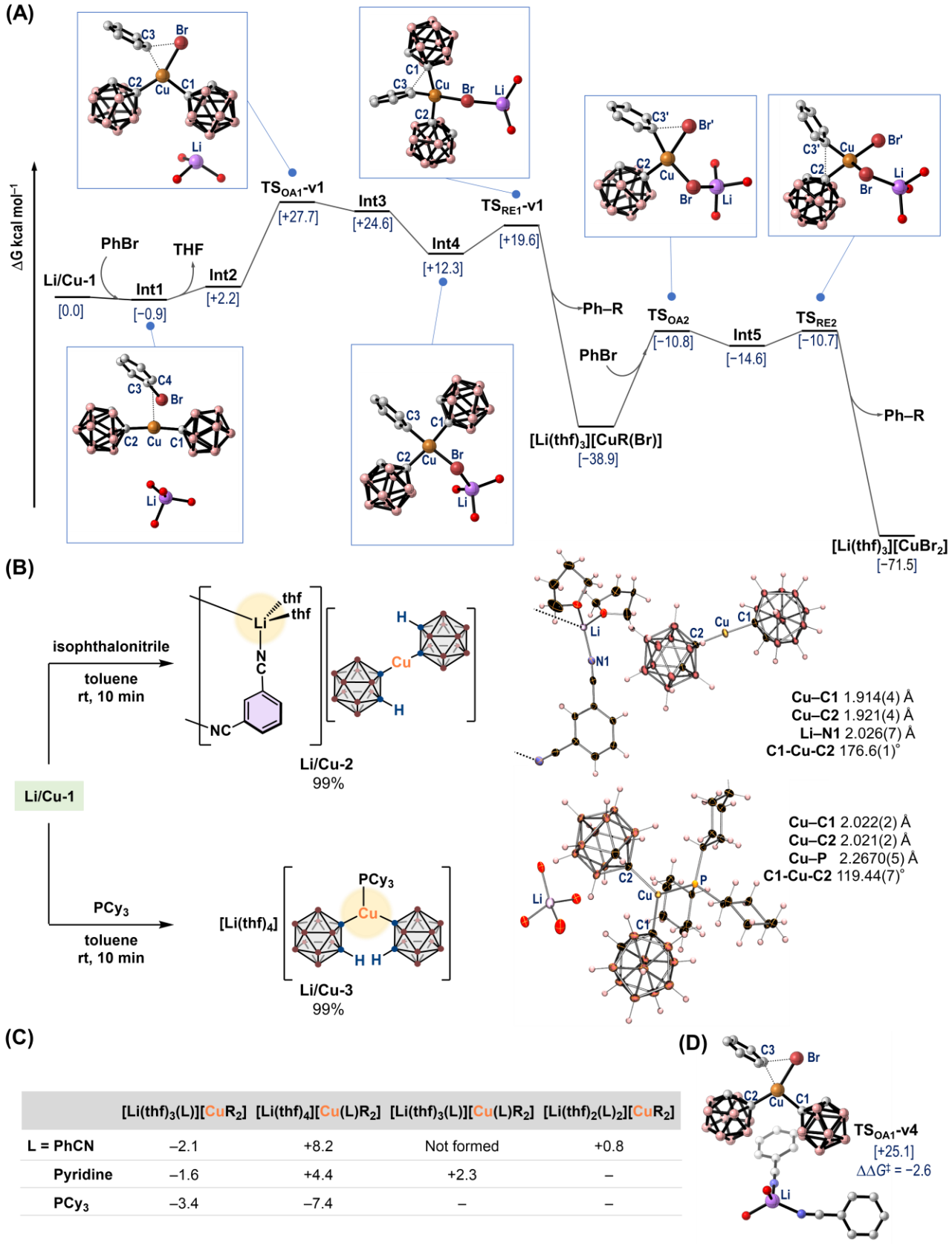
Figure 2.5. Substrate scope. (A) Synthesis of **C13–C30**; isolated yields are given. [a]Reactions using the corresponding aryl chlorides. [b]Reaction was carried out with 4-iodotoluene (**A13′′**) at 60 °C for 48 h. [c]1.5 equiv of **Li/Cu-1** and isophthalonitrile were used. [d]1.5 equiv of **Li/Cu-1** and isophthalonitrile vs. **A17** (0.50 mmol) were used. *o*-Carborane (0.95 mmol) and isophthalonitrile (0.71 mmol) were recovered. [e]2.0 equiv of **Li/Cu-1**

and isophthalonitrile were used. (B) Synthesis of **D31–D34**. The molecular structure of **D33**, determined by an SC-XRD analysis, is shown with thermal ellipsoids at 30% probability. For carborane or carboranyl groups, brown spheres represent B–H units and blue spheres represent C atoms, as shown in Figure 2.2A.

To investigate the reaction mechanisms for the C–C bond formation between **Li/Cu-1** and PhBr, the author performed DFT calculations at the PBE0-D3/Def2-TZVPD(Cu) and Def2-TZVP(others) level in the gas phase. A plausible reaction pathway is depicted in Figure 2.6A along with the structures of selected molecules (*o*-carboranyl groups are shown as R). The relative Gibbs free energies of each molecule are given with respect to [**Li/Cu-1** + 2 PhBr] (0.0 kcal mol^{-1}). First, the *ortho*-carbon (labeled as C4) in PhBr coordinates to the Cu center in **Li/Cu-1** to give energetically slightly favorable **Int1** (−0.9 kcal mol^{-1}). Then, dissociation of one THF molecule from the Li center generates **Int2 (+2.2 kcal** mol^{-1}**)**, which undergoes an oxidative addition to the Ph–Br bond via $\mathbf{TS_{OA1}}$**-v1** (+27.7 mol mol^{-1}) as the rate-determining step ($\Delta G^{\ddagger}$ = +28.6 kcal mol^{-1}). The oxidative addition can also occur directly from **Int1** without the dissociation of one THF molecule via $\mathbf{TS_{OA1}}$**-v2** (+29.9 kcal mol^{-1}; Figure 2.S39), although this transition state is rather unfavorable ($\Delta G^{\ddagger}$ = +30.0 kcal mol^{-1}). In addition, the author confirmed that $[Li(thf)_3]^+$ does not facilitate the oxidative addition, proceeding via $\mathbf{TS_{OA1}}$**-v3 (+33.3** kcal mol^{-1}; Figure 2.S39), by acting as a Lewis acid to promote cleavage of the C−Br bond. The formed distorted square-planar *cis*-R_2Cu(III) complex (**Int3**, +24.6 kcal mol^{-1}) can be expected to readily isomerize to its *trans*-conformer (**Int4**; +12.3 kcal mol^{-1}), which contains a Br---Li^+ interaction. This interaction effectively promotes the subsequent reductive elimination via $\mathbf{TS_{RE1}}$**-v1** (+19.6 mol mol^{-1}) to produce PhR and $[Li(thf)_3][CuR(Br)]$. In contrast, the author also found a substantially less stable transition state $\mathbf{TS_{RE1}}$**-v2** (+29.9 mol mol^{-1}; Figure 2.S35), which includes a $[Li(thf)_4]^+$ unit and thus cannot form the corresponding interaction between the Li^+ and Br centers during the reductive elimination. As **Li/Cu-1** can transfer two carboranyl groups (i.e., CBT > 50%; Figure 2.3B), the author further explored the reaction pathways to generate another equivalent of PhR from $[Li(thf)_3][CuR(Br)]$ and PhBr. The author identified two key transition states, i.e., $\mathbf{TS_{OA2}}$ (−10.8 kcal mol^{-1}) and $\mathbf{TS_{RE2}}$ (−10.7 kcal mol^{-1}), in the pathway leading to the final products (PhR + $[Li(thf)_3][CuBr_2]$; −71.5 kcal mol^{-1}). Possible higher-order structures derived from $[Li(thf)_3][CuR(Br)]$ have not yet been investigated. Such pathways, which may involve multi-centered bonding or aggregation states analogous to Gilman-type reagents, remain unexplored and will be addressed in future studies. It should be noted that a reaction pathway proceeding via the generation of $[Li(thf)_n][CuR_2]$ and $[Li(thf)_n][CuBr_2]$ from $[Li(thf)_3][CuR(Br)]$ cannot be ruled out. The energy barrier to overcome $\mathbf{TS_{RE2}}$ **(**$\Delta G^{\ddagger}$ = +28.2 kcal mol^{-1}**)** limits the reaction progress after the generation of $[Li(thf)_3][CuR(Br)]$. Combining all these results, the overall energy barrier of approximately +28 kcal mol^{-1} to overcome $\mathbf{TS_{OA1}}$**-v1** and $\mathbf{TS_{RE2}}$ is consistent with the sluggish progress of the reaction in the absence of a ligand (Figure 2.3B, run 1).

N-Donor ligands such as pyridine have been proposed to coordinate to the Cu(I) center in Ullmann-type coupling reactions.[28] To explore whether isophthalonitrile can similarly coordinate to the Cu center, the author conducted a stoichiometric reaction between isophthalonitrile and **Li/Cu-1**, and quantitatively isolated complex **Li/Cu-2**, which comprises polymeric $[Li(thf)_2]^+$ structures bridged by isophthalonitriles (Figure 2.6B, top). In stark contrast, the phosphine-coordinated Cu complex **Li/Cu-3** was isolated in 99% yield when

equimolar amounts of **Li/Cu-1** and PCy_3 were mixed (Figure 2.6B, bottom). The molecular structures of these complexes were unambiguously determined by SC-XRD analyses. The structure of the bis(*o*-carboran-1-yl)cuprate unit in **Li/Cu-2** is almost identical to the corresponding structure in **Li/Cu-1**, suggesting that the oxidative addition of aryl halides can be expected to proceed similarly. However, the coordination of PCy_3 to the Cu center causes significant changes in the geometry of the cuprate unit, which would prevent the key oxidative-addition step in **Li/Cu-3**. Furthermore, the author theoretically compared the stability of $[Li(thf)_3(L)][CuR_2]$ and $[Li(thf)_4][Cu(L)R_2]$ complexes (R = *o*-carboranyl) using pyridine, PCy_3, and PhCN as a model for isophthalonitrile to facilitate the discussion of monomeric lithium-cuprate complexes (the relative Gibbs free energies are given with respect to [**Li/Cu-1** + 2 L]; Figure 2.6C). As expected, based on the experimental results, PhCN afforded $[Li(thf)_3(CNPh)][CuR_2]$ (−2.1 kcal mol^{-1}), which is more stable than $[Li(thf)_4][Cu(CNPh)R_2]$ (+8.2 kcal mol^{-1}). Although $[Li(thf)_3(CNPh)_2][CuR_2]$ (+0.8 kcal mol^{-1}) is also a plausible species, optimization of $[Li(thf)_3(CNPh)][Cu(CNPh)R_2]$ failed due to dissociation of PhCN from the Cu center. The critical benefit of using isophthalonitrile is thus rationalized by its coordination to the Li center while leaving the Cu center available for the oxidative addition. In fact, the oxidative addition to PhBr proceeded via $\mathbf{TS_{OA1}}$**-v4** (+25.1 kcal mol^{-1}; Figure 2.6D and Figure 2.S40) from $[Li(thf)_3(CNPh)_2][CuR_2]$, whereby this path is far more favorable ($\Delta\Delta G^{\ddagger}$ = −2.6 kcal mol^{-1}) than the pathway proceeding via $\mathbf{TS_{OA1}}$**-v1** (Figure 2.6A). In this context, based on the atoms-in-molecules analysis, the author confirmed that non-covalent interactions participate between PhCN and carboranyl units, efficiently stabilizing $\mathbf{TS_{OA1}}$**-v4** and therefore promoting the transformation of the R–Cu–R geometry (Figure 2.S41). Conversely, in the case of PCy_3, its coordination to the Cu center was clearly preferred over the formation of $[Li(thf)_3(PCy_3)][CuR_2]$. These experimental and theoretical results are consistent with the fact that no reaction occurred in the presence of PCy_3 (Figure 2.3B). In the case of pyridine, the energy gaps between $[Li(thf)_3(pyridine)][CuR_2]$ (−1.6 kcal mol^{-1}) and pyridine-cuprate species such as $[Li(thf)_4][Cu(pyridine)R_2]$ (+4.4 kcal mol^{-1}) and $[Li(thf)_3(pyridine)][Cu(pyridine)R_2]$ (+2.3 kcal mol^{-1}) are smaller than the case using PhCN. Therefore, the lower CBT value of 37% (Figure 2.3B, run 2) can be attributed to the partial formation of such pyridine-cuprate species, which would exist in an equilibrium with pyridine-lithium species under the applied reaction conditions.[46]



	[Li(thf)$_3$(L)][CuR$_2$]	[Li(thf)$_4$][Cu(L)R$_2$]	[Li(thf)$_3$(L)][Cu(L)R$_2$]	[Li(thf)$_2$(L)$_2$][CuR$_2$]
L = PhCN	–2.1	+8.2	Not formed	+0.8
Pyridine	–1.6	+4.4	+2.3	–
PCy$_3$	–3.4	–7.4	–	–

Figure 2.6. Mechanistic studies (R = *o*-carboranyl group). (A) Plausible reaction pathway and selected optimized molecular structures in the gas phase calculated at the PBE0-D3/Def2-TZVPD(Cu) and Def2-

TZVP(others) level. Selected atoms (Li: purple; B: pink; C: gray; O: red; Cu: orange; Br: reddish brown) and relative Gibbs free energies (kcal mol^{-1}) with respect to [**Li/Cu-1** + 2 PhBr] are shown. (B) Isolation of **Li/Cu-2** and **Li/Cu-3**. Their molecular structures, determined via SC-XRD analyses, are shown with thermal ellipsoids at 30% probability (THF molecules in **Li/Cu-3** are omitted for clarity). (C) Relative Gibbs free energies of {[$Li(thf)_3(L)$][CuR_2] + THF + L}, {[$Li(thf)_4$][$Cu(L)R_2$] + L}, {[$Li(thf)_3(L)$][$Cu(L)R_2$] + THF}, and {[$Li(thf)_2(L)_2$][CuR_2] + 2 THF} with respect to [**Li/Cu-1** + 2 L]. (D) Optimized gas-phase structure of **TS_{OA1}-v4** and its relative Gibbs free energy with respect to [**Li/Cu-1** + 2 PhCN].

2.3 Conclusions

The author has developed a novel cuprate complex that bears two *o*-carboranyl groups **(Li/Cu-1)**, which enables the incorporation of multiple *o*-carborane groups into arenes via an efficient and practical dump-and-stir synthesis with readily available (hetero)aryl bromides and chlorides. The author has also demonstrated that isophthalonitrile coordinates to the Li center rather than to the cuprate unit, allowing the Cu center to undergo the rate-determining oxidative addition to carbon−halide bonds. This counterintuitive ligand design represents a paradigm shift from traditional approaches that focus on the coordination of pyridines and phosphines to Cu. Overall, our findings demonstrate that well-characterized isolated reagents can overcome the limitations of traditional *in-situ* approaches, not only rendering the synthetic process more straightforward and practical but also facilitating the optimization of reaction conditions and providing access to a wider range of molecules.

2.4 Supporting information

2.4.1 General considerations

Unless otherwise noted, all manipulations were conducted under a N_2 atmosphere using standard Schlenk line or grove box (GB) techniques. ^1H, ^{11}B, ^{13}C, ^{19}F, and ^{31}P NMR spectra were recorded on a Bruker AVANCE III 400 or at 25 °C. The chemical shifts in the ^1H NMR spectra were recorded relative to Me_4Si or residual protonated solvent ($CHCl_3$ (δ 7.26), $CDCl_2H$ (δ 5.32), C_6D_5H (δ 7.16)). The chemical shifts in the ^{11}B NMR spectra were recorded relative to $BF_3{\cdot}Et_2O$. The chemical shifts in the ^{13}C spectra were recorded relative to Me_4Si or deuterated solvent ($CDCl_3$ (δ 77.16), CD_2Cl_2 (δ 53.84), C_6D_6 (δ 128.06), DMSO-d_6 (δ 39.52)). The chemical shifts in the ^{19}F NMR spectra were recorded relative to α,α,α-trifluorotoluene (δ −65.64). The chemical shifts in the ^{31}P NMR spectra were recorded relative to 85% H_3PO_4 as an external standard. Assignment of the resonances in ^1H and ^{13}C NMR spectra was based on ^1H−^1H COSY, HMQC, and HMBC experiments. High resolution mass spectrometry (HRMS) and elementary analyses were performed at the Instrumental Analysis Center, Faculty of Engineering, The University of Osaka. Exact mass spectra were obtained using a double-focusing mass spectrometer (JMS-700; JEOL), DART (JMST-100LP; JEOL), and MALDI-TOF (JMS-S3000; JEOL) mass spectrometry.

X-ray crystal data were collected using the Rigaku XtaLAB Synergy equipped with the HyPix-6000HE detector. Using Olex[47], the structure was solved with the SHELXT2[48] structure solution program using Intrinsic Phasing and refined with the SHELXL[49] refinement package using Least Squares minimization. It

should be noted that the boron and carbon atoms in the *o*-carborane moieties might be incorrectly assigned due to the difficulty of distinguishing them by XRD analysis, especially when crystallographic disorder of the pseudo-spherical cluster is observed.[50]

2.4.2 Materials

All commercially available reagents including super-dehydrated solvents (*n*-hexane, toluene, tetrahydrofuran), were purchased from Sigma Aldrich, TCI, and Wako Pure Chemical Industries, and used as received. Benzene-d_6 was distilled from sodium benzophenone ketyl prior to use. CD_2Cl_2 was once degassed by several freeze-pump-thaw cycles and stored inside GB over molecular sieves (4 Å). *o*-Carborane was purchased from Angene and used after sublimation. Substrates used in this work are summarized in Figure 2.S1.

Metrical data for the solid-state structures are available from Cambridge Crystallographic Data Centre: CCDC 2469686 (**Li-1**), 2486445 (**Li/Cu-1**), 2469688 (**Li/Cu-2**), 2469689 (**Li/Cu-3**), 2469669 (**B2**), 2469670 (**B3**), 2469671 (**B4**), 2469672 (**B5**), 2469673 (**B6**), 2469674 (**B7**), 2469675 (**B8**), 2469676 (**B9**), 2469666 (**B10**), 2469667 (**B11**), 2469680 (**B12**), 2469677 (**C14**), 2469678 (**C17**), 2469679 (**C20**), 2469680 (**C21**), 2470754 (**C22**), 2469681 (**C23**), 2469682 (**C24**), 2483553 (**C26**), 2469683 (**C27**), 2469684 (**C28**), 2469685 (**D33**).

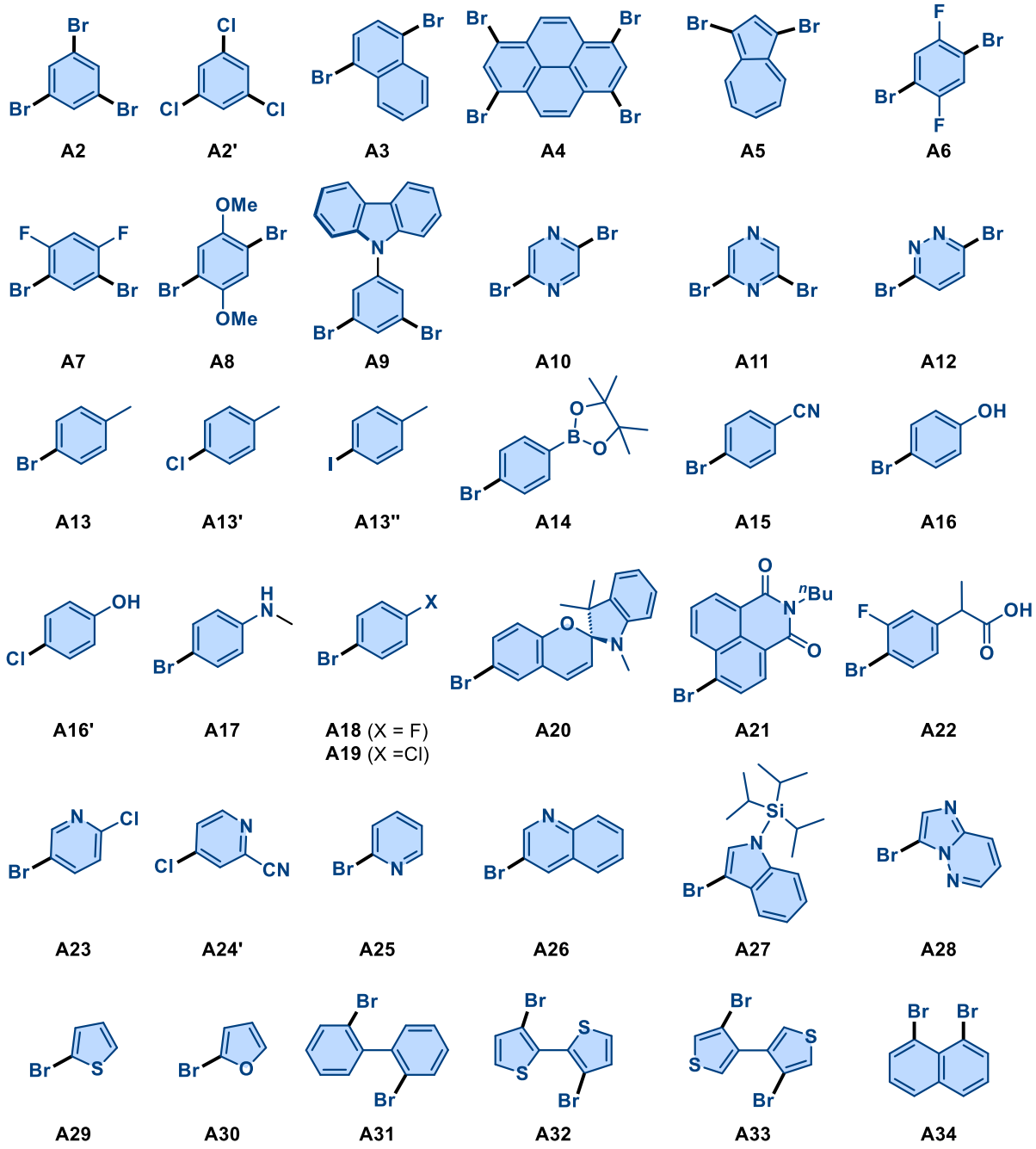


Figure 2.S1. Substrates used in this chapter.

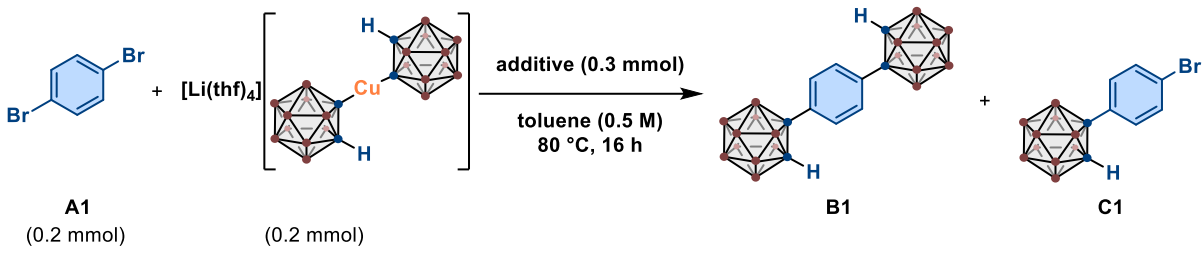
2.4.3 Optimization of reaction conditions

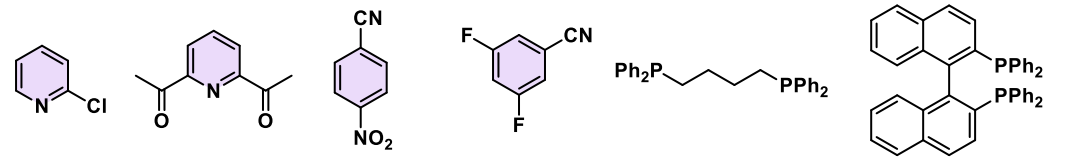
2.4.3.1 Screening of the additives

In a screw-cap reaction vessel equipped with a magnetic stirrer bar, **Li/Cu-1** (0.20 mmol), an additive (0.30 mmol), and 1,4-dibromobenzene (**A1**, 0.20 mmol) were added in this order. Toluene (0.4 mL) was then added, and the vessel was sealed. The mixture was stirred at 80 °C for 16 h. After cooling to rt, the resultant mixture was diluted with wet Et_2O. The resulting mixture was then filtered through filter paper, and the volatiles were removed under reduced pressure. The yields of **B1** and **C1** were determined by NMR analysis using 1,3,5-trimethoxybenzene as an internal standard (Figure 2.3B, and additional results are given in Figure 2.S2). CBT

(carboranyl-group transfer ratio) values were calculated using the following equation:

$$\text{CBT (\%)} = \frac{\text{total moles of carborane units in } \mathbf{B1} \text{ and } \mathbf{C1}}{\text{total moles of carborane units in } \mathbf{Li/Cu-1}} \times 100$$



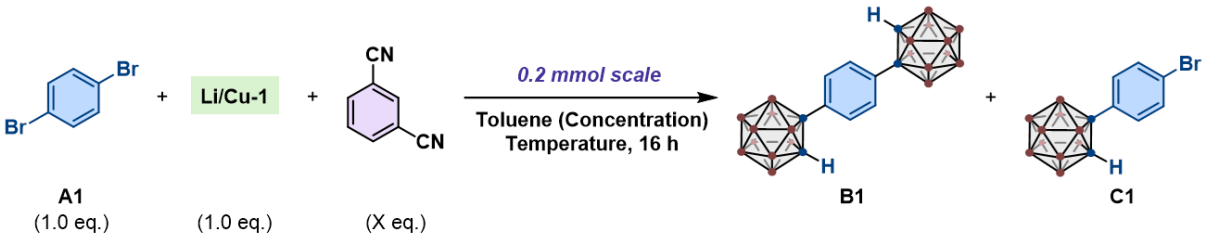


B1 [%]	7	0	12	7	0	0
C1 [%]	32	0	55	42	0	0
CBT [%]	23	0	40	28	0	0

Figure 2.S2. Screening of additives (additional results to those shown in Figure 2.3B).

2.4.3.2 Screening of other parameters

In a screw-cap reaction vessel equipped with a magnetic stirrer bar, **A1** (47.2 mg, 0.200 mmol), **Li/Cu-1** (129.1 mg, 0.200 mmol, 1.0 equiv), isophthalonitrile (X equiv), and an additional additive (1.0 or 2.0 equiv, or none)**,** were added. Toluene (0.25 M, 0.5 M, or 1.0 M with respect to **Li/Cu-1**) was then added, and the vessel was sealed. The mixture was stirred at 70, 80, or 100 °C for 16 h. After cooling to rt, the reaction mixture was diluted with wet Et_2O. The resulting mixture was filtered through filter paper, and the volatiles were removed under reduced pressure. The yields of **B1** and **C1** were determined by NMR analysis using 1,3,5-trimethoxybenzene as an internal standard. The results of the solvent screening are shown in Figure 2.3C, while others are given in Figure 2.S3.



Run	X [eq.]	Concentration	Temperature [°C]	Additive	**B1** [%]	**C1** [%]	CBT [%]
1	0.5	0.5	80	none	7	44	29
2	1.0	0.5	80	none	31	69	66
3	2.0	0.5	80	none	28	72	64
4	2.5	0.5	80	none	23	74	60
5	3.0	0.5	80	none	30	70	65
6	3.5	0.5	80	none	29	71	65
7	1.0	0.25	80	none	4	29	19
8	1.0	1.0	80	none	17	66	50
9	1.0	0.5	70	none	4	18	13
10	1.0	0.5	80	CuCl (1.0 eq.)	14	62	45
11	1.0	0.5	80	LiCl (1.0 eq.)	17	69	52
12	1.0	0.5	80	CuCl (1.0 eq.) + LiCl (1.0 eq.)	16	60	46
13	1.0	0.5	80	CuCl (1.0 eq.) + LiCl (2.0 eq.)	17	64	49
14	1.0	0.5	100	none	33	67	67

Figure 2.S3. Optimization of reaction conditions with isophthalonitrile ligand.

2.4.4. Preparation of carboranyl metal compounds

2.4.4.1 Preparation of **Li-1** (Figure 2.3A)

A solution of *o*-carborane (6.30 g, 43.7 mmol, 1.0 M in THF) was slowly treated with ^{n}BuLi (28.4 mL of a 1.54 M solution in *n*-hexane, 43.7 mmol) at 0 °C, and the mixture was allowed to warm to rt over 1 h with stirring, followed by removal of all volatiles in vacuo. The residue was then washed with *n*-hexane (10 mL × 4) and dried in vacuo, affording **Li-1** as a white solid (15.45 g, 42.2 mmol, 96%). A single crystal of **Li-1** was obtained from a saturated solution of **Li-1** in toluene at rt. **^{1}H NMR** (400 MHz, C_6D_6, rt, δ/ppm): 3.40 (t, J = 6.4 Hz, 12H, O-CH_2), 3.11 (s, 1H, cage C*H*), 1.52–1,31 (m, 12H, CH_2-CH_2-CH_2), 3.80–1.65 (brm, B*H*). **^{11}B NMR** (128 MHz, C_6D_6, rt, δ/ppm): 0.90–−3.30 (m, 2B), −4.53–−6.89 (m, 2B), −7.68–−12.96 (m, 6B). **^{13}C{^{1}H} NMR** (100 MHz, C_6D_6, rt, δ/ppm): 90.7, 68.4, 62.2, 25.6. **Li-1**: M = 366.46, colorless, monoclinic, $P2_1/n$ (#14), a = 13.5724(5) Å, b = 11.5145(5) Å, c = 14.3564(7) Å, α = 90°, β = 96.460(4)°, γ = 90°, V = 2229.36(17) Å^3, Z = 4, $Dcalcd$ = 1.092 g/cm^3 , T = 123.15 K, R_1 (wR_2) = 0.0866 (0.2371).

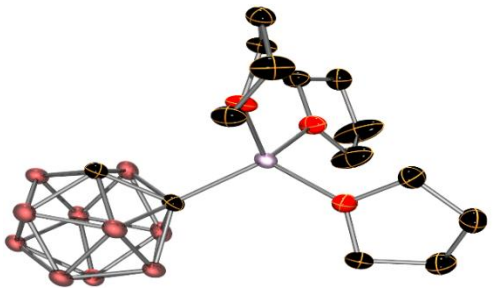


Figure 2.S4. Molecular structure of **Li-1** with ellipsoids set at 30% probability. H atoms are omitted for clarity.

2.4.4.2 Preparation of **Li/Cu-1**

Method A (Figure 2.3A)**:** CuCl (1.53 g, 15.5 mmol, 0.55 equiv) was added to a solution of **Li-1** (10.32 g, 28.2 mmol, 1.0 M in THF) at rt, and the mixture was stirred for 12 h. After removal of all volatiles in vacuo, the residue was washed with *n*-hexane (10 mL × 4). The residue was then extracted with toluene through a Celite pad, followed by removal of all volatiles in vacuo, affording **Li/Cu-1** as a brownish solid (8.53 g, 13.2 mmol, 94%). A single crystal of **Li/Cu-1** was obtained from a saturated solution of **Li/Cu-1** in dichloromethane at rt. **^{1}H NMR** (400 MHz, CD_2Cl_2, rt, δ/ppm): 3.80 (t, J = 6.4 Hz, 16H, O-CH_2), 3.28 (s, 2H, cage C*H*), 2.10–1,95 (m, 16H, CH_2-CH_2-CH$_2$), 2.77–1.18 (brm, B*H*). **^{11}B NMR** (128 MHz, CD_2Cl_2, rt, δ/ppm): −0.25–−4.50 (m, 4B), −6.91–−13.79 (m, 16B). **^{13}C{^{1}H} NMR** (100 MHz, CD_2Cl_2, rt, δ/ppm): 75.3, 69.1 (t, J = 13.1 Hz), 62.2, 25.9. **X-ray** data for **Li/Cu-1** (Figure 2.3A): M = 645.31, colorless, monoclinic, $P2_1/c$ (#14), a = 14.9640(2) Å, b = 14.6836(2) Å, c = 18.0146(3) Å, α = 90°, β = 113.296(2)°, γ = 90°, V = 3635.56(10) Å^3, Z = 4, $Dcalcd$ = 1.179 g/cm^3 , T = 123.15 K, R_1 (wR_2) = 0.0488 (0.1369).

Method B (Figure 2.3A)**:** A solution of *o*-carborane (10.0 g, 69.3 mmol, 1.0 M in THF) was slowly treated with ^{n}BuLi (45.0 mL of a 1.54 M solution in *n*-hexane, 69.3 mmol, 1.0 equiv) at −35 °C, and the mixture was allowed to warm to rt over 1 h with stirring. CuCl (3.78 g, 38.2 mmol, 0.55 equiv) was **then** added to the resultant solution at rt, and **the mixture was** stirred for 12 h. After removal of all volatiles in vacuo, the residue was washed with *n*-hexane (10 mL × 4). **The** residue was **then** extracted with toluene through a Celite pad, followed by removal of all volatiles in vacuo, affording **Li/Cu-1** as a brownish solid (19.9 g, 30.8 mmol, 89%).

Method C (Figure 2.S5): A solution of *o*-carborane (4.66 g, 32.3 mmol, 1.0 M in THF) was slowly treated with ^{n}BuLi (20.9 mL of a 1.55 M solution in *n*-hexane, 32.4 mmol, 1.0 equiv) at −35 °C, and the mixture was allowed to warm to rt over 1 h with stirring. CuCl (3.20 g, 32.3 mmol, 1.0 equiv) was then added to the resultant solution at rt, and the mixture was stirred for 2 h. After removal of all volatiles in vacuo, the residue was washed with *n*-hexane (10 mL × 4) and toluene (10 mL). The residue was then extracted with dichloromethane through a Celite pad, followed by removal of all volatiles in vacuo, affording **Li/Cu-1** as a brownish solid (9.41 g, 14.6 mmol, 90%).

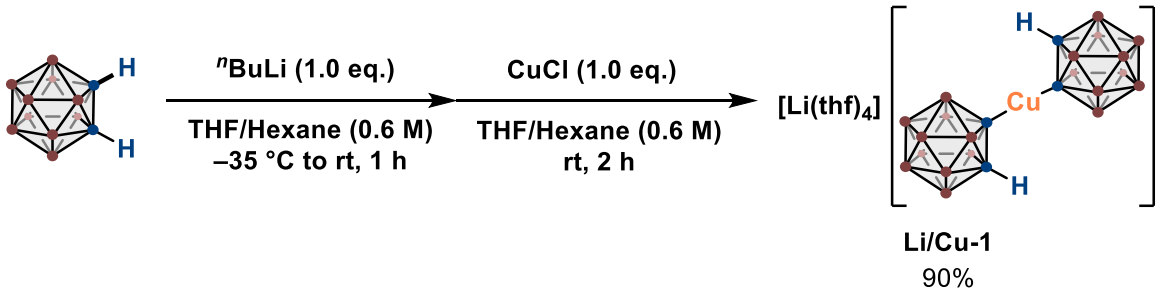


Figure 2.S5. One-pot synthesis of **Li/Cu-1** from *o*-carborane with CuCl (1.0 equiv)

2.4.4.3 Preparation of **Li/Cu-2** (Figure 2.6B)

Isophthalonitrile (64.1 mg, 0.500 mmol, 1.0 equiv) was added to a suspension of **Li/Cu-1** (322.7 mg,

0.500 mmol, 0.5 M in toluene) at rt, and the resultant mixture was stirred for 10 min, followed by removal of all volatiles in vacuo, affording **Li/Cu-2** as a dark brown solid (314.0 mg, 0.499 mmol, 99%). A single crystal of **Li/Cu-2** was obtained from a saturated solution of **Li/Cu-2** in toluene at rt. **^{1}H NMR** (400 MHz, CD_2Cl_2, rt, δ/ppm): 8.10–7.97 (m, 3H, Ar-*H*), 7.77 (brs, 1H, Ar-*H*), 3.85–3.79 (m, 8H, O-C*H*$_2$), 3.30 (m, 2H, cage C*H*), 2.01–1.92 (m, 8H, C*H*$_2$-C*H*$_2$-CH$_2$), 3.16–1.11 (brm, B*H*). **^{11}B NMR** (128 MHz, CD_2Cl_2, rt, δ/ppm): −0.31–−4.64 (m, 4B), −6.81–−13.72 (m, 16B). **^{13}C{^{1}H} NMR** (100 MHz, CD_2Cl_2, rt, δ/ppm): 137.6, 136.5, 131.3, 113.3, 74.9, 69.0 (t, J = 13.9 Hz), 62.2, 25.9. A signal of the ipso-carbon with respect to the cyano group was not identified. **X-ray** data for **(Li/Cu-2)·C$_7$H$_8$**: M = 721.37, colorless, monoclinic, $P2_1/c$ (#14), a = 16.9524(10) Å, b = 11.4965(5) Å, c = 22.1848(15) Å, α = 90°, β = 109.811(7)°, γ = 90°, V = 4067.8(4) Å^3, Z = 4, $Dcalcd$ = 1.178 g/cm^3 , T = 123.15 K, R_1 (wR_2) = 0.0617 (0.1483).

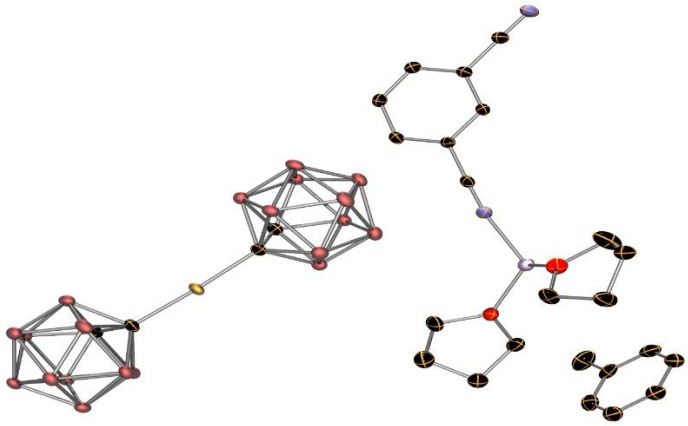


Figure 2.S6. Molecular structure of **(Li/Cu-2)·C$_7$H$_8$** with ellipsoids set at 30% probability. H atoms and a disordered molecule are omitted for clarity.

2.4.4.4 Preparation of **Li/Cu-3** (Figure 2.6B)

PCy_3 (140.2 mg, 0.500 mmol, 1.0 equiv) was added to a **suspension** of **Li/Cu-1** (322.7 mg, 0.500 mmol, 0.5 M in toluene) at rt, and **the resultant mixture was** stirred for 10 min, followed by removal of all volatiles in vacuo, affording **Li/Cu-3** as a gray solid (461.5 mg, 0.500 mmol, 99%). A single crystal of **Li/Cu-3** was obtained from a saturated solution of **Li/Cu-3** in toluene at rt. **^{1}H NMR** (400 MHz, CD_2Cl_2, rt, δ/ppm): 3.82–3.67 (m, 16H, O-C*H*$_2$), 3.28 (m, 2H, cage C*H*), 1.91–1.86 (m, 16H, C*H*$_2$-C*H*$_2$-CH$_2$), 3.06–1.47 (brm, B*H*), 1.41–1.22 (m, 18H, C*H* on PCy_3). **^{11}B NMR** (128 MHz, CD_2Cl_2, rt, δ/ppm): 0.02–−4.44 (m, 4B), −6.26–−14.47 (m, 16B). **^{13}C{^{1}H} NMR** (100 MHz, CD_2Cl_2, rt, δ/ppm): 75.7, 68.7 (t, J = 12.3 Hz), 31.7, 31.5, 31.4, 27.5 (d, J = 11.0 Hz), 26.3, 25.9. **^{31}P{^{1}H} NMR** (162 MHz, CD_2Cl_2, rt, δ/ppm): 29.8 (s, 1P, *P*Cy_3). **X-ray** data for **2(Li/Cu-3)**: M = 1851.44, colorless, triclinic, P-1 (#2), a = 11.95758(14) Å, b = 14.1918(2) Å, c = 17.3976(3) Å, α = 106.0821(13)°, β = 102.3359(11)°, γ = 99.6132(11)°, V = 2689.68(7) Å^3, Z = 1, $Dcalcd$ = 1.143 g/cm^3 , T = 123.15 K, R_1 (wR_2) = 0.0462 (0.1390).

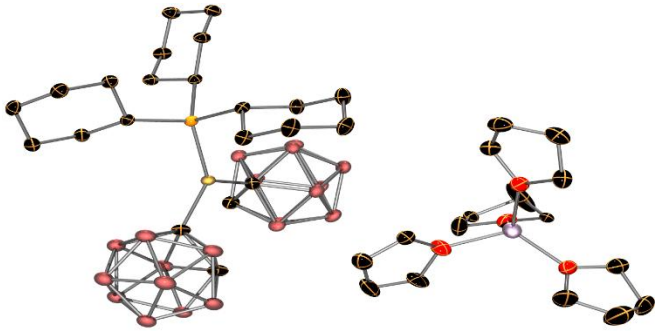
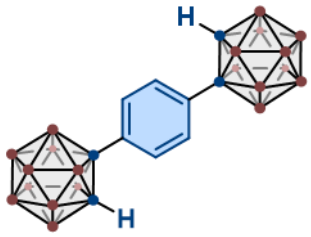


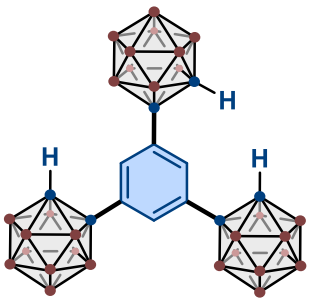
Figure 2.S7. Molecular structure of **Li/Cu-3** with ellipsoids set at 30% probability. H atoms and a disordered molecule are omitted for clarity.

2.5.1 Reaction between aryl halides and Li/Cu-1

General: In a screw-cap reaction vessel equipped with a magnetic stirrer bar, **Li/Cu-1** (1.0 equiv per molar amounts of Br or Cl units), isophthalonitrile (1.0 equiv with respect to **Li/Cu-1**), and the aryl halide were added. Toluene (0.5 M with respect to **Li/Cu-1**) was then added, and the vessel was sealed. The mixture was stirred at 100 °C (or 120 °C when aryl chlorides were used) for 16 h. After cooling to rt, the reaction mixture was diluted with wet Et_2O. The resulting mixture was filtered through filter paper, and the volatiles were removed under reduced pressure *(Note: to prevent the sublimation of o-carborane, removal of volatiles should be conducted at or below rt. If recovery of o-carborane is not necessary, evaporation can be carried out under heating conditions*). The crude product was purified by silica gel column chromatography (*n*-hexane/EtOAc) to afford the product.



B1[51]: The general procedure was followed with **A1** (59.0 mg, 0.250 mmol), **Li/Cu-1** (322.7 mg, 0.500 mmol, 2.0 equiv), isophthalonitrile (64.1 mg, 0.500 mmol, 2.0 equiv), and toluene (1.0 mL). Purification by flash column chromatography on silica gel (*n*-hexane) afforded **B1** as a white solid (88.8 mg, 0.245 mmol, 98%). *The procedure for recovering o-carborane and isophthalonitrile is given in Section 8-1 (vide infra)*. **^{1}H NMR** (400 MHz, $CDCl_3$, rt, δ/ppm): 7.45 (s, 4H, Ar-*H*), 3.92 (s, 2H, cage C*H*), 3.54–1.45 (brm, B*H*).



B2[52]: The general procedure was followed with **A2** (78.7 mg, 0.250 mmol), **Li/Cu-1** (484.0 mg, 0.750 mmol, 3.0 equiv), isophthalonitrile (96.1 mg, 0.750 mmol, 3.0 equiv), and toluene (1.5 mL). Purification by flash column chromatography on silica gel (*n*-hexane/EtOAc = 90/10) afforded **B2** as a white solid (113.5 mg, 0.225 mmol, 90%). A single crystal of **B2** was obtained from a saturated solution of **B2** in acetone at rt. **^{1}H NMR** (400 MHz, $CDCl_3$, rt, δ/ppm): 7.67 (s, 3H, Ar-*H*), 3.87 (s, 3H, cage C*H*), 3.29–1.55 (brm, B*H*). **X-ray** data for **B2·2(C_3H_6O)**: M = 620.86, colorless, monoclinic, $P2_1/n$ (#14), a = 6.8908(4) Å, b = 19.4046(10) Å, c = 27.7383(15) Å, α = 90°, β =

91.390(4)°, γ = 90°, V = 3707.9(4) Å^3, Z = 4, $Dcalcd$ = 1.112 g/cm^3 , T = 123.15 K, R_1 (wR_2) = 0.0555 (0.1288).

B2 was also synthesized by following the general procedure with **A2′** (45.4 mg, 0.250 mmol), **Li/Cu-1** (484.0 mg, 0.750 mmol, 3.0 equiv), isophthalonitrile (96.1 mg, 0.750 mmol, 3.0 equiv), and toluene (1.5 mL). Purification by flash column chromatography on silica gel (*n*-hexane/EtOAc = 90/10) afforded **B2** as a white solid (89.3 mg, 0.177 mmol, 71%).

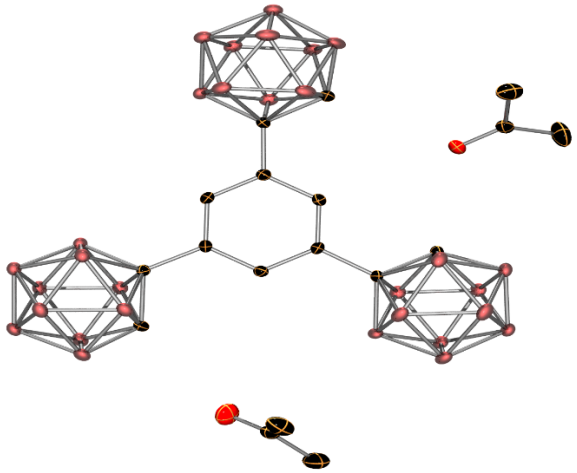
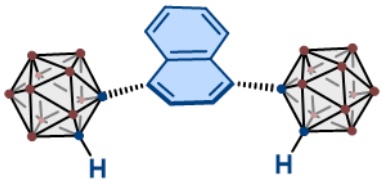


Figure 2.S8. Molecular structure of **B2·2(C_3H_6O)** with ellipsoids set at 30% probability. H atoms are omitted for clarity.



B3: The general procedure was followed with **A3** (71.5 mg, 0.250 mmol), **Li/Cu-1** (322.7 mg, 0.500 mmol, 2.0 equiv), isophthalonitrile (64.1 mg, 0.500 mmol, 2.0 equiv), and toluene (1.0 mL). Purification by flash column chromatography on silica gel (*n*-hexane/EtOAc = 95/5 to 85/15) afforded **B3** as a white solid (88.7 mg, 0.215 mmol, 86%). A single crystal of **B3** was obtained from a saturated solution of **B3** in acetone at rt. **^{1}H NMR** (400 MHz, $CDCl_3$, rt, δ/ppm): 8.88–8.81 (m, 2H, Ar-*H*), 7.69–7.60 (m, 4H), 4.56 (s, 2H, cage C*H*), 3.75–1.25 (brm, B*H*). **^{11}B NMR** (128 MHz, $CDCl_3$, rt, δ/ppm): −0.25–−3.57 (m, 4B), −6.23–−16.71 (m, 16B). **^{13}C{^{1}H} NMR** (100 MHz, $CDCl_3$, rt, δ/ppm): 131.8, 131.3, 127.2, 126.9, 125.6, 76.3, 61.5. **HRMS** (EI$^+$): m/z Calculated for $C_{14}H_{28}B_{20}$ ([M]$^+$) 416.4052, found 416.4110. **X-ray** data for **2(B3)**: M = 825.12, colorless, monoclinic, $P2_1/n$ (#14), a = 20.4921(5) Å, b = 11.6173(3) Å, c = 21.1929(5) Å, α = 90°, β = 113.695(3)°, γ = 90°, V = 4619.9(2) Å^3, Z = 4, $Dcalcd$ = 1.186 g/cm^3 , T = 153.15 K, R_1 (wR_2) = 0.0456 (0.1229).

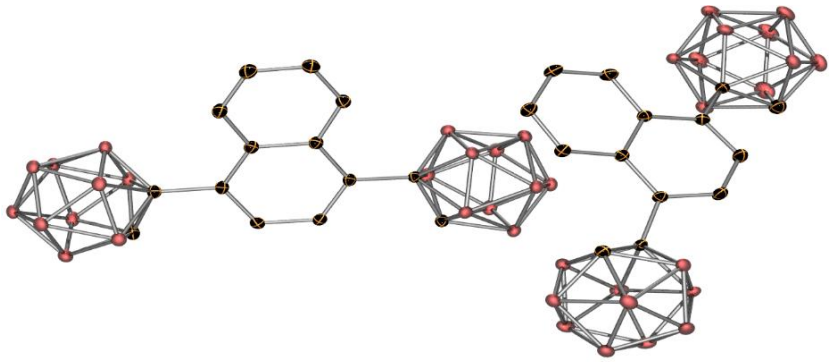
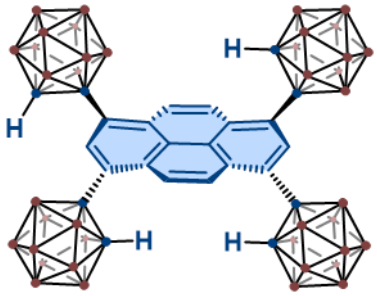


Figure 2.S9. Molecular structure of **2(B3)** with ellipsoids set at 30% probability. H atoms are omitted for clarity.



B4: The general procedure was followed with **A4** (129.5 mg, 0.250 mmol), **Li/Cu-1** (645.3 mg, 1.00 mmol, 4.0 equiv), isophthalonitrile (128.1 mg, 1.00 mmol, 4.0 equiv), and toluene (2.0 mL). Purification by flash column chromatography on silica gel (*n*-hexane/acetone = 2/1) afforded **B4** as a white solid (122.2 mg, 0.158 mmol, 63%). A single crystal of **B4** was obtained from a saturated solution of **B4** in EtOAc at rt. **^{1}H NMR** (400 MHz, $CDCl_3$/acetone-d_6 = 1/1, rt, δ/ppm): 8.69 (s, 4H, Ar-*H*), 8.24 (s, 2H, Ar-*H*), 5.02 (s, 4H, cage C*H*), 3.20–0.97 (brm, B*H*). **^{11}B NMR** (128 MHz, $CDCl_3$/acetone-d_6 = 1/1, rt, δ/ppm): 4.81–1.60 (m, 8B), −0.53–−12.02 (m, 32B). **^{13}C{^{1}H} NMR** (100 MHz, $CDCl_3$/EtOAc-d_8 = 1/1, rt, δ/ppm): 128.2, 126.9, 125.9, 125.2, 76.3, 62.1 (d, J = 7.2 Hz). One carbon resonance was observed at approximately 123.9 ppm, but it was not significant enough to be automatically detected, leaving its details unclear. **HRMS** (MALDI-TOF, m/z): Calculated for $C_{24}H_{50}{}^{10}B_7{}^{11}B_{33}$ ($[M]^+$) 771.7879, found 771.7896. **X-ray** data for **B4·2($C_4H_8O_2$)**: M = 1035.35, colorless, orthorhombic, $P2_12_12_1$ (#19), a = 11.6992(2) Å, b = 17.4486(3) Å, c = 28.7669(4) Å, α = 90°, β = 90°, γ = 90°, V = 5872.32(16) Å^3, Z = 4, $Dcalcd$ = 1.171 g/cm^3 , T = 153.15 K, R_1 (wR_2) = 0.0593 (0.1568). A solvent mask was calculated and 196 electrons were found in a volume of 708 Å^3 in 1 void per unit cell. This is consistent with the presence of 1[$CH_3COOCH_2CH_3$] per formula unit which accounts for 192 electrons per unit cell.

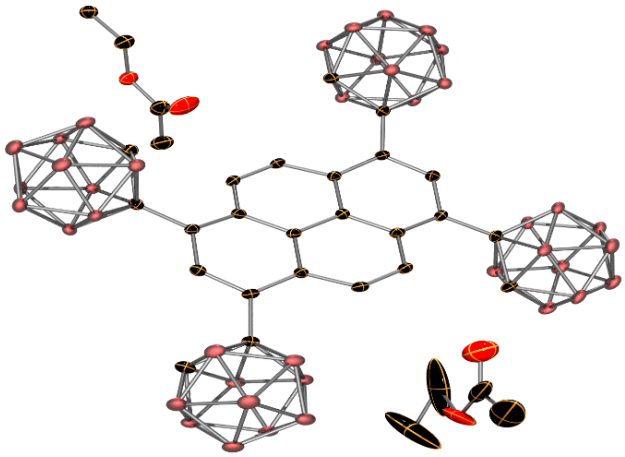
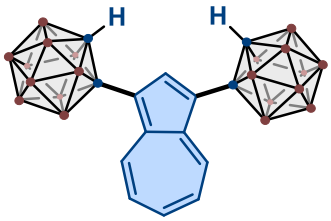


Figure 2.S10. Molecular structure of **B4·2($C_4H_8O_2$)** with ellipsoids set at 30% probability. H atoms are omitted for clarity.



B5: The general procedure was followed with **A5** (71.5 mg, 0.250 mmol), **Li/Cu-1** (322.7 mg, 0.500 mmol, 2.0 equiv), isophthalonitrile (64.1 mg, 0.500 mmol, 2.0 equiv), and toluene (1.0 mL). Purification by flash column chromatography on silica gel (*n*-hexane/EtOAc = 95/5) afforded **B5** as a purple solid (97.7 mg, 0.237 mmol, 95%). A single crystal of **B5** was obtained from a saturated solution of **B5** in acetone at rt. **^{1}H NMR** (400 MHz, $CDCl_3$, rt, δ/ppm): 9.15 (d, J = 10.4 Hz, 2H, Ar-*H*), 8.08 (s, 1H, Ar-*H*), 7.93 (t, J = 9.8 Hz, 1H, Ar-*H*), 7.57 (dd, J = 10.4 Hz, 10.0 Hz, 2H, Ar-*H*), 4.04 (s, 2H, cage C*H*), 3.68–1.41 (brm, B*H*). **^{11}B NMR** (128 MHz, $CDCl_3$, rt, δ/ppm): −0.51–−5.02 (m, 4B), −6.09–−16.18 (m, 16B). **^{13}C{^{1}H} NMR** (100 MHz, $CDCl_3$, rt, δ/ppm): 141.8, 140.0 (d, J = 4.6 Hz), 138.5, 137.5, 127.7, 117.7, 74.1, 64.0 (d, J = 15.4 Hz). **HRMS** (EI^+): m/z Calculated for $C_{14}H_{28}B_{20}$ ($[M]^+$) 416.4052, found 416.4063. **X-ray** data for **2(B5)**: M = 825.12, dark violet, triclinic, P-1 (#2), a = 12.02530(10) Å, b = 12.17120(10) Å, c = 17.05730(10) Å, α = 81.4290(10)°, β = 79.4140(10)°, γ = 73.8090(10)°, V = 2344.04(3) Å^3, Z = 2, $Dcalcd$ = 1.169 g/cm^3 , T = 153.15 K, R_1 (wR_2) = 0.0476 (0.1267).

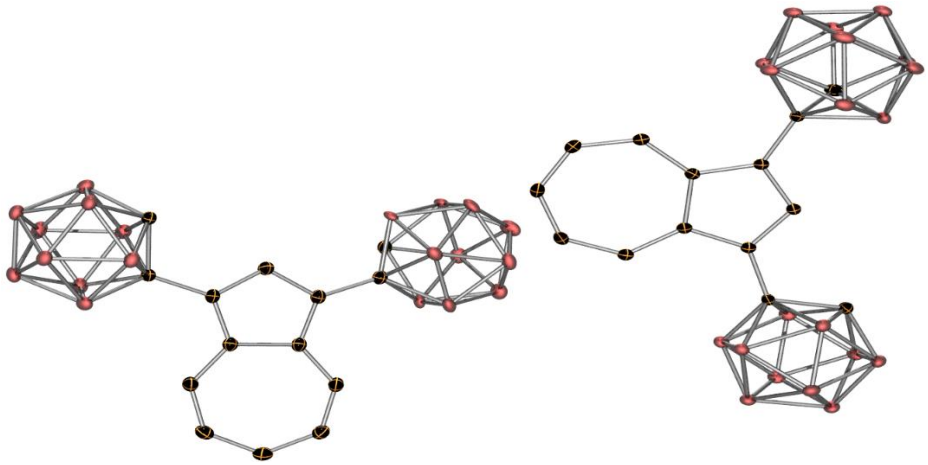
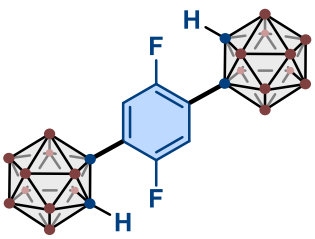


Figure 2.S11. Molecular structure of **2(B5)** with ellipsoids set at 30% probability. H atoms and a disordered molecule are omitted for clarity.



B6: The general procedure was followed with **A6** (68.0 mg, 0.250 mmol), **Li/Cu-1** (322.7 mg, 0.500 mmol, 2.0 equiv), isophthalonitrile (64.1 mg, 0.500 mmol, 2.0 equiv), and toluene (1.0 mL). Purification by flash column chromatography on silica gel (*n*-hexane/EtOAc = 95/5 to 85/15) afforded **B6** as a white solid (92.6 mg, 0.232 mmol, 93%). A single crystal of **B6** was obtained from a saturated solution of **B6** in acetone at rt. **^{1}H NMR** (400 MHz, $CDCl_3$, rt, δ/ppm): 7.35 (t, 2H, J = 10.0 Hz, Ar-*H*), 4.57 (s, 2H, cage C*H*), 3.35–1.39 (brm, B*H*). **^{11}B NMR** (128 MHz, $CDCl_3$, rt, δ/ppm): −0.04–−4.20 (m, 4B), −6.85–−16.02 (m, 16B). **^{13}C{^{1}H} NMR** (100 MHz, $CDCl_3$, rt, δ/ppm): 154.5 (dd, $^1J_{C,F}$ = 248.7

Hz, $^{4}J_{C,F}$ = 3.8 Hz, *C*-F), 124.4 (t, *J* = 10.1 Hz), 120.6 (m), 70.1, 58.9 (m). **^{19}F NMR** (376 MHz, $CDCl_3$, rt, *δ*/ppm): −121.2 (t, 2F, *J* = 10.0 Hz). **HRMS** (EI^+): m/z Calculated for $C_{10}H_{24}B_{20}F_2$ ($[M]^+$) 402.3707, found 402.3736. **X-ray** data for **1/2(B6)**: *M* = 199.25, colorless, monoclinic, $P2_1/c$ (#14), *a* = 7.2815(5) Å, *b* = 11.6189(9) Å, *c* = 12.6617(7) Å, *α* = 90°, *β* = 97.341(6)°, *γ* = 90°, *V* = 1062.44(13) Å^3, *Z* = 4, *Dcalcd* = 1.246 g/cm^3 , *T* = 153.15 K, R_1 (wR_2) = 0.0648 (0.1688).

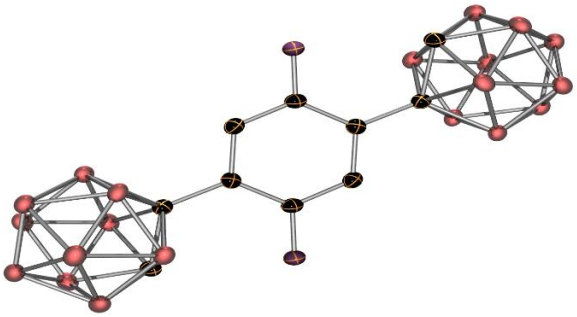
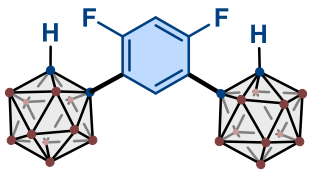


Figure 2.S12. Molecular structure of **B6** with ellipsoids set at 30% probability. H atoms are omitted for clarity.



B7: The general procedure was followed with **A7** (4.84 g, 17.8 mmol), **Li/Cu-1** (23.0 g, 35.6 mmol, 2.0 equiv), isophthalonitrile (4.56 g, 35.6 mmol, 2.0 equiv), and toluene (71.2 mL). Purification by flash column chromatography on silica gel (*n*-hexane/EtOAc = 90/10) afforded **B7** as a white solid (3.49 g, 8.76 mmol, 49%). A single crystal of **B7** was obtained from a saturated solution of **B7** in acetone at rt. **^{1}H NMR** (400 MHz, $CDCl_3$, rt, *δ*/ppm): 7.98 (t, *J* = 8.8 Hz, 1H, Ar-*H*), 7.13 (t, *J* = 12.0 Hz, 1H, Ar-*H*), 4.52 (s, 2H, cage C*H*), 3.41–1.22 (brm, B*H*). **^{11}B NMR** (128 MHz, $CDCl_3$, rt, *δ*/ppm): 0.50–−4.98 (m, 4B), −7.01–−14.50 (m, 16B). **^{13}C{^{1}H} NMR** (100 MHz, $CDCl_3$, rt, *δ*/ppm): 159.3 (dd, $^{1}J_{C,F}$ = 256.9 Hz, $^{3}J_{C,F}$ = 13.6 Hz), 136.0, 119.1–118.7 (m), 107.1–106.3 (m), 70.6, 59.1–58.7 (m). **^{19}F NMR** (376 MHz, $CDCl_3$, rt, *δ*/ppm): −111.4 (t, 2F, $^{4}J_{F,F}$ = 10.2 Hz). **HRMS** (EI^+): m/z Calculated for $C_{10}H_{24}B_{20}$ ($[M]^+$) 402.3707, found 402.3795. **X-ray** data for **B7**: *M* = 398.49, colorless, monoclinic, $P2_1/c$ (#14), *a* = 6.99490(10) Å, *b* = 18.25550(10) Å, *c* = 16.97230(10) Å, *α* = 90°, *β* = 97.1190(10)°, *γ* = 90°, *V* = 2150.58(4) Å^3, *Z* = 4, *Dcalcd* = 1.231 g/cm^3 , *T* = 123.15 K, R_1 (wR_2) = 0.0407 (0.1061).

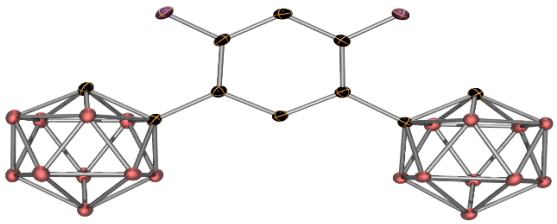
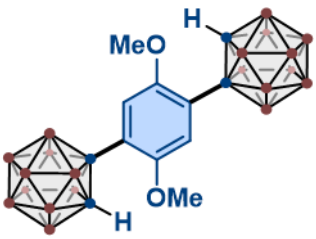


Figure 2.S13. Molecular structure of **B7** with ellipsoids set at 30% probability. H atoms are omitted for clarity.



B8: The general procedure was followed with **A8** (74.0 mg, 0.250 mmol), **Li/Cu-1** (322.7 mg, 0.500 mmol, 2.0 equiv), isophthalonitrile (64.1 mg, 0.500 mmol, 2.0 equiv), and toluene (1.0 mL) , and the reaction was carried out for 32 h. Purification by flash column chromatography on silica gel (*n*-hexane/EtOAc = 90/10) afforded **B8** as a white solid (97.1 mg, 0.230 mmol, 92%). A single crystal of **B8** was obtained from a saturated solution of **B8** in acetone at rt. **^{1}H NMR** (400 MHz, $CDCl_3$, rt, δ/ppm):7.11 (s, 2H, Ar-*H*), 5.28 (s, 2H, cage C*H*). 3.83 (s, 6H, CH_3), 3.24–1.38 (brm, B*H*). **^{11}B NMR** (128 MHz, $CDCl_3$, rt, δ/ppm): −1.31–−5.15 (m, 4B), −6.71–−17.96 (m, 16B). **^{13}C{^{1}H} NMR** (100 MHz, $CDCl_3$, rt, δ/ppm): 149.8, 123.4, 116.9, 73.7, 59.6 (d, J = 11.1 Hz), 56.7 (d, J = 9.2 Hz). **HRMS** (EI^+): m/z Calculated for $C_{12}H_{30}B_{20}O_2$ ($[M]^+$) 426.4107, found 426.4159. **X-ray** data for **1/2(B8)**: M = 211.28, colorless, monoclinic, *C*2/*c* (#15), a = 10.6054(9) Å, b = 10.5708(13) Å, c = 22.338(2) Å, α = 90°, β = 101.970(9)°, γ = 90°, V = 2449.9(4) Å^3, Z = 8, *Dcalcd* = 1.146 g/cm^3 , T = 263.15 K, R_1 (wR_2) = 0.0845 (0.215).

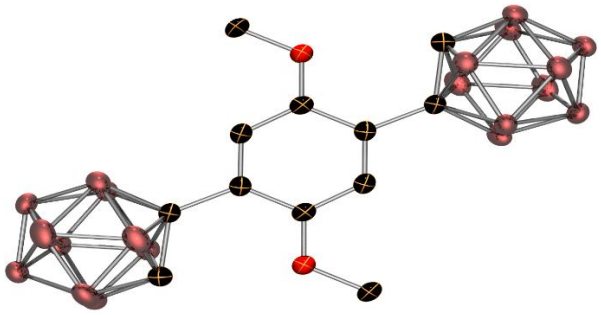
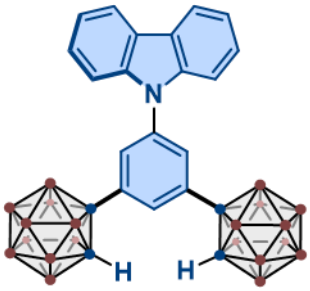


Figure 2.S14. Molecular structure of **B8** with ellipsoids set at 30% probability. H atoms are omitted for clarity.



B9: The general procedure was followed with **A9** (100.3 mg, 0.250 mmol), **Li/Cu-1** (322.7 mg, 0.500 mmol, 2.0 equiv), isophthalonitrile (64.1 mg, 0.500 mmol, 2.0 equiv), and toluene (1.0 mL). Purification by flash column chromatography on silica gel (*n*-hexane/EtOAc = 95/5) afforded **B9** as a white solid (114.0 mg, 0.216 mmol, 86%). A single crystal of **B9** was obtained from a saturated solution of **B9** in acetone at rt. **^{1}H NMR** (400 [1.6 Hz, Ar-*H*), 7.70 (d, 1H, J = 1.6 Hz, Ar-*H*), 7.48 (m, 2H), 7.37 (t, 2H, J = 7.4 Hz, Ar-*H*), 7.31 (d, 2H, J = 8.0 Hz, Ar-*H*), 3.97 (s, 2H, cage C*H*), 3.51–1.47 (brm, B*H*). **^{11}B NMR** (128 MHz, $CDCl_3$, rt, δ/ppm): 1.83–−5.10 (m, 4B), −6.62–−18.64 (m, 16B). **^{13}C{^{1}H} NMR** (100 MHz, $CDCl_3$, rt, δ/ppm): 140.0, 139.3, 136.4, 127.3, 126.8, 125.5, 124.1, 121.4, 121.0, 109.0, 74.6, 60.2 (d, J = 12.9 Hz). **HRMS** (EI^+): m/z Calculated for $C_{22}H_{33}B_{20}N_1$ ($[M]^+$) 531.4474, found 531.4506. **X-ray** data for **B9·(C_3H_6O)**: M = 643.85, colorless, orthorhombic, $P2_12_12_1$ (#19), a = 7.1744(4) Å, b = 21.0702(13) Å, c = 24.1870(12) Å, α = 90°, β = 90°, γ = 90°, V = 3656.3(4) Å^3, Z = 4, *Dcalcd* = 1.170 g/cm^3 , T = 153.15 K, R_1 (wR_2) = 0.0485 (0.1042). A solvent mask was calculated and 108 electrons were found in a volume of 448 Å^3 in 1 void per unit cell. This is consistent with the presence of [C_3H_6O] per formula unit, which accounts for 128 electrons per unit cell.

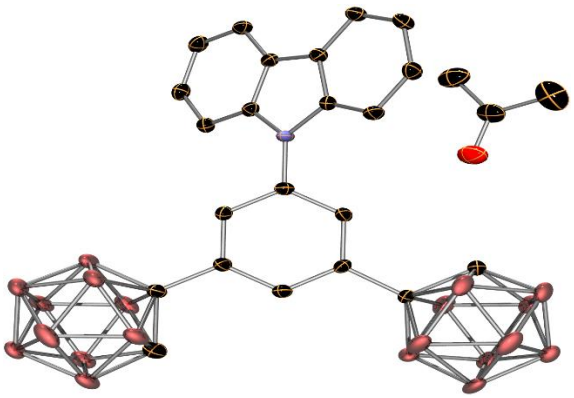
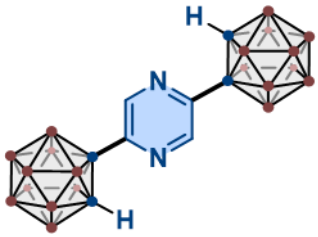


Figure 2.S15. Molecular structure of **B9·(C_3H_6O)** with ellipsoids set at 30% probability. H atoms are omitted for clarity.



B10[53]: The general procedure was followed with **A10** (59.5 mg, 0.250 mmol), **Li/Cu-1** (322.7 mg, 0.500 mmol, 2.0 equiv), isophthalonitrile (64.1 mg, 0.500 mmol, 2.0 equiv), and toluene (1.0 mL). Purification by flash column chromatography on silica gel (*n*-hexane/EtOAc = 90/10) afforded **B10** as a white solid (47.8 mg, 0.131 mmol, 52%). A single crystal of **B10** was obtained from a saturated solution of **B10** in acetone at rt. **^{1}H NMR** (400 MHz, $CDCl_3$, rt, δ/ppm): 8.60 (s, 2H, Ar-*H*), 4.77 (s, 2H, cage C*H*), 3.42–1.33 (brm, B*H*). **X-ray** data for **1/2(B10)**: M = 182.25, colorless, monoclinic, $P2_1/c$ (#14), a = 7.1448(4) Å, b = 11.7803(7) Å, c = 12.3900(7) Å, α = 90°, β = 97.814(6)°, γ = 90°, V = 1033.16(10) Å^3, Z = 4, *Dcalcd* = 1.172 g/cm^3 , T = 153.15 K, R_1 (wR_2) = 0.0479 (0.1293).

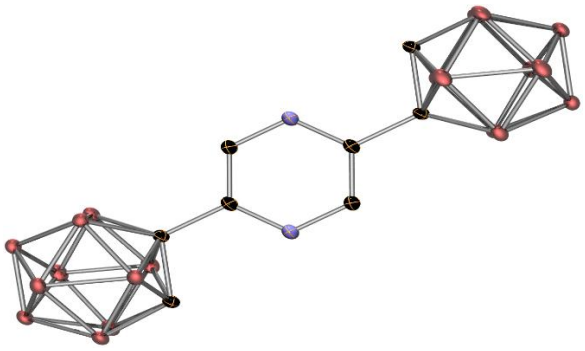
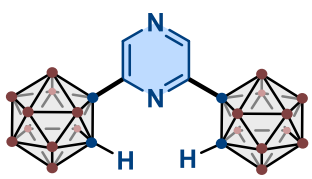


Figure 2.S16. Molecular structure of **B10** with ellipsoids set at 30% probability. H atoms are omitted for clarity.



B11: The general procedure was followed with **A11** (59.5 mg, 0.250 mmol), **Li/Cu-1** (322.7 mg, 0.500 mmol, 2.0 equiv), isophthalonitrile (64.1 mg, 0.500 mmol, 2.0 equiv), and toluene (1.0 mL). Purification by flash column chromatography on silica gel (*n*-hexane/EtOAc = 90/10) afforded **B11** as a white solid (88.7 mg, 0.243 mmol, 97%). A single crystal of **B11** was obtained from a saturated solution of **B11** in acetone at rt. **^{1}H NMR** (400 MHz, $CDCl_3$, rt, δ/ppm): 8.90 (s, 2H, Ar-*H*), 4.42 (s,

2H, cage C*H*), 3.32–1.43 (brm, B*H*). **^{11}B NMR** (128 MHz, $CDCl_3$, rt, δ/ppm): −0.29–−4.68 (m, 4B), −6.04–−15.15 (m, 16B). **^{13}C{^{1}H} NMR** (100 MHz, $CDCl_3$, rt, δ/ppm): 145.6, 143.8 (d, J = 3.7 Hz), 71.5, 56.8 (d, J = 7.3 Hz). **HRMS** (EI^+): m/z Calculated for $C_8H_{24}B_{20}N_2$ ($[M]^+$) 368.3800, found 368.3871. **X-ray** data for **B11**: M = 364.49, colorless, monoclinic, *I*1*a*1 (#9), a = 11.9825(5) Å, b = 14.3028(5) Å, c = 12.7724(5) Å, α = 90°, β = 106.159(4)°, γ = 90°, V = 2102.50(15) Å^3, Z = 4, *Dcalcd* = 1.151 g/cm^3 , T = 153.15 K, R_1 (wR_2) = 0.0488 (0.1282).

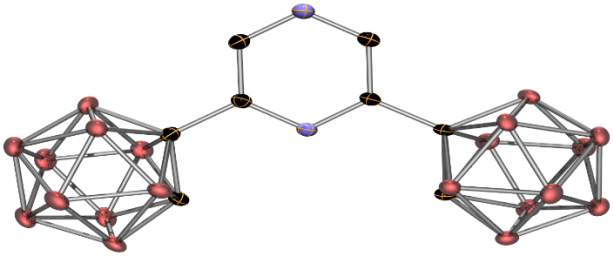
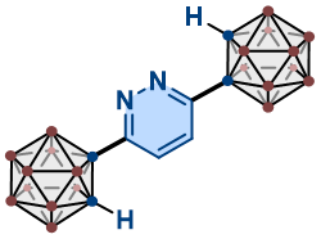


Figure 2.S17. Molecular structure of **B11** with ellipsoids set at 30% probability. H atoms are omitted for clarity.



B12: The general procedure was followed with **A12** (59.5 mg, 0.250 mmol), **Li/Cu-1** (322.7 mg, 0.500 mmol, 2.0 equiv), isophthalonitrile (64.1 mg, 0.500 mmol, 2.0 equiv), and toluene (1.0 mL). Purification by flash column chromatography on silica gel (*n*-hexane/EtOAc = 90/10) afforded **B12** as a white solid (76.1 mg, 0.209 mmol, 83%). A single crystal of **B12** was obtained from a saturated solution of **B12** in acetone at rt. **^{1}H NMR** (400 MHz, $CDCl_3$, rt, δ/ppm): 7.74 (s, 2H, Ar-*H*), 5.03 (s, 2H, cage C*H*), 3.28–1.39 (brm, B*H*). **^{11}B NMR** (128 MHz, $CDCl_3$, rt, δ/ppm): −0.78–−4.87 (m, 4B), −6.93–−15.88 (m, 16B). **^{13}C{^{1}H} NMR** (100 MHz, $CDCl_3$, rt, δ/ppm): 155.5, 126.5, 71.8, 57.0 (d, J = 10.2 Hz). **HRMS** (EI^+): m/z Calculated for $C_8H_{24}B_{20}N_2$ ($[M]^+$) 368.3800, found 368.3856. **X-ray** data for **B12**: M = 364.49, colorless, orthorhombic, *Pna*2$_1$ (#33), a = 24.7124(3) Å, b = 6.75550(10) Å, c = 12.4271(2) Å, α = 90°, β = 90°, γ = 90°, V = 2074.64(5) Å^3, Z = 4, *Dcalcd* = 1.167 g/cm^3 , T = 153.15 K, R_1 (wR_2) = 0.0374 (0.0967).

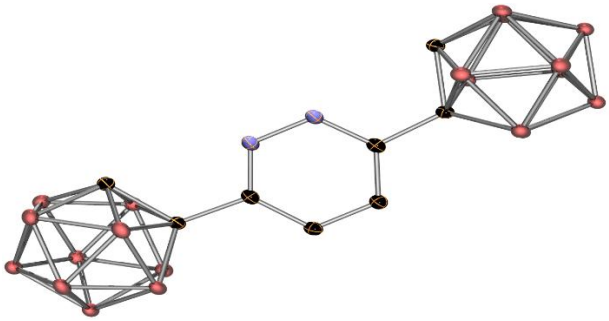
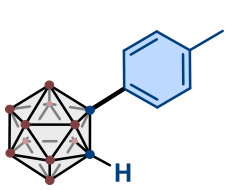


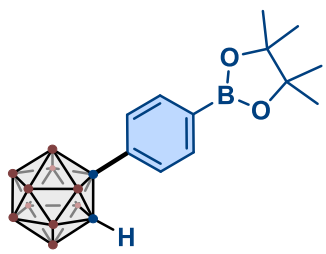
Figure 2.S18. Molecular structure of **B12** with ellipsoids set at 30% probability. H atoms are omitted for clarity.



C13[54]: The general procedure was followed with **A13** (42.8 mg, 0.250 mmol), **Li/Cu-1** (161.3 mg, 0.250 mmol, 1.0 equiv), isophthalonitrile (32.0 mg, 0.250 mmol, 1.0 equiv), and toluene (0.5 mL). Purification by flash column chromatography on silica gel (*n*-hexane) afforded **C13** as a white solid (56.6 mg, 0.242 mmol, 97%). **^{1}H NMR** (400 MHz, $CDCl_3$, rt, δ/ppm): 7.36 (d, 2H, J = 8.4 Hz, Ar-*H*), 7.13 (d, 2H, J = 8.0 Hz, Ar-*H*), 3.92 (s, 1H, cage C*H*), 2.34 (s, 3H, CH_3), 3.32–1.64 (brm, B*H*).

C13 was also synthesized by following the general procedure with **A13′** (63.2 mg, 0.499 mmol), **Li/Cu-1** (322.7 mg, 0.500 mmol, 1.0 equiv), isophthalonitrile (64.1 mg, 0.500 mmol, 1.0 equiv), and toluene (1.0 mL). Purification by flash column chromatography on silica gel (*n*-hexane) afforded **C13** as a white solid (83.3 mg, 0.355 mmol, 71%).

C13 was also synthesized by following the general procedure with **A13″** (54.5 mg, 0.250 mmol), **Li/Cu-1** (161.3 mg, 0.250 mmol, 1.0 equiv), isophthalonitrile (32.0 mg, 0.250 mmol, 1.0 equiv), and toluene (0.5 mL), and the reaction was carried out for 48 h. Purification by flash column chromatography on silica gel (*n*-hexane) afforded **C13** as a white solid (55.7 mg, 0.238 mmol, 95%).



C14: The general procedure was followed with **A14** (70.7 mg, 0.250 mmol), **Li/Cu-1** (161.3 mg, 0.250 mmol, 1.0 equiv), isophthalonitrile (32.0 mg, 0.250 mmol, 1.0 equiv), and toluene (0.5 mL). Purification by flash column chromatography on silica gel (*n*-hexane/EtOAc = 80/20) afforded **C14** as a white solid (79.6 mg, 0.230 mmol, 92%). A single crystal of **C14** was obtained from a saturated solution of **C14** in acetone at rt. **^{1}H NMR** (400 MHz, $CDCl_3$, rt, δ/ppm): 7.76 (d, J = 8.4 Hz, 2H, Ar-*H*), 7.46 (d, J = 8.4 Hz, 2H, Ar-*H*), 3.99 (s, 1H, cage C*H*), 1.33 (s, 12H, C-CH_3), 3.01–1.66 (brm, B*H*). **^{11}B NMR** (128 MHz, $CDCl_3$, rt, δ/ppm): 30.3 (s, 1B, Ar-*B*Pin), −0.0–−6.6 (m, 2B), −6.9–−15.9 (m, 8B). **^{13}C{^{1}H} NMR** (100 MHz, $CDCl_3$, rt, δ/ppm): 136.2, 135.3, 126.7, 84.4, 76.5, 59.9 (d, J = 15.3 Hz), 25.0 (d, J = 6.6 Hz). A signal of the ipso-carbon bonded to the boron was not identified. **HRMS** (EI^+): m/z Calculated for $C_{14}H_{27}B_{11}O_2$ ([M]$^+$) 348.3030, found 348.3057. **X-ray** data for **C14**: M = 346.26, colorless, monoclinic, $P2_1/n$ (#14), a = 7.6804(3) Å, b = 23.5249(11) Å, c = 11.3975(4) Å, α = 90°, β = 91.154(4)°, γ = 90°, V = 2058.89(14) Å^3, Z = 4, $Dcalcd$ = 1.117 g/cm^3 , T = 153.15 K, R_1 (wR_2) = 0.0459 (0.1198).

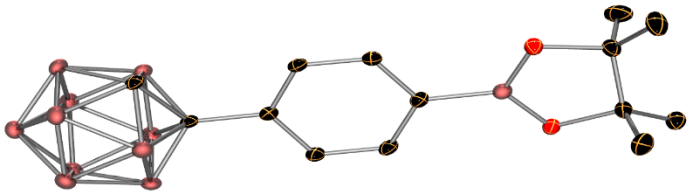
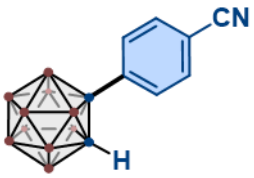
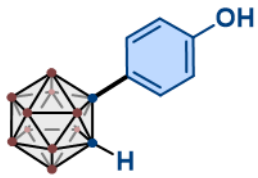


Figure 2.S19. Molecular structure of **C14** with ellipsoids set at 30% probability. H atoms are omitted for clarity.

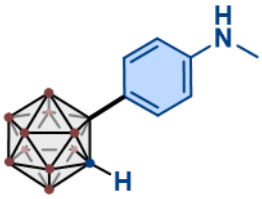


C15[55]: The general procedure was followed with **A15** (45.5 mg, 0.250 mmol), **Li/Cu-1** (161.3 mg, 0.250 mmol, 1.0 equiv), isophthalonitrile (32.0 mg, 0.250 mmol, 1.0 equiv), and toluene (0.5 mL). Purification by flash column chromatography on silica gel (*n*-hexane/EtOAc = 90/10) afforded **C15** as a white solid (60.4 mg, 0.246 mmol, 99%). **^{1}H NMR** (400 MHz, $CDCl_3$, rt, δ/ppm): 7.68–7.58 (m, 4H, Ar-*H*), 4.00 (s, 1H, cage C*H*), 3.49–1.45 (brm, B*H*). **HRMS** (EI^+): m/z Calculated for $C_9H_{15}B_{10}N_1$ ([M]$^+$) 247.2135, found 247.2141.



C16[56]: The general procedure was followed with **A16** (43.3 mg, 0.250 mmol), **Li/Cu-1** (242.0 mg, 0.375 mmol, 1.5 equiv), isophthalonitrile (48.0 mg, 0.375 mmol, 1.5 equiv), and toluene (0.75 mL). Purification by flash column chromatography on silica gel (*n*-hexane/EtOAc = 70/30) afforded **C16** as a white solid (47.6 mg, 0.202 mmol, 81%). **^{1}H NMR** (400 MHz, $CDCl_3$, rt, δ/ppm): 7.42–7.35 (m, 2H, Ar-*H*), 6.81–6.71 (m, 2H, Ar-*H*), 5.01 (s, 1H, O*H*), 3.86 (s, 1H, cage C*H*), 3.41–1.46 (brm, B*H*).

C16 was also synthesized by following the general procedure with **A16′** (64.2 mg, 0.499 mmol), **Li/Cu-1** (484.0 mg, 0.750 mmol, 1.5 equiv), isophthalonitrile (96.1 mg, 0.750 mmol, 1.5 equiv), and toluene (1.5 mL). Purification by flash column chromatography on silica gel (*n*-hexane/EtOAc = 70/30) afforded **C16** as a white solid (63.6 mg, 0.270 mmol, 54%).



C17: The general procedure was followed with **A17** (93.0 mg, 0.500 mmol), **Li/Cu-1** (484.0 mg, 0.750 mmol, 3.0 equiv), isophthalonitrile (96.1 mg, 0.750 mmol, 3.0 equiv), and toluene (1.5 mL). Purification by flash column chromatography on silica gel (*n*-hexane/EtOAc = 85/15) afforded **C17** as a white solid (109.4 mg, 0.441 mmol, 88%). *The procedure for recovering o-carborane and isophthalonitrile is given in Section 8-2 (see Figure 2.S33).* A single crystal of **C17** was obtained from a saturated solution of **C17** in acetone at rt. **^{1}H NMR** (400 MHz, $CDCl_3$, rt, δ/ppm): 7.30 (m, 2H, Ar-*H*), 6.47 (m, 2H, Ar-*H*), 3.95 (brs, N*H*), 3.82 (s, 1H, cage C*H*), 2.84 (s, 3H, CH_3), 3.44–1.22 (brm, B*H*). **^{11}B NMR** (128 MHz, $CDCl_3$, rt, δ/ppm): −0.50–−3.09 (m, 1B), −3.63–−6.63 (m, 1B), −8.17–−15.34 (m, 8B). **^{13}C{^{1}H} NMR** (100 MHz, $CDCl_3$, rt, δ/ppm): 150.4, 129.3, 121.6, 111.8 (d, J = 6.0 Hz), 78.2, 61.6 (d, J = 14.2 Hz), 30.4 (d, J = 8.4 Hz). **HRMS** (EI^+): m/z Calculated for $C_9H_{19}B_{10}N_1$ ($[M]^+$) 251.2448, found 251.2452. **X-ray** data for **C17**: M = 249.35, colorless, monoclinic, $P2_1/n$ (#14), a = 7.1546(2) Å, b = 18.9206(7) Å, c = 10.4931(4) Å, α = 90°, β = 92.876(3)°, γ = 90°, V = 1418.65(9) Å^3, Z = 4, *Dcalcd* = 1.167 g/cm^3 , T = 153.15 K, R_1 (wR_2) = 0.0599 (0.1613).

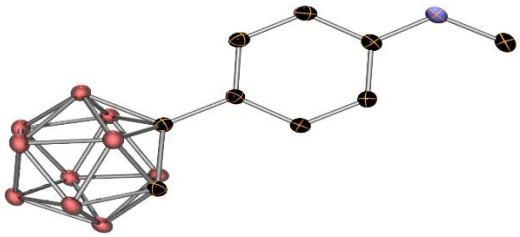
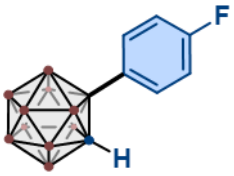
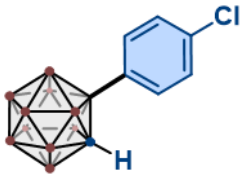


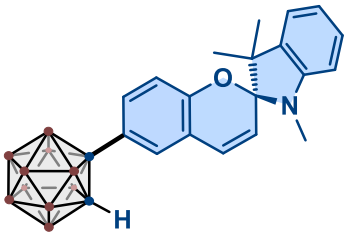
Figure 2.S20. Molecular structure of **C17** with ellipsoids set at 30% probability. H atoms are omitted for clarity.



C18[36]: The general procedure was followed with **A18** (43.8 mg, 0.250 mmol), **Li/Cu-1** (161.3 mg, 0.250 mmol, 1.0 equiv), isophthalonitrile (32.0 mg, 0.250 mmol, 1.0 equiv), and toluene (0.5 mL). Purification by flash column chromatography on silica gel (*n*-hexane) afforded **C18** as a white solid (58.1 mg, 0.244 mmol, 97%). **^{1}H NMR** (400 MHz, $CDCl_3$, rt, δ/ppm): 7.52–7.44 (m, 2H, Ar-*H*), 7.05–6.99 (m, 2H, Ar-*H*), 3.90 (s, 1H, cage C*H*), 3.38–1.36 (brm, B*H*). **^{19}F NMR** (376 MHz, $CDCl_3$, rt, δ/ppm): −113.74–−113.84 (m, 1F, Ar-*F*).



C19[36]: The general procedure was followed with **A19** (47.9 mg, 0.250 mmol), **Li/Cu-1** (161.3 mg, 0.250 mmol, 1.0 equiv), isophthalonitrile (32.0 mg, 0.250 mmol, 1.0 equiv), and toluene (0.5 mL). Purification by flash column chromatography on silica gel (*n*-hexane) afforded **C19** as a white solid (59.0 mg, 0.232 mmol, 93%) **^{1}H NMR** (400 MHz, $CDCl_3$, rt, δ/ppm): 7.46–7.39 (m, 2H, Ar-*H*), 7.34–7.28 (m, 2H, Ar-*H*), 3.92 (s, 1H, cage*CH*), 3.40–1.46 (brm, B*H*).



C20[12]: The general procedure was followed with **A20** (89.1 mg, 0.250 mmol), **Li/Cu-1** (161.3 mg, 0.250 mmol, 1.0 equiv), isophthalonitrile (32.0 mg, 0.250 mmol, 1.0 equiv), and toluene (0.5 mL). Purification by flash column chromatography on silica gel (*n*-hexane/EtOAc = 99/1 to 90/10) afforded **C20** as a pale yellow solid (83.2 mg, 0.198 mmol, 79%). A single crystal of **C20** was obtained from a saturated solution of **C20** in acetone at rt. **^{1}H NMR** (400 MHz, $CDCl_3$, rt, δ/ppm): 7.24–7.14 (m, 3H, Ar-*H*), 7.07 (d, J = 7.6 Hz, 1H, Ar-*H*), 6.89–6.78 (m, 2H, Ar-*H* and Ar-C*H*-CH), 6.63 (d, J = 7.6 Hz, 1H, Ar-*H*), 6.53 (d, J = 7.6 Hz, 1H, Ar-*H*), 5.76 (d, J = 10.4 Hz, 1H, C-C*H*-CH), 3.85 (s, 1H, cage C*H*), 2.71 (s, 3H, N-CH_3), 1.28 (s, 3H, C-CH_3), 1.16 (s, 3H, C-CH_3), 3.35–1.42 (brm, B*H*). **^{11}B NMR** (128 MHz, $CDCl_3$, rt, δ/ppm): −0.93–−5.68 (m, 2B), −8.04–−16.22 (m, 8B). **^{13}C{^{1}H} NMR** (100 MHz, $CDCl_3$, rt, δ/ppm): 155.9, 148.1, 136.5, 129.3, 128.7 (d, J = 4.8 Hz), 127.9, 126.6, 125.0, 121.7, 121.2, 119.6, 118.9, 115.3 (d, J = 5.6 Hz), 107.1, 105.3, 61.2 (d, J = 13.5 Hz), 52.1, 29.0 (d, J = 8.5 Hz), 26.0 (d, J = 4.6 Hz), 20.2 (d, J = 5.4 Hz). **HRMS** (EI^+): m/z Calculated for $C_{21}H_{29}B_{10}N_1O_1$ ($[M]^+$) 421.3180, found 421.3230. **X-ray** data for **C20**: M = 419.55, orange, orthorhombic, *Pbca* (#61), a = 14.9882(9) Å, b = 12.2029(7) Å, c = 25.5284(13) Å, α = 90°, β = 90°, γ = 90°, V = 4669.1(5) Å^3, Z = 8, *Dcalcd* = 1.194 g/cm^3 , T = 153.15 K, R_1 (wR_2) = 0.0731 (0.1684).

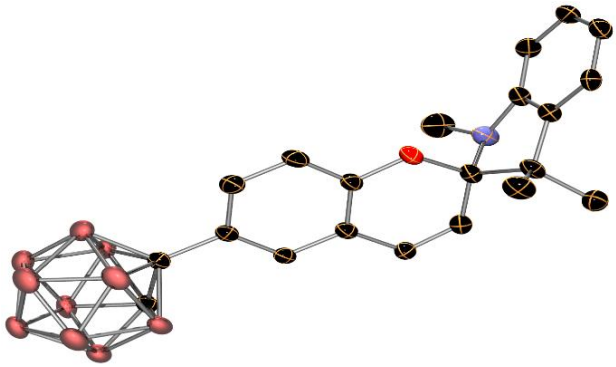
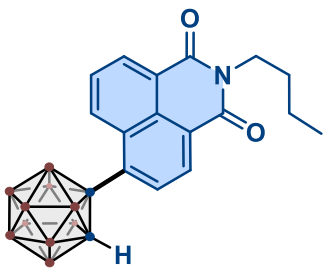


Figure 2.S21. Molecular structure of **C20** with ellipsoids set at 30% probability. H atoms are omitted for clarity.



C21: The general procedure was followed with **A21** (83.0 mg, 0.250 mmol), **Li/Cu-1** (161.3 mg, 0.250 mmol, 1.0 equiv), isophthalonitrile (32.0 mg, 0.250 mmol, 1.0 equiv), and toluene (0.5 mL). Purification by flash column chromatography on silica gel (*n*-hexane only) afforded **C21** as a white solid (89.5 mg, 0.226 mmol, 91%). A single crystal of **C21** was obtained from a saturated solution of **C21** in acetone at rt. **^{1}H NMR** (400 MHz, $CDCl_3$, rt, δ/ppm): 9.16 (d, 1H, J = 9.2 Hz, Ar-*H*), 8.68 (d, 1H, J = 7.2 Hz, Ar-*H*), 8.52 (d, 1H, J = 8.0 Hz, Ar-*H*), 7.93 (d, 1H, J = 8.0 Hz, Ar-*H*), 7.86 (dd, 1H, J = 8.8 Hz, 7.2 Hz, Ar-*H*), 4.67 (s, 1H, cage C*H*), 4.16 (t, 2H, J = 7.6 Hz, N-CH_2), 1.70 (quin, 2H, J = 7.6 Hz, CH_2-CH_2-CH_2) 1.43 (sx, 2H, J = 7.5 Hz, CH_2-CH_2-CH_3), 0.97 (t, 3H, J = 7.2 Hz, CH_2-CH_3), 3.63–1.50 (brm, B*H*). **^{11}B NMR** (128 MHz, $CDCl_3$, rt, δ/ppm): −0.04–−3.85 (m, 2B), −6.47–−15.71 (m, 8B). **^{13}C{^{1}H} NMR** (100 MHz, $CDCl_3$, rt, δ/ppm): 163.8, 163.1, 135.4, 131.8, 131.2, 129.7, 129.6, 129.0, 127.8,

124.7, 123.8, 76.0, 61.4, 40.6, 30.2, 20.5, 13.9. **HRMS** (EI^+): m/z Calculated for $C_{18}H_{25}B_{10}N_1O_2$ ($[M]^+$) 397.2816, found 397.2840. **X-ray** data for **C21**: M = 395.49, colorless, triclinic, P-1 (#2), a = 7.3843(3) Å, b = 8.7494(4) Å, c = 16.6349(8) Å, α = 77.660(4)°, β = 78.871(4)°, γ = 88.299(4)°, V = 1030.10(8) Å^3, Z = 2, $Dcalcd$ = 1.275 g/cm^3 , T = 153.15 K, R_1 (wR_2) = 0.0578 (0.1508).

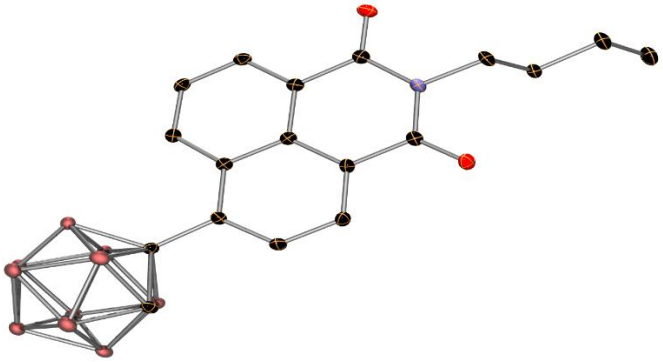
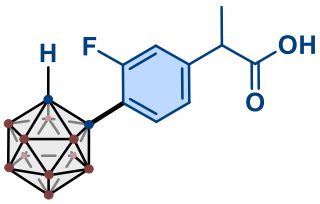


Figure 2.S22. Molecular structure of **C21** with ellipsoids set at 30% probability. H atoms are omitted for clarity.



C22: The general procedure was followed with **A22** (61.8 mg, 0.250 mmol), **Li/Cu-1** (322.7 mg, 0.500 mmol, 2.0 equiv), isophthalonitrile (64.1 mg, 0.500 mmol, 2.0 equiv), and toluene (1.0 mL). Purification by flash column chromatography on silica gel (*n*-hexane/EtOAc = 1/2 to 2/3) afforded **C22** as a white solid (47.3 mg, 0.152 mmol, 61%). A single crystal of **C22** was obtained from a saturated solution of **C22** in acetone at rt. **^{1}H NMR** (400 MHz, $CDCl_3$, rt, δ/ppm): 7.57 (t, J = 8.6 Hz, 1H, Ar-*H*), 7.11 (d, J = 8.4 Hz, 1H, Ar-*H*), 7.04 (d, J = 14.4 Hz, 1H, Ar-*H*), 4.63 (s, 1H, cage C*H*), 3.73 (q, J = 7.1 Hz, 1H, CH_3-C*H*), 1.51 (d, J = 7.2 Hz, 3H, CH-CH_3), 3.36–1.15 (brm, B*H*). **^{11}B NMR** (128 MHz, $CDCl_3$, rt, δ/ppm): −1.37–−4.20 (m, 2B), −4.85–−16.10 (m, 8B). **^{13}C{^{1}H} NMR** (100 MHz, $CDCl_3$, rt, δ/ppm): 178.6, 159.0 (d, $^1J_{C,F}$ = 248.8 Hz), 143.9 (d, J = 8.7 Hz), 132.2, 124.5, 120.2 (d, J = 8.4 Hz), 116.4 (d, J = 24.9 Hz), 72.1, 59.4 (d, J = 18.6 Hz), 44.5, 18.0. **^{19}F NMR** (376 MHz, $CDCl_3$, rt, δ/ppm): −117.7 (s, 1F). **HRMS** (EI^+): m/z Calculated for $C_{11}H_{19}B_{10}F_1O_2$ ($[M]^+$) 312.2300, found 312.2322. **X-ray** data for **C22**: M = 310.36, colorless, triclinic, P-1 (#2), a = 6.88599(18) Å, b = 9.9543(3) Å, c = 12.7186(2) Å, α = 96.886(2)°, β = 101.2502(19)°, γ = 101.555(2)°, V = 826.17(4) Å^3, Z = 2, $Dcalcd$ = 1.248 g/cm^3, T = 123.15 K, R_1 (wR_2) = 0.0539 (0.1406).

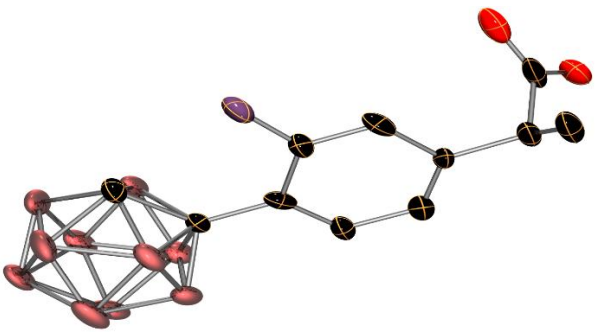
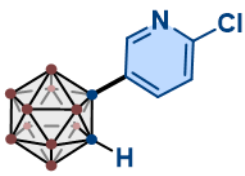


Figure 2.S23. Molecular structure of **C22** with ellipsoids set at 30% probability. One of the disordered

molecules is shown. H atoms are omitted for clarity.



C23: The general procedure was followed with **A23** (48.1 mg, 0.250 mmol), **Li/Cu-1** (161.3 mg, 0.250 mmol, 1.0 equiv), isophthalonitrile (32.0 mg, 0.250 mmol, 1.0 equiv), and toluene (0.5 mL). Purification by flash column chromatography on silica gel (*n*-hexane/EtOAc = 90/10) afforded **C23** as a white solid (50.9 mg, 0.199 mmol, 80%). A single crystal of **C23** was obtained from a saturated solution of **C23** in acetone at rt. **^{1}H NMR** (400 MHz, $CDCl_3$, rt, δ/ppm): 8.52 (d, 1H, J = 2.8 Hz, Ar-*H*), 7.78 (dd, 1H, J = 8.4 H, 2.8 Hz, Ar-*H*), 7.33 (d, 1H, J = 8.8 Hz, Ar-*H*), 3.92 (s, 1H, cage C*H*), 3.42–1.41 (brm, B*H*). **^{11}B NMR** (128 MHz, $CDCl_3$, rt, δ/ppm): −0.02–−5.34 (m, 2B), −7.17–−15.25 (m, 8B). **^{13}C{^{1}H} NMR** (100 MHz, $CDCl_3$, rt, δ/ppm): 153.5, 148.5, 138.3, 128.8, 124.3, 72.7, 60.3. **HRMS** (EI^+): m/z Calculated for $C_7H_{14}B_{10}Cl_1N_1$ ($[M]^+$) 257.1745, found 257.1766. **X-ray** data for **C23**: M = 255.74, colorless, orthorhombic, $Pna2_1$ (#33), a = 26.0585(9) Å, b = 7.1993(3) Å, c = 7.1951(3) Å, α = 90°, β = 90°, γ = 90°, V = 1349.82(9) Å^3, Z = 4, $Dcalcd$ = 1.258 g/cm^3 , T = 153.15 K, R_1 (wR_2) = 0.0310 (0.0829).

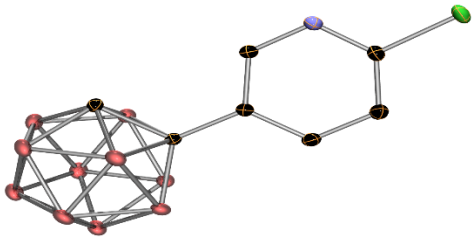
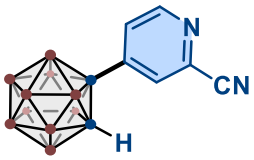


Figure 2.S24. Molecular structure of **C23** with ellipsoids set at 30% probability. H atoms are omitted for clarity.



C24: The general procedure was followed with aryl chloride **A24′** (69.3 mg, 0.500 mmol), **Li/Cu-1** (322.7 mg, 0.500 mmol, 2.0 equiv), isophthalonitrile (64.1 mg, 0.500 mmol, 2.0 equiv), and toluene (1.0 mL). Purification by flash column chromatography on silica gel (*n*-hexane/EtOAc = 90/10) afforded **C24** as a white solid (31.9 mg, 0.130 mmol, 26%). A single crystal of **C24** was obtained from a saturated solution of **C24** in acetone at rt. **^{1}H NMR** (400 MHz, $CDCl_3$, rt, δ/ppm): 8.78–8.71 (m, 1H, Ar-*H*), 7.74 (s, 1H, Ar-*H*), 7.59 (d, 1H, J = 4.8 Hz, Ar-*H*), 4.00 (s, 1H, cage C*H*), 3.30–1.05 (brm, B*H*). **^{11}B NMR** (128 MHz, $CDCl_3$, rt, δ/ppm): 0.14–−3.74 (m, 2B), −6.03–−15.32 (m, 8B). **^{13}C{^{1}H} NMR** (100 MHz, $CDCl_3$, rt, δ/ppm): 151.9, 143.9, 135.2, 126.5, 125.0, 116.3, 72.1, 59.1 (d, J = 13.8 Hz). **HRMS** (EI^+): m/z Calculated for $C_8H_{14}B_{10}N_2$ ($[M]^+$) 248.2087, found 248.2085. **X-ray** data for **2(C24)**: M = 492.62, colorless, monoclinic, $P2_1/c$ (#14), a = 6.7996(2) Å, b = 20.5686(6) Å, c = 19.3753(5) Å, α = 90°, β = 91.061(2)°, γ = 90°, V = 2709.33(13) Å^3, Z = 4, $Dcalcd$ = 1.208 g/cm^3 , T = 153.15 K, R_1 (wR_2) = 0.0663 (0.1602).

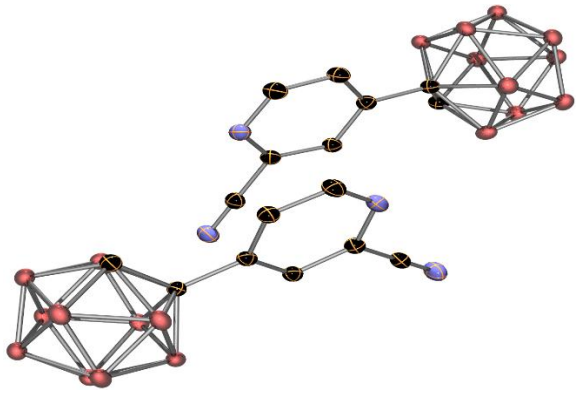
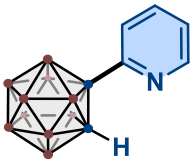
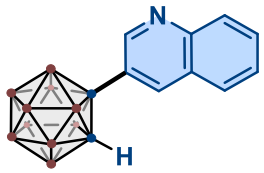


Figure 2.S25. Molecular structure of **2(C24)** with ellipsoids set at 30% probability. H atoms are omitted for clarity.



C25[58]:The general procedure was followed with **A25** (39.5 mg, 0.250 mmol), **Li/Cu-1** (161.3 mg, 0.250 mmol, 1.0 equiv), isophthalonitrile (32.0 mg, 0.250 mmol, 1.0 equiv), and toluene (0.5 mL). Purification by flash column chromatography on silica gel (*n*-hexane/EtOAc = 90/10) afforded **C25** as a white solid (47.1 mg, 0.213 mmol, 85%). **^{1}H NMR** (400 MHz, $CDCl_3$, rt, δ/ppm): 8.41 (d, J = 4.8 Hz, 1H, Ar-*H*), 7.70 (t, J = 7.8 Hz, 1H, Ar-*H*), 7.53 (d, J = 8.0 Hz, 1H, Ar-*H*), 7.31 (dd, J = 7.8 Hz, J = 5.0 Hz, 1H, Ar-*H*), 4.99 (s, 1H, cage C*H*), 3.351–0.73 (brm, B*H*).



C26: The general procedure was followed with **A26** (52.0 mg, 0.250 mmol), **Li/Cu-1** (161.3 mg, 0.250 mmol, 1.0 equiv), isophthalonitrile (32.0 mg, 0.250 mmol, 1.0 equiv), and toluene (0.5 mL). Purification by flash column chromatography on silica gel (*n*-hexane/EtOAc = 90/10) afforded **C26** as a white solid (57.6 mg, 0.212 mmol, 85%). A single crystal of **C26** was obtained from a saturated solution of **C26** in acetone at rt. **^{1}H NMR** (400 MHz, $CDCl_3$, rt, δ/ppm): 8.99 (d, J = 2.0 Hz, 1H, Ar-*H*), 8.30 (d, J = 2.0 Hz, 1H, Ar-*H*), 8.12 (d, J = 8.4 Hz, 1H, Ar-*H*), 7.84 (d, J = 8.0 Hz, 1H, Ar-*H*), 7.80 (t, J = 7.6 Hz, 1H, Ar-*H*), 7.64 (t, J = 7.8 Hz, 1H, Ar-*H*), 4.07 (s, 1H, cage C*H*), 3.62–1.11 (brm, B*H*). **^{11}B NMR** (128 MHz, $CDCl_3$, rt, δ/ppm): 0.03–−4.99 (m, 2B), −6.09–−15.73 (m, 8B). **^{13}C{^{1}H} NMR** (100 MHz, $CDCl_3$, rt, δ/ppm): 148.3, 148.2, 135.8, 131.5, 129.5, 128.4–127.9 (m, two kinds of peaks overlapped), 126.6, 126.4, 74.2, 60.6 (d, J = 15.8 Hz). **HRMS** (EI^+): m/z Calculated for $C_{10}H_{24}B_{20}$ ($[M]^+$) 273.2291, found 273.2301. **X-ray** data for **C26**: M = 271.35, colorless, orthorhombic, *Pna*2$_1$ (#33), a = 6.98320(10) Å, b = 21.0279(3) Å, c = 10.1776(2) Å, α = 90°, β = 90°, γ = 90°, V = 1494.50(4) Å^3, Z = 4, *Dcalcd* = 1.206 g/cm^3 , T = 123.15 K, R_1 (wR_2) = 0.0433 (0.1106).

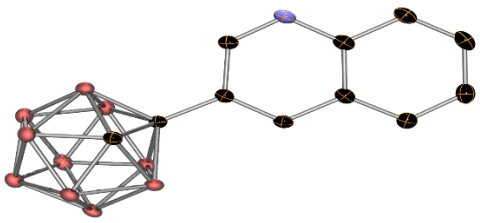
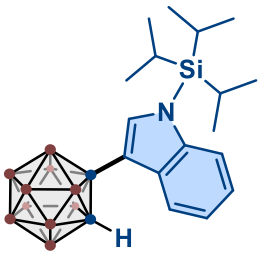


Figure 2.S26. Molecular structure of **C26** with ellipsoids set at 30% probability. H atoms are omitted for clarity.



C27: The general procedure was followed with **A27** (88.1 mg, 0.250 mmol), **Li/Cu-1** (161.3 mg, 0.250 mmol, 1.0 equiv), isophthalonitrile (32.0 mg, 0.250 mmol, 1.0 equiv), and toluene (0.5 mL). Purification by flash column chromatography on silica gel (*n*-hexane) afforded **C27** as a white solid (101.0 mg, 0.243 mmol, 97%). A single crystal of **C27** was obtained from a saturated solution of **C27** in acetone at rt. **^{1}H NMR** (400 MHz, $CDCl_3$, rt, δ/ppm): 7.96–7.89 (m, 1H, Ar-*H*), 7.54–7.46 (m, 2H, Ar-*H*), 7.25–7.17 (m, 2H, Ar-*H*), 3.96 (s, 1H, cage C*H*), 1.69 (m, 3H, C*H*$(CH_3)_2$), 1.15 (d, 18H, J = 7.6 Hz, CH(CH_3)$_2$), 3.60–1.46 (brm, B*H*). **^{11}B NMR** (128 MHz, $CDCl_3$, rt, δ/ppm): −0.49–−5.97 (m, 2B), −6.79–−17.52 (m, 8B). **^{13}C{^{1}H} NMR** (100 MHz, $CDCl_3$, rt, δ/ppm): 141.2, 133.8 (d, J = 2.2 Hz), 128.2, 122.7, 121.3, 119.8, 114.7, 112.0, 73.7, 63.9 (d, J = 13.6 Hz), 18.1, 12.9. **HRMS** (EI$^+$): m/z Calculated for $C_{19}H_{37}B_{10}N_1Si_1$ ([M]$^+$) 417.3626, found 417.3669. **X-ray** data for **C27**: M = 415.68, colorless, monoclinic, $P2_1/c$ (#14), a = 13.7789(4) Å, b = 7.3417(2) Å, c = 24.5423(7) Å, α = 90°, β = 91.987(3)°, γ = 90°, V = 2481.22(12) Å^3, Z = 4, $Dcalcd$ = 1.113 g/cm^3, T = 153.15 K, R_1 (wR_2) = 0.0363 (0.0976).

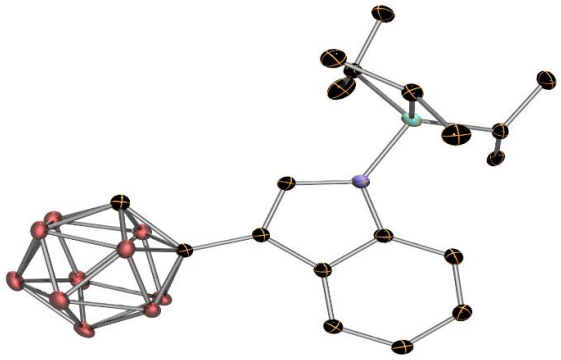
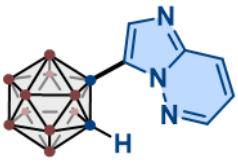


Figure 2.S27. Molecular structure of **C27** with ellipsoids set at 30% probability. H atoms and a disordered molecule are omitted for clarity.



C28: The general procedure was followed with **A28** (49.5 mg, 0.250 mmol), **Li/Cu-1** (161.3 mg, 0.250 mmol, 1.0 equiv), isophthalonitrile (32.0 mg, 0.250 mmol, 1.0 equiv), and toluene (0.5 mL). Purification by flash column chromatography on silica gel (*n*-hexane/EtOAc = 90/10) afforded **C28** as a white solid (61.0 mg, 0.233 mmol, 93%). A single crystal of **C28** was obtained from a saturated solution of **C28** in acetone at rt. **^{1}H NMR** (400 MHz, $CDCl_3$, rt, δ/ppm): 8.40 (d, J = 3.6 Hz, 1H, C*H*-N), 8.03 (d, J = 8.8 Hz, 1H, C-C*H*-CH), 7.95 (s, 1H, N-C*H*-C), 7.15 (dd, 1H, J = 9.2 Hz, 4.4 Hz, CH-C*H*-CH), 5.52 (s, 1H, cage C*H*), 3.49–0.60 (brm, B*H*). **^{11}B NMR** (128 MHz, $CDCl_3$, rt, δ/ppm): −1.29–−5.00 (m, 2B), −6.63–−16.2 (m, 8B). **^{13}C{^{1}H} NMR** (100 MHz, DMSO-d_6, rt, δ/ppm): 144.3, 140.0, 136.4 (d, J = 4.7 Hz), 126.4, 119.3, 119.1, 67.3, 63.1. **HRMS** (DART$^+$, m/z): Calculated for $C_8H_{16}B_{10}N_3$ ([M+H]$^+$) 264.22693, found 264.22858. **X-ray** data for **C28**: M = 261.33, colorless, monoclinic, $P2_1/n$ (#14), a = 6.9911(2) Å, b = 9.4471(3) Å, c = 20.9966(6) Å, α = 90°, β = 96.610(3)°, γ = 90°, V = 1377.52(7) Å^3, Z = 4,

Dcalcd = 1.260 g/cm^3, *T* = 123.15 K, R_1 (wR_2) = 0.0411 (0.1152).

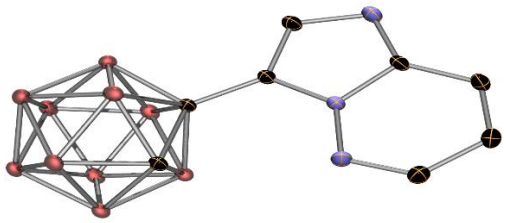
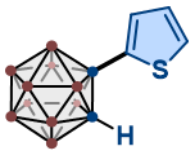
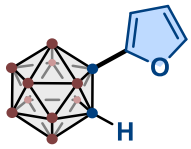


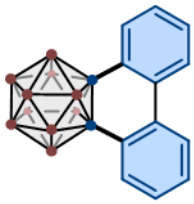
Figure 2.S28. Molecular structure of **C28** with ellipsoids set at 30% probability. H atoms are omitted for clarity.



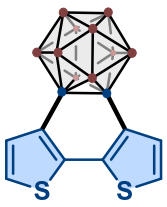
C29[59]: The general procedure was followed with **A29** (40.8 mg, 0.250 mmol), **Li/Cu-1** (161.3 mg, 0.250 mmol, 1.0 equiv), isophthalonitrile (32.0 mg, 0.250 mmol, 1.0 equiv), and toluene (0.5 mL). Purification by flash column chromatography on silica gel (*n*-hexane only) afforded **C29** as a white solid (56.4 mg, 0.249 mmol, 99%). **^{1}H NMR** (400 MHz, $CDCl_3$, rt, *δ*/ppm): 7.29–7.17 (m, 2H, S-C*H*-CH and C-C*H*-CH, overlapped with $CHCl_3$), 6.91 (dd, 1H, *J* = 5.2 Hz, 4.0 Hz, CH-C*H*-CH), 3.85 (s, 1H, cage C*H*), 3.58–1.40 (brm, B*H*).



C30: The general procedure was followed with **A30** (73.5 mg, 0.500 mmol), **Li/Cu-1** (322.7 mg, 0.500 mmol, 2.0 equiv), isophthalonitrile (64.1 mg, 0.500 mmol, 2.0 equiv), and toluene (1.0 mL). Purification by flash column chromatography on silica gel (*n*-hexane only) afforded **C30** as a colorless liquid (100.0 mg, 0.476 mmol, 95%). **^{1}H NMR** (400 MHz, $CDCl_3$, rt, *δ*/ppm): 7.31 (m, 1H, O-C*H*-CH), 6.51 (d, 1H, *J* = 3.6 Hz, CH-C*H*-C), 6.34 (dd, 1H, *J* = 3.4 Hz, 1.8 Hz, CH-C*H*-CH), 3.93 (s, 1H, cage C*H*), 3.56–1.41 (brm, B*H*). **^{11}B NMR** (128 MHz, $CDCl_3$, rt, *δ*/ppm): 0.40–−5.58 (m, 2B), −7.44–−15.35 (m, 8B). **^{13}C{^{1}H} NMR** (100 MHz, $CDCl_3$, rt, *δ*/ppm): 146.0, 143.7, 111.7 (d, *J* = 6.1 Hz), 111.2 (d, *J* = 6.8 Hz), 68.5, 60.8 (d, *J* = 14.1 Hz). **HRMS** (EI^+): m/z Calculated for $C_6H_{14}B_{10}O_1$ ($[M]^+$) 212.1975, found 212.1986.

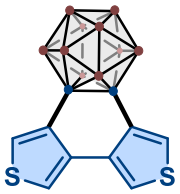


D31[43]: The general procedure was followed with **A31** (78.0 mg, 0.250 mmol), **Li/Cu-1** (322.7 mg, 0.500 mmol, 2.0 equiv), isophthalonitrile (64.1 mg, 0.500 mmol, 2.0 equiv), and toluene (1.0 mL). Purification by flash column chromatography on silica gel (*n*-hexane only) afforded **D31** as a white solid (69.4 mg, 0.236 mmol, 94%). **^{1}H NMR** (400 MHz, $CDCl_3$, rt, *δ*/ppm): 8.11 (d, 2H, *J* = 7.6 Hz, Ar-*H*), 7.72 (dd, 2H, *J* = 8.0 Hz, *J* = 1.2 Hz, Ar-*H*), 7.52 (td, 2H, *J* = 7.6 Hz, *J* = 1.2 Hz, Ar-*H*), 7.42 (td, 2H, *J* = 7.6 Hz, *J* = 1.2 Hz, Ar-*H*), 3.65–1.04 (brm, B*H*).



D32[45]: The general procedure was followed with **A32** (81.0 mg, 0.250 mmol), **Li/Cu-1** (322.7 mg, 0.500 mmol, 2.0 equiv), isophthalonitrile (64.1 mg, 0.500 mmol, 2.0 equiv), and toluene (1.0 mL). Purification by flash column chromatography on silica gel (*n*-hexane/EtOAc = 97/3) afforded **D32** as a white solid (74.0 mg, 0.241 mmol, 97%). **^{1}H NMR** (400 MHz, $CDCl_3$, rt, *δ*/ppm): 7.29 (d, *J* = 5.2 Hz, 2H, S-C*H*), 7.22 (d, *J* = 5.2 Hz, 2H, C-C*H*-CH), 3.64–0.76 (brm,

B*H*).



D33: The general procedure was followed with **A33** (81.0 mg, 0.250 mmol), **Li/Cu-1** (322.7 mg, 0.500 mmol, 2.0 equiv), isophthalonitrile (64.1 mg, 0.500 mmol, 2.0 equiv), and toluene (1.0 mL). Purification by flash column chromatography on silica gel (*n*-hexane/EtOAc = 97/3) afforded **D33** as a white solid (66.2 mg, 0.216 mmol, 86%). A single crystal of **D33** was obtained from a saturated solution of **D33** in acetone at rt. **^{1}H NMR** (400 MHz, $CDCl_3$, rt, δ/ppm): 7.55–7.48 (m, 4H, S-C*H*), 3.40–1.53 (m, cage B*H*), 3.59–1.55 (brm, B*H*). **^{11}B NMR** (128 MHz, $CDCl_3$, rt, δ/ppm): −4.18–−6.79 (m, 2B), −7.99–−13.08 (m, 8B). **^{13}C{^{1}H} NMR** (100 MHz, $CDCl_3$, rt, δ/ppm): 131.4, 128.4, 124.8, 119.6, 71.4. **HRMS** (EI^+): m/z Calculated for $C_{10}H_{14}B_{10}S_2$ ($[M]^+$) 308.1467, found 308.1495. **X-ray** data for **2(D33)**: M = 612.86, colorless, monoclinic, $P2_1/c$ (#14), a = 13.8635(2) Å, b = 11.52150(10) Å, c = 20.2307(3) Å, α = 90°, β = 108.359(2)°, γ = 90°, V = 3066.94(8) Å^3, Z = 4, $Dcalcd$ = 1.327 g/cm^3, T = 123.15 K, R_1 (wR_2) = 0.0453 (0.1236).

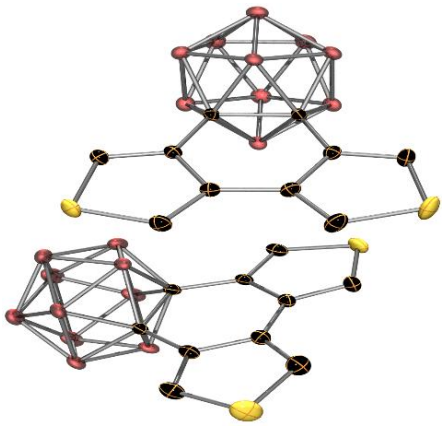
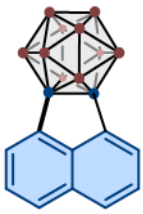


Figure 2.S29. Molecular structure of **2(D33)** with ellipsoids set at 30% probability. H atoms are omitted for clarity.



D34[44]: The general procedure was followed with **A34** (71.5 mg, 0.250 mmol), **Li/Cu-1** (322.7 mg, 0.500 mmol, 2.0 equiv), isophthalonitrile (64.1 mg, 0.500 mmol, 2.0 equiv), and toluene (1.0 mL). Purification by flash column chromatography on silica gel (*n*-hexane only) afforded **D34** as a white solid (26.8 mg, 0.100 mmol, 40%). A single crystal of **D34** was obtained from a saturated solution of **D34** in acetone at rt. **^{1}H NMR** (400 MHz, $CDCl_3$, rt, δ/ppm): 7.80 (d, 2H, J = 8.0 Hz, Ar-*H*), 7.59 (d, 2H, J = 7.2 Hz, Ar-*H*), 7.52 (dd, 2H, J = 8.4 Hz, 7.2 Hz, Ar-*H*), 3.42–1.20 (brm, B*H*). **^{11}B NMR** (128 MHz, $CDCl_3$, rt, δ/ppm): −2.86–−8.82 (m, 6B), −10.46–−14.15 (m, 8B). **^{13}C{^{1}H} NMR** (100 MHz, $CDCl_3$, rt, δ/ppm): 139.4, 135.9, 131.5, 127.8, 126.9, 81.7. **HRMS** (EI^+): m/z Calculated for $C_{12}H_{16}B_{10}$ ($[M]^+$) 270.2183, found 270.2181.

2.4.5 Reaction of Li/Cu-1 with pyridine

Li/Cu-1 (32.3 mg, 0.050 mmol) and pyridine (1.0 equiv, 5.0 equiv, or none) were mixed in CD_2Cl_2

(0.7 mL), and the resultant mixture was transferred into a J. Young NMR tube. After standing at rt for 1 h, ^{1}H NMR data were collected (Figure 2.S30). Upon increasing the amount of pyridine, signals of THF and some pyridine signals were obviously upfield-shifted, suggesting the existence of a coordination equilibrium.

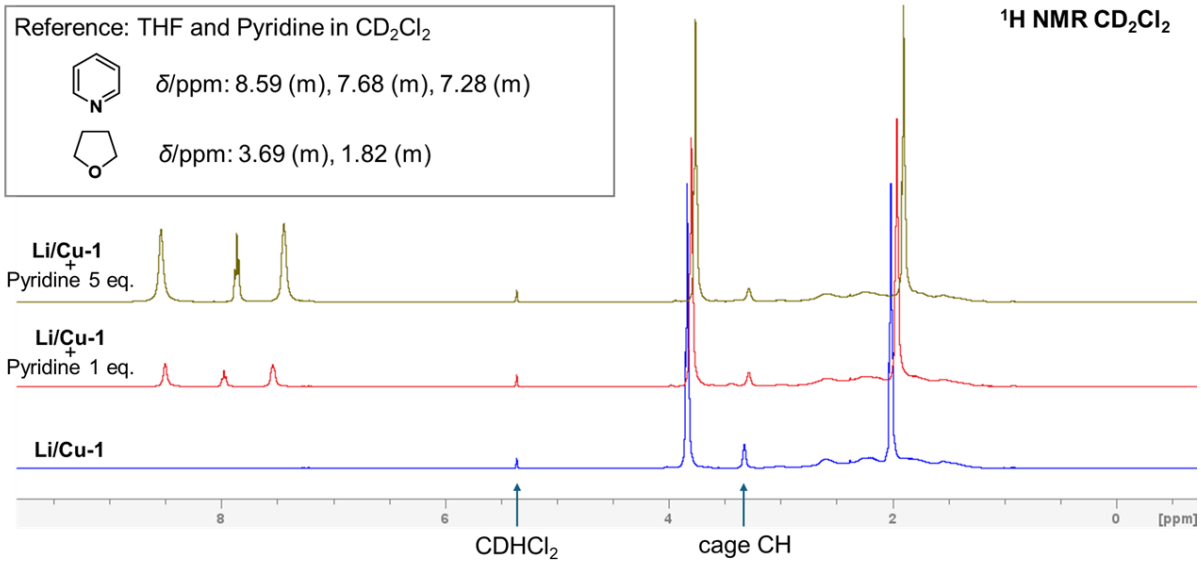
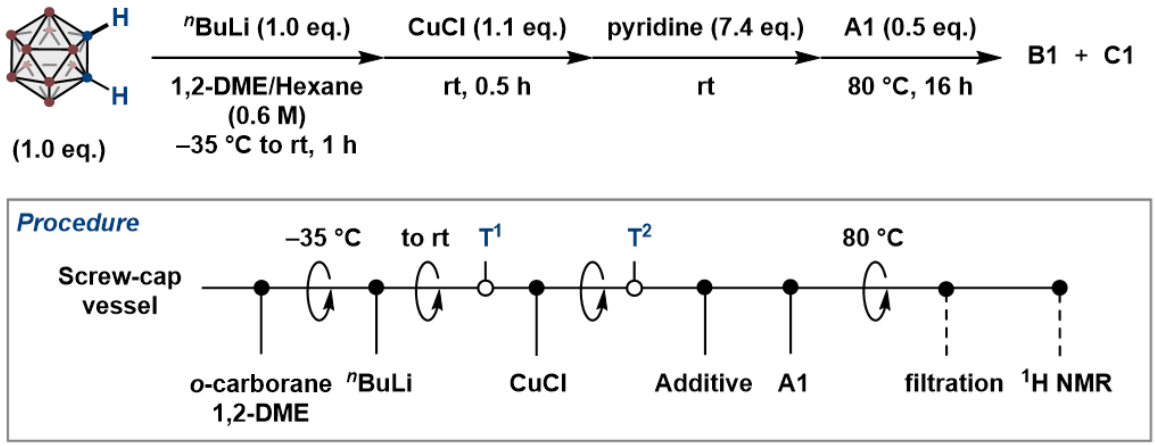


Figure 2.S30. ^{1}H NMR of **Li/Cu-1** (bottom); after the addition of 1 equiv of pyridine (middle); after the addition of 5 equiv of pyridine (top).

2.4.6. Results of *in-situ* experiments

2.4.6.1. *In-situ* generation of carboranyl copper species



Run	Variation from the standard conditions	B1 [%]	C1 [%]	CBT [%]
1	None	1	18	10
2	CuI (1.1 eq.) instead of CuCl (1.1 eq.) was used	0	12	6
3	$[CuOTf]_2 \cdot C_6H_6$ (1.1 eq.) instead of CuCl (1.1 eq.) was used	0	4	2
4	^{i}PrMgCl (1.1 eq.) instead of ^{n}BuLi (1.1 eq.) was used	0	9	5
5	A premixed solution of CuCl (1.1 eq.) and pyridine (7.4 eq.) was added at T^1	1	16	9
6	Pyridine (3.8 eq.) was used	2	19	12
7	Pyridine (20.0 eq.) was used	0	12	6
8	DME/Hexane (1.0 M) instead of DME/Hexane (0.6 M)	1	15	9
9	DME/Hexane (0.6 M) was removed in vacuo and THF (0.6 M) was then added at T^1	2	23	14
10	DME/Hexane (0.6 M) was removed in vacuo and THF (0.6 M) was then added at T^2	2	19	12
11	DME/Hexane (0.6 M) was removed in vacuo and DMSO (0.6 M) was then added at T^1	1	27	15
12	DME/Hexane (0.6 M) was removed in vacuo and DMF (0.6 M) was then added at T^1	2	17	11
13	DME/Hexane (0.6 M) was removed in vacuo and 1,4-dioxane (0.6 M) was then added at T^1	1	19	11
14	DME/Hexane (0.6 M) was removed in vacuo and MeCN (0.6 M) was then added at T^1	0	0	0
15	DME/Hexane (0.6 M) was removed in vacuo and Toluene (0.6 M) was then added at T^1	2	27	16
16	DME/Hexane (0.6 M) was removed in vacuo and Toluene (0.6 M) was then added at T^1; pyridine (3.8 equiv) was used.	5	26	18
17	DME/Hexane (0.6 M) was removed in vacuo and Toluene (0.6 M) was then added at T^1; pyridine (2.0 equiv) was used.	5	29	20

Figure 2.S31. Results of *in-situ* experiments. T^1 and T^2 represent the points at which reagents were added.

General conditions (Figure 2.S31, run 1): Based on the reported procedure[21], in a screw-cap reaction vessel equipped with a magnetic stirrer bar, a solution of *o*-carborane (86.5 mg, 0.600 mmol, 1.0 equiv, 1.0 M in DME) was slowly treated with ^{n}BuLi (0.397 mL, 0.599 mmol, 1.0 equiv, 1.51 M in hexane) at −35 °C, and the mixture was stirred for 1 h while gradually warming to rt. CuCl (65.9 mg, 0.666 mmol, 1.1 equiv) was then added, and the mixture was stirred for an additional 30 min, followed by the addition of pyridine (0.360 mL, 4.46 mmol, 7.4 equiv). Subsequently, A1 (70.8 mg, 0.30 mmol, 0.5 equiv) was added, and the reaction mixture was stirred at 80 °C for 16 h. After cooling to rt, the resulting mixture was diluted with wet Et_2O. The mixture was then filtered through filter paper, and the volatiles were removed under reduced pressure. The yields of B1 and C1 were determined by NMR analysis using 1,3,5-trimethoxybenzene as an internal standard.

2.4.6.2. Ni-catalyzed carboranylation of **A1**

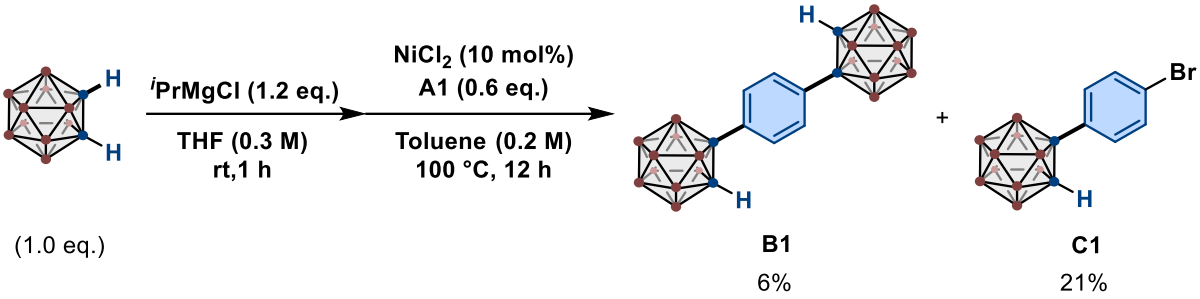


Figure 2.S32. Ni-catalyzed carboranylation of **A1**

Based on the reported procedure[36], a solution of *o*-carborane (79.0 mg, 0.548 mmol, 1.0 equiv, 0.5 M in THF) was slowly treated with ^{i}PrMgCl (0.666 mL of a 1.0 M solution in THF, 0.666 mmol, 1.2 equiv) at rt, and the mixture was stirred for 1 h at rt. After removing all volatiles under reduced pressure, the residue was treated with toluene (2.78 mL), $NiCl_2$ (7.2 mg, 0.056 mmol, 10 mol%), and **A1** (78.3 mg, 0.308 mmol, 0.6 equiv). The mixture was then stirred at 100 °C for 12 h. After cooling to rt, the reaction mixture was diluted with wet Et_2O. The resulting mixture was filtered through filter paper, and the volatiles were removed under reduced pressure. The yields of **B1** and **C1** were determined by NMR analysis using 1,3,5-trimethoxybenzene as an internal standard.

2.4.7 Recovery of *o*-carborane and isophthalonitrile

2.4.7.1. Reaction between **A1** and **Li/Cu-1** (Figure 2.3D)

The procedure follows the steps outlined in Section 5. After quenching the reaction synthesizing **B1**, the crude mixture was subjected to sublimation for 15 min at 100 °C under 0.2 mmHg. The remaining residue was purified by silica gel column chromatography, yielding **B1** (*vide supra*) and isophthalonitrile (60.4 mg, 0.471 mmol, 94%). The sublimated solid was collected with *n*-hexane, and the solvent was removed under reduced pressure to obtain *o*-carborane (64.8 mg, 0.449 mmol).

2.4.7.2. Reaction between **A17** and **Li/Cu-1** (Figure 2.5A)

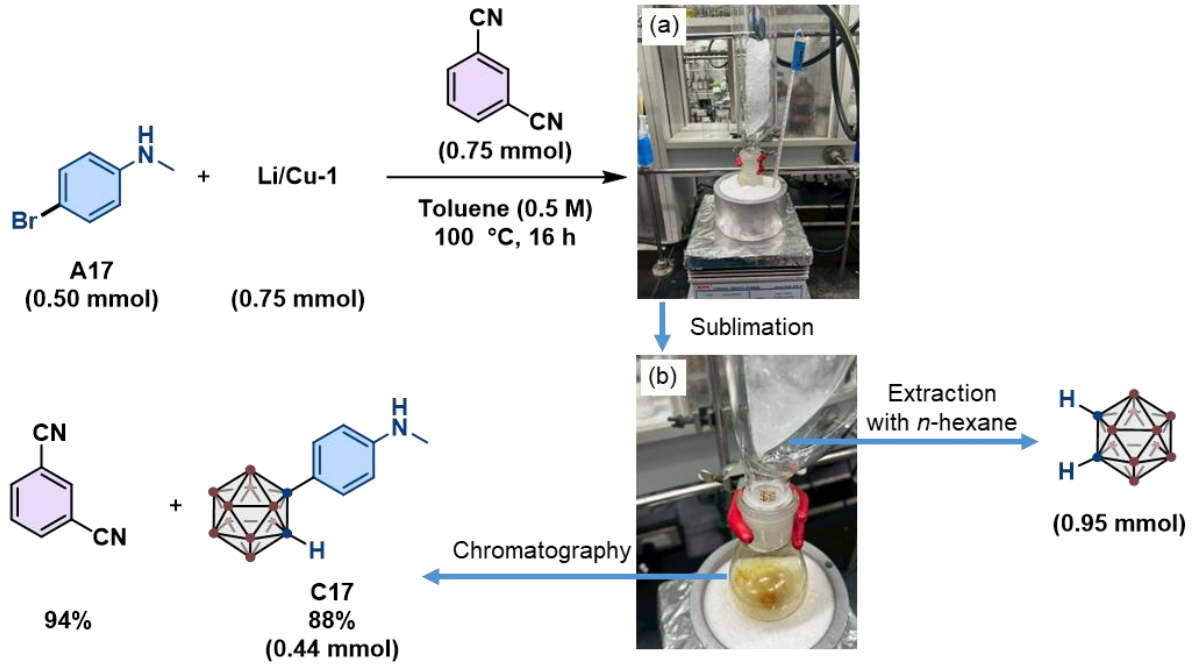


Figure 2.S33. Recovery of *o*-carborane and isophthalonitrile from the reaction between **A17** and **Li/Cu-1**

The procedure follows the steps outlined in Section 2.5.1. After quenching the reaction synthesizing **C17** (Figure 2.S33a), the crude mixture was subjected to sublimation for 15 min at 100 °C under 0.2 mmHg (Figure 2.S33b). The remaining residue was purified by silica gel column chromatography, which yielded **C17** (*vide supra*) and isophthalonitrile (90.4 mg, 0.706 mmol, 94%). The sublimated solid was collected with *n*-hexane, and the solvent was removed under reduced pressure to afford *o*-carborane (136.3 mg, 0.945 mmol).

2.4.8 Synthesis of 1,1′-bis(*o*-carborane)[42]

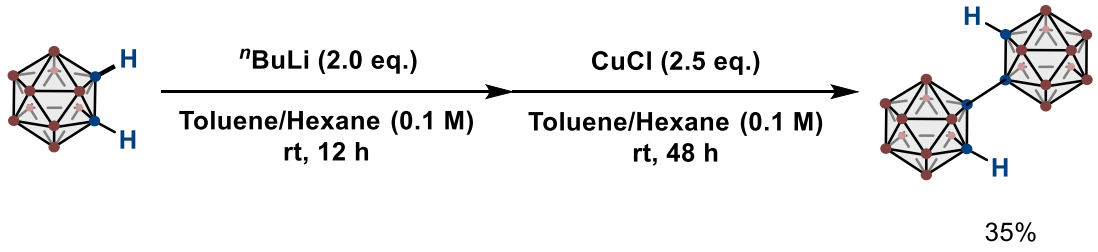


Figure 2.S34. Synthesis of 1,1′-bis(*o*-carborane)

A solution of *o*-carborane (432 mg, 3.00 mmol, 0.15 M in Toluene) was slowly treated with ^{n}BuLi (3.90 mL of a 1.54 M solution in hexane, 6.01 mmol, 2.0 equiv) at rt and stirred for 12 h. CuCl (750 mg, 7.58 mmol, 2.5 equiv) was then added to the resultant solution at rt, and the mixture was stirred for 48 h. The reaction mixture was quenched with 3 M HCl, and the organic layer was separated. The aqueous phase was extracted with Et_2O, and the combined organic extracts were removed under reduced pressure. The crude product was purified by silica gel column chromatography (*n*-hexane) afforded as a 1,1′-bis(*o*-carborane) (147.2 mg, 0.514

mmol, 34%). **<u>^{1}H NMR</u>** (400 MHz, $CDCl_3$, rt, δ/ppm): 3.81 (s, 2H, cage C*H*), 3.60–1.23 (brm, B*H*).

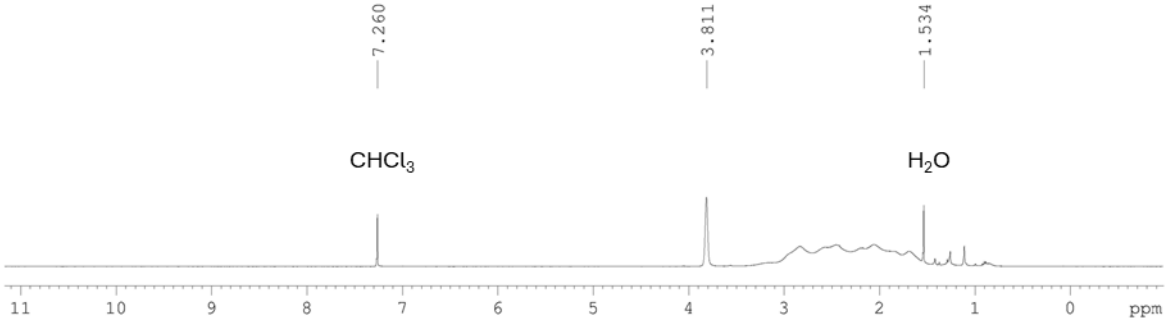


Figure 2.S35. ^{1}H NMR (400 MHz, $CDCl_3$, rt) of the 1,1′-bis(*o*-carborane)

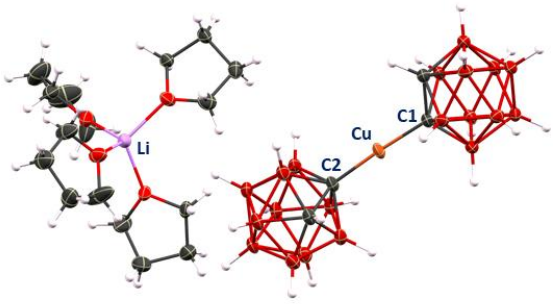
2.4.9 Theoretical studies

2.4.9.1 Computational details

Density functional theory (DFT) calculations were performed using Gaussian 16 (Revision C.01) software[60]. Molecular structures were optimized and their single-point energies were calculated at the PBE0-D3 level with the Def2-TZVPD (Cu) and Def2-TZVP (others) basis sets in the gas phase [61,62]. Harmonic frequency calculations were performed at the same level of theory to verify that intermediates have no imaginary frequency, whereas transition states have only one imaginary frequency. The appropriateness of the connections between each reactant and product via a transition state was confirmed using intrinsic reaction coordinate (IRC) calculations[63]. The reported Gibbs free energies were calculated at 298.15 K. It should be noted that these calculations involve a certain margin of error. The Def2-TZVPD basis sets were obtained from the Basis Set Exchange website (https://www.basissetexchange.org/).[64]

2.4.9.2 Method Optimization

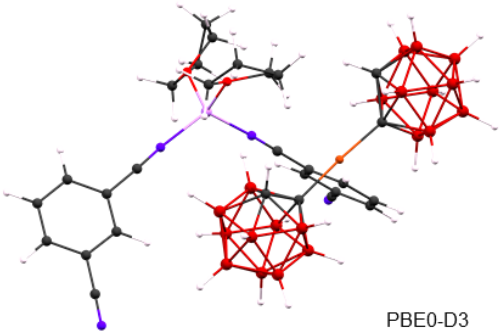
The author carried out optimization of the gas-phase structure of **Li/Cu-1** at various theoretical levels shown in Figure S36 with the Def2-TZVPD (Cu) and Def2-TZVP (others) basis sets. By comparing the obtained structural parameters with the SC-XRD results, the author decided to use the PBE0-D3 level in this work due to its high reproducibility.



	XRD	B3LYP-D3	M06-D3	PBE0-D3	PBE0	wB97XD
Cu-C1	1.91	1.95	1.93	1.93	1.94	1.94
Cu-C2	1.91	1.95	1.94	1.93	1.94	1.94
Ave. Li-O	1.93	1.95	1.95	1.94	1.96	1.95
C1-Cu-C2	176.7	177.0	162.4	177.0	176.1	173.8

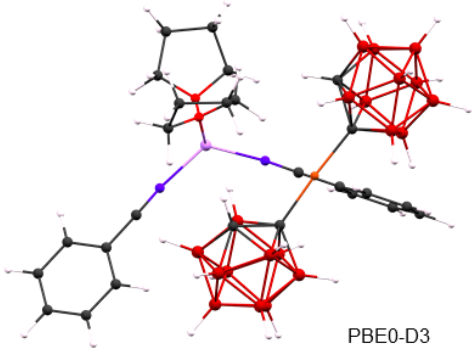
Figure 2.S36. Optimization of theoretical levels. Bond lengths (Å) and angles (deg) are given.

To discuss the suitability of using PhCN as a mimicetic ligand for isophthalonitrile in the mechanistic studies, the author compared the structures of **Li/Cu-2** and its mimic $[Li(thf)_2(CNPh)_2][Cu(o\text{-carboran-1-yl})_2]$ under the optimized calculation conditions, as shown in Figure 2.S37. To evaluate the long-range dispersion corrections, the ωB97XD level was also tested[25]. As a result, the author confirmed the PBE0-D3 can adequately reproduce the monomeric structure of **Li/Cu-2** without the long-range dispersion corrections, although the distance between the Li and Cu centers found in the SC-XRD analysis was not reproduced as it would be sensitive to crystal packing effects.



	XRD[1]	PBE0-D3	wB97XD
Cu-C1	1.91	1.93	1.94
Cu-C2	1.92	1.94	1.94
Ave. N-Li	2.03	2.02	2.07
Ave. Li-O	1.90	1.94	1.96
C1-Cu-C2	176.6	175.5	176.2
Ave. C-N-Li	172.0	174.1	171.0
Li---Cu	8.39	5.11	5.05

[1]Including toluene in the crystal lattice



	PBE0-D3	wB97XD
Cu-C1	1.94	1.94
Cu-C2	1.94	1.94
Ave. N-Li	2.01	2.05
Ave. Li-O	1.96	1.99
C1-Cu-C2	176.5	177.2
Ave. C-N-Li	173.4	171.8
Li---Cu	5.13	5.02

Figure 2.S37. Comparison of structural parameters between DFT-optimized **Li/Cu-2** and $[Li(thf)_2(CNPh)_2][Cu(o\text{-carboran-1-yl})_2]$. Bond lengths (Å) and angles (deg) are given.

2.4.9.3 Mechanistic Studies

First, the author examined how the number of coordinated THF molecules impacts the stability of **Li/Cu-1** (Figure 2.S38). The author found that dissociation of one THF molecule is possible, but dissociation of more than two THFs is unfavorable from the Li center. Additionally, forming the neutral Cu(*o*-carboran-1-yl) species is thermodynamically very unfavorable.

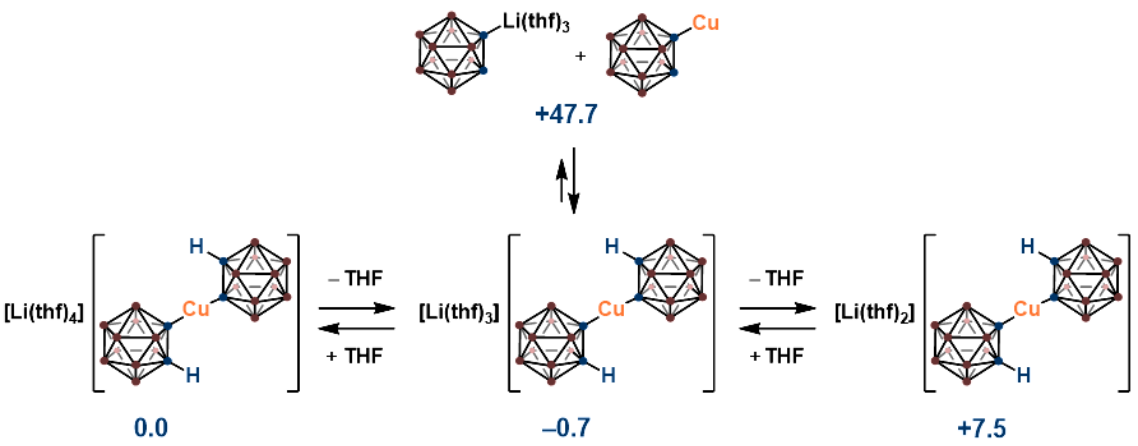


Figure 2.S38. Influence of THF coordination on the Li center.

Then, the author explored possible reaction mechanisms and found that the mechanism shown in Figure 2.6A is plausible after conducting the conformational searches for intermediates and transition states when required at the PBE0-D3/Def2-SVPD(Cu) and Def2-SVP(others) level of theory. The optimized structures of the involved compounds and transition states, along with their selected geometrical parameters, are shown in Figure 2.S35.

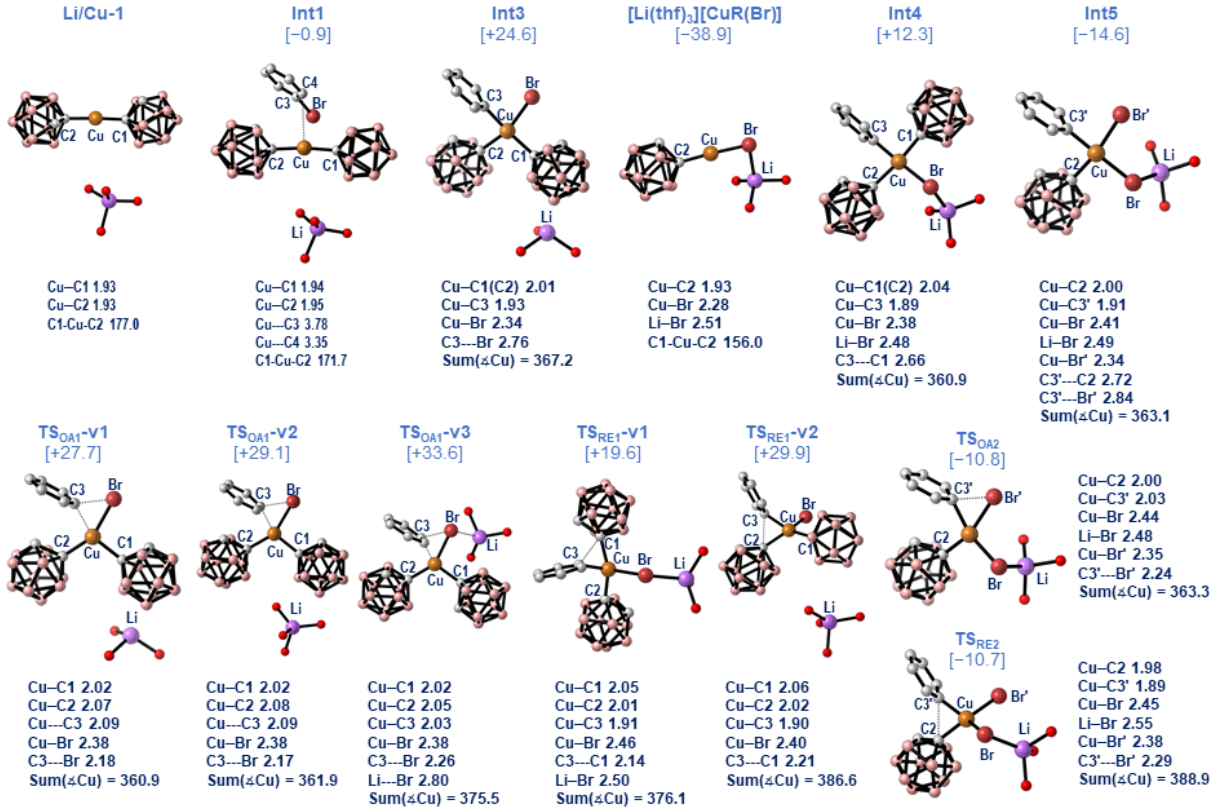


Figure 2.S39. Optimized structures of the involved compounds and transition states, shown in Figure 2.6A. Their relative Gibbs free energies [kcal mol^{-1}] with respect to **Li/Cu-1** and selected geometrical parameters (bond lengths in Å and angles in degrees) are given.

Moreover, the author explored the plausible oxidative addition paths from [Li(thf)$_3$(CNPh)][Cu(*o*-carboran-1-yl)$_2$] and [Li(thf)$_2$(CNPh)$_2$][Cu(*o*-carboran-1-yl)$_2$] to clarify the influence of PhCN molecules on the rate-determining steps (Figure 2.6C, Figure 2.6D, and Figure 2.S40). The path proceeding via **TS$_{OA1}$-v1** from **Int1** (i.e., $\Delta G_{v1}^{\ddagger}$ = +29.8 kcal mol^{-1}) is also shown for comparison. It should be noted that the potential energy surface is different in the presence of PhCN and thus $\Delta G_{v1}^{\ddagger}$ has changed from the values shown in Figure 2.6A. In the presence of one molecule of PhCN, oxidative addition occurs via **TS$_{OA1}$-v5** with a nearly identical energy barrier ($\Delta G_{v5}^{\ddagger}$ = +29.9 kcal mol^{-1}). On the other hand, the coordination of two molecules of PhCN, as seen in the SC-XRD structure of **Li/Cu-2**, significantly promotes the oxidative addition by stabilizing **TS$_{OA1}$-v4** (+25.1 kcal mol^{-1}; $\Delta G_{v4}^{\ddagger}$ = +27.2 kcal mol^{-1}) through non-covalent interactions between phenyl groups in PhCN and carboranyl B−H bonds. Indeed, such interactions are confirmed by the atoms in molecules (AIM) analysis (Figure 2.S41).

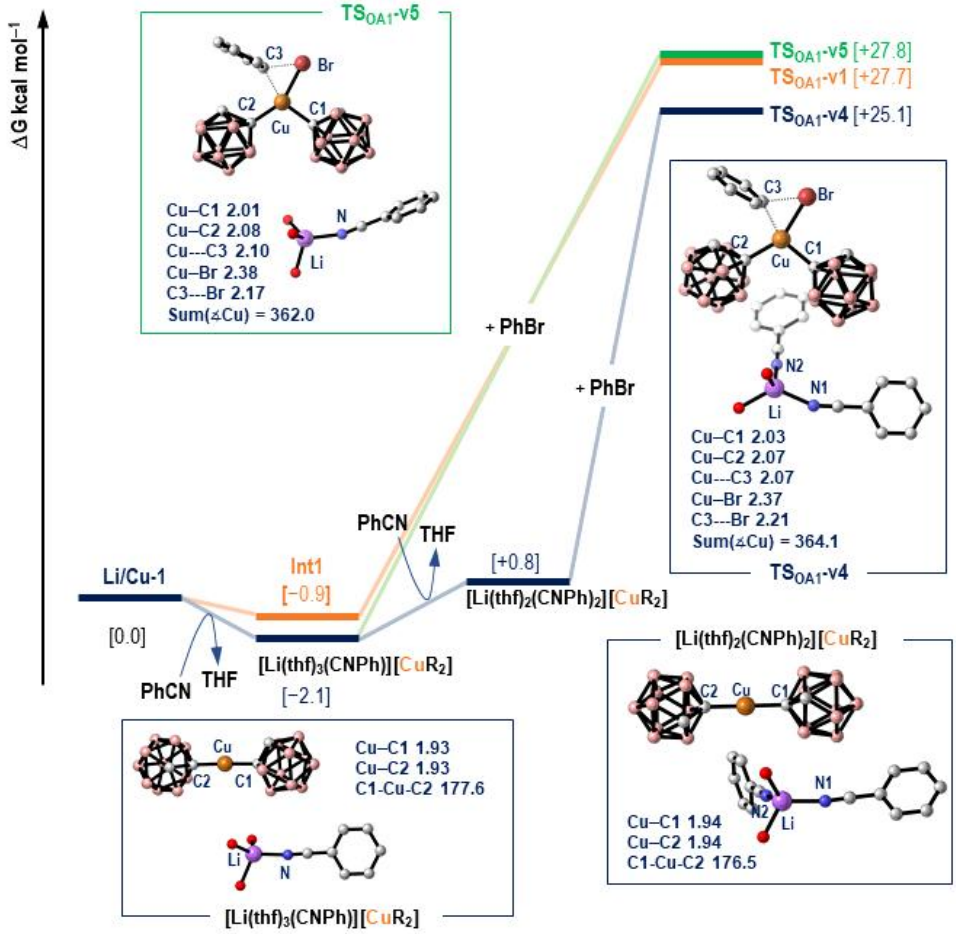


Figure 2.S40. Oxidative addition processes in the presence of PhCN ligands. The relative Gibbs free energies [kcal mol^{-1}] with respect to [**Li/Cu-1** + 2 PhCN + PhBr] and selected geometrical parameters (bond lengths in Å and angles in degrees) are given.

2.4.9.4 Atoms in molecule (AIM) analysis

The analysis on the quantum theory of the atoms in molecules were carried out using the AIMAll program (Version 19.10.12)[66], in which wave functional files were prepared based on the SCF density at the PBE0-D3/Def2-TZVPD (Cu) and Def2-TZVP (others)/gas-phase level. In Table 2.S1, details of the AIM analysis are given, wherein atom labels are identical to those found in the optimized DFT structures (Rho, electron density in $e\ r_{Bohr}^{-3}$ oat BCPs; G and V, the kinetic and potential energy densities in $E_h\ r_{Bohr}^{-3}$; δ(BCP) values show the average number of electrons shared at a BCP). In Figure 2.S41, the AIM bond paths (white lines) are shown with the bond critical points (BCP; $e\ r_{Bohr}^{-3}$; green dots), while C–H/B–H bonds that do not form NCIs and THF molecules are omitted for clarity. As demonstrated, several NCIs participate between the carborane and PhCN groups to stabilize **TS$_{OA1}$-v4**.

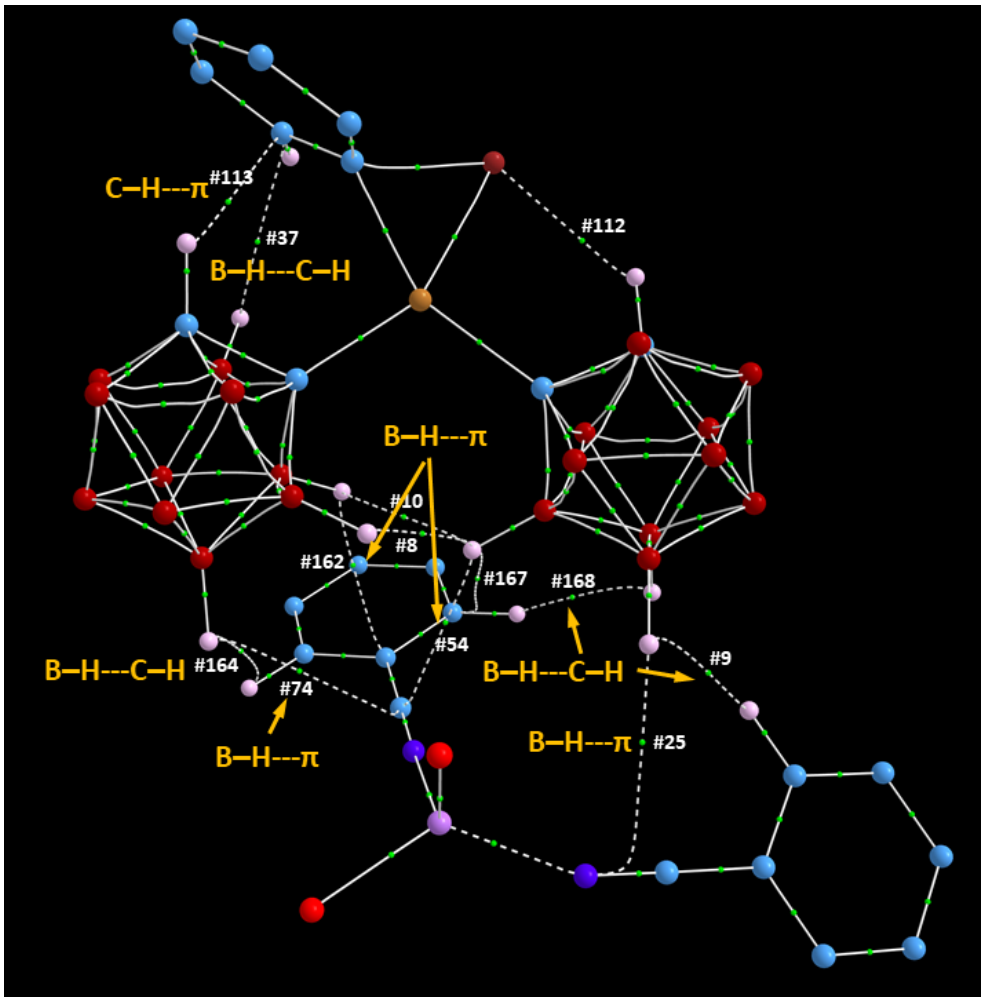


Figure 2.S41. Selected bond paths, their names, and critical points for **TS_{OA1}-v4**.

Table 2.S1. Results of the AIM analysis for **TS_{OA1}-v4**

BCP#	*Atoms*	*Rho*	*DelSqRho*	*G*	*V*	*δ(BCP)*
1	C2 - H3	0.293919	-1.088791	0.03453	-0.341258	0.884006
2	Cu1 - C4	0.095207	0.230127	0.093827	-0.130122	0.620709
3	C2 - C4	0.177698	-0.158615	0.079643	-0.19894	0.98941
4	B14 - B36	0.116378	-0.097534	0.039914	-0.104211	0.293687
5	H35 - H70	0.009082	0.025417	0.005369	-0.004384	0.032562
6	C4 - B5	0.127016	0.019615	0.119064	-0.233224	0.533071
7	B14 - H15	0.185698	-0.328168	0.129022	-0.340087	0.646499
8	H11 - H33	0.010623	0.030483	0.006521	-0.005422	0.040925
9	H35 - H92	0.008738	0.026491	0.005465	-0.004306	0.025706
10	H6 - H33	0.007536	0.021819	0.004593	-0.003731	0.028633
11	B5 - H6	0.184648	-0.308352	0.131773	-0.340635	0.666525
12	Cu1 - C7	0.087138	0.227172	0.086888	-0.116983	0.570129
13	C7 - B58	0.127755	0.007484	0.116949	-0.232028	0.527899

14	B32 - B58	0.119837	-0.11288	0.041268	-0.110755	0.324446
15	B32 - B38	0.120929	-0.122553	0.038663	-0.107965	0.446041
16	B27 - B42	0.121225	-0.126464	0.038608	-0.108833	0.459431
17	C7 - B8	0.125473	-0.071948	0.089677	-0.197342	0.409757
18	B8 - H9	0.185657	-0.331304	0.128148	-0.339121	0.651167
19	C2 - B36	0.126533	0.096698	0.136562	-0.24895	0.519905
20	C2 - B14	0.127392	0.049121	0.127404	-0.242527	0.409139
21	H11 - H24	0.008791	0.024884	0.005306	-0.004391	0.034872
22	C4 - B10	0.126205	0.015759	0.116888	-0.229836	0.53076
23	B5 - B10	0.119513	-0.113264	0.040626	-0.109568	0.332265
24	B14 - B20	0.122101	-0.129724	0.039138	-0.110708	0.452574
25	H35 - N99	0.004131	0.01306	0.002551	-0.001837	0.019803
26	C4 - B14	0.124725	-0.069243	0.089253	-0.195816	0.407167
27	B5 - B14	0.121084	-0.121658	0.040953	-0.11232	0.333804
28	B10 - H11	0.186396	-0.312579	0.133518	-0.345181	0.661891
29	C2 - B12	0.127851	0.056048	0.129682	-0.245351	0.409592
30	C4 - B12	0.124998	-0.06344	0.091962	-0.199783	0.408298
31	H11 - H68	0.006333	0.019982	0.004119	-0.003243	0.016562
32	B10 - B12	0.120946	-0.12107	0.040922	-0.112112	0.330111
33	C2 - B18	0.12779	0.099325	0.138813	-0.252794	0.522908
34	H24 - H68	0.007715	0.020927	0.004528	-0.003824	0.027475
35	B12 - H13	0.185482	-0.330224	0.128143	-0.338842	0.648517
36	B25 - B34	0.118644	-0.116223	0.037886	-0.104828	0.45599
37	H15 - C48	0.007267	0.022117	0.004565	-0.0036	0.025332
38	Cu1 - C47	0.08628	0.113071	0.059294	-0.090321	0.527354
39	B16 - B25	0.121687	-0.127875	0.0388	-0.109568	0.449742
40	C7 - B16	0.123815	-0.079569	0.082983	-0.185859	0.403943
41	C7 - C59	0.176025	-0.150668	0.079734	-0.197136	0.993413
42	B22 - B27	0.121622	-0.12868	0.038493	-0.109156	0.465498
43	B16 - H17	0.185866	-0.331655	0.128467	-0.339847	0.65157
44	B12 - B45	0.121663	-0.127252	0.03872	-0.109252	0.451171
45	C66 - H68	0.281617	-0.976077	0.040142	-0.324304	0.908163
46	B10 - B45	0.120588	-0.121377	0.038808	-0.10796	0.444386
47	C69 - H71	0.285743	-1.016782	0.035783	-0.325762	0.919403
48	C66 - C72	0.245532	-0.597481	0.062267	-0.273904	0.977735
49	B12 - B18	0.115208	-0.091318	0.040241	-0.103311	0.281329
50	B18 - H19	0.183503	-0.309538	0.129578	-0.33654	0.684036
51	B5 - B20	0.119662	-0.118187	0.038456	-0.10646	0.436842

52	B20 - B36	0.121306	-0.1287	0.038217	-0.108608	0.461473
53	B5 - B29	0.120219	-0.121724	0.03809	-0.106611	0.455597
54	H33 - C100	0.007332	0.022784	0.004774	-0.003853	0.019247
55	B36 - H37	0.183425	-0.309384	0.129488	-0.336323	0.685257
56	B18 - B45	0.122493	-0.134102	0.038177	-0.109879	0.471349
57	B20 - H21	0.179475	-0.277403	0.130714	-0.330779	0.71065
58	B42 - C59	0.127576	0.094556	0.137432	-0.251224	0.524534
59	B8 - C59	0.127977	0.060471	0.130903	-0.246689	0.409666
60	B16 - B22	0.115932	-0.095826	0.039783	-0.103522	0.289597
61	B22 - C59	0.126501	0.094867	0.136103	-0.248489	0.520011
62	B22 - H23	0.183743	-0.31213	0.129366	-0.336764	0.686231
63	B22 - B25	0.121363	-0.129379	0.038218	-0.10878	0.462262
64	B25 - H26	0.179813	-0.281417	0.130316	-0.330987	0.714849
65	B25 - B27	0.117234	-0.10886	0.037884	-0.102984	0.437803
66	C7 - B32	0.127867	0.015048	0.118972	-0.234181	0.523424
67	B27 - H28	0.178228	-0.269301	0.130723	-0.328771	0.705406
68	H11 - H65	0.007093	0.022964	0.004719	-0.003698	0.017681
69	B10 - B29	0.121032	-0.124594	0.03855	-0.108249	0.457406
70	B36 - B40	0.121426	-0.128554	0.038602	-0.109342	0.46266
71	O61 - C63	0.247842	-0.513753	0.201924	-0.532287	0.847616
72	Li60 - N112	0.026248	0.180317	0.037447	-0.029816	0.068052
73	B20 - B29	0.118601	-0.117104	0.037647	-0.10457	0.459427
74	H30 - C100	0.004123	0.013534	0.00263	-0.001876	0.00962
75	Li60 - N99	0.023981	0.164079	0.033812	-0.026604	0.06342
76	O61 - H85	0.006464	0.026431	0.005298	-0.003988	0.020055
77	B20 - B40	0.117064	-0.108464	0.037866	-0.102847	0.434628
78	B29 - H30	0.176183	-0.246109	0.132929	-0.327385	0.69331
79	Cu1 - Br46	0.065985	0.175121	0.059775	-0.075769	0.604608
80	B27 - B34	0.119714	-0.121882	0.037897	-0.106264	0.472589
81	B8 - B32	0.120948	-0.119865	0.041676	-0.113318	0.32151
82	C88 - C89	0.31392	-0.920263	0.104874	-0.439813	1.317054
83	B38 - H39	0.176213	-0.247972	0.132357	-0.326707	0.699179
84	B32 - H33	0.187063	-0.311159	0.134875	-0.34754	0.658728
85	B32 - B34	0.121324	-0.124877	0.038575	-0.108369	0.453608
86	B34 - H35	0.177071	-0.245426	0.134353	-0.330062	0.688665
87	B18 - B36	0.117614	-0.102344	0.039633	-0.104852	0.316696
88	B8 - B38	0.121726	-0.127198	0.038406	-0.108611	0.453439
89	B27 - B38	0.117607	-0.109426	0.038219	-0.103795	0.441993

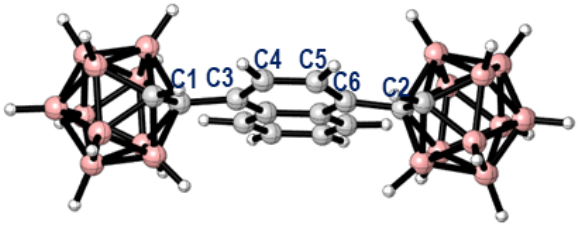
90	B34 - B38	0.119106	-0.116396	0.038269	-0.105636	0.46073
91	H44 - B45	0.17798	-0.25881	0.132606	-0.329914	0.699272
92	C63 - H64	0.282526	-0.989637	0.037171	-0.321752	0.903946
93	B18 - B40	0.120892	-0.125144	0.038751	-0.108789	0.454261
94	B29 - B40	0.119506	-0.12158	0.037703	-0.105801	0.469298
95	B40 - B45	0.117669	-0.110324	0.038146	-0.103874	0.438775
96	C63 - H65	0.289956	-1.047651	0.034356	-0.330625	0.882588
97	O62 - C84	0.253457	-0.542584	0.20636	-0.548367	0.861585
98	H65 - H82	0.004598	0.016749	0.003294	-0.0024	0.007828
99	B40 - H41	0.179955	-0.284419	0.129868	-0.330841	0.713957
100	H44 - H82	0.00249	0.007888	0.001512	-0.001052	0.009936
101	B8 - B42	0.114995	-0.090817	0.039997	-0.102699	0.279071
102	B16 - C59	0.127757	0.055877	0.129508	-0.245046	0.411275
103	B22 - B42	0.117415	-0.101283	0.039429	-0.104179	0.313531
104	B38 - B42	0.12233	-0.133592	0.03807	-0.109538	0.473657
105	B42 - H43	0.183291	-0.307893	0.129642	-0.336256	0.684962
106	H44 - H65	0.008846	0.026506	0.005559	-0.004492	0.027211
107	C69 - H70	0.289105	-1.038724	0.034311	-0.328304	0.887132
108	Li60 - O61	0.028117	0.210481	0.043877	-0.035133	0.068273
109	B29 - B45	0.118771	-0.115878	0.037981	-0.104932	0.458407
110	H64 - H85	0.006099	0.023763	0.004847	-0.003754	0.009415
111	Br46 - C47	0.089327	0.032016	0.037303	-0.066602	0.672665
112	H31 - Br46	0.016036	0.046236	0.010342	-0.009124	0.072641
113	H3 - C48	0.014493	0.045862	0.010017	-0.008568	0.027264
114	B16 - B58	0.121446	-0.123879	0.040843	-0.112655	0.334868
115	C48 - H51	0.287195	-1.030633	0.03716	-0.331978	0.928468
116	C47 - C48	0.316731	-0.930463	0.108269	-0.449154	1.30147
117	C47 - C49	0.316151	-0.923384	0.109005	-0.448856	1.313166
118	C48 - C50	0.318458	-0.932139	0.11037	-0.453775	1.389948
119	C49 - C52	0.31656	-0.924408	0.108826	-0.448754	1.380976
120	C49 - H53	0.28544	-1.01842	0.037514	-0.329633	0.931917
121	C50 - C54	0.317704	-0.93786	0.105889	-0.446243	1.369771
122	C52 - C54	0.31927	-0.945111	0.107172	-0.450622	1.383798
123	C50 - H55	0.285435	-1.017822	0.037386	-0.329228	0.949947
124	C52 - H56	0.285508	-1.018516	0.037357	-0.329344	0.949626
125	C54 - H57	0.285473	-1.01528	0.038352	-0.330525	0.955032
126	B25 - B58	0.119947	-0.118892	0.038587	-0.106897	0.438006
127	H24 - B58	0.182962	-0.291374	0.133097	-0.339037	0.661729

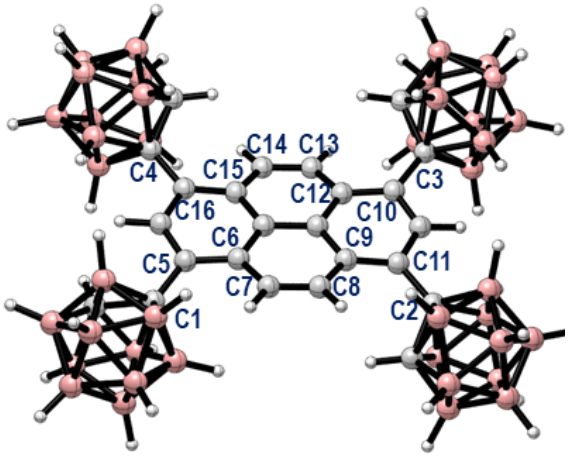
128	B34 - B58	0.121147	-0.12439	0.038397	-0.107891	0.460499
129	H31 - C59	0.290947	-1.065778	0.034633	-0.33571	0.898624
130	H30 - H77	0.003967	0.011421	0.002355	-0.001855	0.01616
131	Li60 - O62	0.025725	0.193955	0.040016	-0.031543	0.061744
132	O61 - C69	0.245413	-0.501711	0.199701	-0.52483	0.844905
133	C69 - C72	0.255575	-0.656814	0.061363	-0.28693	0.966076
134	C63 - C66	0.256859	-0.662311	0.062437	-0.290451	0.963096
135	C66 - H67	0.279273	-0.96394	0.041263	-0.32351	0.942447
136	C72 - H73	0.279606	-0.967276	0.040593	-0.323006	0.940617
137	C72 - H74	0.27771	-0.947251	0.042379	-0.321571	0.943588
138	O62 - C75	0.252527	-0.515661	0.21707	-0.563056	0.85117
139	C75 - H76	0.281961	-0.987436	0.036209	-0.319277	0.915545
140	C75 - H77	0.289485	-1.047897	0.033849	-0.329671	0.895068
141	C78 - H79	0.280106	-0.966774	0.041584	-0.324862	0.943497
142	C78 - H80	0.279885	-0.962109	0.042003	-0.324533	0.946711
143	C84 - H85	0.287338	-1.028439	0.035118	-0.327346	0.906433
144	C75 - C81	0.25717	-0.663986	0.062008	-0.290014	0.963493
145	C78 - C81	0.241445	-0.579951	0.060192	-0.265372	0.975993
146	C81 - H82	0.281061	-0.971809	0.040543	-0.324038	0.924521
147	C81 - H83	0.279402	-0.964503	0.041061	-0.323248	0.944485
148	C78 - C84	0.245815	-0.609389	0.05749	-0.267328	0.953093
149	C84 - H86	0.28435	-1.003284	0.036119	-0.323059	0.918737
150	C87 - C88	0.288461	-0.853202	0.096675	-0.406651	1.082345
151	C91 - C95	0.320457	-0.955684	0.106389	-0.451699	1.38893
152	C88 - C90	0.313566	-0.917102	0.104104	-0.437484	1.315956
153	C89 - C91	0.322955	-0.967128	0.108741	-0.459264	1.396931
154	C91 - H96	0.287419	-1.03476	0.035812	-0.330315	0.941387
155	C89 - H92	0.290651	-1.066605	0.033244	-0.333139	0.897131
156	C90 - C93	0.322944	-0.964139	0.109828	-0.460692	1.409484
157	C90 - H94	0.287112	-1.030955	0.036489	-0.330716	0.94509
158	C93 - C95	0.319274	-0.949289	0.105654	-0.44863	1.381555
159	C93 - H97	0.286395	-1.024474	0.037145	-0.330408	0.949849
160	C95 - H98	0.286885	-1.029512	0.036374	-0.330125	0.949563
161	C87 - N99	0.494742	-0.139599	0.939325	-1.913549	2.206744
162	H6 - C101	0.007748	0.023737	0.004951	-0.003969	0.02711
163	H77 - N112	0.007858	0.02851	0.0058	-0.004473	0.02982
164	H30 - H107	0.005263	0.017043	0.003385	-0.00251	0.016155
165	C100 - N112	0.49485	-0.134655	0.940673	-1.91501	2.177364

166	C100 - C101	0.289863	-0.861741	0.098392	-0.41222	1.077433
167	H33 - C102	0.005929	0.020134	0.004009	-0.002986	0.016029
168	H39 - H105	0.007568	0.021594	0.004459	-0.003519	0.029423
169	C101 - C102	0.314453	-0.922958	0.104874	-0.440488	1.305949
170	C101 - C103	0.31453	-0.922961	0.104774	-0.440288	1.306225
171	C102 - H105	0.289526	-1.053341	0.034609	-0.332554	0.913226
172	C102 - C104	0.323374	-0.968174	0.109498	-0.461039	1.397543
173	C103 - C106	0.323561	-0.968948	0.109785	-0.461807	1.396781
174	C103 - H107	0.288465	-1.0425	0.035733	-0.33209	0.932751
175	C104 - C108	0.320011	-0.953493	0.106055	-0.450484	1.382694
176	C106 - C108	0.320046	-0.953636	0.106106	-0.450622	1.381465
177	C104 - H109	0.286792	-1.028243	0.036738	-0.330536	0.947063
178	C106 - H110	0.286933	-1.029221	0.036784	-0.330873	0.946871
179	C108 - H111	0.286801	-1.028699	0.036515	-0.330204	0.950284

2.4.9.5 Comparison of gas-phase-optimized and SC-XRD structures of **B3** and **B4**

To confirm that distortions found in **B3** and **B4** by SC-XRD analyses are not caused by crystal packing effects, the author optimized their isolated gas-phase structures at the PBE0-D3/Def2-SVP. As shown in Figure 2.S42, the distorted structures are reproduced by DFT, showing that the repulsions between carboranyl C–H/B–H and aromatic C–H bonds are responsible for these distortions.





	XRD	PBE0-D3
C1-C3	1.52	1.52
C2-C6	1.52	1.52
C4-C5	1.40	1.40
C1-C3-C4-C5	168.0	173.8
C2-C6-C5-C4	−165.4	-173.7

	XRD	PBE0-D3
C1-C5-C6-C7	−21.4	−15.7
C2-C11-C9-C8	19.6	17.1
C3-C10-C12-C13	18.9	16.0
C4-C16-C15-C14	−17.7	−15.0

Figure 2.S42. Selected geometrical parameters (bond lengths in Å and angles in degrees) for **B3** and **B4**

2.5 References and Notes

1. Erdmann, P.; Greb, L. *Angew. Chem., Int. Ed.* **2022**, *61*, e202114550.
2. Issa, F.; Kassiou, M.; Rendina, L. M. *Chem. Rev.* **2011**, *111*, 5701–5722.
3. Valliant, J. F.; Guenther, K. J.; King, A. S.; Morel, P.; Schaffer, P.; Sogbein, O. O.; Stephenson, K. A. *Coord. Chem. Rev.* **2002**, *232*, 173–230.
4. Tanaka, K.; Gon, M.; Ito, S.; Ochi, J.; Chujo, Y. *Coord. Chem. Rev.* **2022**, *472*, 214779.
5. Núñez, R.; Tarrés, M.; Ferrer-Ugalde, A.; De Biani, F. F.; Teixidor, F. *Chem. Rev.* **2016**, *116*, 14307–14378.
6. Li, J.; Kim, J. S.; Fan, J.; Peng, X.; Matějíček, P. *Chem. Soc. Rev.* **2025**, *54*, 4104–4134.
7. Ochi, J.; Tanaka, K.; Chujo, Y. *Angew. Chem., Int. Ed.* **2020**, *59*, 9841–9855.
8. Sivaev, I. B.; Stogniy, M. Y.; Bregadze, V. I. *Coord. Chem. Rev.* **2021**, *436*, 213795.
9. Shi, J.; Li, M.; Xu, S.; Chen, M.; Zhang, X.; Zhang, Y.; Wu, L.; Ji, L. *Cryst. Growth Des.* **2024**, *24*, 9440–9446.
10. Aniés, F.; Hamilton, I.; De Castro, C. S. P.; Furlan, F.; Marsh, A. V.; Xu, W.; Pirela, V.; Patel, A.; Pompilio, M.; Cacialli, F.; Martín, J.; Durrant, J. R.; Laquai, F.; Gasparini, N.; Bradley, D. D. C.; Heeney, M. *J. Am. Chem. Soc.* **2024**, *146*, 13607–13616.
11. Yuhara, K.; Tanaka, K. *Chem. Sci.* **2025**, *16*, 6495–6506.
12. Yu, X.; Cui, D.; Wang, M.; Wang, Z.; Wang, M.; Tu, D.; Bregadze, V.; Lu, C.; Zhao, Q.; Chen, R.; Yan, H. *Chinese Chem. Lett.* **2025**, *36*, 110520.
13. Wei, X.; Zhu, M. J.; Cheng, Z.; Lee, M.; Yan, H.; Lu, C.; Xu, J. J. *Angew. Chem., Int. Ed.* **2019**, *58*, 3162–3166.
14. King, R. B. *Chem. Rev.* **2001**, *101*, 1119–1152.
15. Grimes, R. N. *Dalton Trans.* **2015**, *44*, 5939–5956.
16. Ali, H. A.; Ismail, M. A.; Fouda, A. E. A. S.; Ghaith, E. A. *RSC Adv.* **2023**, *13*, 18262–18305.
17. Zhou, N.; Ren, H.; Li, X.; Peng, J.; Sun, Z.; Cao, H.; Tu, D.; Lu, C.; Yan, H. *J. Am. Chem. Soc.* **2025**, *147*, 27030–27042.
18. Xu, S.; Zhang, H.; Zong, J.; Cao, H.; Tu, D.; Lu, C. S.; Yan, H. *J. Am. Chem. Soc.* **2025**, *147*, 12845–12857.
19. Marfavi, A.; Kavianpour, P.; Rendina, L. M. *Nat. Rev. Chem.* **2022**, 6, 486–504.
20. Qiu, Z. *Tetrahedron Lett.* **2015**, *56*, 963–971.
21. Coult, R.; Fox, M. A.; Gill, W. R.; Herbertson, P. L.; MacBride, J. A. H.; Wade, K. *J. Organomet. Chem.* **1993**, *462*, 19–29.
22. Zhang, J.; Xie, Z. *Synthesis* **2025**, *57*, 495–521.
23. Dziedzic, R. M.; Spokoyny, A. M. *Chem. Commun.* **2019**, *55*, 430–442.
24. Quan, Y.; Xie, Z. *Chem. Soc. Rev.* **2019**, *48*, 3660–3673.
25. Anderson, K. P.; Mills, H. A.; Mao, C.; Kirlikovali, K. O.; Axtell, J. C.; Rheingold, A. L.; Spokoyny, A. M. *Tetrahedron* **2019**, *75*, 187–191.
26. Sun, M.; Feng, L.; Lu, J. Y. *Org. Lett.* **2024**, *26*, 3697–3702.

27. El-Zaria, M. E.; Arii, H.; Nakamura, H. *Angew. Chem., Int. Ed.* **2014**, *53*, 5156–5160.
28. Sambiagio, C.; Marsden, S. P.; Blacker, A. J.; McGowan, P. C. *Chem. Soc. Rev.* **2014**, *43*, 3525–3550.
29. Lu, J. Y.; Zhao, B.; Du, Y.; Yang, J.; Lu, J. *Org. Biomol. Chem.* **2019**, *17*, 7438–7441.
30. Pearce, K. G.; Anderson, N. H.; Fox, M. A.; Albesa-Jové, D.; Pålsson, L. O.; Rosair, G. M.; Welch, A. J. *Dalton Trans.* **2024**, *53*, 6653–6659.
31. Yang, Q.; Zhao, Y.; Ma, D. *Org. Process Res. Dev.* **2022**, *26*, 1690–1750.
32. Recently, bis(carboran-1-yl)aurate species have been detected and proposed to play crucial roles in stabilizing gold nanoparticles and controlling regioselectivity in catalytic reactions, though structural characterization of such complexes remains limited. See: Wang, M.; Zhang, S.; Gong, Y.; Zhang, W.; Wang, Y.; Chen, Y.; Zheng, Q.; Liu, Z.; Tang, C. *Angew. Chem., Int. Ed.* **2024**, *63*, e202409283.
33. Willans, C. E.; Kilner, C. A.; Fox, M. A. *Chem. Eur. J.* **2010**, *16*, 10644–10648.
34. Sakuraba, M.; Hoshimoto, Y. *Synthesis* **2024**, *56*, 3421–3430.
35. Hisata, Y.; Washio, T.; Takizawa, S.; Ogoshi, S.; Hoshimoto, Y. *Nat. Commun.* **2024**, *15*, 3708.
36. Tang, C.; Xie, Z. *Angew. Chem., Int. Ed.* **2015**, *54*, 7662–7665.
37. Cahiez, G.; Gager, O.; Buendia, J. *Synlett* **2010**, 299–303.
38. Ledwon, P. *Org. Electron.* **2019**, *75*, 105422.
39. Sanaullah; Walczak, K. *Org. Biomol. Chem.* **2025**, *23*, 6287–6319.
40. Xia, H.; Xie, K.; Zou, G. *Molecules* **2017**, *22*, 2236.
41. The corresponding carboranylation of 8-bromoquinoline failed, and debrominated quinoline was predominantly obtained at 120 °C.
42. Ren, S.; Xie, Z. *Organometallics* **2008**, *27*, 5167–5168.
43. Morisaki, Y.; Tominaga, M.; Ochiai, T.; Chujo, Y. *Chem. Asian J.* **2014**, *9*, 1247–1251.
44. Jia, C.; Wang, L.; Ma, Y. N.; Duan, Z. *Organometallics* **2025**, *44*, 938–943.
45. Morisaki, Y.; Tominaga, Y.; Chujo, Y. *Chem. Eur. J.* **2012**, *18*, 11251–11257.
46. Although the Details Were Unclear, NMR Signals Showing the Dissociation of THF from the Li Center Were Observed upon Mixing **Li/Cu-1** and Pyridine (1–5 equiv) in CD_2Cl_2 at Room Temperature, Together with a Concomitant Upfield Shift of the Pyridine Signals, Possibly Indicating the Occurrence of a Ligand-Exchange Reaction and/or Coordination of Pyridine to the Cu Center (Figure 2.S30).
47. Dolomanov, O. V.; Bourhis, L. J.; Gildea, R. J.; Howard, J. A. K.; Puschmann, H. *J. Appl. Crystallogr.* **2009**, *42*, 339–341.
48. Sheldrick, G. M. *Acta Crystallogr. A* **2015**, *71*, 3–8.
49. Sheldrick, G. M. *Acta Crystallogr. C* **2015**, *71*, 3–8.
50. Fox, M. A.; Hughes, A. K. *Coord. Chem. Rev.* **2004**, *248*, 457–476.
51. Songkram, C.; Ohta, K.; Yamaguchi, K.; Pichierri, F.; Endo, Y. *Inorg. Chem.* **2010**, *49*, 11174–11183.
52. Jiang, W.; Knobler, C. B.; Hawthorne, M. F. *Inorg. Chem.* **1996**, *35*, 3056–3058.
53. Li, Y.; Zhao, P.; Jia, C.; Sun, N.; Ma, Y.-N.; Duan, Z. *Organometallics* **2024**, *43*, 1077–1084.
54. Wyzlic, I. M.; Tjarks, W.; Soloway, A. H.; Perkins, D. J.; Burgos, M.; O'Reilly, K. P. *Inorg. Chem.* **1996**, *35*, 4541–4547.

55. Murphy, D. M.; Mingos, D. M. P.; Forward, J. M. *J. Mater. Chem.* **1993**, *3*, 67–76.
56. Causey, P. W.; Besanger, T. R.; Valliant, J. F. *J. Med. Chem.* **2008**, *51*, 2833–2844.
57. Lee, S. H.; Kwon, Y. B.; Yoon, C. M. *Synth. Commun.* **2009**, *39*, 4069–4078.
58. Lu, J. Y.; Wan, H.; Zhang, J.; Wang, Z.; Li, Y.; Du, Y.; Li, C.; Liu, Z. T.; Liu, Z. W.; Lu, J. *Chem. Eur. J.* **2016**, *22*, 17542–17546.
59. Fabre, B.; Hao, E.; LeJeune, Z. M.; Amuhaya, E. K.; Barrière, F.; Garno, J. C.; Vicente, M. G. H. *ACS Appl. Mater. Interfaces* **2010**, *2*, 691–702.
60. Frisch, M. J.; Trucks, G. W.; Schlegel, H. B.; Scuseria, G. E.; Robb, M. A.; Cheeseman, J. R.; Scalmani, G.; Barone, V.; Petersson, G. A.; Nakatsuji, H.; Li, X.; Caricato, M.; Marenich, A. V.; Bloino, J.; Janesko, B. G.; Gomperts, R.; Mennucci, B.; Hratchian, H. P.; Ortiz, J. V.; Izmaylov, A. F.; Sonnenberg, J. L.; Williams-Young, D.; Ding, F.; Lipparini, F.; Egidi, F.; Goings, J.; Peng, B.; Petrone, A.; Henderson, T.; Ranasinghe, D.; Zakrzewski, V. G.; Gao, J.; Rega, N.; Zheng, G.; Liang, W.; Hada, M.; Ehara, M.; Toyota, K.; Fukuda, R.; Hasegawa, J.; Ishida, M.; Nakajima, T.; Honda, Y.; Kitao, O.; Nakai, H.; Vreven, T.; Throssell, K.; Montgomery, J. A., Jr.; Peralta, J. E.; Ogliaro, F.; Bearpark, M. J.; Heyd, J. J.; Brothers, E. N.; Kudin, K. N.; Staroverov, V. N.; Keith, T. A.; Kobayashi, R.; Normand, J.; Raghavachari, K.; Rendell, A. P.; Burant, J. C.; Iyengar, S. S.; Tomasi, J.; Cossi, M.; Millam, J. M.; Klene, M.; Adamo, C.; Cammi, R.; Ochterski, J. W.; Martin, R. L.; Morokuma, K.; Farkas, O.; Foresman, J. B.; Fox, D. J. Gaussian, Inc., Wallingford CT, 2016.
61. Adamo, C.; Barone, V. *J. Chem. Phys.* **1999**, *110*, 6158–6170.
62. Grimme, S.; Antony, J.; Ehrlich, S.; Krieg, H. *J. Chem. Phys.* **2010**, *132*, 154104.
63. Fukui, K. *Acc. Chem. Res.* **1981**, *14*, 363–368.
64. Pritchard, B. P.; Altarawy, D.; Didier, B.; Gibson, T. D.; Windus, T. L. *J. Chem. Inf. Model.* **2019**, *59*, 4814–4820.
65. Chai, J. D.; Head-Gordon, M. *Phys. Chem. Chem. Phys.* **2008**, *10*, 6615–6620.
66. Keith, T. A. AIMAll (Version 19.10.12, Professional): Computational Chemistry Using the Quantum Theory of Atoms in Molecules (QTAIM). TK Gristmill Software, Overland Park, KS, 2017. Available at: http://aim.tkgristmill.com/.

Chapter 3

Triarylboranes Bearing (*ortho*-Carboran-1-yl)aryl Groups for Catalytic Hydrogenation with Pure or Crude H_2

Abstract: Structural diversification of triarylboranes with previously unexplored substituents offers new opportunities for catalytic transformations. In this study, the author developed triarylboranes incorporating 2,6-F_2-4-(*o*-carboran-1-yl)phenyl (Ar) groups and investigated their Lewis acidity and catalytic performance. Among them, B(2,6-$Cl_2C_6H_3$)Ar_2 exhibited remarkable activity in reductive alkylation of aliphatic amino-acid esters using molecular hydrogen, achieving efficient C–N bond formation under mild conditions. This borane also demonstrated high turnover numbers in hydrogenation of N-heteroaromatics (TON up to 3960 with pure H_2; up to 2400 with crude H_2) and enabled dehydrogenation of tetrahydroquinoline. These results represent the first catalytic applications of carboranyl-substituted triarylboranes in diverse hydrogen-mediated transformations, highlighting their potential as versatile Lewis acidic catalysts.

3.1 Introduction

Triarylboranes (BAr_3) have been widely used as electron-accepting units in photo- and electro-functional materials and as key Lewis acids to generate frustrated Lewis pairs (FLPs) between Lewis bases.[1–5] Intense research efforts have been devoted to regulating the Lewis acidity of BAr_3 by introducing substituents onto the aromatic rings, such as halogens (especially F and Cl atoms), alkyl (especially the CH_3 group), and other unsaturated hydrocarbon groups.[1,6,7] However, the limited availability of methods for the construction of three C_{Ar}–B bonds without occupying the empty p orbital on boron has left many functional groups unexplored. Our group has contributed to this field with the synthesis of BAr_3 compounds as catalysts for the hydrogenation of *N*-heteroaromatic and carbonyl compounds using H_2 or a gaseous mixture of H_2, CO, CO_2, and/or CH_4 (crude H_2)[8–10] as well as for the reductive alkylation of amino acids with aldehydes,[11,12] using remote back-strain[13] and machine-learning-assisted strategies.[12]

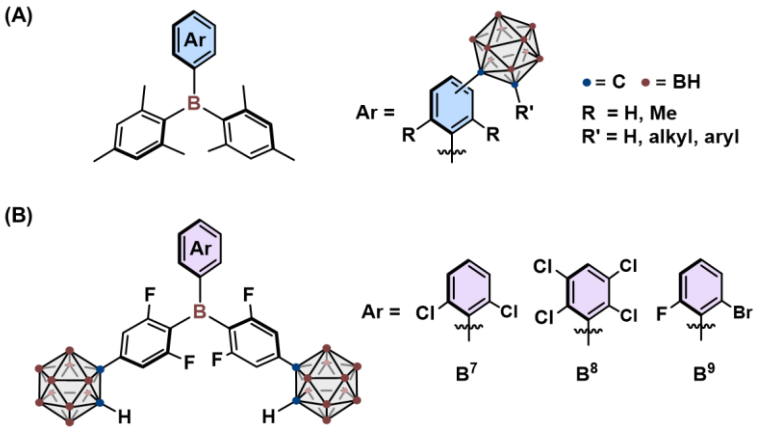


Figure 3.1. (A) Hitherto reported heteroleptic triarylboranes containing (*o*-carboran-1-yl)arenes. (B) Structure of **B[7]–B[9]** synthesized in this work. *Reprinted with permission from* Organic Letters. © American Chemical Society.

Motivated by the unique properties of *o*-carboranes, such as strong electron-withdrawing ability, high thermal stability, three-dimensional aromaticity, and remarkable hydrophobicity,[14–19] the author became interested in exploring the introduction of *closo*-1,2-carboranes (*o*-carboranes, *o*-1,2-$C_2B_{10}H_{12}$; Figure 3.1A) as substituents on the aryl groups of BAr_3 and in applying the obtained boranes to catalytic hydrogenation reactions. Several examples of homo- and heteroleptic BAr_3 that bear (*o*-carboran-1-yl)arenes have been synthesized (Figure 3.1A),[20–26] and their Lewis acidity and photophysical properties have been explored. However, these molecules simultaneously contain more than two 2,6-dimethylaryl units, such as the mesityl group (Mes), limiting their application as Lewis-acidic catalysts in molecular transformations. In fact, catalytic molecular transformations using boranes that bear carboranyl aryl groups have not been reported to date.[27] Here, the author report the synthesis of heteroleptic boranes **B[7]–B[9]**, which bear two 2,6-F_2-4-(*o*-carboran-1-yl)C_6H_2 groups (Figure 3.1B), and their application to the catalytic hydrogenation of *N*-heteroaromatics using H_2 or gaseous mixtures including H_2, CO_2, and/or CO, as well as the reductive alkylation of aliphatic amino-acid esters with H_2 as a reductant. The key to the successful synthesis of **B[7]–B[9]** is the straightforward and multigram-scale preparation of 3,5-F_2-(*o*-carboran-1-yl)C_6H_3 based on the method shown in Chapter 2 using [Li(thf)$_4$][(*o*-carboran-1-yl)$_2$Cu] complex (**Li/Cu-1**).[28]

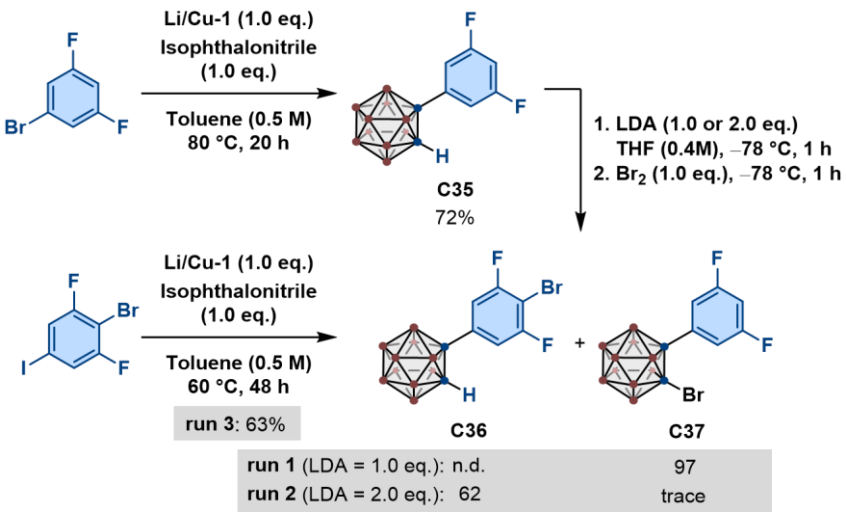


Figure 3.2. Reactions of aryl halides with **Li/Cu-1**. Yields of isolated products are shown. *Reprinted with permission from* Organic Letters. © American Chemical Society.

The carboranylation of 1-bromo-3,5-difluorobenzene with an equimolar amount of **Li/Cu-1** and isophthalonitrile in toluene at 80 °C furnished **C35** in 72% isolated yield (14.1 mmol, 3.62 g) (Figure 3.2). Then, the author explored the bromination at the *para* position of **C35** with respect to the carboranyl unit via deprotonation with lithium diisopropylamide (LDA, 1.0 equiv) followed by addition of Br_2 (1.0 equiv); however,

bromination of the carboranyl C–H group occurred predominantly to furnish **C37** in 97% yield (Figure 3.2, run 1). Conversely, using 2.0 equiv of LDA afforded the targeted aryl C–H brominated product **C36** in 62% yield, together with a trace amount of **C37** (Figure 3.2, run 2). These results suggest that bromination proceeds preferentially at the aryl C–Li unit relative to the carboranyl C–Li unit when both the aryl and carboranyl C–H bonds are fully deprotonated. Furthermore, the reaction of 2-bromo-1,3-difluoro-5-iodobenzene with **Li/Cu-1** at 60 °C proceeded via selective carboranylation at the iodide position to afford **C36** in 63% yield (Figure 3.2, run 3), demonstrating a more step-efficient approach to **C36** than the conditions described in run 2 (Figure 3.2). However, using 1-bromo-3,5-difluorobenzene would be more cost-effective than using 2-bromo-1,3-difluoro-5-iodobenzene.

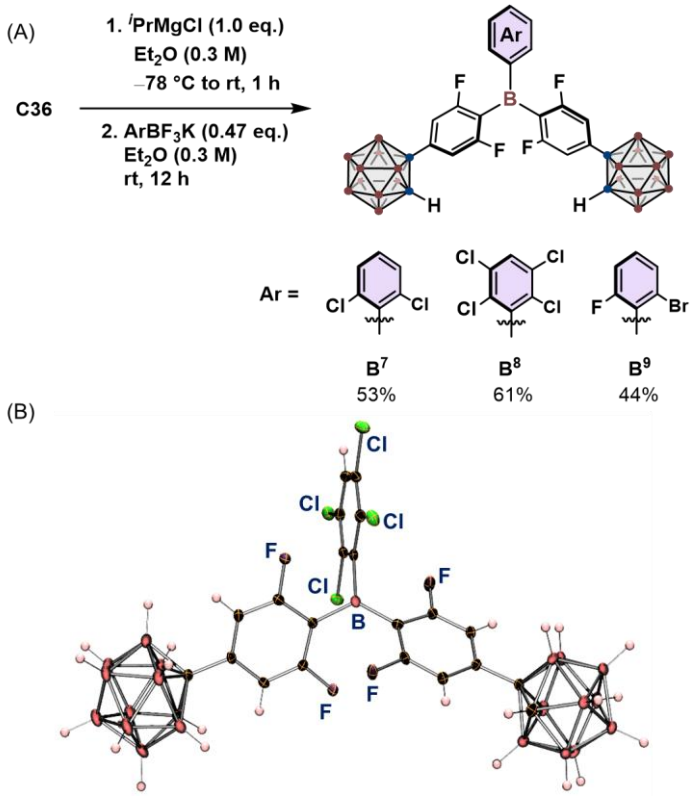
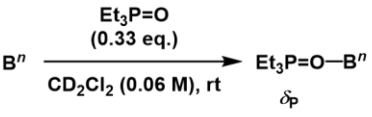


Figure 3.3. (A) Synthesis of **B**^{7}–**B**^{9}. Yields of isolated products are shown. (B) Molecular structure of **B**^{8} with thermal ellipsoids at 30% probability. *Reprinted with permission from* Organic Letters. © American Chemical Society.

With precursor **C36** in hand, the author then synthesized boranes **B**^{7} (53%), **B**^{8} (61%), and **B**^{9} (44%) via C–B bond formation between an (*o*-carboran-1-yl)aryl Grignard reagent generated from **C36** and ^{i}PrMgCl in Et_2O and the corresponding $ArBF_3K$ salt (Ar = 2,6-Cl_2-C_6H_3 for **B**^{7}, 2,3,5,6-Cl_4C_6H for **B**^{8}, and 2-Br-6-F-C_6H_3 for **B**^{9}; Figure 3.3A). The author selected these *ortho*-dihalogenated aryl groups because they are known to endow BAr_3 with superior performance in catalytic hydrogenation and hydrosilylation reactions.[8,10–12, 29–33] However, polyhalogenated boranes tend to be less soluble (or nearly insoluble) in common organic solvents such as toluene or *n*-hexane, making the purification process to remove inorganic salt byproducts laborious and

time-consuming. In contrast, owing to the lipophilicity of the carboranyl groups, **B⁷**–**B⁹** readily dissolve in *n*-hexane and can thus be easily extracted from the crude mixture. Their molecular structures were unambiguously confirmed by multinuclear NMR and single-crystal X-ray diffraction analyses (the molecular structure of **B⁸** is shown in Figure 3.3B).

Next, the author evaluated the effective Lewis acidity of **B⁷**–**B⁹** using the Gutmann–Beckett method,[33] i.e., by comparing the deviation in chemical shifts ($\Delta\delta_P$) upon the formation of $Et_3P{=}O$–**B***ⁿ* (*n* = 7–9) relative to free $Et_3P{=}O$ (δ_P = 51.4 in CD_2Cl_2). A larger $\Delta\delta_P$ value is expected for BAr_3 compounds that exhibit higher Lewis acidity toward $Et_3P{=}O$. The author furthermore included $B(C_6F_5)_3$ and $B(2,6\text{-}Cl_2\text{-}C_6H_3)(2,6\text{-}F_2\text{-}3,5\text{-}X_2C_6H)_2$ (**B³ᵃ**: X = Br; **B¹ᵃ**: X = F) in our study because **B³ᵃ** exhibited remarkable catalytic performance in the hydrogenation of 1-methylindole (**MeInd**) and 2-methylquinoline (**MeQin**),[8,10,29] while **B¹ᵃ** showed reasonable activity toward the reductive alkylation of natural amino-acid derivatives.[11] As shown in Figure 3.4, the $\Delta\delta_P$ values (and the corresponding acceptor numbers, ANs)[1] follow the order **B⁷** ($\Delta\delta_P$ = +22.5; AN = 72.7) < **B⁹** = **B³ᵃ** ($\Delta\delta_P$ = +23.3; AN = 74.5) ≈ **B⁸** ($\Delta\delta_P$ = +23.4; AN = 74.7) ≈ **B¹ᵃ** ($\Delta\delta_P$ = +23.6; AN = 75.1) < $B(C_6F_5)_3$ ($\Delta\delta_P$ = +26.3; AN = 81.1). The LUMO energy levels of **B⁷**–**B⁹** indicate that their intrinsic Lewis acidity is higher than that of **B³ᵃ** and **B¹ᵃ** but lower than that of $B(C_6F_5)_3$, further supporting the strongly electron-withdrawing nature of the *o*-carboranyl groups. A comparison of their global electrophilicity indices (ω [eV])[35,36] corroborates this conclusion.



	B⁷	**B⁸**	**B⁹**	**B³ᵃ**	**B¹ᵃ**	$B(C_6F_5)_3$
δ_P [ppm] (AN)	73.9 (72.7)	74.8 (74.7)	74.7 (74.5)	74.7 (74.5)	75.0 (75.1)	77.7 (81.1)
LUMO [eV] (ω [eV])	−1.41 (1.81)	−1.57 (1.89)	−1.43 (1.81)	−1.28 (1.71)	−1.33 (1.76)	−1.93 (2.18)

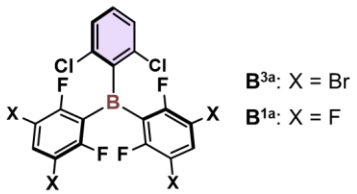
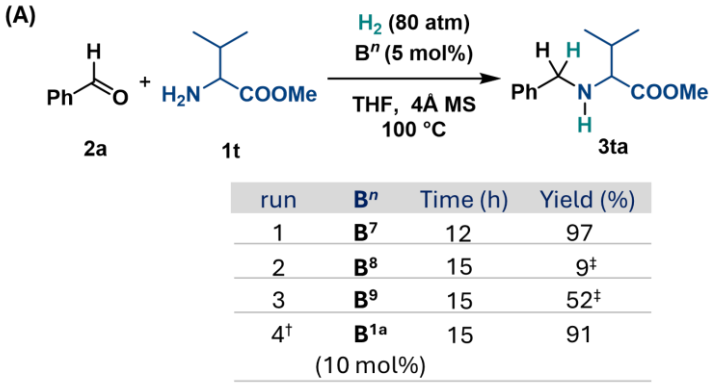


Figure 3.4. Reaction between **B***ⁿ* (*n* = 7–9) and $Et_3P{=}O$ (0.33 equiv) in CD_2Cl_2. Each δ_P value and the corresponding acceptor number (AN) are shown. LUMO energy levels (eV), calculated at the ωB97X-D/6-311+G(d,p)//ωB97X-D/6-31G(d,p) level (gas phase), are also given. Values for **B⁴**, **B⁵**, and $B(C_6F_5)_3$ are reproduced from ref. 13. For details on the calculation of the global electrophilicity index (ω [eV]), see the Supporting Information 3.4.9.3.

Then, **B⁷**–**B⁹** were applied to the reductive alkylation of natural amino-acid derivatives in the presence of H_2 as a reductant (Figure 3.5). So far, developing a BAr_3 that effectively mediates the reductive alkylation of

aliphatic amino acids (or their ester derivatives) has remained challenging. In this context, the author previously reported that **B**[1a] catalyzed the reaction between valine ester (**1t**) and benzaldehyde (**2a)** in the presence of H_2 (80 atm), even though 10 mol% of the catalyst was required to produce **3ta** in 91% yield after 15 h (Figure 3.5A).[11] Remarkably, the author found that **3ta** was afforded in 97% yield after 12 h when 5 mol% **B**[7] was used, further highlighting its superior catalytic performance compared to hitherto reported boranes, albeit that **B**[8] and **B**[9] were less active. The author then applied **B**[7] (5 mol%) to transform dimethyl glutamate (**1u**) with **2a** and H_2, which eventually isolated cyclic amide **3ua** in 50% yield via the reductive alkylation, followed by the intramolecular cyclization with concomitant elimination of MeOH (Figure 3.5B).



run	B^n	Time (h)	Yield (%)
1	**B**[7]	12	97
2	**B**[8]	15	9‡
3	**B**[9]	15	52‡
4†	**B**[1a] (10 mol%)	15	91

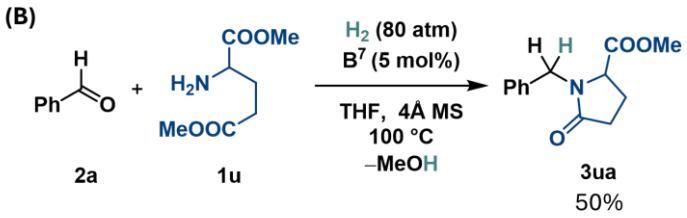
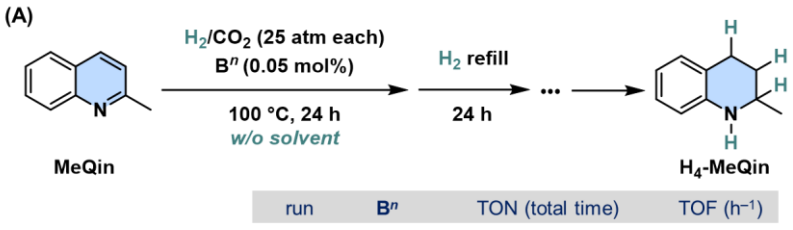


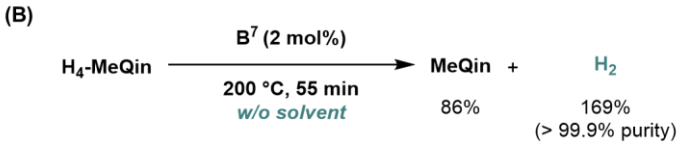
Figure 3.5. (A) Reductive alkylation of **1t** with **2a** in the presence of **B**[7]–**B**[9] (5 mol%) and H_2 (80 atm). †Results reproduced from ref. 11. ‡NMR yields. (B) Sequential reductive alkylation/intramolecular amidation reaction from **1u**. *Reprinted with permission from* Organic Letters. © American Chemical Society.

Finally, the author examined the catalytic activity of **B**[7]–**B**[9] in the solvent-free hydrogenation of **MeQin** using an equimolar gaseous mixture of H_2/CO_2 (25 atm each) or $H_2/CO/CO_2$ (30 atm each) as well as in that of **MeInd** using H_2 (60 atm) to yield 1,2,3,4-tetrahydroquinoline (**H_4-MeQin**) (Figure 3.6A) and 1-methylindoline (**H_2-MeInd**) (Figure 3.6C), respectively. It should be noted that these gaseous mixtures are commonly accepted models for crude H_2, which is widely produced from various carbon-based resources, such as natural gas and biomass. As previously reported,[8,10,29] $B(C_6F_5)_3$ does not efficiently catalyze the hydrogenation of **MeQin** (Figure 3.6A, run 5) or **MeInd** under such solvent-free and/or mixed gas conditions. In contrast, **B**[3a] exhibited a high catalyst turnover number (TON) and turnover frequency (TOF per hour) in the production of **H_4-Qin** and **H_2-Ind** under otherwise identical conditions (Figures 3.6A and 3.6C, runs 4). These results have rendered **B**[3a] one of the best BAr_3 catalysts for the hydrogenation of *N*-heteroaromatics explored so far, owing to the precise regulation of remote back-strain.[8,10,29] Interestingly, **B**[7] exhibited promising activity for

the hydrogenation of **MeQin** using H_2/CO_2, yielding a TON of 2400 after 48 h (Figure 3.6A, run 1), which corresponds to a higher TOF (50.0 h^{-1}) than that obtained with $\mathbf{B^{3a}}$ (20.0 h^{-1}). This significant increase in the initial reaction rate was attributed to the higher intrinsic Lewis acidity of $\mathbf{B^7}$ compared to that of $\mathbf{B^{3a}}$ (Figure 3.4); however, BAr_3 compounds with higher intrinsic Lewis acidity are more susceptible to deactivation under Lewis-base-rich conditions. In fact, under solvent-free conditions using $H_2/CO/CO_2$ (30 atm each), $\mathbf{B^7}$ (0.1 mol%) afforded a TON of 1440 after 48 h, which is slightly lower than that using $\mathbf{B^{3a}}$ (1520), most likely because suppression of the catalytic activity by reversible coordination of CO to the boron center should be more critical for $\mathbf{B^7}$.[37] Interestingly, the $\mathbf{B^7}$ catalyzed solvent-free dehydrogenation from **H_4-MeQin** proceeded smoothly to regenerate **MeQin** (86%) with concomitant generation of H_2 (169% yield with >99.9 purity) within 55 min (Figure 3.6B). Similarly, the author confirmed the promising reactivity of $\mathbf{B^8}$ in the hydrogenation of **MeQin** (TOF = 25.0 h^{-1}; Figure 3.6A, run 2); however, $\mathbf{B^8}$ gave **H_2-MeInd** only in a lower yield (Figure 3.6C, run 2). $\mathbf{B^9}$ was ineffective in the hydrogenation of **MeQin** and **MeInd** under the applied reaction conditions (Figures 3.6A and 3.6C, runs 3).



run	B^n	TON (total time)	TOF (h^{-1})
1	$\mathbf{B^7}$	2400 (48 h) [1440]‡	50.0
2	$\mathbf{B^8}$	1200 (48 h)	25.0
3	$\mathbf{B^9}$	16 (24 h)	0.7
4†	$\mathbf{B^{3a}}$	2400 (120 h) [1520]‡	20.0
5†	$B(C_6F_5)_3$	21 (72 h)	0.3





run	B^n	TON	TOF (h^{-1})
1	$\mathbf{B^7}$	2300	95.8
2	$\mathbf{B^8}$	300	12.5
3	$\mathbf{B^9}$	50	2.1
4†	$\mathbf{B^{3a}}$	2850	118.8

Figure 3.6. (A) Evaluation of the catalytic activity and robustness of $\mathbf{B^7}$–$\mathbf{B^9}$ (0.05 mol%) in the hydrogenation of **MeQin** (50 mmol) in terms of TON and TOF (h^{-1}). (B) Solvent-free catalytic dehydrogenation of **H_4-MeQin** (3.77 mmol) using $\mathbf{B^7}$. The yield of **MeQin** was determined by GC analysis. The yield of H_2 was calculated based on the collected volume (V = 143 mL, 6.38 mmol). (C) Catalytic hydrogenation of **MeInd** (25 mmol)

with **B**^{7}**–B**^{9} (0.02 mol%). The product yield was determined by GC analysis. †Results reproduced from ref. 13. ‡Reaction with 0.1 mol% borane, **MeQin** (25 mmol), and $H_2/CO/CO_2$ (30 atm each) for 48 h. *Reprinted with permission from* Organic Letters. © American Chemical Society.

3.3 Conclusion

In summary, the author has synthesized novel heteroleptic boranes **B**^{7}**–B**^{9}, which bear 2,6-F_2-4-(*o*-carboran-1-yl)C_6H_2 groups, and evaluated their Lewis acidity experimentally and theoretically. In contrast to previously reported polyhalogenated BAr_3 compounds, **B**^{7}**–B**^{9} show excellent solubility in *n*-hexane owing to the lipophilicity of the carboranyl moieties, which significantly simplifies their purification after synthesis. Moreover, the author confirmed for the first time the promising catalytic activity of boranes that carry (*o*-carboran-1-yl)aryl groups. **B**^{7} exhibited reductive alkylation of aliphatic amino-acid esters, reflecting the strong electron-withdrawing nature of the *o*-carboranyl groups. Remarkably, **B**^{7} can also serve as a good catalyst for the a TON of up to 2400 (TOF up to 50 h^{-1}) in the catalytic hydrogenation of 2-methylquinoline even under solvent-free conditions using crude H_2 (H_2/CO_2 or $H_2/CO/CO_2$). **B**^{7} also effectively catalyzes the dehydrogenation of 2-methyl-1,2,3,4-tetrahydroquinoline and the hydrogenation of 1-methylindole. Given that archetypal $B(C_6F_5)_3$ shows only limited utility under such Lewis-base-rich conditions, the structural diversification of BAr_3 with hitherto unexplored functional groups can be expected to significantly expand their utility in catalytic molecular transformations.

3.4 Supporting information

3.4.1 General considerations

Unless otherwise noted, all manipulations were conducted under a N_2 atmosphere using standard Schlenk line or grove box (GB) techniques. ^{1}H, ^{11}B, ^{13}C, ^{19}F, and ^{31}P NMR spectra were recorded on a Bruker AVANCE III 400 or at 25 °C. The chemical shifts in the ^{1}H NMR spectra were recorded relative to Me_4Si or residual protonated solvent ($CHCl_3$ (δ 7.26), $CDCl_2H$ (δ 5.32), C_6D_5H (δ 7.16)). The chemical shifts in the ^{11}B NMR spectra were recorded relative to $BF_3{\cdot}Et_2O$. The chemical shifts in the ^{13}C spectra were recorded relative to Me_4Si or deuterated solvent ($CDCl_3$ (δ 77.16), CD_2Cl_2 (δ 53.84), C_6D_6 (δ 128.06)). The chemical shifts in the ^{19}F NMR spectra were recorded relative to α,α,α-trifluorotoluene (δ −65.64). The chemical shifts in the ^{31}P NMR spectra were recorded relative to 85% H_3PO_4 as an external standard. Heating and stirring experiments were carried out using an oil bath for standard reactions. For gas-pressurized experiments conducted in an autoclave, the author used a solid metal block heater. Analytical gas chromatography (GC) was carried out on a Shimadzu GC-2025 gas chromatograph equipped with a flame ionization detector. The purity of hydrogen obtained from the dehydrogenation reaction was determined using a Shimadzu Nexis™ GC-2030 gas chromatograph. High resolution mass spectrometry (HRMS) was performed at the Analytical Instrumentation Facility, Graduate School of Engineering, The University of Osaka. HRMS spectra were obtained using a double-focusing mass spectrometer (JMS-700; JEOL) mass spectrometry.

X-ray crystal data were collected using the Rigaku XtaLAB Synergy equipped with the HyPix-6000HE detector. Using Olex[38], the structure was solved with the SHELXT2[39] structure solution program using

Intrinsic Phasing and refined with the SHELXL[40] refinement package using Least Squares minimization. It should be noted that the boron and carbon atoms in the *o*-carborane moieties might be incorrectly assigned due to the difficulty of distinguishing them by XRD analysis, especially when crystallographic disorder of the pseudo-spherical cluster is observed.[41]

Figures in this section are reproduced from our article published in Organic Letters, with permission from the American Chemical Society.

3.4.2 Materials

All commercially available reagents, including super-dehydrated solvents (*n*-hexane, toluene, tetrahydrofuran), were purchased from Sigma Aldrich, Tokyo Chemical Industry TCI, and Wako Pure Chemical Industries, and used as received. Benzene-d_6 was distilled from sodium benzophenone ketyl prior to use. CD_2Cl_2 was once degassed by several freeze-pump-thaw cycles and stored inside GB over molecular sieves (4 Å). 1-Methylindole (**MeInd**), 2-methylquinoline (**MeQin**) and tetradecane (for an internal standard of the GC analysis) were purchased from TCI or Angene Chemical, and used after distillation over CaH_2. *o*-Carborane was purchased from Angene and used after sublimation. **Li/Cu-1** was prepared based on the reported procedure.[28]

Metrical data for the solid-state structures are available from Cambridge Crystallographic Data Centre: CCDC 2500155 (**C37**), 2500157 (**B^7**), 2500156 (**B^8**), 2500158 (**B^9**).

3.4.3 Preparation of materials

3.4.3.1 Preparation of **C35** (Figure 3.2B)

In a screw-cap reaction vessel equipped with a magnetic stirrer bar, **Li/Cu-1** (12.65 g, 19.6 mmol, 1.0 equiv), isophthalonitrile (2.51 g, 19.6 mmol, 1.0 equiv), and 1-bromo-3,5-difluorobenzene (3.78 g, 19.6 mmol, 1.0 equiv) were added. Toluene (39.2 mL) was then added, and the vessel was sealed. The mixture was stirred at 80 °C for 20 h. After cooling to rt, the reaction mixture was diluted with wet Et_2O. The resulting mixture was filtered through a filter paper, and the volatiles were removed under reduced pressure. The crude product was purified by distillation (160 °C, 0.2 mmHg) to afford **C35** as a white solid (3.62 g, 14.1 mmol, 72%). **^{1}H NMR** (400 MHz, $CDCl_3$, rt, δ/ppm): 7.05–7.01 (m, 2H), 6.91–6.84 (m, 1H), 3.92 (s, 1H), 3.48–1.64 (brm). **^{11}B NMR** (128 MHz, $CDCl_3$, rt, δ/ppm): −0.71–−4.35 (m, 2B), −6.98–−14.01 (m, 8B). **^{13}C{^{1}H} NMR** (100 MHz, $CDCl_3$, rt, δ/ppm): 162.9 (dd, J = 249.7 Hz, J = 12.9 Hz), 137.0 (t, J = 10.0 Hz), 111.5 (d, J = 28.3 Hz), 106.2–105.3 (m), 74.3, 60.1 (d, J = 14.2 Hz). **^{19}F NMR** (376 MHz, $CDCl_3$, rt, δ/ppm): −110.2 (t, J = 7.5 Hz, 2F). **HRMS** (CI^-): m/z Calculated for $C_8H_{14}B_{10}F_2$ ($[M]^-$) 258.1994, found 258.2005.

3.4.3.2 Preparation of **C36**

Method A (Figure 3.2B, run 2): A solution of ^{i}Pr$_2$NH (2.86 mL, 20.3 mmol, 1.0 M in THF) was slowly treated with ^{n}BuLi (12.1 mL, 18.5 mmol, 1.53 M in hexane) at −78 °C. After stirring at −78 °C for 1 h, the resultant LDA was slowly transferred into a solution of **1** (2.37 g, 9.25 mmol, 0.5 M in THF) at −78 °C. After stirring for 1 h at −78 °C, Br_2 (1.47 g, 9.20 mmol, 1.0 equiv) was added, and the resultant mixture was stirred for an additional 1 h at −78 °C. After being diluted with saturated aqueous NH_4Cl solution at −78 °C, the organic layer

was extracted with Et_2O and dried over Na_2SO_4. The volatile was then removed in vacuo. Purification by flash column chromatography on silica gel (*n*-hexane only) afforded **C36** as a white solid (1.92 g, 5.73 mmol, 62%). ^{1}**H NMR** (400 MHz, $CDCl_3$, rt, δ/ppm): 7.15–7.05 (m, 2H), 3.90 (s, 1H), 3.48–1.05 (brm). **^{11}B NMR** (128 MHz, $CDCl_3$, rt, δ/ppm): −0.02–−5.74 (m, 2B), −6.19–−15.60 (m, 8B). **^{13}C{^{1}H} NMR** (100 MHz, $CDCl_3$, rt, δ/ppm): 160.0 (dd, J = 249.6 Hz, J = 4.9 Hz), 135.2, 112.0 (d, J = 26.9 Hz), 100.8, 73.8, 60.1. **^{19}F NMR** (376 MHz, $CDCl_3$, rt, δ/ppm): −105.4 (t, J = 6.0 Hz, 2F). **HRMS** (CI^-): m/z Calculated for $C_8H_{13}B_{10}Br_1F_2$ ($[M]^-$) 336.1099, found 336.1135.

Method B (Figure 3.2B, run 3)**:** In a screw-cap reaction vessel equipped with a magnetic stirrer bar, **Li/Cu-1** (9.49 g, 14.7 mmol, 1.0 equiv), isophthalonitrile (1.88 g, 14.7 mmol, 1.0 equiv), and 2-bromo-1,3-difluoro-5-iodobenzene (4.69 g, 14.7 mmol, 1.0 equiv) were added. Toluene (29.4 mL) was then added, and the vessel was sealed. The mixture was stirred at 60 °C for 48 h. After cooling to rt, the reaction mixture was diluted with wet Et_2O. The resulting mixture was filtered through filter paper, and the volatiles were removed under reduced pressure. The crude product was purified by silica gel column chromatography (*n*-hexane only) to afford **C36** as a white solid (3.12 g, 9.31 mmol, 63%).

3.4.3.3 Preparation of **C37** (Figure 3.2B, run 1)

A solution of ^{i}Pr$_2$NH (0.71 mL, 5.05 mmol, 1.0 M in THF) was slowly treated with ^{n}BuLi (3.00 mL, 4.59 mmol, 1.53 M in hexane) at −78 °C. After stirring at −78 °C for 1 h, the resultant LDA was slowly transferred into a solution of **C35** (1.18 g, 4.60 mmol, 0.5 M in THF) at −78 °C. After stirring for 1 h at −78 °C, Br_2 (733 mg, 4.59 mmol) was added, and the resultant mixture was stirred for an additional 1 h at −78 °C. After being diluted with saturated aqueous NH_4Cl solution at −78 °C, the organic layer was extracted with Et_2O and dried over Na_2SO_4. The volatile was then removed in vacuo. Purification by flash column chromatography on silica gel (*n*-hexane only) afforded **C37** as a white solid (1.50 g, 4.48 mmol, 97%). **^{1}H NMR** (400 MHz, $CDCl_3$, rt, δ/ppm): 7.25–7.15 (m, 2H), 7.04–6.91 (m, 1H), 3.89–1.00 (brm). **^{11}B NMR** (128 MHz, $CDCl_3$, rt, δ/ppm): −0.01–−5.94 (m, 2B), −5.99–−14.00 (m, 8B). **^{13}C{^{1}H} NMR** (100 MHz, $CDCl_3$, rt, δ/ppm): 162.7 (dd, J = 249.4 Hz, J = 12.8 Hz), 134.5 (t, J = 10.1 Hz), 115.5–114.9 (m), 107.5–106.5 (m), 81.8, 59.2. **^{19}F NMR** (376 MHz, $CDCl_3$, rt, δ/ppm): −110.4 (t, J = 7.7 Hz, 2F). **HRMS** (CI^-): m/z Calculated for $C_8H_{13}B_{10}Br_1F_2$ ($[M]^-$) 336.1099, found 336.1135. **X-ray** data for **3**: M = 335.19, colorless, triclinic, P-1 (#2), a = 6.9543(4) Å, b = 7.8497(6) Å, c = 14.4731(9), α = 94.006(6)°, β = 90.188(5)°, γ = 112.131(7)°, V = 729.70(9) Å^3, Z = 2, $Dcalcd$ = 1.526 g/cm^3 , T = 173.15 K, R_1 (wR_2) = 0.0577 (0.1612).

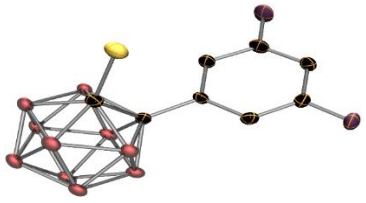


Figure 3.S1. Molecular structure of **C37** with ellipsoids set at 30% probability. H atoms are omitted for clarity.

Reprinted with permission from Organic Letters. © American Chemical Society.

3.4.3.4 Synthesis of **B**^{7} (Figure 3.3A)

A solution of **C36** (1.68 g, 5.01 mmol, 0.3 M in Et_2O) was slowly treated with ^{i}PrMgCl (5.01 mL, 1.0 equiv, 1.0 M in Et_2O) at −78 °C. After stirring for 1 h (−78 °C to rt), (2,6-dichlorophenyl)trifluoro-λ^4-borane, potassium salt[42] (596 mg, 2.36 mmol, 0.47 equiv) was added into the reaction solution, and stirred for another 12 h. After the removal of all volatiles in vacuo, the residue was dissolved in a small amount of toluene and then passed through a Celite pad, then concentrated in vacuo and washed with *n*-hexane to afford **B**^{7} as a white solid (834 mg, 1.25 mmol, 53%) after removal of all volatiles in vacuo. A single crystal of **B**^{7} was obtained from a saturated solution of **B**^{7} in benzene at rt. **^{1}H NMR** (400 MHz, C_6D_6, rt, δ/ppm): 6.92 (d, J = 8.0 Hz, 2H), 6.67 (d, J = 8.4 Hz, 4H), 6.62 (t, J = 8.0 Hz, 1H), 2.54 (s, 2H), 3.60–1.04 (brm). **^{11}B NMR** (128 MHz, C_6D_6, rt, δ/ppm): 0.32–−4.29 (m, 4B), −6.69–−15.22 (m, 16B). **^{13}C{^{1}H} NMR** (100 MHz, C_6D_6, rt, δ/ppm): 165.9 (dd, $^{1}J_{C,F}$ = 253.8 Hz, $^{4}J_{C,F}$ = 12.2 Hz), 142.5–142.0 (m, two kinds of peaks were overlapping.), 134.9, 131.6, 127.3, 118.8–118.4 (m), 111.9 (dd, J = 29.0 Hz, J = 7.5 Hz), 73.7, 59.9 (d, J = 10.7 Hz). **^{19}F NMR** (376 MHz, C_6D_6, rt, δ/ppm): −98.7 (d, J = 8.3 Hz, 4F). **X-ray data for B**^{7}: M = 667.36, colorless, monoclinic, I_12/a_1 (#15), a = 28.2482(7) Å, b = 7.00801(14) Å, c = 34.8584(9), α = 90°, β = 108.758(3)°, γ = 90°, V = 6534.2(3) Å^3, Z = 8, *Dcalcd* = 1.357 g/cm^3 , T = 153.15 K, R_1 (wR_2) = 0.0515 (0.1484).

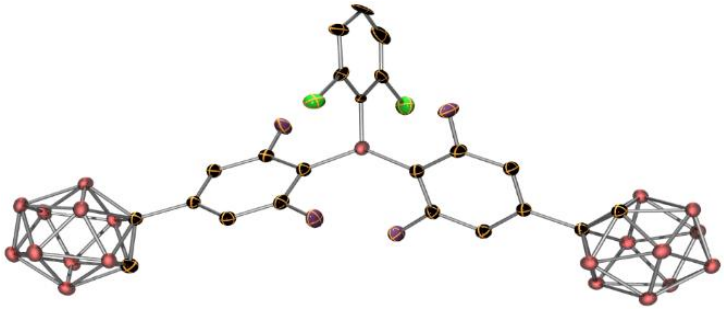


Figure 3.S2. Molecular structure of **B**^{7} with ellipsoids set at 30% probability. H atoms and a disordered molecule are omitted for clarity. *Reprinted with permission from* Organic Letters. © American Chemical Society.

3.4.3.5 Synthesis of **B**^{8} (Figure 3.3A)

A solution of **C36** (1.09 g, 3.25 mmol, 1.0 equiv, 0.3 M in Et_2O) was slowly treated with ^{i}PrMgCl (3.25 mL, 1.0 equiv, 1.0 M in Et_2O) at −78 °C. After stirring for 1 h (−78 °C to rt), trifluoro(2,3,5,6-tetrachlorophenyl)-λ^4-borane, potassium salt[12] (492 mg, 1.53 mmol, 0.47 equiv) was added into the reaction solution, and stirred for another 12 h. After the removal of all volatiles in vacuo, the residue was dissolved in a small amount of toluene and then passed through a Celite pad, then concentrated in vacuo and washed with *n*-hexane to afford **B**^{8} as a white solid (689 mg, 0.936 mmol, 61%) after removal of all volatiles in vacuo. A single crystal of **B**^{8} was obtained from a saturated solution of **B**^{8} in toluene at rt. **^{1}H NMR** (400 MHz, C_6D_6, rt, δ/ppm): 7.05 (s, 1H), 6.66 (d, J = 8.8 Hz, 4H), 2.54 (s, 2H), 3.74–1.06 (brm). **^{11}B NMR** (128 MHz, C_6D_6, rt, δ/ppm): 1.04–−6.05 (m, 4B), −6.06–−17.33 (m, 16B). **^{13}C{^{1}H} NMR** (100 MHz, C_6D_6, rt, δ/ppm): 166.0 (dd, J = 254.6

Hz, J = 12.1 Hz), 145.0, 142.9 (t, J = 12.0 Hz), 132.5, 131.7 (d, J = 4.1 Hz), 130.6, 117.9–117.1 (m), 112.3–111.4 (m), 73.5, 59.9 (d, J = 11.8 Hz). **^{19}F NMR** (376 MHz, C_6D_6, rt, δ/ppm): −98.3 (d, J = 8.3 Hz, 4F). **X-ray data for B[8]** (Figure 3.3B): M = 736.24, colorless, orthorhombic, *Pna*2$_1$ (#33), a = 39.9368(15) Å, b = 6.9768(3) Å, c = 12.4184(6), α = 90°, β = 90°, γ = 90°, V = 3460.2(3) Å^3, Z = 4, $Dcalcd$ = 1.413 g/cm^3, T = 143.15 K, R_1 (wR_2) = 0.0364 (0.0868).

3.4.3.6. Synthesis of **B[9]** (Figure 3.3A)

A solution of **C36** (1.20 g, 3.58 mmol, 1.0 equiv, 0.3 M in Et_2O) was slowly treated with ^{i}PrMgCl (3.58 mL, 1.0 equiv, 1.0 M in Et_2O) at −78 °C. After stirring for 1 h (−78 °C to rt), (2-bromo-6-fluorophenyl)trifluoro-λ^4-borane, potassium salt[33] (469 mg, 1.67 mmol, 0.47 equiv) was added into the reaction solution, and stirred for another 12 h. After the removal of all volatiles in vacuo, the residue was dissolved in a small amount of toluene and then passed through a Celite pad, then concentrated in vacuo and washed with *n*-hexane to afford **B[9]** as a white solid (505 mg, 0.726 mmol, 44%) after removal of all volatiles in vacuo. A single crystal of **B[9]** was obtained from a saturated solution of **B[9]** in benzene at rt. **^{1}H NMR** (400 MHz, C_6D_6, rt, δ/ppm): 7.06–7.01 (m, 1H), 6.71–6.55 (m, 6H), 2.54 (s, 2H), 3.57–1.03 (brm). **^{11}B NMR** (128 MHz, C_6D_6, rt, δ/ppm): 0.48–−4.60 (m, 4B), −6.55–−15.44 (m, 16B). **^{13}C{^{1}H} NMR** (100 MHz, CD_2Cl_2, rt, δ/ppm): 165.6 (dd, J = 253.3 Hz, J = 12.3 Hz), 162.8 (d, J = 243.7 Hz), 141.8, 132.9 (d, J = 8.7 Hz), 128.7, 128.4, 123.6, 114.2 (d, J = 23.5 Hz), 111.8 (d, J = 29.6 Hz), 74.4, 60.5 (d, J = 15.8 Hz). A signal of the ipso-carbon with respect to the boron atoms was not identified. **^{19}F NMR** (376 MHz, C_6D_6, rt, δ/ppm): −98.9 (d, J = 8.3 Hz, 4F), −105.5 (s, 1F). **X-ray data for B[9]**: M = 695.37, colorless, monoclinic, $I_1$2/a$_1$ (#15), a = 27.8460(14) Å, b = 6.9880(2) Å, c = 34.618(2), α = 90°, β = 107.686(6)°, γ = 90°, V = 6417.9(6) Å^3, Z = 8, $Dcalcd$ = 1.439 g/cm^3 , T = 293(2) K, R_1 (wR_2) = 0.0689 (0.1741).

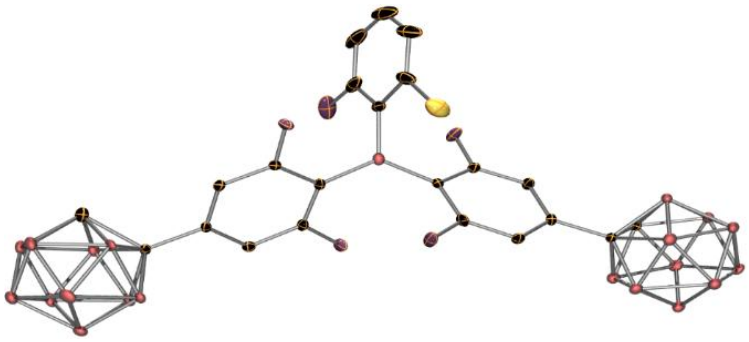


Figure 3.S3. Molecular structure of **B[9]** with ellipsoids set at 30% probability. H atoms are omitted for clarity. *Reprinted with permission from* Organic Letters. © American Chemical Society.

3.4.4 Catalytic hydrogenation of MeQin[8]

Condition A: A 30 mL autoclave was charged with **MeQin** (ca. 50.0 mmol) and **B^n** (ca. 0.025 mmol, 0.05 mol%). Tetradecane was added as an internal standard. Once sealed, the autoclave was pressurized with H_2/CO_2 (25 atm each) and heated at 100 °C. Through this experiment, the author repeatedly pressurized H_2 to reach the total pressure of 50 atm at rt once a day, if the total pressure significantly decreased within the last 24 h. After

confirming that the decrease in total pressure became insignificant, the author further heated the system for an additional 24 h. Then, the reaction was degassed at rt and the yield of **H_4-MeQin** was determined by GC analysis (Figure 3.6A).

Using B^7: Followed by the general procedure, **MeQin** (7.08 g, 49.4 mmol), **B^7** (17.0 mg, 0.0255 mmol), and tetradecane (230 mg, 1.16 mmol) were employed, and the autoclave was heated for 48 h, giving **H_4-MeQin** in 60% GC yield and TON 2400 (TOF 50.0 h^{-1}).

Using B^8: Followed by the general procedure, **MeQin** (7.05 g, 49.2 mmol), **B^8** (19.1 mg, 0.0259 mmol), and tetradecane (236 mg, 1.19 mmol) were employed, and the autoclave was heated for 48 h, giving **H_4-MeQin** in 30% GC yield and TON 1200 (TOF 25.0 h^{-1}).

Using B^9: Followed by the general procedure, **MeQin** (7.14 g, 49.9 mmol), **B^9** (17.2 mg, 0.0247 mmol), and tetradecane (247 mg, 1.25 mmol) were employed, and the autoclave was heated for 24 h, giving **H_4-MeQin** in 0.4% GC yield and TON 16 (TOF 0.7 h^{-1}).

Condition B: A 30 mL autoclave was charged with **MeQin** (3.59 g, 25.1 mmol) and **B^7** (16.8 mg, 0.0252 mmol, 0.1 mol%). Tetradecane (246 mg, 1.24 mmol) was added as an internal standard. Once sealed, the autoclave was pressurized with H_2/CO/CO_2 (30 atm each) and heated at 100 °C for 48 h. Then, the reaction was degassed at rt. The yield of **H_4-MeQin** was confirmed in 72% (TON 1440) by GC yield.

Condition C: A 30 mL autoclave was charged with **MeQin** (ca. 50.0 mmol) and **B''** (ca. 0.025 mmol, 0.05 mol%). Tetradecane was added as an internal standard. Once sealed, the autoclave was pressurized with H_2 (85 atm) and heated at 100 °C. Through this experiment, the author repeatedly pressurized H_2 to reach the total pressure of 85 atm at rt once a day, if the total pressure significantly decreased within the last 24 h. After confirming that the decrease in total pressure became insignificant, the author further heated the system for an additional 24 h. Then, the reaction was degassed at rt and the yield of **H_4-MeQin** was determined by GC analysis.

Using B^7: Followed by the general procedure, **MeQin** (7.04 g, 49.2 mmol), **B^7** (17.3 mg, 0.0259 mmol), and tetradecane (240.3 mg, 1.21 mmol) were employed, and the autoclave was heated for 48 h, giving **H_4-MeQin** in >99% GC yield and TON 3960 (TOF 82.5 h^{-1}).

Using $B(C_6F_5)_3$: Followed by the general procedure, **MeQin** (7.13 g, 49.8 mmol), **$B(C_6F_5)_3$** (14.3 mg, 0.0279 mmol,), and tetradecane (241.1 mg, 1.22 mmol) were employed, and the autoclave was heated for 24 h, giving **H_4-MeQin** in 5% GC yield and TON 200 (TOF 8.3 h^{-1}).

3.4.5 Catalytic dehydrogenation of MeQin

A 10 mL one-necked reaction vial was charged with **H_4-MeQin** (554.7 mg, 3.77 mmol), **B^7** (50.1 mg,

0.0751 mmol, 2 mol%), and tetradecane (97.5 mg, 0.491 mmol) as an internal standard. The reaction mixture was heated at 200 °C for 55 min and then allowed to cool to rt. Hydrogen gas was collected in a graduated cylinder, and the yield of H_2 was calculated based on the collected volume (143 mL), corresponding to 169% yield (6.38 mmol). The yield of MeQin was 86%, and the purity of the collected H_2 was 99.978%, as determined by GC analysis (Figure 3.S4) by calibrating for the contaminated amounts of CO_2 from air.[8]

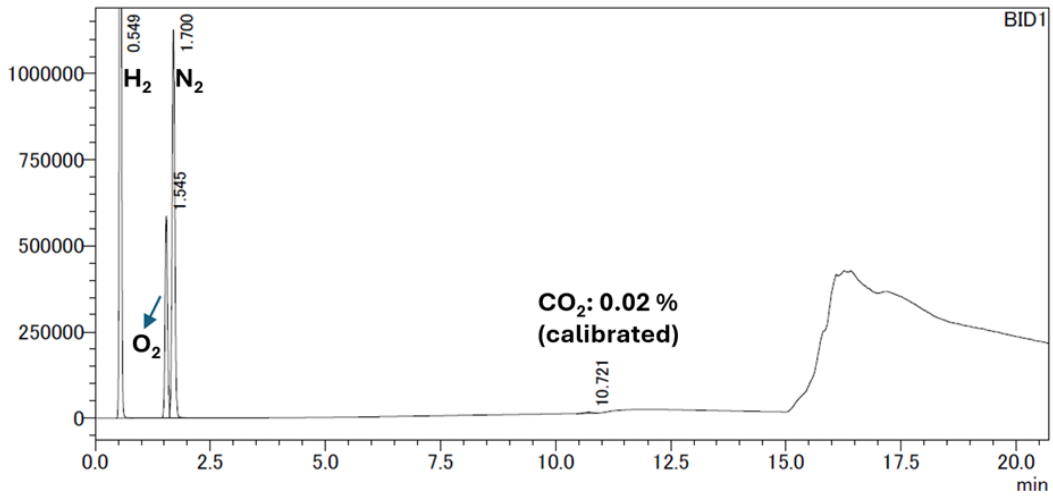


Figure 3.S4 The GC chromatogram for the collected H_2 *Reprinted with permission from* Organic Letters. © American Chemical Society.

3.4.6 Catalytic hydrogenation of MeInd[29]

General: A 30 mL autoclave was charged with **MeInd** (ca. 100 mmol), **B″** (ca. 0.020 mmol, 0.02 mol%) and tetradecane as an internal standard. Once sealed, the autoclave was pressurized with H_2 (60 atm) and heated at 100 °C for 24 h. After degassing at rt, the yield of **H_2-MeInd** was determined by GC analysis (Figure 3.6C).

Using B[7]: Followed by the general procedure, **MeInd** (13.1 g, 99.9 mmol), **B[7]** (13.7 mg, 0.0205 mmol), and tetradecane (987 mg, 4.98 mmol) were employed, giving **H_2-MeInd** in 46% GC yield and TON 2300 (TOF 95.8 h^{-1}).

Using B[8]: Followed by the general procedure, **MeInd** (13.0 g, 99.1 mmol), **B[8]** (14.7 mg, 0.0200 mmol), and tetradecane (848 mg, 4.27 mmol) were employed, giving **H_2-MeInd** in 6% GC yield and TON 300 (TOF 12.5 h^{-1}).

Using B[9]: Followed by the general procedure, **MeInd** (13.0 g, 99.1 mmol), **B[9]** (13.3 mg, 0.0191 mmol), and tetradecane (927 mg, 4.67 mmol) were employed, giving **H_2-MeInd** in 1% GC yield and TON 50 (TOF 2.1 h^{-1}).

3.4.7 Reductive alkylation of amino-acid derivatives with benzaldehyde[12]

General: A 10 mL autoclave was charged with **2a** (ca. 0.20 mmol), **1t** or **1u** (ca. 0.20 mmol), **B″** (ca. 0.01 mmol),

4Å MSiv (50 mg), and THF (4 mL). Once sealed, the vessel was pressurized with H_2 (80 atm) and the reaction mixture was stirred at 100 °C for 12 h or 24 h. Then degassed at rt followed by addition of acetone, the resultant mixture was filtered to remove MS and other solids when generated. Subsequently, all volatiles were removed in vacuo to give crude mixture (Figures 3.6A, 6B). The NMR yield was determined by using 1,3,5-trimethoxybenzen as an internal standard.

Using 1t (Figure 3.5A, run 1): Followed by the general procedure, **2a** (21.7 mg, 0.204 mmol), **1t** (26.8 mg, 0.204 mmol), and **B**[7] (6.7 mg, 0.0100 mmol) were employed, and the autoclave was heated for 12 h, giving **3ta** (43.8 mg, 0.198 mmol, 97%) as pale-yellow liquid.

Using 1u (Figure 3.5B): Followed by the general procedure, **2a** (21.2 mg, 0.200 mmol), **1u** (35.0 mg, 0.200 mmol), and **B**[7] (6.7 mg, 0.0100 mmol) were employed, and the autoclave was heated for 24 h, giving **3ua** (23.2 mg, 0.0995 mmol, 50%) as pale-yellow liquid. The author also isolated 3,5-F_2-(*o*-carboran-1-yl)C_6H_3 (0.002 mmol) from the crude mixture and confirmed that the carborane structure remained intact.

Identification of **3ta**[43]:
^{1}H NMR (400 MHz, $CDCl_3$, rt, δ/ppm): 7.55–7.20 (m, 5H), 3.83 (d, J = 12.8 Hz, 1H), 3.72 (s, 3H), 3.58 (d, J = 13.2 Hz, 1H), 3.02 (d, J = 6.4 Hz, 1H), 1.96–1.86 (m, 1H), 1.77 (s, 1H), 0.94 (d, J = 6.8 Hz, 6H).

Identification of **3ua**[44]:
^{1}H NMR (400 MHz, $CDCl_3$, rt, δ/ppm): 7.35–7.17 (m, 5H), 5.02 (d, J = 14.8 Hz, 1H), 4.00 (d, J=14.8 Hz, 1H), 3.99 (dd, J = 9.1 Hz, J = 3.1 Hz, 1H), 3.67 (s, 3H), 2.58 (dt, J = 17.5, J = 9.3 Hz, 1H), 2.42 (dq, J = 9.6, J = 3.7 Hz, 1H), 2.26 (dt, J = 13.1, J = 9.3 Hz, 1H), 2.08 (ddt, J = 13.0, J = 9.6, J = 3.4 Hz, 1H).

3.4.8 Comparison of Lewis acidity[12]

A J. Young tube was charged with **B**[7], **B**[8] or **B**[9] (0.03 mmol each), Et_3P=O (1.3 mg, 0.01 mmol, 0.33 equiv), and CD_2Cl_2 (0.5 mL). Then, the ^{31}P NMR analyses were conducted (Figure 3.4).

3.4.9 Theoretical studies

3.4.9.1 Computational details

Density functional theory (DFT) calculations were performed using Gaussian 16 (Revision C.01).[45] All the structures were optimized at the ωB97X-D[46] level of theory with the 6-31G(d,p) basis sets. Frequency calculations were performed to verify that intermediates have no imaginary frequency. Single-point energy calculations were carried out at ωB97X-D/6-311+G(d,p)/gas-phase level of theory. The reported Gibbs free energies were calculated at 298.15 K. These calculations involve a certain margin of error. The coordinates of the optimized structures are separately given.

3.4.9.2 Selected frontier molecular orbitals (FMOs) for B^n

FMOs, including the p orbitals of the boron, calculated at the *ω*B97X-D/6-311+G(d,p)//*ω*B97X-D/6-31G(d,p) level, are shown in Figure 3.S5.

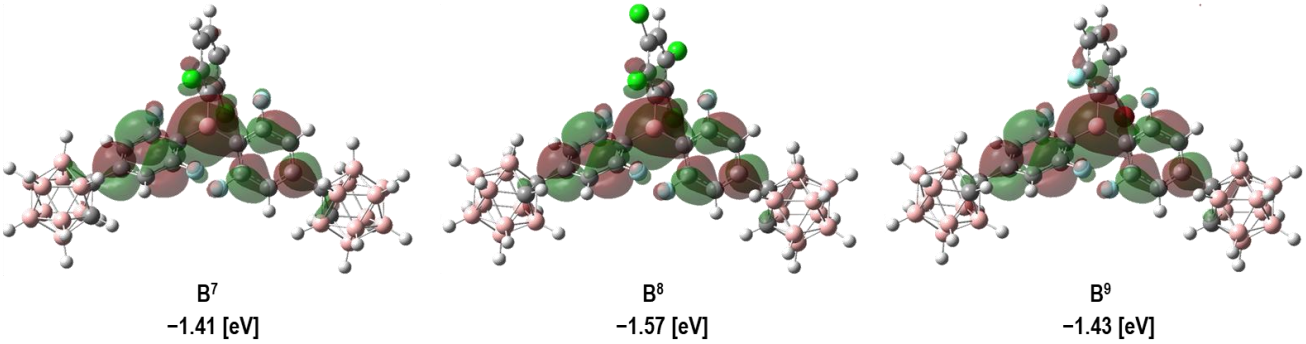


Figure 3.S5. Selected FMOs (LUMO in most cases) for **B*ⁿ*** (n = 7–9). *Reprinted with permission from* Organic Letters. © American Chemical Society.

3.4.9.3 Calculation of Global Electrophilicity Index

The global electrophilicity index (ω) was calculated according to the literature method (Figure 3.S6).[35,36,47] This index provides a quantitative measure of the electrophilic power of a molecule and is defined as:

$$\omega = \mu^2/(2\eta)$$

where μ is the electronic chemical potential, and η is the chemical hardness, which are defined as:

$$\mu = -(I + A)/2$$

$$\eta = I - A$$

In this work, I and A were approximated using Koopmans' theorem:

$$I \approx -\omega_{HOMO}$$

$$A \approx -\omega_{LUMO}$$

This leads to the operational formulas:

$$\mu \approx (\omega_{HOMO} + \omega_{LUMO})/2$$

$$\eta \approx \omega_{LUMO} - \omega_{HOMO}$$

Borane	ε_{HOMO} (eV)	ε_{LUMO} (eV)	μ (eV)	η (eV)	ω (eV)
B[7]	-9.23	-1.41	-5.32	7.82	1.81
B[8]	-9.17	-1.57	-5.37	7.61	1.89
B[9]	-9.17	-1.43	-5.30	7.74	1.81
B[3a]	-9.00	-1.28	-5.14	7.72	1.71
B[1a]	-9.19	-1.33	-5.26	7.87	1.76
B(C_6F_5)$_3$	-9.78	-1.93	-5.85	7.86	2.18

Figure 3.S6. HOMO and LUMO energies, chemical potential (μ), chemical hardness (η), and global electrophilicity indices (ω) for boranes. *Reprinted with permission from* Organic Letters. © American Chemical Society.

3.4.9.4 Conformers for $Et_3P{=}O{-}$**B**[9]

The author confirmed that $Et_3P{=}O{-}$**B**[9] would include isomers **I** or **II**, depending on whether $Et_3P{=}O$ coordinates to the boron center from the F or Br side of the 2-Br-6-F-C_6H_3 ring. The author performed DFT calculations to compare the relative Gibbs free energies (ΔG) of isomers **I** and **II** with respect to that of [$Et_3P{=}O$ + **B**[9]] (0.0 kcal mol^{-1}) (Figure 3.S7). The author confirmed that the formation of isomer **II** (ΔG = −13.3 kcal mol^{-1}) is thermodynamically more favorable than that of isomer **I** (ΔG = −12.2 kcal mol^{-1}), suggesting that coordination of $Et_3P{=}O$ preferentially proceeds from the bulkier Br side rather than from the less crowded F side. Similar discussions were reported by Soós et al.[48]

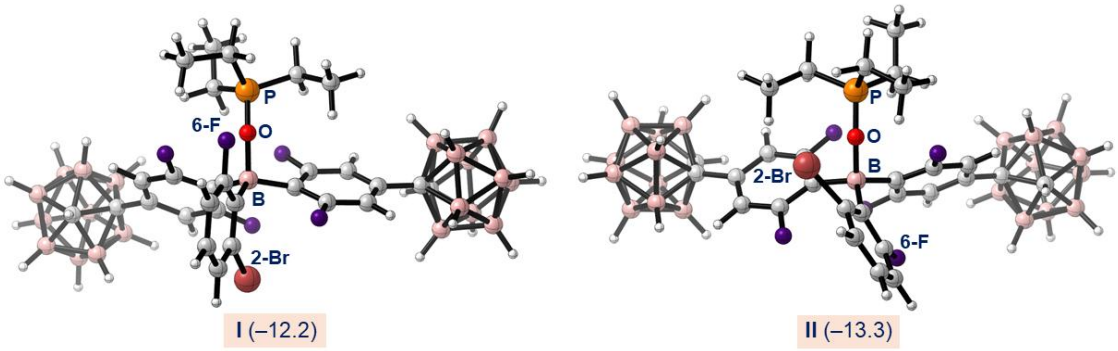


Figure 3.S7. Comparison of the relative Gibbs free energies (kcal mol^{-1}) of isomers **I** and **II**, which are determined with respect to [$Et_3P{=}O$ + **B**^{9}] (0.0 kcal mol^{-1}) at the ωB97X-D/6-311+G(d,p)//ωB97X-D/6-31G(d,p) level (gas phase). Selected bond lengths (Å) and angles (°): **I**; O–B 1.55; P–O–B 146.0. **II**; O–B 1.55; P–O–B 148.4. *Reprinted with permission from* Organic Letters. © American Chemical Society.

3.5 References and notes

1. Carden, J. L.; Dasgupta, A.; Melen, R. L. *Chem. Soc. Rev.* **2020**, *49*, 1706–1725.
2. Berger, S. M.; Ferger, M.; Marder, T. B. *Chem. Eur. J.* **2021**, *27*, 7043–7058.
3. Stephan, D. W. *J. Am. Chem. Soc.* **2021**, *143*, 20002–20014.
4. Berger, S. M.; Marder, T. B. *Mater. Horiz.* **2022**, *9*, 112–120.
5. Afrin, A.; Chinna Ayya Swamy, P. *Mater. Chem. Front.* **2025**, *9*, 1794–1820.
6. Sakuraba, M.; Hoshimoto, Y. *Synthesis* **2024**, *56*, 3421–3430.
7. Ferger, M.; Berger, S. M.; Rauch, F.; Schönitz, M.; Rühe, J.; Krebs, J.; Friedrich, A.; Marder, T. B. *Chem. Eur. J.* **2021**, *27*, 9094–9101.
8. Hashimoto, T.; Asada, T.; Ogoshi, S.; Hoshimoto, Y. *Sci. Adv.* **2022**, *8*, eade0189.
9. Sakuraba, M.; Ogoshi, S.; Hoshimoto, Y. *Tetrahedron Chem* **2024**, *9*, 100059.
10. Hashimoto, T.; Harabuchi, Y.; Ogoshi, S.; Maeda, S.; Hoshimoto, Y. *Bull. Chem. Soc. Jpn.* **2025**, *98*, uoae145.
11. Hoshimoto, Y.; Kinoshita, T.; Hazra, S.; Ohashi, M.; Ogoshi, S. *J. Am. Chem. Soc.* **2018**, *140*, 7292–7300.
12. Hisata, Y.; Washio, T.; Takizawa, S.; Ogoshi, S.; Hoshimoto, Y. *Nat. Commun.* **2024**, *15*, 3708.
13. Sakuraba, M.; Morishita, T.; Hashimoto, T.; Ogoshi, S.; Hoshimoto, Y. *Synlett* **2023**, *34*, 2187–2192.
14. Issa, F.; Kassiou, M.; Rendina, L. M. *Chem. Rev.* **2011**, *111*, 5701–5722.
15. Valliant, J. F.; Guenther, K. J.; King, A. S.; Morel, P.; Schaffer, P.; Sogbein, O. O.; Stephenson, K. A. *Coord. Chem. Rev.* **2002**, *232*, 173–230.
16. Tanaka, K.; Gon, M.; Ito, S.; Ochi, J.; Chujo, Y. *Coord. Chem. Rev.* **2022**, *472*, 214779.
17. Núñez, R.; Tarrés, M.; Ferrer-Ugalde, A.; de Biani, F. F.; Teixidor, F. *Chem. Rev.* **2016**, *116*, 14307–14378.
18. Li, J.; Kim, J. S.; Fan, J.; Peng, X.; Matejíček, P. *Chem. Soc. Rev.* **2025**, *54*, 4104–4134.
19. Sivaev, I. B.; Stogniy, M. Y.; Bregadze, V. I. *Coord. Chem. Rev.* **2021**, *436*, 213795.

20. Lee, Y. H.; Lee, H. D.; Ryu, J. Y.; Lee, J.; Lee, M. H. *J. Organomet. Chem.* **2017**, *846*, 81–87.
21. Kim, S. Y.; Lee, A. R.; Cho, Y. J.; Son, H. J.; Han, W. S.; Kang, S. O. *J. Organomet. Chem.* **2015**, *798*, 245–251.
22. Nghia, N. Van; Jana, S.; Sujith, S.; Ryu, J. Y.; Lee, J.; Lee, S. U.; Lee, M. H. *Angew. Chem., Int. Ed.* **2018**, *57*, 12483–12488.
23. Choi, B. H.; Lee, J. H.; Hwang, H.; Lee, K. M.; Park, M. H. *Organometallics* **2016**, *35*, 1771–1777.
24. Song, K. C.; Kim, H.; Lee, K. M.; Lee, Y. S.; Do, Y.; Lee, M. H. *Dalton Trans.* **2013**, *42*, 2351–2354.
25. Lee, K. M.; Huh, J. O.; Kim, T.; Do, Y.; Lee, M. H. *Dalton Trans.* **2011**, *40*, 11758–11764.
26. Huh, J. O.; Kim, H.; Lee, K. M.; Lee, Y. S.; Do, Y.; Lee, M. H. *Chem. Commun.* **2010**, *46*, 1138–1140.
27. Although it is not a triarylborane, tris(*o*-carboran-1-yl)borane was confirmed to catalyze the defluorinative functionalization of 1-fluoroadamantane; for details, see: Akram, M. O.; Tidwell, J. R.; Dutton, J. L.; Martin, C. D. *Angew. Chem., Int. Ed.* **2022**, *61*, e202212073.
28. Hisata, Y.; Morishita, D.; Hoshimoto, Y. *J. Am. Chem. Soc.* **2025**, *147*, 37677–37687.
29. Hashimoto, T.; Tanigawa, M.; Kambe, K.; Ogoshi, S.; Hoshimoto, Y. *Precis. Chem.* **2025**, *3*, 128–134.
30. Dorkó, E.; Kótai, B.; Földes, T.; Gyömöre, Á.; Papai, I.; Soós, T. *J. Organomet. Chem.* **2017**, *847*, 258–262.
31. Dorkó, É.; Szabó, M.; Kótai, B.; Pápai, I.; Domján, A.; Soós, T. *Angew. Chem., Int. Ed.* **2017**, *56*, 9512–9516.
32. Gyömöre, Á.; Bakos, M.; Földes, T.; Pápai, I.; Domján, A.; Soós, T. *ACS Catal.* **2015**, *5*, 5366–5372.
33. Dudás, Á.; Gyömöre, Á.; Mészáros, B. B.; Gondár, S.; Adamik, R.; Fegyverneki, D.; Papp, D.; Otte, K. B.; Ayala, S.; Daru, J.; Répási, J.; Soós, T. *J. Am. Chem. Soc.* **2025**, *147*, 1112–1122.
34. Erdmann, P.; Greb, L. *Angew. Chem., Int. Ed.* **2022**, *61*, e202114550.
35. Parr, R. G.; von Szentpály, L.; Liu, S. *J. Am. Chem. Soc*. **1999**, *121*, 1922–1924.
36. Geerlings, P.; De Proft, F.; Langenaeker, W. *Chem. Rev*. **2003**, *103*, 1793–1874.
37. When H_2 (85 atm) was used for the hydrogenation of **MeQin**, **B**[7] (0.05 mol%) exhibited a TON of 3960 within 48 h, while $B(C_6F_5)_3$ resulted in a TON of 200 after 48 h. Under otherwise identical conditions, **B**[8] exhibited a TON of 2960 (*cf.* ref. 8).
38. Dolomanov, O. V.; Bourhis, L. J.; Gildea, R. J.; Howard, J. A. K.; Puschmann, H. *J. Appl. Crystallogr.* **2009**, *42*, 339–341.
39. Sheldrick, G. M. *Acta Crystallogr. A* **2015**, *71*, 3–8.
40. Sheldrick, G. M. *Acta Crystallogr. C* **2015**, *71*, 3–8.
41. Fox, M. A.; Hughes, A. K. *Coord. Chem. Rev.* **2004**, *248*, 457–476.
42. Vedejs, E.; Chapman, R. W.; Fields, S. C.; Lin, S.; Schrimpf, M. R. *J. Org. Chem.* **1995**, *60*, 3020–3027.
43. Salvatore, R. N.; Nagle, A. S.; Kyung, W. J. *J. Org. Chem.* **2002**, *67*, 674–683.
44. Weigl, M.; Wnsch, B. *Tetrahedron* **2002**, *58*, 1173–1183.
45. Frisch, M. J.; Trucks, G. W.; Schlegel, H. B.; Scuseria, G. E.; Robb, M. A.; Cheeseman, J. R.; Scalmani, G.; Barone, V.; Petersson, G. A.; Nakatsuji, H.; Li, X.; Caricato, M.; Marenich, A. V.; Bloino, J.; Janesko, B. G.; Gomperts, R.; Mennucci, B.; Hratchian, H. P.; Ortiz, J. V.; Izmaylov, A. F.; Sonnenberg, J. L.;

Williams-Young, D.; Ding, F.; Lipparini, F.; Egidi, F.; Goings, J.; Peng, B.; Petrone, A.; Henderson, T.; Ranasinghe, D.; Zakrzewski, V. G.; Gao, J.; Rega, N.; Zheng, G.; Liang, W.; Hada, M.; Ehara, M.; Toyota, K.; Fukuda, R.; Hasegawa, J.; Ishida, M.; Nakajima, T.; Honda, Y.; Kitao, O.; Nakai, H.; Vreven, T.; Throssell, K.; Montgomery, J. A., Jr.; Peralta, J. E.; Ogliaro, F.; Bearpark, M. J.; Heyd, J. J.; Brothers, E. N.; Kudin, K. N.; Staroverov, V. N.; Keith, T. A.; Kobayashi, R.; Normand, J.; Raghavachari, K.; Rendell, A. P.; Burant, J. C.; Iyengar, S. S.; Tomasi, J.; Cossi, M.; Millam, J. M.; Klene, M.; Adamo, C.; Cammi, R.; Ochterski, J. W.; Martin, R. L.; Morokuma, K.; Farkas, O.; Foresman, J. B.; Fox, D. J. Gaussian, Inc., Wallingford CT, 2016.

46. Chai, J. D.; Head-Gordon, M. *Phys. Chem. Chem. Phys.* **2008**, *10*, 6615–6620.
47. Chattaraj, P. K.; Sarkar, U.; Roy, D. R. *Chem. Rev.* **2006**, *106*, 2065–2091.
48. Kovács, B.; Földes, T.; Szabó, M.; Dorkó, É.; Kótai, B.; Laczkó, G.; Holczbauer, T.; Domján, A.; Pápai, I.; Soós, T. *Chem. Sci.* **2024**, *15*, 15679–15689.

Conclusions

In this thesis, the author has developed reductive alkylation of aniline-derived amino acids or natural amino acid derivatives using H_2 and aldehydes in the presence of the well-characterized BAr_3 catalysts. The key to achieving this work was optimizing the BAr_3 structure by screening various substituents, both theoretically and experimentally.

In Chapter 1, the author constructed an *in-silico* library of 54 BAr_3 molecules using DFT calculations and developed machine-learning regression models with experimental data as the objective variable. As a result of catalyst optimization, the author demonstrated that B(2,3,5,6-Cl_4-C_6H)(2,6-F_2-3,5-$(CF_3)_2$-$C_6H)_2$ effectively catalyzed the reductive alkylation of aniline-derived amino acids and peptides using H_2.

In Chapter 2, the author reported a synthetic method for preparing *o*-carboranyl arenes, which serve as synthetic precursors to BAr_3 catalysts used in the reductive alkylation of natural amino acid derivatives. To this end, the author developed an isolated lithium bis(*o*-carboran-1-yl)cuprate reagent that converts the previously complicated and unreproducible *in-situ* carboranylation reaction into a "dump-and-stir" synthesis from readily available bromides and chlorides. This reagent enabled gram-scale synthesis, allowing efficient introduction of multiple carboranyl groups and even construction of carborane-fused π-systems. Mechanistic studies revealed that isophthalonitrile coordinates to the Li center, stabilizing the rate-determining oxidative addition transition state at the Cu center, while phosphines deactivate the cuprate.

In Chapter 3, the author used the synthetic method for *o*-carboranyl arenes developed in Chapter 2 to synthesize BAr_3 bearing 2,6-F_2-4-(*o*-carboran-1-yl)phenyl groups. The *o*-carboranyl aryl groups enhanced the intrinsic Lewis acidity and improved solubility in *n*-hexane, facilitating the purification process. This BAr_3 was confirmed to be an efficient catalyst for the reductive alkylation of the aliphatic amino acid derivatives. Furthermore, it exhibited effective catalytic activity in the hydrogenation and dehydrogenation of nitrogen-containing cyclic compounds using crude hydrogen (H_2/CO/CO_2) and pure H_2.

Through these achievements, the author has established a conceptual framework and practical guidelines for the design and identification of BAr_3 as catalysts for the reductive alkylation of amino acids using H_2. By exploiting the unique electronic and steric properties of well-optimized BAr_3, this research not only broadens the scope of FLP catalysis but also introduces strategies to simplify downstream purification steps in organic synthesis. These contributions are expected to accelerate the development of highly efficient and environmentally sustainable synthetic methodologies, thereby promoting greener and more resource-conscious practices in chemical manufacturing.

List of Publications

1. “In-silico-assisted derivatization of triarylboranes for the catalytic reductive functionalization of aniline-derived amino acids and peptides with H_2”
   Yusei Hisata; Takashi Washio, Shinobu Takizawa, Sensuke Ogoshi, Yoichi Hoshimoto
   Nat. Commun. **2024**, *15*, 3708 (DOI: 10.1038/s41467-024-47984-0).
2. “An Isolated Lithium *ortho*-Carboranyl Cuprate Complex for the Synthesis of Multiple-Carborane-Substituted Arenes from (Hetero)Aryl Bromides and Chlorides”
   Yusei Hisata, Daina Morishita, Yoichi Hoshimoto
   J. Am. Chem. Soc. **2025**, *147*, 37677–37687 (DOI: 10.1021/jacs.5c13004).
3. “Triarylboranes Bearing (*ortho*-Carboran-1-yl)aryl Groups for Catalytic Hydrogenation with Pure or Crude Hydrogen”
   Yusei Hisata, Riku Ikeda, Anil Chauhan, Yoichi Hoshimoto
   Org. Lett. **2026**, *28*, 372–376 (DOI: 10.1021/acs.orglett.5c04669).

Supplementary Publications

1. “Triarylborane Catalysis: From Hydrogenation of Unsaturated Molecules to H_2 Purification”
   Taichi Morishita, Yusei Hisata, Taiki Hashimoto, Sensuke Ogoshi, Yoichi Hoshimoto
   J. Synth. Org. Chem. Jpn. **2024**, *82*, 1097–1106 (DOI: 10.5059/yukigoseikyokaishi.82.1097).
2. “Palladium-Catalyzed γ-Arylation of Acylketene Synthons with Aryl Chlorides Enabled by Ylide-Functionalized Phosphines (YPhos)”
   Sourav Manna, Florian Papp, Yusei Hisata, Julian Löffler, Martyna Rybka, Viktoria H. Gessner, Yoichi Hoshimoto, Lukas J. Gooßen
   Adv. Synth. Catal. **2024**, *366*, 1107–1112 (DOI: 10.1002/adsc.202301474).